Biomimetic gastric tract simulator

A thesis presented in partial fulfilment of the requirements
for the degree of

Doctor of Philosophy
in
Engineering

at Massey University, Manawatu,
New Zealand.

Gerald Keith Olson

2023

Abstract

Mimicry of the biomechanical functioning of the human gastric tract can play a significant role in study of the behaviour of foods and food structures as they are broken down and digested in the human body. The gastric tract wall produces peristaltic waves and other deformation patterns providing movement, accommodation, mixing and evacuation of foods in the stomach and connected gastric tract organs. This thesis presents an advanced biomimetic dynamic *in vitro* model of the human gastric tract that simulates anatomic geometry and demonstrates the mixing and movement of gastric tract contents. Materials, methods, and techniques suitable for mimicking the gastric tract wall were investigated and artificial membrane layers, artificial muscles, muscle activation and control mechanisms, and feedback sensors were developed and integrated into a dynamic physical model of the gastric tract. A composite material of silicone rubber reinforced with a nylon elastic fabric provides a thin, watertight, and highly elastic artificial membrane that forms the shell of the tract. Artificial muscles made from loops of coiled nylon monofilament line, attached to the artificial membrane, are contracted, and expanded through the pulling and releasing of flexible tendons or cables. Contraction and expansion of the artificial muscles is carried out using winding mechanisms and motors, while feedback and control systems track and maintain the desired mechanical activity of the tract. Mimicry of the muscle and membrane layers of the gastric tract wall is a novel approach to simulating gastric tract biomechanics, resulting in a soft, highly flexible, and dynamic physical *in vitro* modelling of the geometrical, anatomic, and biomechanical functioning of the human gastric tract.

Acknowledgements

First and foremost, I am indebted to my supervisor Professor Clive Davies for his immeasurable wisdom, advice, constant support, and heartfelt encouragement throughout my PhD journey. I could not have done it without you Clive! I also want to thank my co-supervisors Professor Gourab Sen Gupta, Doctor Rose Davies, and Doctor Luke Fullard for all the help and direction they have provided over the years, and for all the encouraging feedback they have given that made my work enjoyable. I want to acknowledge the financial support and professional experience provided by the Riddet Institute and its members, and for the opportunity they provided to undertake this project. Finally, thank you to my family who have always been there for me and travelled with me along the way.

Table of Contents

List of Figures

List of Tables

Glossary

Actuation: fact of making a machine start to work or a process starts to happen.

Amylase: any of a class of digestive enzymes, present in saliva that break down complex carbohydrates such as starch into simpler sugars such as glucose.

Axial: located on, around, or in the direction of an axis.

Biomechanics: the study of the structure, function and motion of the mechanical aspects of biological systems using the methods of mechanics.

Biomimicry: the emulation of the models, systems, and elements of nature for the purpose of solving complex human problems.

Chyme: results from the mechanical and chemical breakdown of a bolus and consists of partially digested food, water, hydrochloric acid, and various digestive enzymes.

Digesta: something undergoing digestion.

Distal: situated away from the point of attachment or origin or a central point especially of the body.

Enteric nervous system: one of the main divisions of the autonomic nervous system and consists of a mesh-like system of neurons that governs the function of the gastrointestinal tract.

Epithelium: a membranous cellular tissue that covers a free surface or lines a tube or cavity of an animal body and serves especially to enclose and protect the other parts of the body, to produce secretions and excretions, and to function in assimilation

Gastric: of or relating to the stomach.

In silico: done or produced by using computer software or simulation.

In vitro: outside the living body and in an artificial environment.

In vivo: in the living body of a plant or animal.

Lumen: the cavity of a tubular organ or part.

Mesentery: a double layer of peritoneum that encloses the intestines and attaches them to the posterior abdominal wall.

Morphogenesis: the formation and differentiation of tissues and organs.

Motility: the ability of the muscles of the digestive tract to undergo contraction.

Mucosa: a membrane rich in mucous glands.

Occlude: to close up or block off.

Oesophagus: a muscular tube that conveys food from the mouth to the stomach.

Omentum: a double fold of peritoneum extending from the stomach to adjacent abdominal organs.

Peritoneum: the smooth transparent serous membrane that lines the cavity of the abdomen of a mammal.

Pharynx: the muscular tubular passage of the vertebrate digestive and respiratory tracts extending from the back of the nasal cavity and mouth to the oesophagus.

Phasic contractions: a regularly recurring cycle of contractions.

Plexus: a network of anastomosing or interlacing blood vessels or nerves.

Polypeptide: a continuous, unbranched chain of amino acids joined by peptide bonds.

Proteoglycans: proteins that are heavily glycosylated.

Proximal: next to or nearest the point of attachment or origin, a central point, or the point of view.

Rugae: a series of ridges produced by folding of the wall of an organ.

Serous: of thin watery constitution.

Strain: the change in form or shape of an object or physical body on which stress is applied.

Stress: Force per unit area or the magnitude of a force - a force that can cause a change in an object or physical body.

Submucosa: a layer of dense irregular connective tissue that supports the mucosa and joins it to the muscular layer.

Supine*:* lying on the back or with the face upward.

Tonic contractions: the sustained contractions of various groups of muscle fibres in a muscle to keep persistent muscular tension.

Transverse: made at right angles to the long axis of the body.

Villi: tiny projections on the inner surface of the small intestine which help in absorbing nutrients from digested food.

Viscoelastic: Viscoelastic materials combine the properties of *viscous* fluids and *elastic* solids when they are deformed. Viscoelastic materials include polymers and many biological tissues.

Chapter One

Introduction

Chapter 1 – Introduction

Understanding the biomechanics of the human gastrointestinal tract (GIT) plays an important role in understanding human digestion and health. The gastrointestinal tract is a highly complex system of tubular organs that processes ingested food material, through both mechanical and non-mechanical means, so that nutrients and other chemicals can be digested and absorbed into the body [1, 2]. Mimicry of the biomechanical functioning of the layers of the gastrointestinal tract wall has the potential to advance the accuracy of *in vitro* simulations, or simulations outside their normal biological context, by more closely reproducing the deformation patterns of the human digestive system.

This research aims to develop a biomimetic *in vitro* model of the stomach. The *in vitro* model mimics the biological mechanical properties of the gastric tract wall and simulates the contractive and expansive actions of the gastric tract muscle layers using controlled 'soft' actuators. This chapter introduces the study by first discussing the background and context, followed by the research problem, the research aims, objectives and questions, the significance and finally, the limitations and scope of the study.

1.1. Background and context

The gastrointestinal tract, also referred to as the digestive tract, consists of the mouth, pharynx, oesophagus, stomach, duodenum, small intestine, large intestine or colon and rectum (Fig. 1). Each component of the tract has a particular role to play in the process of digestion. The oesophagus transports food from the mouth to the stomach. The prime role of the stomach is to accommodate and break down food, which then passes as chyme through to the duodenum where bile is added. The chyme then passes to the small intestine

which extracts nutrients and provides the body with energy from the digested food. It then passes to the large intestine, or colon, which extracts water from the residual chyme before it reaches the rectum and is finally passed as excreta.

The gastric tract is a section of the gastrointestinal tract consisting of the mouth, pharynx, oesophagus, stomach and duodenum. The stomach has anatomically defined regions called the fundus, corpus or body, antrum and pylorus (Fig. 2). It also has functional regions

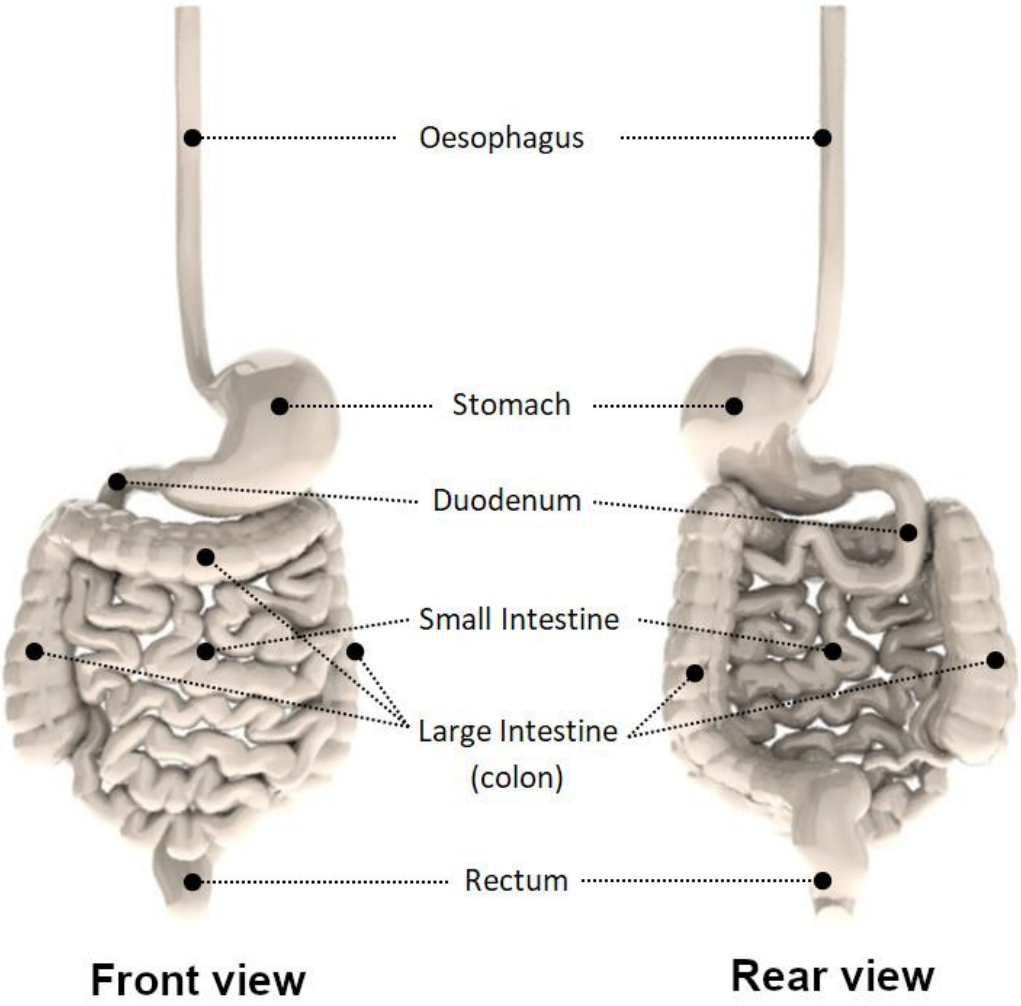

Fig. 1: The human gastrointestinal tract - mouth and pharynx are not shown.
(This work includes rendered derivatives of BodyParts3D, © The Database Center for Life Science licensed under CC Attribution-Share Alike 2.1 Japan:
https://dbarchive.biosciencedbc.jp/en/bodyparts3d/lic.html)

referred to as the gastric reservoir, where tonic contractions take place, and the gastric pump, where phasic contractions such as peristaltic waves occur [3].

The entire gastrointestinal tract is formed from an uninterrupted tube during the foetal development stage [1]. The wall of the tract therefore has the same layered structure throughout its length which consists of an innermost mucosal layer, an extracellular matrix composed of collagen and elastin that fills space between cell tissue, layers of smooth muscle cells, and an outer protective layer called the serosa that coats the organs and *dictates their final shape [4].

The muscle layers are the biomechanical driving mechanism behind the tracts' motility actions. There are two distinct layers of smooth muscle that are found throughout the entire

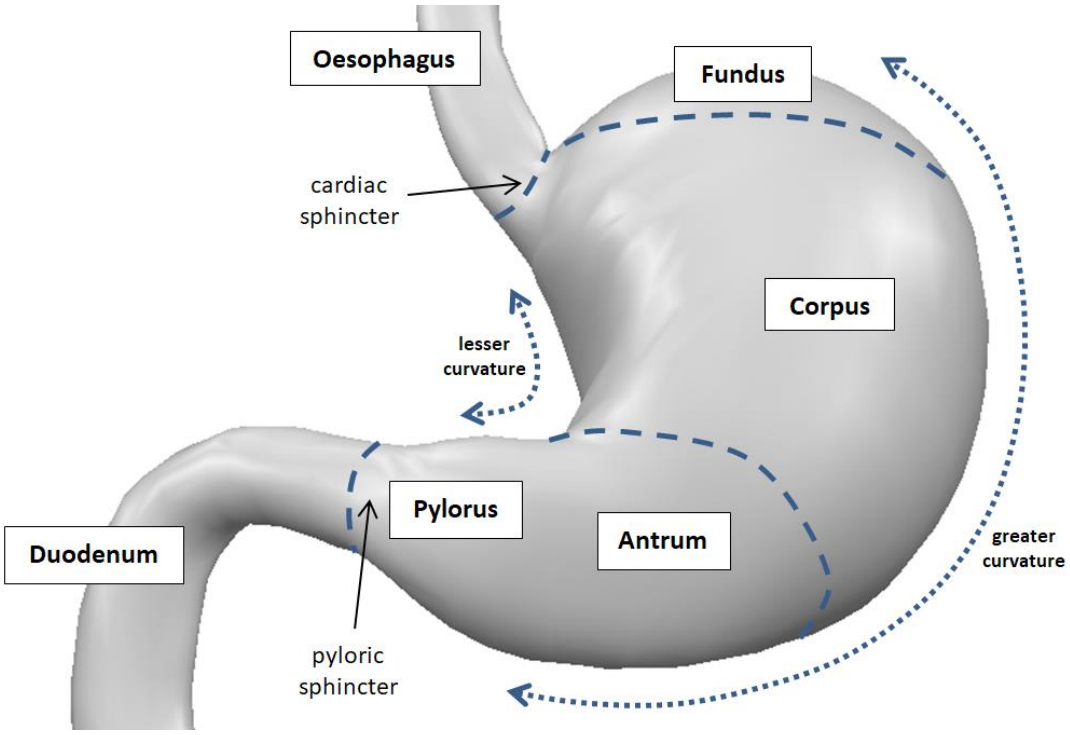

Fig. 2: Anatomical regions of the stomach and attached organs.
(This work includes rendered derivatives of BodyParts3D, © The Database Center for Life Science licensed under CC Attribution-Share Alike 2.1 Japan:
https://dbarchive.biosciencedbc.jp/en/bodyparts3d/lic.html)

tract, these layers are called the longitudinal muscle and circumferential muscle layers and take their name from the orientation of the muscle cells within the layers [1]. The stomach is the only organ of the tract that has an additional muscle layer, known as the oblique layer, and exhibits a larger range of dynamic movement behaviours than other regions of the tract.

The gastrointestinal tract is connected to the body through a thin serous membrane called the peritoneum [1, 5]. The peritoneum provides pathways for blood and lymphatic transfer to and from the tract as well as acting as a conduit for nervous and bioelectrical connections. Peritoneal tissue is connected to the stomach body along the lesser curvature, where the membrane is called the lesser omentum, and the greater curvature which is referred to as the greater omentum [6]. This attachment provides the stomach with flexibility for undergoing deformation and motility within the abdominal cavity.

From a simplistic biomechanical point of view, the motility patterns of the gastrointestinal tract create the moving, mixing, and grinding of its contents. The oesophagus moves boluses of food to the stomach. The stomach adds gastric and digestive juices and mixes, grinds, and moves the contents to the duodenum as chyme. The duodenum mixes bile from the gallbladder with the chyme and moves it into the small intestine. The small and large intestines then extract nutrients and water from the chyme, mixing and moving it gradually throughout the remainder of the intestinal tract to the rectum where it is eventually expelled.

Three major types of biomechanical gut motility can be observed in the gastrointestinal tract: segmentation, tonic contraction and peristalsis [7] (Fig. 3). Segmentation occurs in the small and large intestine and is a non-propulsive contractive action of the circumferential muscles that mixes intestinal chyme in a back and forth squeezing action. Tonic

contractions occur in the fundus of the stomach during volume adjustments in the accommodation of food, and at regions that divide the gut into functional segments such as sphincters. Peristalsis is a highly integrated, complex motor action for moving contents along the tract via a sweeping propulsive action. The action of peristalsis involves a sequential contraction and relaxation of the circumferential and longitudinal muscles with one layer of muscle contracting as the other layer relaxes and extends.

Ideally, study of the effects of gastrointestinal biodynamics on the digestion of foods or pharmaceuticals would be carried out within the living human body, or *in vivo*. However, there are significant costs and ethical considerations associated with the undertaking of *in vivo* studies of the digestion of food and pharmaceuticals. The desire to replicate the biological characteristics of the gastrointestinal tract (GIT) within a controlled environment, with less cost, difficulty and concern for safety than is experienced with *in vivo* studies, has led to the application of *in vitro* models to simulate the GIT digestive processes.

In vitro models of the human gastrointestinal tract have been developed since the early

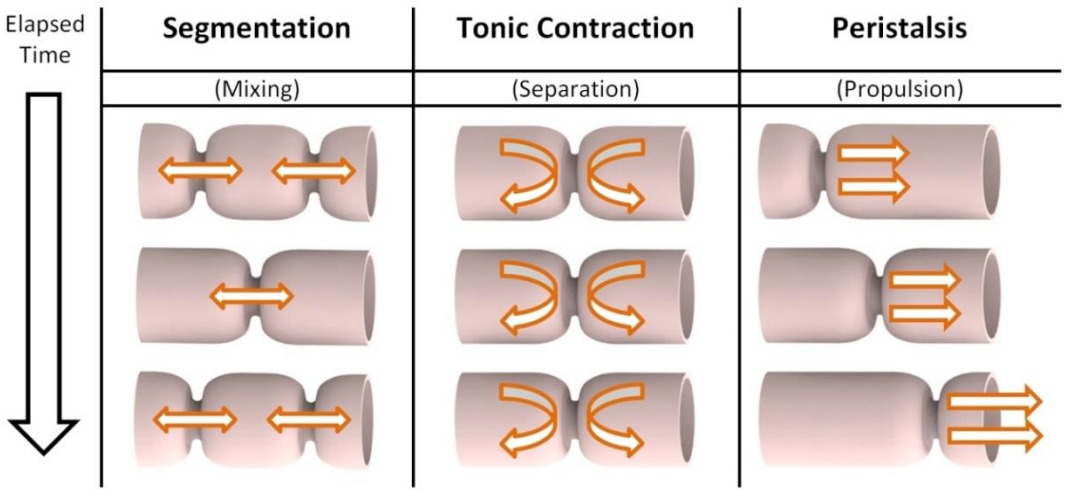

Fig. 3: Major types of biomechanical gut motility.

1990's and can be divided into two categories, static and dynamic [8]. Static *in vitro* models focus primarily on the chemical and absorptive processes that take place during digestion, but do not include any dynamic aspects such as the gastric emptying of small particles or changes in pH or secretion flows [9], nor do they recreate the biomechanical action of the *in vivo* GIT such as peristaltic motion or transit of materials [10].

Dynamic *in vitro* simulation models of the GIT attempt to recreate, integrate and control a varied range of parameters of the GIT digestive process, such as body temperature, gastric pH control, stomach mixing, gastric emptying, intestinal pH control, digestive secretions, intestinal tract motility, intestinal absorption and intestinal microbiota [8]. The highly complex and dynamic nature of the human digestive system presents significant challenges in the development of a simulated system that can suitably emulate this wide range of parameters.

Recent developments have shown an increased trend towards the use of biomimetic models and soft robotics for simulating the dynamic aspects of the gastrointestinal tract. Biomimicry is defined by the Oxford dictionary of English [11] as "*the design and production of materials, structures, and systems that are modelled on biological entities and processes*". The use of biomimetic modelling can add enhanced realism to simulations of the modelled system as many of the physical forms and processes are performed in a manner as close as possible to those of the biological system being studied. Soft robotics [12-14] is a new area of engineering that is increasingly being used as the preferred method of delivery for the dynamic behaviour of biomimetic models and offers great potential in simulating the entirely soft structures of an actual biological system in a bio-relevant manner.

1.2. Research problem

The current state of research, regarding dynamic *in vitro* modelling of the biomechanics of the gastric tract, involves the use of mechanical or robotic systems to mimic muscle contractions against a flexible membrane wall using hydraulic or pneumatic [15-23] actuation or mechanically driven [24-28] actuation systems. These actuation systems apply external forces against a flexible membrane wall to deform it within controlled, localised areas and recreate desired motility patterns. The externally applied forces typically require fixed or rigid backing materials to function properly, such as sealed pneumatic or hydraulic enclosures or a housing for mechanical rollers.

The use of soft robotics is increasing, particularly with models implementing pneumatic actuation systems for the mimicry of muscle constrictions. However, these systems require some form of rigid backing material to actuate the pneumatic pressure against the flexible wall, which limits the artificial muscle system from being entirely soft or flexible in form and suggests that a fully 'soft' biomimetic simulation of the GIT is still to be demonstrated. There is also a degree of separation between the muscle actuation system and the membrane wall which prevents the artificial muscles from flexing and moving with the tract wall as it deforms. This mechanical structure differs from that exhibited by biological systems where the muscles are embedded within the wall and are an integral part of it.

These constraints currently prevent *in vitro* models from replicating the entire range of actual physiological deformations that occur, producing only a limited range of deformation actions over a localised region. The ability of these models to simulate in a biomimetic manner the highly dynamic nature of the gastrointestinal tract wall is therefore reduced. These limitations need to be addressed to better understand the interactions between

individual muscle layers, and how they effectively contribute to the overall observed motility, breakdown and mixing of the gastrointestinal contents.

1.3. Aims

This thesis proposes a novel approach to mimicking the biomechanical characteristics and properties of the gastric tract wall and the modelling of its complex motility patterns via a controllable flexi-walled reactor. It proposes to address knowledge gaps in physiologically representative *in vitro* models for simulating human gastric tract biomechanical functioning. The aim of this research is to develop a bio-relevant physical simulation model of the biomechanics of the human gastric tract by mimicking the physical structure, function and characteristics of the interactive layers of tissue that form the tract wall. The goal of this research is the development of a physical flexi-walled reactor with peristaltic capability that can demonstrate applied mixing, grinding and transport action of liquids, slurries and semi-solid contents. Mimicry of the biomechanical activity of the biological gastric tract system could allow for more accurate assessment, both quantitatively and qualitatively, of the physical effects of the gastric tract wall on the mechanical processes of digestion.

1.4. Objectives

The aims of this research will be realised through the following three objectives:

Research Objective 1: Identify materials, methods, and techniques that can be used to develop a biomimetic physical model simulating gastric tract biomechanics.

i. Identify and determine, through appropriate reference to the literature, key biomechanical principles and processes involved in human gastrointestinal tract digestion.

ii. Identify artificial muscles, muscle simulation techniques, and methods of actuation that display similarities to the biological layers of gastrointestinal tract muscle that can be suitably fabricated using available means.

iii. Identify materials and properties of materials that display similarities to actual gastrointestinal tract tissue, or layers of tissue, and that can be suitably fabricated using available means.

iv. Develop a method of combining the artificial muscles and membranes for mimicry of the morphology and functioning of actual gastric tract wall layers.

v. Provide a means for simulating the biological mixing and transportation of a variety of liquid, semi-solid and solid food materials, and provide subsequent feedback of relevant simulation data.

Research Objective 2: Create a physical model of the biomimetic materials, methods, and simulation techniques with control and feedback mechanisms.

i. Build or fabricate artificial muscles, or unit constrictors, as identified in RO1, that can be embedded within or connected to a layer or layers of artificial tissue material.

ii. Create or fabricate membrane layers from candidate materials, or composite materials, as identified in RO1.

iii. Construct an anatomically relevant model of the gastric tract, or regions thereof, from the developed artificial muscle and membrane layers.

iv. Provide a means of control for the constrictions and expansions of the artificial muscles that allow for simulated demonstration of peristalsis, gastric emptying and other common biomechanical gastric processes as identified in RO1.

Research Objective 3: Evaluate the mechanical characteristics and material properties of the physical model and integrate them with the requirements of a biomimetic *in vitro* simulation model.

i. Measure the mechanical and material properties of the proposed artificial muscle and membrane layers through testing and measurement devices such as tensile and compression tests, strain gauges or stretch sensors, load cells and pressure sensors.

ii. Evaluate the mechanical properties and characteristics of the simulated gastric tract model(s) with the properties and characteristics obtained from *in vivo* and *ex vivo* data representing actual biological gastric tract tissue. Adjustments of the material and mechanical parameters of the physical model may be undertaken, as required, to align the physical model with the *in vitro* simulation model requirements.

1.5. Research questions

Research questions to be answered through biomimetic simulation of the gastric tract include the following:

Research Question 1: *What materials, methods, and techniques are suitable for developing a biomimetic physical model that simulates human gastric tract biomechanics?*

Research Question 2: *How can the methods, materials and techniques identified in RQ1 be used to create a biomimetic physical simulation model of the gastric tract with peristaltic capability, control and feedback mechanisms, and demonstration of mixing and transport?*

Research Question 3: *How do the mechanical characteristics, material properties and operational aspects of the physical model identified in RQ2 integrate with the requirements of a biomimetic model simulating biomechanical action of the human gastric tract?*

Much is already known about the human gastrointestinal tract that can assist in the development of an *in vitro* biomimetic simulation model. Several areas of research including the anatomical form of the GIT, motility initiation mechanisms, gastrointestinal motility patterns and characteristics of the tract wall tissue layers provide impetus and direction for this research.

Anatomical form

A basis for the required structural form and attachment constraints of the biomimetic model can be derived from 3D representations of actual morphological and anatomical form and positioning of the organs involved in the digestive system [29], and knowledge about their connection points to the body [30]. However, the representative shapes of the gastric organs obtained this way can vary between individuals and depend on factors such as the amount of contents present, the stage of the digestive process, the degree of development of the gastric musculature, the condition of the surrounding organs, looping of the small and large intestines, physique, sex and age [4]. This suggests that there may also be temporal changes in organ morphology that should be accounted for in the development of an *in vitro* model.

Motility initiation mechanisms

There is knowledge of the electrical and nervous inputs that drive or trigger GIT muscle contractions, how the visceral muscles are contracted and relaxed, the transference

mechanisms of the trigger signals across and between the muscle layer boundaries, and the chemical and mechanical feedback mechanisms that initiate the different motility patterns involved in the digestive process [1-4, 31, 32]. These drivers of biological motility suggest implementation of various feedback and control mechanisms that may be required for the *in vitro* simulation model.

Motility patterns

Knowledge of the different types and timings of motility patterns and associated trigger events during different stages of digestion [2, 7, 33-35] offer a basis for the programmable control of the simulated system. Deformation patterns of the *in vitro* model can therefore be based on actual observed deformation patterns and recorded timings of contractions and phasic deformations. This approach would align the mimicked deformations with *in vivo* observations and allow for more accurate assessment of the appropriate operation of the *in vitro* system.

Tissue layers

Experimental evidence of the structure, properties and characteristics of the tissue layers of the gastrointestinal tract wall suggest suitable target specifications for the material properties and characteristics of the simulated tract. This includes observations made on the similarities and differences between the GIT wall layers within the different organs and sub-regions of the organs [36-38]. However, questions remain on whether these specifications are attainable with currently available materials and technology and whether the actual observations are representative of the population.

In addition to the research questions presented in Section 1.5 there remain other questions that require consideration in response to the research objectives, such as how can an effective simulation model of the biomechanical action of the gastric tract accurately be evaluated? Limitations still exist in producing accurate physical modelling of the complex mechanical forces and the reproduction of complex biological motility patterns, such as gastric emptying and peristalsis [9], and there is limited consensus on the best methods to use for measuring these actions [1].

1.6. Significance of the research

The findings of this thesis, and the development of a biomimetic gastric tract simulator, provide close-to-reality simulation to advance several areas of knowledge in the domain of human digestion. Biomimetic simulation of the mechanical activity and material properties of the human gastric tract wall, coupled with consideration for the provision of chemical pathways, natural system bioactivity, and interactive feedback mechanisms, could provide significant *in vitro* systems for accurately evaluating the complex physiological morphology and biomechanical motility patterns of the human digestive tract.

Potential contributions from the development of a biomimetic gastric tract simulator include:

i. Improved physiological accuracy in simulating gut motility and the biomechanical digestive action of food and fluids during ingestion and digestion.
ii. More accurate means for quantitative analysis of gastric tract deformation characteristics and measurement of the forces and pressures involved in digestive processes.

iii. Provision of an alternative model to *in vivo* studies for studying the human gastric tract.

iv. Providing a comparison with biomechanical data obtained from *in silico* and virtual simulations.

v. Improved testing of the biomechanical breakdown effects on potential functional foods.

vi. Improved pharmaceutical testing of pill and drug transition throughout the gastric tract.

vii. Enhanced realism of gastric tract form and motility for surgical simulation and practice *e.g.*, endoscopic and surgical training.

viii. More realistic simulation of the gastric tract internal cavity for the design and development of smart pills and other gastric devices *e.g.*, stent and gastric balloon or band placements, identification of potential device migration problems.

ix. An increased potential for the development of innovative nature-inspired methods for moving and mixing of a wide variety of liquid, semi-solid and solid materials *e.g.*, slurry pumps and industrial processes mimicking the multi-stage digestive processes of the gastric tract.

There are various other aspects pertaining to *in vitro* modelling of the gastrointestinal tract that have been identified as requiring further attention. Gregersen [39] suggests little is known about tone and distensibility of the tract and its effects on content flow, and attributes this to a lack of applicable methods for obtaining and interpreting quantitative data. Biomimetic *in vitro* modelling of the gastric tract may provide a suitable testbed from which new and improved methods for the measurement of tone and distensibility can be extensively trialled and developed.

Cleary et al. [40] indicates that some of the challenges facing adequate modelling of stomach function include:

i. Characterising stomach geometry and mechanical / contractile properties and their variation between populations; and
ii. Simulating the compliance of stomach wall deformation with contractions. There is a perceived need for simulation models that can change the morphology of the stomach wall in a natural manner, whilst maintaining the same characteristics of the wall that are evident throughout all morphological forms of the stomach.

Singh, Ye, & Ferrua [41] suggest there exists a need for the development of more advanced models that can precisely simulate gastric motility and gastric emptying, while Drechsler & Ferrua [42] add a requirement for *in vitro* modelling that provides information on the shear stresses that develop *in vivo*. Both these requests highlight a need for simulation models that more closely mimic the actual biomechanical functioning of the gastrointestinal tract.

Furthermore, Gregersen & Christensen [1] propose that improved mechanical analysis of the operation of the gastrointestinal tract can advance the knowledge of:

i. The elastic and viscoelastic, or passive, properties of the wall.
ii. Wall responses to mechanoreceptor stimulation.
iii. The peristaltic reflexes.
iv. The mechanics of bolus transport.
v. The origin of gastrointestinal perceptions or sensations.
vi. The nature and origin of tone in smooth muscle.
vii. The development and growth of the gut.
viii. Remodelling of the geometry and biomechanical properties in the gut.

ix. The origin of mechanical dysfunction related gastrointestinal diseases.

x. The development of new clinical tests for mechanical dysfunction in the gut.

1.7. Scope and limitations

In scope

This study covers the biomimetic *in vitro* simulation modelling of the biomechanics of the human gastric tract wall. The scope of this study as laid out in this section includes the anatomical regions of interest, forms of biomechanical activity and control to be demonstrated, feedback and sensing mechanisms to be included, provisions for tract content sample acquisition and provisions for chemical pathways.

The anatomical regions of the gastric tract that are within scope of this study are the distal region of the oesophagus, the stomach and the proximal region of the duodenum (Fig. 4). This relates to a section of the gastric tract that is approximately 250 mm in height for an average human adult. It also includes the cardiac, or lower-oesophageal sphincter, and pyloric sphincter that designate the relative boundaries between these distinct sections of the tract.

Several forms of biomechanical activity fall within the scope of this study. These include the applied demonstration of peristaltic wave deformations that take place in the oesophagus, stomach and the proximal region of the duodenum, tonic contraction and expansion of muscles within the fundus region of the stomach and standing wave muscle activity within the duodenum. Also included within scope are the tonic contractions or membrane closure actions carried out by the cardiac or lower oesophageal sphincter, and the pyloric sphincter where gastric emptying of the stomach contents takes place.

Several sensing and feedback mechanisms required for the monitoring of mechanical, chemical, and thermal activity fall within scope of this study. Quantitative feedback is required for ascertaining the appropriate level of contraction force and amplitude of contraction ratios being applied to the artificial membrane wall of the tract. Sensing of the amount of stretch occurring over the stomach membrane wall, particularly in the fundus region, is useful for controlling contraction amplitudes and adjusting stomach volume for the accommodation of food. Other feedback and sensing mechanisms may involve

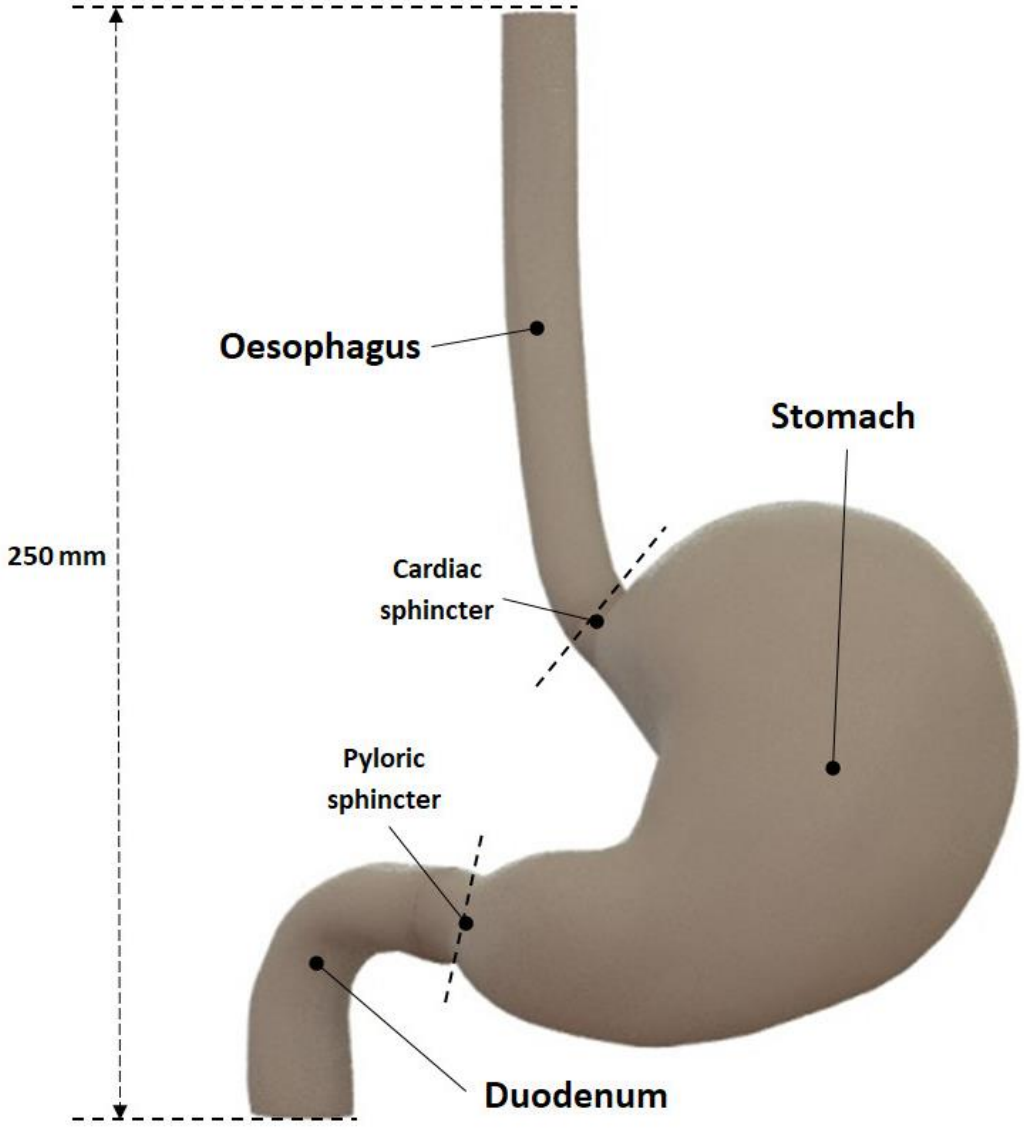

Fig. 4: Anatomical sections of the human gastric tract within scope of this study.

monitoring and controlling the reactor environmental and internal contents temperature and monitoring the levels of pH of the stomach contents.

For the biomimetic *in vitro* gastric tract simulator to be useful as a tool in researching the digestion of food materials within the gastric tract, the scope of this study also includes provision for accessing the contents of the stomach at various stages of digestion. This includes the collection of materials after digestive actions have taken place and the materials have been emptied from the stomach reactor. It also includes any means that allow for the periodic sampling of, or direct access to, the digested materials that can be found at specific locations within the stomach itself, including the fundus, corpus or antrum regions.

The provision of chemical pathways that can pass fluidic chemicals into the internal cavity of the *in vitro* reactor is within scope of this study. The introduction of gastric juices and fluids to the contents within the stomach is an essential aspect of human digestion in the breakdown of food structures. Simulated mucosal and saliva secretions may also prove useful in providing some form of lubricant to assist in the moving of food materials throughout the artificial tract. This includes investigation of suitable methods for the controlled passage of fluidic materials from an external source, through the gastric wall membrane material or down the oesophageal tract, and into the inner cavity of the stomach.

Outside of scope

This study does not include any complete tests or trials involving the digestion of foods or food materials. Only the means for actuating and controlling the muscles and contraction deformations have been included in this study. It is beyond the scope of this study to consider, demonstrate, and propose as to when and to what amplitude specific muscle actuations, or sequences of gastric tract wall deformations, are likely to occur during various

simulated digestion phases. This includes the development of programmed code providing specified timed sequences for controlling the operational actuation of the artificial muscles.

The timing and occurrence of specific motility patterns can be highly variable and dependent on many factors other than the basic feedback mechanisms that are considered within the scope of this study. The operation and inclusion of biological feedback mechanisms initiating from the endocrine, gastrointestinal, and nervous systems are therefore not included in the *in vitro* model. These feedback mechanisms control the type and timing of motility actions during digestion. They are not included because they determine the generation of contractile patterns, rather than the actuation of the muscles themselves.

Also outside of scope are the chemo-physical aspects of digestion simulation such as the breakdown of food materials by gastric juices and acids, mastication actions in the mouth and chewing of a food bolus, and biomechanical and biochemical aspects of the intestinal tract beyond the pyloric sphincter. Simulation of the intestinal tract biomechanics is considered beyond scope of this study due to the length of this portion of the tract, approximately 6 metres, and the functional absorbency of nutrients and water that occur within the small and large intestines.

Limitations

This study is limited to present understanding of the biomechanical activity involved in the human gastric tract bio-system. Visual observation of the actual deformation patterns occurring in human stomachs, and the gastrointestinal tract in general, is limited to the availability of medical scans, endoscopy or surgical video recordings and still images. While many aspects of the biomechanical activity of the human gastric tract and the structure and

functions of the tract wall have been extensively studied, the complexity of the gastric tract biological system and its interactions with other biological systems in the human body is not yet fully understood. This is particularly so regarding the complexity of the neurological interactivity and chemical and hormonal feedback mechanisms regulating biomechanical activity within the biological system. Biological variances found between different populations and individuals also limit the ability of a singular *in vitro* model of the gastric tract to potentially represent the full range of physical variations that occur.

The use of synthetic materials for mimicking biological matter limits the complete range of physical and chemical properties and characteristics of the resulting *in vitro* simulation model. Self-healing and organic re-growth of complex cellular structures is one aspect of biological organisms that is difficult, if not impossible, to fully reproduce with synthetic materials. This is compounded when additional requirements of the *in vitro* simulation model may include accessing internal regions of the artificial reactor for examination of its content, cleaning of the internals of the reactor model after use, and general ease-of-access to the artificial tract without requiring some form of surgical removal or dissection of the synthetic membrane.

Dissection of an artificial stomach membrane for the analysis of its contents mid-way through the digestive process is not recommended. This is because cutting of the synthetic membrane typically results in an irreparable membrane or irreversible alteration to the biomechanical deformation characteristics of the membrane surface. It may be considered here that the closer an *in vitro* system comes to mimicking that of an *in vivo* biological system, the closer it comes to inheriting many of the challenges involved with study of the *in vivo* system.

Delimitations

Methods and materials included in the development of the *in vitro* simulation model should be readily available, low cost and easy to implement or fabricate. This delimitation improves the potential for the *in vitro* simulation model to be replicated easily and at low cost. The ability to reproduce an *in vitro* gastric tract simulation model easily and affordably would promote a wider community of researchers to contribute towards determining dynamic *in vitro* model testing specifications, assist in the ongoing development of *in vitro* simulation model capabilities, and share and compare results from the testing of different food materials. The *in vitro* simulation model reactor materials have also been derived from a variety of non-ferritic materials so that magnetic particle tracing methods can be used for mapping translational and mixing effects on the internal contents of the reactor.

1.8. Layout of the thesis

In **Chapter One**, the context of the study has been introduced. The research objectives and questions have been identified, and the value of the research presented. The limitations and scope of the study have also been discussed.

Chapter Two presents a review of the literature exploring *in vitro* models that have been developed for simulating various physical or chemical digestion aspects of the human gastrointestinal tract.

Chapter Three provides a more detailed context of the biological tract membrane and describes two innovative approaches for the development of an artificial membrane for mimicking the stomach wall including a composite elastic membrane and poroelastic silicone sponge shells.

Chapter Four describes the muscle layers of the biological system and the development and implementation of artificial muscles including the use of unit constrictors, braided structures that deform in a predictable peristaltic manner, tendons and Bowden cables, and techniques for achieving membrane and muscle interconnectivity.

Chapter Five introduces methods for providing actuation of the artificial muscles for an artificial stomach and programmable simulation of many forms of deformation that occur in the biological system. Included are mechanical actuation methods for creating multiple constrictions from a single rotating mechanism, and a pulley-driven actuation system for driving individual unit constrictor contractions.

Chapter Six introduces control and feedback methods for an artificial stomach including membrane stretch and deformation, muscle contraction, pressure sensing, and the potential for incorporating simulation and visualisation methods within the feedback process.

Chapter Seven presents an advanced biomimetic gastric tract simulator, derived from the conclusions of Sections 3-7, for the development of a controlled "morphing" stomach physical model that simulates the contractive and expansive actions of the muscle layers found within the stomach wall, as well as considered methods for containment and temperature regulation of the modelled reactor.

Chapter Eight closes with conclusions of the thesis and answers the research questions posed by the study.

Chapter Two

Literature Review

Chapter 2 – Literature Review

This section presents a review of the literature exploring *in vitro* - performed outside the living body and in an artificial environment - models that have been developed for simulating various physical or chemical aspects of the human gastrointestinal tract (GIT). An emphasis is placed on dynamic *in vitro* models that have incorporated a stomach or upper gastric tract component, with a particular focus on the approaches used in simulating GIT biomechanical and biochemical actions. Some background to the biological characteristics of the human GIT is introduced, followed by a review of stomach and gastrointestinal *in vitro* models and other relevant methods and models used for simulating GIT structure and behaviour. A brief overview of instruments used in measurement of biomechanical activity and material properties of real and simulated tracts is also discussed.

2.1 Background - biological aspects of the gastrointestinal tract

The dynamic mechanical nature of the gastrointestinal tract wall is dependent on the functional interaction between several distinct layers of tissue. The hollow organs of the GIT are comprised of a surrounding wall of external smooth or visceral muscle and inner mucosal tissue [1]. The outermost layer of the tract wall is called the serosa, a protective skin formed of densely packed collagen and elastin fibres that covers all other layers and dictates the overall shape of the shell. There are two layers of muscle tissue evident throughout the length of the gastrointestinal tract. These muscle layers are oriented in the circumferential and longitudinal directions. Exceptions to this are the stomach, that has an additional oblique layer of muscle extending over the fundus [43], and the oesophagus, which has a layer of skeletal muscle that begins from the pharynx and blends into the smooth muscle halfway along its length [1]. The soft and flexible inner mucosal tissue is comprised of the

submucosa and the plexus, the muscularis mucosa or mucosal muscle, and mucosa which have an epithelial surface layer that comes into direct contact with internal cavity contents. The mucosal layers vary in function and form along the tract, providing chemical transfer pathways for fluids for the release of gastric juices into the stomach cavity and bile into the duodenum, nutrient absorption via the small intestine and water absorption from the colon.

Akhmadeev and Miftahof [44] characterise the soft tissue of the stomach wall as a "*transversely anisotropic nonhomogenous viscoelastic biocomposite that undergoes finite strains*." This is a description of the tract wall in general as the gastrointestinal compartments all share common layers of biomaterial between them. The GIT has evolved from a single tubular form during embryonic morphogenesis to provide a range of functional characteristics dependent on the organ position, location and role within the human digestive system [1]. The mechanical forces from contractive and expansive action of the outer muscle layers, acting on the material properties of the inner mucosal layers, are considered the single most important factor contributing to the deformation, motility and mixing characteristics of the tract [45]. The mucosal and sub-mucosal layers' contribution to the biomechanical characteristics of the tract is considered to be negligible [4].

Connecting these layers together is a fibrous extracellular matrix (ECM) composed of proteoglycans, glycol-proteins, and fibres such as collagen and elastin [4]. The ECM provides the elasticity and structural strength of the tract wall within a biochemically stable microenvironment for the tissue. Elastin is composed of a flexible cross-linked polypeptide and has a linear stress-strain relationship up to approximately 200% maximum strain. However, the collagen fibres become stiff when under load and exhibit highly non-linear stress-strain characteristics. The overall strength of the GIT wall at various locations along

the tract is strongly correlated with the content of collagen-elastin that exists at these locations [4].

The structure of the muscle wall layers varies in thickness and mechanical properties throughout the length of the GIT. Mechanical properties such as stiffness, elongation of the material and tensile strength, are significantly affected by wall layer thicknesses and levels of collagen and elastin present within the inter-connective tissue and the mucosal layers [45]. Wall layer thickness varies depending on the specific role at a particular location within an organ; for instance, muscle layer thickness tends to be increased at sphincters and where mechanical break-down of material is likely to occur, such as in the antrum and pylorus of the stomach. It is less thick where absorption of broken-down digesta or chyme is the prominent mechanism, such as in the small intestine.

There are characteristic forms of folding and buckling of the biological tract wall that could potentially be mimicked. These include intestinal gut looping [46, 47] and the folding of the luminal wall surface in the manner of ridges such as the formation of intestinal villi [47-49] and internal rugae of the stomach. The intestine, when separated from the mesentery tissue, takes on the form of a long un-looped tubular structure [46], but when attached to the mesentery it forms characteristic looping. The looping of the tract provides efficient containment of the entire length of the intestine, typically 3-5 metres in total, within the abdominal cavity. The mesentery connections are flexible and elastic to enable the looped intestine to continue to effectively transport and mix its contents within the space it occupies.

Boundary constraints imposed on the inner mucosal layers during tissue cell growth and expansion are suggested to create internal folding structures on the tract wall inner surface,

including the formation of intestinal villi in the small intestines and the rugae of the stomach [47-49]. These constraints are caused by the compressive action of the muscle layers of the tract wall. The circular and longitudinal layers of muscle create multidirectional compressive stress on the inner mucosal tissue during its formation, and in so doing the mucosal layer forms a patterned sequence of folding and buckling over the luminal surface. Initially, action from the circular muscle layer creates a set of waved ridges on the mucosal surface which is directed along the axis of the tract. The longitudinal muscles then create a compressive constraint perpendicular to the circular muscle contraction which causes the ridges to buckle and form a zig-zag pattern over the inner surface. However, the patterning of folds within the stomach wall is different. The complex, multidirectional and random folding patterns of the stomach rugae may be additionally influenced by the presence of the oblique muscle layer in the stomach wall.

Nelson [47] proposes that the attachment of membrane layers exhibiting unequal growth rates cause the buckling and folding of the inner surface of the gastrointestinal tract, and that these unequal growth rates can be simulated by attaching synthetic elastic materials together that exhibit different amounts of stretch. The stress imbalance between the two unequally stretched materials can create buckling and folding characteristics that are like conditions observed within the biological tract. However, there may still be considerable residual stress remaining within the composite material even though no external load is being applied.

A zero-stress state occurs when a material has been relieved of residual stresses and has reached a no-load state *i.e.*, when all external and internal forces have been removed. Residual strain is the strain difference between the zero-stress state and the no-load state of

a material [45]. Gregersen and Kassab [45] identified the importance of residual strain in relieving stress concentrations developed in the mucosal layer of the gastrointestinal tract during bolus transport, and that residual stress may also serve as a growth regulating factor on the tissue layers. A circular ring section of a tubular tract can be cut so that the tissue is allowed to uncurl, and the opening angle of the resulting sector can be used to quantify the amount of residual stress that is present [39, 45]. This method for determining the zero-stress state of a tubular section of tract may also be used to determine whether residual stresses exist within sections of fabricated tubular artificial membranes.

2.2 Stomach and gastrointestinal tract models

In vitro models are used to simulate the digestive processes of the gastrointestinal tract. Several reviews of the state of *in vitro* gastrointestinal models have been published over the years [8, 9, 50-56] with correlation of many of these models against data obtained from *in vivo* measurements. There are two types of *in vitro* models used in simulating the GI and digestive processes, static models and dynamic models. A recent research trend has also emerged on the use of biomimetic and soft robotic GI simulation models.

2.2.1 Static *in vitro* models

Static *in vitro* models focus primarily on the chemical and absorptive processes that take place during digestion. They consist of a single or series of separate containers that include the addition of chemicals to food materials such as gastric acids and enzymes recreating the chemical digestive break-down of food and, in some cases, emulating the extraction of nutrients within the GIT [57, 58]. Static simulators may also incorporate some form of mechanical mixing of the partially digested food to approximate mixing processes, such as a

"head over heels" rotor mixing [58], or the pre-mixing or blending of samples before adding them to the simulation.

The static model approach has widespread use because it is cheaper and less time consuming than dynamic simulation models and provides the potential for multiple simulations to be undertaken simultaneously which can be useful for the screening of different foods [55]. Static models also show good repeatability and reproducibility of results, and the experimental conditions and procedures involved have been incorporated into the INFOGEST international consensus and standardisation on static digestive simulations [59-61]. At present, there is no similar consensus for the standardisation of dynamic *in vitro* models.

A major limitation of static models is that they do not include any dynamic aspects of digestion, such as the gastric emptying of small particles or changes in pH or secretion flows [9], nor do they recreate the kinetic aspects involved in the biomechanical action of the *in vivo* GIT such as peristaltic motion or transit of materials [10]. Static *in vitro* GIT models are limited in usefulness to the study of simple meals or single substrates that can be tested under specific conditions [59].

2.2.2 Dynamic *in vitro* models

Dynamic *in vitro* simulation models attempt to recreate, integrate and control a varied range of parameters of the GIT digestive process, such as body temperature, gastric pH control, stomach mixing, gastric emptying, intestinal pH control, digestive secretions, intestinal tract motility, intestinal absorption and intestinal microbiota [8]. Table 1 and Table 2 display a chronological listing of some of the developed dynamic gastric models, as well as their

related mechanical aspects and operational characteristics. Only models that have incorporated a stomach component have been included in the tables.

While dynamic models may provide good simulation of *in vivo* biochemical digestive processes and attempt to simulate GIT contraction and mixing, they do not closely replicate actual physiological forces and pressures underlying organ wall deformation as they appear *in vivo* or are limited to replicating the effects only over a specific region. The mechanical properties and morphology of an actual GI tract widely varies over its entirety [62] and little is known about how the physical deformation of the tract wall contributes to GIT motility and mixing processes. Aspects of the developed models for simulating GIT wall behaviour are outlined in the following section, including: the type of intended application, incorporated components, reactor materials, component orientation, gastric secretion, mixing and emptying, transfer of contents, feedback and control, and biomimicry.

Table 1: Chronological listing of dynamic *in vitro* models reviewed from the literature.

Year	Name	Full Name	Reference
1992	TIM-1	The TNO Gastrointestinal Model	[52] Verhoeckx, K., Cotter, P., López-Expósito, I., et al. [63] Minekus, M., Marteau, P., Havenaar, R., & Veld, J.
1993	SHIME	Simulated Human Intestinal Microbial Ecosystem	[64] Molly, K., Woestyne, M. V., & Verstraete, W.
2008	DGM	Dynamic Gastric Model	[65] Vardakou, M., Mercuri, A., Barker, S. A., Craig, D. Q., Faulks, R. M., & Wickham, M. S. [66] Wickham, M. J. S., Faulks, R. M., Mann, J., & Mandalari, G.
2010	HGS	Human Gastric Simulator	[67] Kong, F., & Singh, R. P. [68] Phinney, D. M., & Singh, R. P.
2011	Stomach sim	Stomach simulator	[69] Condino, S., Harada, K., Pak, N. N., Piccigallo, M., Menciassi, A., & Dario, P.
2014	c-GDS	Continuous-type Gastric Digestion Simulator	[70] Kozu, H., Kobayashi, I., Nakajima, M., et al. [71] Kozu, H., Nakata, Y., Nakajima, M., et al.
	DIDGI	Dynamic Digester Gastro-intestinal	[72] Ménard, O., Picque, D., & Dupont, D.
2015	SIMGI	Dynamic SIMulator of the GastroIntestinal tract	[73] Barroso, E., Cueva, C., Peláez, C., Martínez-Cuesta, M. C., & Requena, T. [74] Cueva, C., Jiménez-Girón, A., Muñoz-González, I., et al.
	ESIN	Engineered Stomach and small INtestine	[75] Guerra, A., Denis, S., le Goff, O., et al.
	RD-IV-	Rope-Driven *In Vitro* Human Stomach Model	[76] Chen, L., Xu, Y., Fan, T., et al.
2016	TIMagc	TIM + advanced gastric compartment	[52] Verhoeckx, K., Cotter, P., López-Expósito, I., et al. [77] Bellmann, S., Lelieveld, J., Gorissen, T., Minekus, M., & Havenaar, R.
	DGSM	Dynamic Gastric Simulating Model	[78] Do, D. H. T., Kong, F., Penet, C., Winetzky, D., & Gregory, K.
	IMGS	*In vitro* Mechanical Gastric System	[79] Barros, L., Retamal, C., Torres, H., Zúñiga, R. N., & Troncoso, E.
2018	DHS-IV	Dynamic *In Vitro* Human Stomach System	[24] Peng, Z., Wu, P., Wang, J., et al. [25] Wang, J., Wu, P., Liu, M., et al.
	i HGS	Improved Human Gastric Simulator	[26] Keppler, S., O'Meara, S., Bakalis, S., Fryer, P., & Bornhorst, G.
2019	AGS	Advanced Gastric Simulator	[27] Hribar, M., Trontelj, J., Berglez, S., et al.
	AGDS	Artificial Gastric Digestive System	[28] Liu, W., Fu, D., Zhang, X., Chai, J., Tian, S., & Han, J.
	GSM	Gastric Simulation Model	[15] Li, Y., Fortner, L., & Kong, F.
	BGR		[23] Li, Z.-t., Zhu, L., Zhang, W.-l., Zhan, X.-b., & Gao, M.-j.
	IV-DGS	*In Vitro* Distal Gastric Simulator	[16] Donis-Rabanales, L. F., Escalona-Ortiz, M., Ruiz-Huerta, L., de la Fuente, E. B., Caballero-Ruiz, A., & Ascanio-Gasca, G. [17] Donis-Rabanales, F., López-Ruiz, T., Ruiz-Huerta, L., Ascanio, G., Brito-de la Fuente, E., & Caballero-Ruiz, A.
2020	SoGut	Soft Robotic Gastric Simulator	[18] Dang, Y., Liu, Y., Hashem, R., et al. [80] Dang, Y. [19] Dang, Y., Stommel, M., Cheng, L. K., & Xu, W. [20] Dang, Y., Cheng, L. K., Stommel, M., & Xu, W. [21] Hashem, R., Xu, W., Stommel, M., & Cheng, L. K. [22] Hashem, R., Xu, W., Stommel, M., & Cheng, L.

Table 2: Characteristics of dynamic *in vitro* models.

Model Name	Year	Component volume: (ml)								Intended application			Reactor material				Component orientation	
		oesophagus	stomach	duodenum	jejunum	ileum	ascending colon	transverse colon	descending colon	food digestion	pharmaceutical	medical device testing	glass	polymer	latex	silicone	fixed	variable
TIM-1 [52, 63]	1992		300	55	130	130				■			■		■		■	
SHIME [64]	1993		300	300		300	1000	1600	1200	■			■				■	
DGM [65, 66]	2008		800							■	■			■	■		■	
HGS [67, 68]	2010		5700							■					■		■	
stomach simulator [69]	2011		1400									■				■		■
c-GDS [70, 71]	2014		550							■				■	■		■	
DIDGI [72]			200	x	x	x				■			■				■	
SIMGI [73, 74]	2015		x	x			x			■				■		■	■	
ESIN [75]		-	500	100	170	170					■		■				■	
RD-IV-HSM [76]			500							■						■	■	
TIMagc [52, 77]	2016		300	55	130	130				■			■		■		■	
DGSM [78]			300							■				■			■	
IMGS [79]			900							■					■		■	
DHS-IV [24, 25]	2018	x	650	x						■						■		■
improved HGS [26]			5000							■					■		■	
AGS [27]	2019		250								■					■	■	
AGDS [28]			1700							■						■	■	
GSM [15]			600							■					■		■	
BGR [23]			500	x	x	x	x	x	x	■	■		■			■	■	
IV-DGS [16, 17]			256							■	■			■		■	■	
SoGut [18-22, 80]	2020		1000							■	■	■				■		■

Continues next page

Model Name	Year	Controlled gastric additions / secretions				Gastric emptying / sieving						Secretion introduction method						Motility mechanism - gastric mixing & moving								
		rate (ml / min)	saliva	gastric fluid	HCl	valve	Teflon membrane	mesh net	pump	elastic annulus	contraction	syringe / peristaltic pump	perforated tube	dispensed along wall	distributed tubing	added at inlet to stomach	diaphragm pump	hydraulic pressure (flexible wall)	magnetic stirring	hydraulic pressure (piston & barrel)	mechanical rollers	rope driven	impellor stirring	pneumatic pressure (flexible wall)	pistons	iris diaphragm
TIM-1 [52, 63]	1992	1	■	■	■	■						■	■					■								
SHIME [64]	1993		■	■	■				■			■							■							
DGM [65, 66]	2008		■	■	■					■		■		■						■						
HGS [67, 68]	2010	0.03-8.2	■	■	■			■				■			■						■					
stomach simulator [69]	2011																					■				
c-GDS [70, 71]	2014							■	■							■	■				■					
DIDGI [72]			■	■	■		■					■											■			
SIMGI [73, 74]	2015		■	■	■							■				■		■								
ESIN [75]			■	■	■				■			■								■						
RD-IV-HSM [76]												■			■							■				
TIMagc [52, 77]	2016		■	■	■	■						■						■								
DGSM [78]		1	■	■	■							■				■				■						
IMGS [79]																■								■		
DHS-IV [24, 25]	2018	0-10		■	■	■						■									■					
improved HGS [26]									■							■					■					
AGS [27]	2019					■						■				■									■	
AGDS [28]									■							■					■					
GSM [15]		2-3		■	■						■	■			■									■		
BGR [23]												■						■								
IV-DGS [16, 17]		0.5-1.0		■	■	■						■				■		■								
SoGut [18-22, 80]	2020										■					■								■		

Continues next page

Model Name	Year	Motility mechanism - intestinal transit				Wall membrane thickness (mm)	Feedback				Control - pH		Control - temperature				Bioaccessibility		Intestinal microbiota
		hydraulic pressure (flexible wall)	volume flow	peristaltic valve pump	pneumatic pressure (flexible wall)	stomach	Max. intraluminal pressure - (mm Hg)	Max. contraction force - (N)	pH	temperature	gastric pH	intestinal pH	water jacket	lamp / light	heater	chamber	dialysis system	filtration system	
TIM-1 [52, 63]	1992																		
SHIME [64]	1993																		
DGM [65, 66]	2008	n/a	n/a	n/a	n/a							n/a					n/a	n/a	n/a
HGS [67, 68]	2010	n/a	n/a	n/a	n/a			3.4				n/a					n/a	n/a	n/a
stomach simulator [69]	2011	n/a	n/a	n/a	n/a												n/a	n/a	n/a
c-GDS [70, 71]	2014	n/a	n/a	n/a	n/a												n/a	n/a	n/a
DIDGI [72]																			
SIMGI [73, 74]	2015																		
ESIN [75]																			
RD-IV-HSM [76]		n/a	n/a	n/a	n/a	6											n/a	n/a	n/a
TIMagc [52, 77]	2016																		
DGSM [78]		n/a	n/a	n/a	n/a												n/a	n/a	n/a
IMGS [79]		n/a	n/a	n/a	n/a	1		1.89									n/a	n/a	n/a
DHS-IV [24, 25]	2018	n/a	n/a	n/a	n/a	5-7											n/a	n/a	n/a
improved HGS [26]		n/a	n/a	n/a	n/a												n/a	n/a	n/a
AGS [27]	2019	n/a	n/a	n/a	n/a												n/a	n/a	n/a
AGDS [28]		n/a	n/a	n/a	n/a		27	2.67									n/a	n/a	n/a
GSM [15]		n/a	n/a	n/a	n/a	2	70										n/a	n/a	n/a
BGR [23]							20-220	0.72											
IV-DGS [16, 17]		n/a	n/a	n/a	n/a		200										n/a	n/a	n/a
SoGut [18-22, 80]	2020	n/a	n/a	n/a	n/a			1									n/a	n/a	n/a

2.2.2.1 Components and component orientation

Single or multiple components

Some of the dynamic models may be designed around a single component or include multiple components of the gastrointestinal tract, such as the oesophagus, stomach, small intestine (duodenum, jejunum and ileum) and colon (ascending, transverse and descending). Multiple components are restricted to models that use a rigid containment compartment, such as glass, with some provision for basic transit of the contents between them (TIM-1 [52, 63], SHIME [64], DIDGI [72], SIMGI [73], ESIN [75], TIMagc [52, 77], BGR [23]). The transit and mixing mechanisms involved with these models are, to a large extent, typically lacking biomimetic accuracy, and the shape or form of the compartments is un-representative of the true form and flexibility of the actual GIT components.

With reference to Table 2, models representing a singular component such as the stomach tend to introduce more advanced biomimetic mechanisms within their designs (DGM [65, 66], HGS [67, 68], stomach simulator [69], c-GDS [70, 71], RD-IV-HSM [76], DGSM [78], IMGS [79], improved HGS [26], AGS [27], AGDS [28], GSM [15], distal gastric simulator [16], and SoGut [18-22, 80]). However, these mechanisms may be useful only for bio-mimicry of a single component or localised action, such as antral grinding, and may not be suitable in replicating the bio-mechanical actuation of other gastrointestinal components or range of motility actions. This may be a reason dynamic models exhibiting advanced bio-mechanical action have not yet extended into replicating the full gastrointestinal tract. Another reason may be that the materials and mechanisms used may be too costly or too complex to implement over a wider range of gastrointestinal components.

Component orientation

One of the most overlooked aspects to the design of the dynamic models is an ability to change the orientation of the model to reflect a change of body posture or position. Most models have a fixed orientation to the components involved, apart from DHS-IV [24, 25] that can be rotated 90° about a single axis only [24, 25]. The components cannot be rotated, flexed or varied in any direction other than the one they are originally fixed to. These models therefore do not attempt to mimic the wide variations in posture that the human body may assume during the hours-long process of digestion. A change in posture alters the GIT component orientation and has potential to influence changes in internal pressure of the components. Changes in pressure arising from alteration in posture are particularly evident in the stomach [81] and can be because of gravity, as well as from pressure from the surrounding organs and tissues.

A major limitation of a model's capability to provide variable orientation to the modelled components may relate to the types of mechanisms, materials and design that are used for containing and deforming the component membrane wall. Heavy, large, rigid and inflexible materials are too difficult to alter in orientation, particularly if they are attached to or require to be positioned relative to a static wall or framework. If a containment vessel cannot be fully enclosed or sealed, such as through the actuation of artificial sphincters or valves, then its contents could also potentially fall out if it is rotated. Applied membrane deformation mechanisms *i.e.*, mechanisms that apply forces directly to the membrane wall, will need to be rotated along with the membrane shell, and if they are bulky in design then this complicates achievement of a re-orientation of the compartment.

Reducing the complexity of actuation mechanisms for GIT motility to be as light, compact, and flexible as possible would help improve a model's potential to re-orient its component's position. From a biomimicry perspective this would mean reducing the footprint of the actuation devices to be as close as possible to that of the actual membrane being mimicked, containing the deformation actuation mechanisms within the membrane itself. Ideally this means fabricating artificial muscles that can be contained entirely within the GIT wall membrane, with the same orientation and contractibility that the biological membrane muscle layers exhibit while also displaying similar flexibility.

The directional orientation of the muscle layers in various regions of the GIT, such as the stomach muscle orientations depicted in Fig. 5, suggest they approximate a crossover grid-like patterned formation when layered upon each other. Pseudo-muscle unit constrictors may be aligned along these directional surface lines within an artificial muscle membrane layer. Subsequent manipulation, such as contraction and relaxation of the unit constrictors, could then create deformation patterns and promote a morphing of the overall shape of the organ into various forms. Similar morphological transformations of organic forms have previously been described by D'Arcy Thompson in "On Growth and Form" [82]. Thompson's work has provided a theoretical basis for explaining the formation of looping in the gut [46], the buckling and wrinkling of the internal GIT wall from mechanical instabilities between epithelial tissues and their surroundings [47, 83], and may also provide insight for prediction of the morphological deformation of the GIT wall in general.

A structured, orientated patterning of the muscle layers *i.e.*, along the lines as shown in Fig. 5, provides a basis from which controlled morphing of the entire length of the GIT wall could be achieved. In this way, different stomach shapes and organ morphology could be

programmed into a simulation through independent constriction and relaxation of the artificial muscle lines. At the same time, reproducing the anatomic orientation of the muscle layers may provide improved mimicry of the actual longitudinal and circumferential constriction characteristics that produce the motility patterns of the natural system.

2.2.2.2 Reactor materials

The most used materials in the fabrication of gastric reactors *i.e.*, the vessel within which the digestive actions take place, include glass, acrylic, PVC, ABS, latex or silicone rubber (PDMS). These materials are chosen because of their physical characteristics including resistance to chemical degradation, transparency, flexibility, elasticity and the ability to form them in a suitable manner for containment. However, not all characteristics are usually obtainable within any one type of material, so combinations of these materials are commonly found within the models reviewed.

The SHIME [64] and DIDGI [72] models use a purely glass containment for their

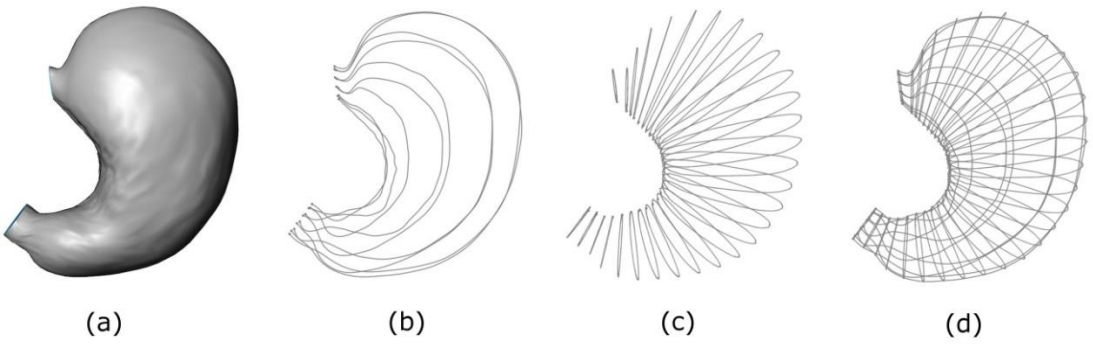

Fig. 5: (a) 3D CAD model of a human stomach derived from magnetic resonance imaging (MRI) scans. (b, c & d) Surface lines depicting approximated longitudinal and circumferential muscle orientations. The oblique layer is not shown.
(This work includes rendered derivatives of BodyParts3D, © The Database Center for Life Science licensed under CC Attribution-Share Alike 2.1 Japan:
https://dbarchive.biosciencedbc.jp/en/bodyparts3d/lic.html)

components but do not involve any flexible membrane. The DGSM [78] is similar but uses acrylic instead of glass. Other models (TIM-1 [52, 63], DGM [65, 66], c-GDS [70, 71], SIMGI [73], TIMagc [52, 77], BGR [23]) use a flexible latex or silicone membrane for the reactor wall that is located within a solid *i.e.*, glass or rigid plastic, containment vessel. Component forms are therefore limited to basic shapes such as beakers, cylinders, cones or simple curved sections. Only a few of the models reviewed have been designed with a moulded gastric reactor that takes on a recognisable form resembling that of an actual stomach (IMGS [79], the stomach simulator [69], RD-IV-HSM [76], DHS-IV [24, 25], AGDS [28], GSM [15], the distal gastric simulator [16], SoGut [18-22, 80]). In all instances these designs followed a 'J-shaped' stomach form. AGS [27], HGS [67, 68] and improved HGS [26] use a flexible J-shaped bag or membrane to replicate the stomach shape, but these do not exhibit as close a resemblance to an actual stomach as do the models using a moulded stomach form. The addition of rigid materials and mechanisms used in the design of many of the models prevent them from simulating a form that closely mimics the dynamic morphological capabilities of an actual stomach.

The use of purely rigid materials for reactor containment cannot therefore realistically be considered as entirely suitable for the biomimicry of the biomechanical and material properties of biological tissue. The biological gastrointestinal tract is confined within the abdominal cavity and is surrounded by various organs including the liver, pancreas, spleen, kidney, the diaphragm of the lungs, fatty tissue, skeletal muscles, and inter-connective tissues such as the mesentery. From a biomimicry point of view, a 'soft' approach to confinement is preferred over the use of inflexible or rigid materials.

Single layer membranes without some form of rigid structural support are likely to require a thick layer of an elastomeric material. This is to reduce the possibility of rupture as the shell deforms and assists in returning the shell back to its original shape after constriction. The membranes used by models such as IMGS [79], RD-IV-HSM [76], DHS-IV [24, 25], stomach simulator [69], AGS [27], GSM [15], distal gastric simulator [16] and SoGut [18-22, 80] are of a single layer of elastomeric material directly formed from a static mould. Other attempts have been made to create anatomically correct and distensible copies of parts of the GIT by 3D printing silicone shells using measurement data obtained from manipulated computed tomography scans [55]. This approach affects the ability for the mechanical creation of internal surface folding and buckling as the shell contracts. This may be evident with the model used by Chen et al. [34] as they deliberately fabricate a pattern of rugae, or soft surface folds, onto the inner surface of the silicone shell, rather than allowing rugae to develop on the surface of the wall through the folding deformation action of the membrane. Studies on the formation of buckling or folding behaviours of tissue [47-49, 83] suggest that rugae naturally arise from differences in the properties of the various layers present in the wall membrane, such as differences in mechanical stiffness between layers.

Many of the models in Table 2 involve a single layer, flexible or elastic wall, typically made from silicone or latex, being constricted in some manner at various locations. In using a single layer membrane, these models pay little attention to effects that may occur from the interactions between different layers within the wall membrane. Gastric toning, the expansion and contraction of the stomach wall for the accommodation of food, is also limited by the characteristics of the selected membrane materials used for the stomach reactor and lacks a controllable constrictive and expansive capability over the entirety of the stomach shell. For instance, Chen et al. [76] fabricated a replica human stomach in silicone

and used several 'rope' tendons, embedded within the antrum (lower) region of the silicone stomach, to act as constrictors. A pseudo-peristaltic contraction motion was simulated through the attachment of the tendons to varying positions along a hinged rod, the tip of which is attached to a motorised spindle that pulls the rod tip down and then releases it, allowing the three constrictors to contract and expand at differing amounts. The model, however, has difficulty achieving the disintegration of large food particles and in reproducing the gastric emptying, or sieving, and jet-like retro-propulsive flow effects present in the *in vivo* stomach.

2.2.2.3 Gastric secretion, motility and the emptying of stomach contents

Gastric secretion

For some dynamic models, gastric secretions such as saliva, gastric juices and hydrochloric acid are provided to the system to simulate and promote the chemical breakdown of food structures within the stomach. Rotary peristaltic and syringe pumps feature prominently among models that provide secretions (TIM-1 [52, 63], DGM [65, 66], SIMGI [73], TIMagc [52, 77], HGS [67, 68], ESIN [75], RD-IV-HSM [76], DHS-IV [24, 25], AGS [27], GSM [15], BGR [23]), particularly with the multi-stage, multi-compartmented models employing glass containment of the individual compartments. Some of the pumps distribute the fluids over the container wall, while others employ tubing to feed the fluids through various locations on a flexible membrane. Another common method is the addition of fluids directly into an inlet to the stomach compartment using either a peristaltic or syringe pump, or by manual injection or mixing of the fluids in with the contents before adding them to the reactor (c-GDS [70, 71], SIMGI [73], IMGS [79], improved HGS [26], AGS [27], AGDS [28], distal gastric simulator [16], SoGut [18-22, 80]).

Gastric motility

Biological digestive tract motility is significantly dependent on the interaction of contractions and expansions that occur between muscle layers in the longitudinal and circumferential, and in the case of the stomach, oblique orientations [1]. During peristaltic contractions the longitudinal muscles relax and extend as the circumferential muscles contract, and vice versa. Replication of this expansion and contraction interaction between muscle-layers can be difficult to achieve in a controlled physical simulation.

The models mentioned in Table 2 employ a diverse range of methods for promoting gastric movement or mixing, also referred to as motility, within the stomach compartment. These include the use of hydraulic or pneumatic pressure against a flexible wall (TIM-1 [52, 63], SIMGI [73], TIMagc [52, 77], BGR [23], GSM [15], distal gastric simulator [16], SoGut [18-22, 80]) or from the driving of a piston and barrel (DGM [65, 66], ESIN [75], DGSM [78]), magnetic stirring (SHIME [64]), mechanical rollers against a flexible wall (HGS [67, 68], c-GDS [70, 71], DHS-IV [24, 25], improved HGS [26], AGDS [28]), rope driven contraction (stomach simulator [69], RD-IV-HSM [76]), impellor stirring (DIDGI [72]), direct piston pressure (IMGS [79]) or iris-type diaphragms (AGS [27]).

The methods for transfer of post-gastric contents, typically employed in models that also incorporate intestinal compartments, generally involve straight-forward pumping via peristaltic valve pumps (TIM-1 [52, 63], SHIME [64], TIMagc [52, 77], ESIN [75], DIDGI [72], SIMGI [73]) that may also be assisted by the movement of the digesta through applied hydraulic or pneumatic pressure on a flexible membrane (TIM-1 [52, 63], TIMagc [52, 77]). These methods provide good control for transfer of contents from one compartment to the other but cannot be considered as closely mimicking actual GIT motility deformations.

A useful theoretical framework from which to begin to consider approaching biomimicry of the biomechanical properties of the tract wall membrane is the "three element model" as devised by Hill [39]. Hill's model considers the muscle tissue as a composite consisting of a 'contractile element' connected with a 'series elastic element' for describing the active contraction of the tissue muscle, and a 'parallel element' to describe the connective tissues such as elastin and collagen. Hill's model has also been increasingly used in the development of appropriate finite element analysis methods for biomechanical modelling of muscle mechanics [84].

Gastric emptying

Gastric emptying involves the gradual removal of contents from the stomach into the duodenum. Biologically this is carried out via the opening and contracting of the pyloric sphincter that begins as a slow contraction wave, progressing from the antrum, and increasing in constriction until it reaches the pylorus [3]. The size of particles passing through the sphincter is typically less than 2 mm in diameter [33]. To achieve this particle size the artificial sphincters used in the models may employ a variety of mechanisms for the 'sieving' and release of chyme out of the stomach including valves (TIM-1 [52, 63], TIMagc [52, 77], DHS-IV [24, 25], AGS [27]), Teflon membranes (DIDGI [72]), mesh nets (HGS [67, 68], c-GDS [70, 71]), pumps (SHIME [64], c-GDS [70, 71], ESIN [75], improved HGS [26], AGDS [28]), elastic annuli (DGM [65, 66]) and biomimetic contractions (GSM [15], SoGut [18-22, 80]).

Many of the methods used for replicating the 'gastric sieve' of the pyloric sphincter fall short of achieving a close biomimetic simulation. It is unrealistic to consider that mesh nets or perforated membranes would behave in a similar manner to a rolling wave that terminates

in a constricting aperture when fluidic suspensions or delicate food matrices are propelled along with it. Improvements in the reproduction of the muscular contractions of the pyloric and other GIT sphincters are therefore another area requiring further attention.

Alternative approaches and soft-robotics technology

Other dynamic models have been developed specifically for the biomimetic simulation of the oesophagus [85-90], duodenum [91], or the small or large intestine [92-98], but without the inclusion of a stomach compartment. These models present some unique methods and mechanisms in their design that tend to more closely mimic actual motility and deformation of the GIT wall, the majority of which employ pneumatics to drive the contraction of a flexible membrane wall in a specific manner and sequence. However, the methods employed tend to work only for a specific section of the GIT, or for a specific motility action, and therefore lack some flexibility in applying the same method or mechanism of motility to other GIT components. This is due, in part, to the inclusion of rigid components for achieving suitable operation of the actuation or movements, such as requiring solid outer shells for pneumatic pressures to act against or the use of rigid connectors between individual actuation units.

The trend now is towards the development of soft-robotic systems that use flexible materials and actuation approaches to create entirely 'soft' mechanisms. This is apparent through the recent proliferation of models that employ pneumatics to drive the artificial contractions over a flexible membrane. Artificial muscle contractions could also be realised through use of other alternative technologies such as electroactive/photoactive polymers (EAPs) [99-102], electrically-driven hydrogels [103-107], phase-change materials [108], pneumatic, vacuum and fluid-driven actuators [109-111], shape memory alloys (SMAs) [112], twisted nylon

fishing line [113-121], and origami or kirigami actuators [109, 122-124]. Many of these technologies may provide for artificial muscles to potentially become embedded within a membrane wall itself, which would in turn allow for the simulated component membrane to respond in a dynamic manner more like that of the actual biological component being modelled.

Advances in membrane technologies could also be applied to mimic different parts of the GIT wall or improve the physical properties of reactor membranes, bringing them closer in responsiveness to those of biological membranes. Elastic fabric and elastomer composites have been trialled in replicating the skins of octopi [125-127] and in creating thinner, reinforced viscoelastic membranes with improved resistance to tearing [128]. Braided and mesh structures have been employed to replicate the tubular peristaltic locomotion action of earthworms [129-132] and the design of gastrointestinal stents [133] so that they deliberately deform in a peristaltic manner. There is also potential for embedding of advanced sensor materials, such as flexible plastic bioelectronics [134] and rubbery sensors [135], within the membrane to provide quantitative feedback of membrane characteristics such as strain, pressure and temperature.

2.2.2.4 Feedback and control

To provide realistic simulation of GIT motility *e.g.*, the demonstration of peristaltic slow waves, segmentation, and gastric emptying, some form of control over the appropriate contraction timing and sequence is required. This is complicated by the biological presence of feedback mechanisms, chemical triggers, and mechano-receptors throughout the entirety of the GIT wall that influence the initiation and timing of the contraction processes. For example, the rate of gastric emptying is determined by feedback mechanisms coming from

the stomach, duodenum and the small intestine [3], meaning that all related compartments may require modelling in some manner to approach a realistic biomimetic feedback response.

This does not mean that the modelling of the necessary feedback components is required to be physical in form as they could instead be virtual or computational simulations of selected components or regions. Developments in computational modelling allow for multi-scale control of factors and geometries of the GIT and can include mathematical and finite element analysis of shell deformation [36, 44, 136-140], predictive modelling [139], and computational fluid dynamics [141-143]. This form of modelling could provide simulation results that approximate actual biological feedback responses. Despite the rapid advances in computational modelling Du et al. [144] suggest there is still a disconnect between the mathematical and virtual modelling of slow waves, mechanisms of slow wave propagation, material properties, motility, and luminal content distributions.

Understanding of patterns of slow wave generation *i.e.*, frequency, velocity and amplitude, has been explored through use of magnetic tracing [145] and high-resolution mapping techniques using electrodes [146-153]. The results of these studies may be useful in providing information on proposed timing sequences and patterns for controlling the localised muscle contractions of a physical model. However, the patterns recorded are of limited duration, derived mostly from single pattern occurrences of the constrictions, and in many cases show no indication of the initiation of the motility patterns coming from specific chemical or mechanical feedback receptors within the tract wall layers.

Experimental assessments of the characteristics and properties of a physical biomimetic model could be used in conjunction with computational *in silico* models [144]. There may

also be some potential in driving the motility patterns of dynamic *in vitro* GIT models via feedback directly provided from electrophysiological mapping techniques capturing slow wave propagations from biological systems.

2.3. Instruments

2.3.1. Tensile strength

Studies of biological GIT wall mechanical properties, the contractive forces and pressures involved, and the characteristics of GIT motility, provide a basis from which an assessment of the performance of a biomimetic simulation model can be made. A limited number of studies have been carried out on the tensile properties of GIT soft wall tissue, with tensile testing and analysis undertaken on human post-surgery and cadaver specimens [37] and comparable species such as pigs [62, 140, 154, 155]. The observed differences between results of these studies, for both human and porcine samples, highlight the wide range of variation in physical morphology and mechanical properties that naturally occur between populations. Tensile results also differ significantly between different regions of the GIT (Table 3) [37, 62].

Table 3: Regional differences in the tensile properties of human gastrointestinal tissue.

Location	Maximal Stress	Destructive Strain
Oesophagus	1.2 MPa	140 %
Stomach (axial)	0.7 MPa	190 %
Stomach (transversal)	0.5 MPa	190 %
Small bowel (transversal)	0.9 MPa	140 %
Large Bowel (transversal)	0.9 MPa	180 %

However, the scope of specimen sampling, particularly in human studies, is limited and there can be considerable variation between the locations and orientations of sample tissue strips selected in each case study. The values of Young's modulus obtained between studies can span multiple orders of magnitude [156], and tensile studies that take into consideration the preconditioning and zero-stress states of the materials under test are more likely to provide comparably accurate data [39, 45]. Therefore, specifying a suitable target range of tensile properties *i.e.*, for the selection of any considered biomimetic soft-wall membrane material, will not be straight-forward and depends on the selected methodology used in measuring the tissue properties.

Planar uniaxial, biaxial and triaxial tensile tests are the typical methods employed for measuring the material properties of the wall tissue of the GIT. Uniaxial tensile testing is the most common method but neglects the anisotropic behaviour of the soft tissue [37, 155]. Biaxial and triaxial tests provide a better account of the non-linear anisotropic characteristics of the sample tissue yet they provide challenges in reproducibility due to the difficulty in providing adequate anchorage of the samples during testing [140, 154].

A multi-axial out-of-plane tensile testing machine could be designed to obtain quantitative information on the anisotropic properties and behaviour of artificial tissue layers. One type of tensile testing machine is based on employing flexural loading of the sample fabric specimens and a capacitive sensor array to measure strain of the material in multiple directions [157-159]. These machines have been developed for testing the behaviour of various types of fabric and textiles and therefore could also be employed to evaluate tensile forces acting in multiple directions on fabricated elastic membranes.

2.3.2. Pressure, force and volume

A variety of methods have been used for measurement of *in vivo* forces, pressure, and changes in cross-sectional area or volume occurring during motility within gastrointestinal regions. Several of the most employed methods found within the literature are described in Table 4.

Pressure measurements of the contractions from artificial muscles of *in vitro* models have been demonstrated using a 22 mm hollow thick-walled rubber bulb attached to a hand-held manometer. This technique was used by Kong & Singh [67] for obtaining measurements of contractile force in the Human Gastric Simulator [67, 68]. The amount of force that is applied by the constrictors may be calibrated by compressing the bulb in a universal testing machine and calculating the relationship between pressure readings from the manometer and linear force applied by the universal testing machine.

It is also possible that balloon or inflation bag distension of tubular regions of the tract may be carried out on *in vitro* models to determine membrane compression forces. The procedure for *in vivo* testing, as described in Gregersen et al. [160], relies on inflating a 60 mm long non-compliant 25 micrometre thick balloon in a section of the tract for experimental testing of the membrane tension. The balloon is connected to a container of fluid via a tube and is inflated to pressure by varying the height of the level container. Preconditioning of the membrane by cycling of the inflation and deflation processes may be required until the stress and strain relation is reproducible [160]. Suggested pressure steps may range between 0 to 15 cm H_2O with the distension radius determined through measured grid analysis and timed frame capture with a high-resolution camera [160].

Table 4: Common methods used for measuring biomechanical properties of the gastrointestinal tract.

Method	Measurand	Description	Source
conventional and high-resolution manometry	pressure	Detects pressure changes caused by constrictions. Uses either strain gauges on a probe or perfusion of water from a catheter. Low cost, low precision method measuring only circumferential constrictions. High-resolution manometry uses a larger number of (fibre-optic) electrodes for measurement.	[1, 161]
barostat	volume	Involves the maintaining of a constant pressure in an air-filled bag placed in the lumen, the volume of air entering or leaving during constrictions is measured.	[162-165]
impedance planimetry	cross-sectional area	Cross-sectional area measurements are made from measurements of electrical impedance from electrodes on a probe. Can be combined with bag distension methods.	[1]
ultrasonography and endoscopic ultrasonography	volume	A medical imaging technique using a combination of real-time scanning with Doppler technology. Useful for measuring gastric emptying, however images may be blurred by fat or gas. Measures volume change over time. Endoscopic ultrasonography combines ultrasonic transducer imaging with an endoscopic probe.	[1, 163-165]
magnetic resonance imaging (MRI)	volume	Like ultrasonography, this medical imaging technique measures volume changes over time but uses magnetic resonance as the imaging source, ultrasonography and MRI methods can also be combined with computational fluid dynamics.	[1, 163-166]
single-photon emission computed tomography (SPECT)	volume	A nuclear medicine tomographic imaging technique using gamma rays. Can provide 3D information.	[163-165]
electromyography	force	Uses electrodes to pick up electrical activity of the muscle cells and measure the amount of force produced.	[167]
agar bead fracturing	force	Agar beads are made with predefined fracture strengths (determined through compression tests). The remains of surviving beads in the lumen determine the limits of constrictive force that have been applied.	[168]
inflation bag testing (distension)	external diameter from applied pressure	Like the barostat technique but typically using a fluid and with an emphasis on measuring the tensions on the bag along its length as it is deformed.	[36, 160]
high resolution pill-tracking of forces	force	A pill containing a permanent magnet is swallowed into the stomach and tracked using a matrix of magnetic field sensors. Force and torque data is calculated from the pill's position as a function of time.	[169]

2.4 Conclusions

A review of the literature has identified several knowledge gaps involved with present state-of-the-art gastrointestinal tract simulators:

1. Dynamic gastrointestinal simulation models are significantly lacking in ability to accurately replicate the entire biomechanical action, peristaltic motions, gastric toning, gastric emptying, retro-propulsive flow effects, and the physiological forces and pressures underlying organ wall deformation of the *in vivo* gastrointestinal tract. Biomimetic models that focus primarily on replicating the biomechanical actions of the GIT show a distinct lack in provision for the biochemical digestive processes that the dynamic simulation models have targeted. This highlights the existence of a distinct gap to be bridged between the biochemical systems of the dynamic GIT *in vitro* models and current mechanical GIT biomimicry attempts.
2. Little is known of how differences in morphological form and physical properties of the deformation of the membrane walls contribute to the mixing and motility processes of the GIT.
3. The use of single layer membranes in replicating the tract wall neglects any mechanical interaction effects between the different layers of the *in vivo* tract wall, and how differing orientations of the muscle layers interact to create the natural motility and deformation patterns. The occurrence of internal surface buckling and folding, derived from layers with different mechanical properties, is also omitted from simulations.
4. Much of the data obtained on the tensile properties of the tract wall neglect the anisotropic behaviour of the soft tissue.

5. Although *in silico* models can provide multi-scale control of factors and geometries, they still do not effectively connect through simulation the replication of slow waves, mechanisms of slow wave propagation, material properties, motility, and luminal content distributions.
6. Feedback mechanisms, such as the chemical and mechanical receptors in the layers of the wall and their ability to initiate various motility patterns as food is digested, have not been explored in simulations of gastrointestinal tract mechanics.

The membrane

Chapter 3 – The Membrane

This chapter describes the development of an artificial membrane for mimicking the gastrointestinal tract wall. It includes the fabrication and testing of a composite elastic membrane and a membrane composed of a poroelastic silicone sponge shell. The composite elastic membrane combines a silicone elastomer rubber with a stretchable nylon fabric to provide a very thin, structurally reinforced elastic membrane that can be formed to follow the shape of a typical stomach. A silicone sponge material is also described that can be both expanded and compressed. Due to the porous and elastic nature of the sponge material it demonstrates potential in providing a means of distribution for gastric fluids to and from the internal contents of the reactor.

The mechanical properties and characteristics of the biological tract wall have been investigated for the development of an artificial deformable membrane. The mechanical properties of the artificial membrane should attempt to mimic the elasticity characteristics of the biological tract as dictated by the collagen-elastin content of the ECM, the thickness and strength of the muscle layers over different regions of the tract, and the buckling and folding properties of the biological tissues involved. However, some consideration should also be given to the provision of chemical pathways through the membrane wall material or directly into the internal contents, and the creation of impermeable or semi-permeable surfaces for retention of the contents within the reactor. An ability to provide chemical pathways throughout the artificial membrane wall could provide means to mimic digestive fluid secretions into the stomach cavity, as well as provide some form of surface lubrication along the wall lining for supporting the oesophageal transport of a food bolus to the stomach.

3.1. Composite elastic membrane

A composite elastic membrane is a membrane produced from two or more materials that alter its material properties when merged. These material properties can include improved mechanical or chemical characteristics such as tensile strength, elasticity, flexibility, tear-strength, transparency, durability, and chemical resistance. Changing the physical properties of a material by merging it with other materials can help produce desired characteristics that align it more closely with the requirements of the intended application.

Specifications for the required achievable strain of an artificial tract wall membrane may be derived from observed measurements of maximum strain for wall tissue samples obtained from various locations on the biological tract. According to Egorov et al. [37] the maximum uniaxial strain achieved by actual human gastrointestinal tissue is approximately 190% in the stomach, 140% in the oesophagus and 140% in the small intestine. This suggests that achieving a strain of at least 200% from the artificial membrane material would be sufficient to mimic the maximal strain obtained by actual biological gastric wall tissue.

Wang, Gregory and Minor [128] investigated improvements to the mechanical properties of moulded silicone rubber when composited with a range of fabric materials including nylon, polyester, rayon, silk, cotton, and several blended fabrics. They found that tensile strength, tear strength and puncture resistance were improved when synthetic materials such as nylon, polyester, rayon-spandex, and polyester-cotton fabrics were used within the composite material and that they were more suited to applications that required toughened structures or reduced strain. However, the nylon, polyester and polyester-cotton composites displayed a limited ability to stretch compared to other silicone composites made from elasticated rayon-spandex blended fabrics.

Use of elasticated fabrics combined with a silicone rubber has been studied in development of a skin analogue for a robotic octopus [125-127]. An elasticated knitted nylon fabric combined with two types of silicone rubber of differing softness was used to obtain a suitable stiffness for the elastic artificial octopus skin. The Young's moduli in both the transverse and longitudinal directions were found to be lower than those of actual octopus skin, while the strength, failure strain and fracture toughness were higher. This method of fabric compositing was considered for simulating the soft tissue of the gastrointestinal tract as the artificial octopus skin was proven to be watertight in construction, highly flexible, and displayed unidirectional failure strain beyond 200% from its original length.

A silicone (Ecoflex™ 00-30, Smooth-On Inc., USA) and nylon composite material was fabricated to investigate its potential as a robust elastic membrane, acting as a reactor shell for the containment of food materials and providing a structure onto which the connection of unit constrictors or artificial muscles could be made. A basic stomach shape was constructed by inflating a rubber glove and wrapping rubber-bands around it in various locations to form the fundus, corpus, and antrum regions of the anatomical stomach (Fig. 6). Elasticated nylon knitted fabric, obtained from a pair of nylon stockings, was pulled over the inflated stomach form and liquid silicone was brushed over to seal the fabric and make it watertight. Once the sealed membrane was removed from the form it was filled with water and the openings tied shut with rubber-bands.

The fabricated membrane exhibited high flexibility and good resistance to tear and fracture while also remaining water-tight when stretched or manipulated. The membrane could hold water for several months without any obvious leakage or breakdown of the material. Based on these promising results a repeatable method of fabrication for this type of reactor membrane shell was explored.

Three-dimensional stomach template form

A three-dimensional (3D) stomach model was designed and built as a solid template form onto which a silicone composite membrane could be fabricated. Computer-aided design (CAD) software (SolidWorks) was used to section a 3D surface model created from the dimensions of a human stomach (BodyParts3D, © The Database Center for Life Science licensed under CC Attribution-Share Alike 2.1 Japan) [29] into a series of 3 mm thick slices.

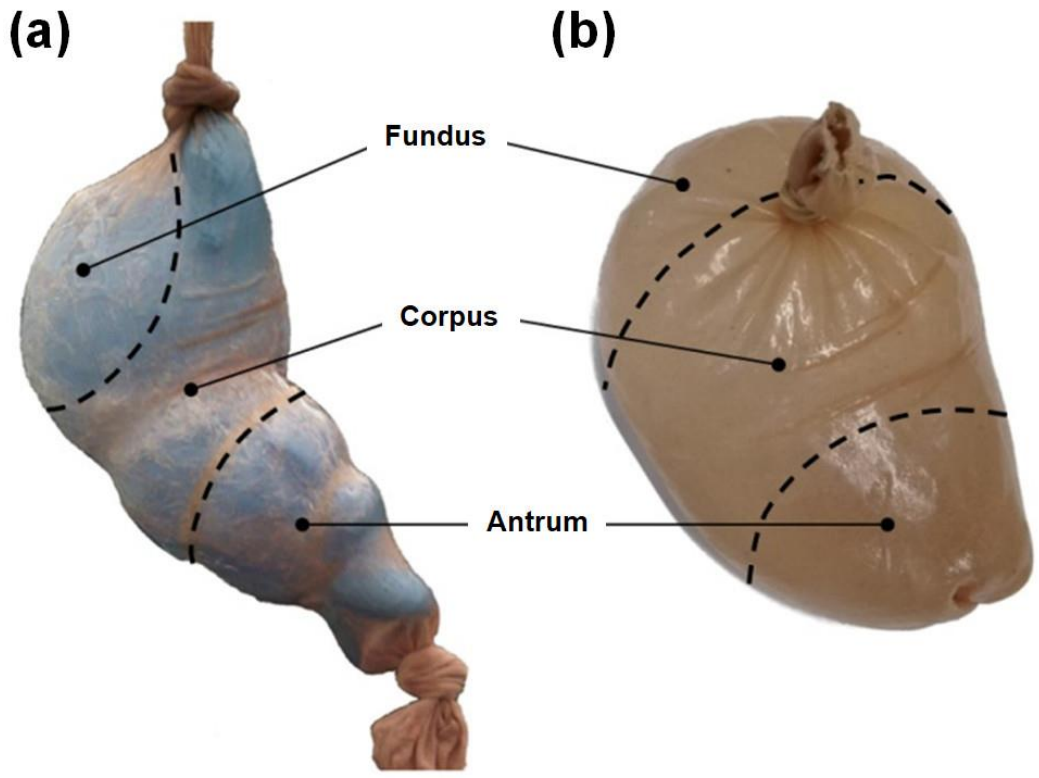

Fig. 6: (a) Artificial membrane formed over a basic stomach shaped mould. (b) The same artificial membrane removed from the mould and filled with water.

The profile outlines of these slices were cut into 3 mm sheets of corrugated cardboard using a laser cutter (Epilog Fusion CO_2 Laser 120W). The slices were then rearranged, slice by slice, back into the original stomach shape and glued together with polyvinyl acetate (PVA) adhesive. The layered cardboard stomach form was finally completely covered with modelling clay and the surface smoothed by hand before allowing it to dry (Fig. 7). The dried clay surface was brushed with a coating of silicone oil to prevent the clay from inhibiting the liquid silicone during curing.

A cylindrical length of elasticated nylon knitted fabric was pulled over the solid stomach form while rubber bands were used to hold the loose fabric against the form at the openings of the oesophagus and duodenum. The fabric-dressed form was suspended over a drip tray and a layer of liquid silicone was brushed over the entire surface and allowed to cure (Fig. 8). This process was repeated two or three times until the thickness of the silicone layer was

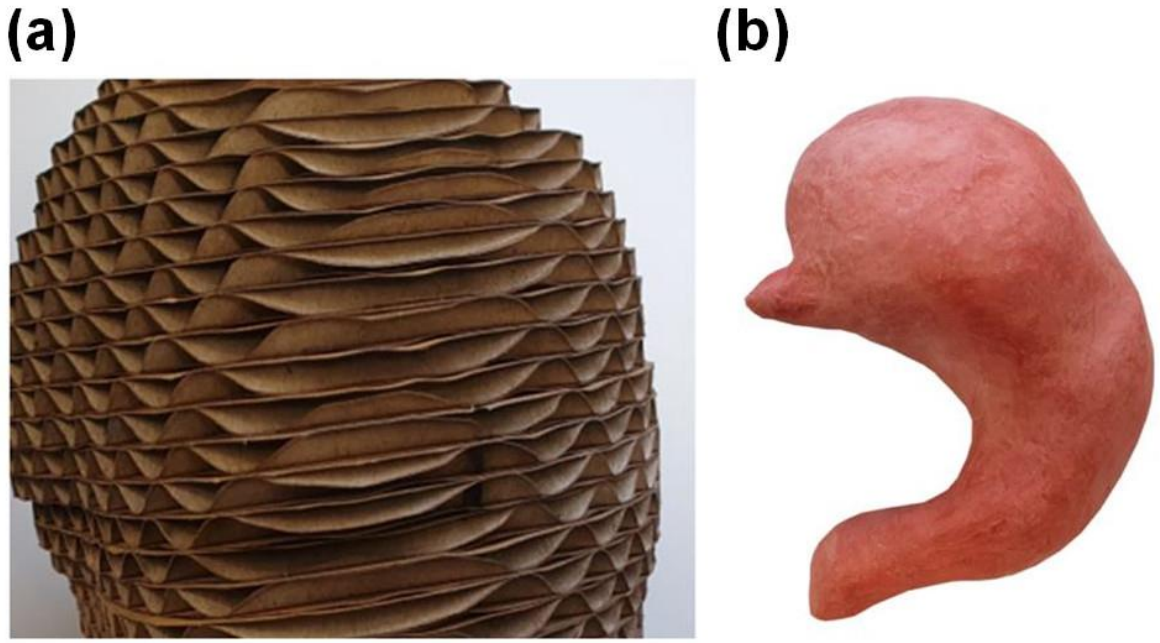

Fig. 7: (a) Close-up image of the stacked corrugated cardboard sheet slices used to form the stomach shape. (b) The completed cardboard stomach shape filled with a surface layer of modelling clay.

between 1-2 mm and there were no visible holes or gaps in the silicone material. The composite layer was removed from the mould by carefully stretching and peeling the elastic material back over the solid form.

Two-dimensional stomach template form

A second fabrication approach was to create a solid form for the membrane from a template stomach shape cut from a sheet of 3 mm thick medium-density fibreboard (MDF). An initial outline of the stomach was drawn on a sheet of paper by pressing out the composite membrane that was created using the solid stomach form described above and tracing around the edges of the membrane. This hand-traced outline was then scanned, placed into CAD software (SolidWorks) as a two-dimensional (2D) image and traced with spline tools to produce a digital copy of the 2D stomach shape that could be cut out with a laser cutter (Epilog Fusion CO_2 Laser 120W). Additional reference lines were drawn on the cut MDF

Fig. 8: Composite membrane formed over the surface of a 3D stomach shape.

template to indicate approximate placement locations of the unit constrictors for the membrane.

The surface of the MDF form was brushed completely with silicone oil to create a suitable surface for curing of the liquid silicone. A tubular length of elasticated nylon knitted fabric was pulled over this form and repeated brushing of multiple layers of silicone completed the fabrication of the composite membrane (Fig. 9). Particular attention was paid to the application of silicone over the edges of the form as this was where inadequate surface coverage was most likely to occur. Once completely covered the form was suspended over a drip tray and any excess liquid silicone was allowed to flow, by gravity, off the form.

To further ensure that no holes were present in the fabricated membrane, and that it was completely waterproof, one opening was tied with a rubber band while water was poured into the other opening, filling the enclosed membrane sac. Any points of leakage were marked and patched with a small amount of liquid silicone after the water was removed. This process was repeated several times with increasing amounts of water being added until five litres could be held without any subsequent leakage occurring.

Tensile testing of the artificial tissue membrane layers attempted to follow procedures for the tensile testing of actual gastrointestinal tract tissue as described in the literature [37, 62, 140, 154, 155]. Artificial membrane samples were obtained from the fundus, corpus, and antrum regions of the fabricated stomach (Fig. 10). Transverse (circumferential) and longitudinal-orientated sections of the artificial tissue were cut into 60 mm long by 10 mm wide sample strips using a guillotine.

To determine the thickness of the membrane, the samples were placed between two 8.00 mm thick machined steel plates and the combined thickness of the steel plates and membrane measured with a micrometer and recorded (Table 5). An average thickness taken from several measurements was calculated as the thickness of the artificial tissue was not uniform, and the sandwiching effect of the material between the steel plates can cause some compression of the membrane. However, plate compression was not considered to alter the measurements by a significant amount. The samples were then subjected to uniaxial

Fig. 9: Composite membrane moulded over the surface of a template stomach form cut from a sheet of MDF.

extension on a universal testing machine (Instron 5960 Dual Column Tabletop) fitted with a 30 kN load cell. A 25 mm length of sample material was held between the clamps and a strain rate velocity of 200 mm per minute applied to the sample under test. Preconditioning of the sample was undertaken by applying 3 cycles of stretching to 100% of original length prior to stretching them to the point of complete failure. No recovery period was allowed between the preconditioning cycles and final stretch cycle.

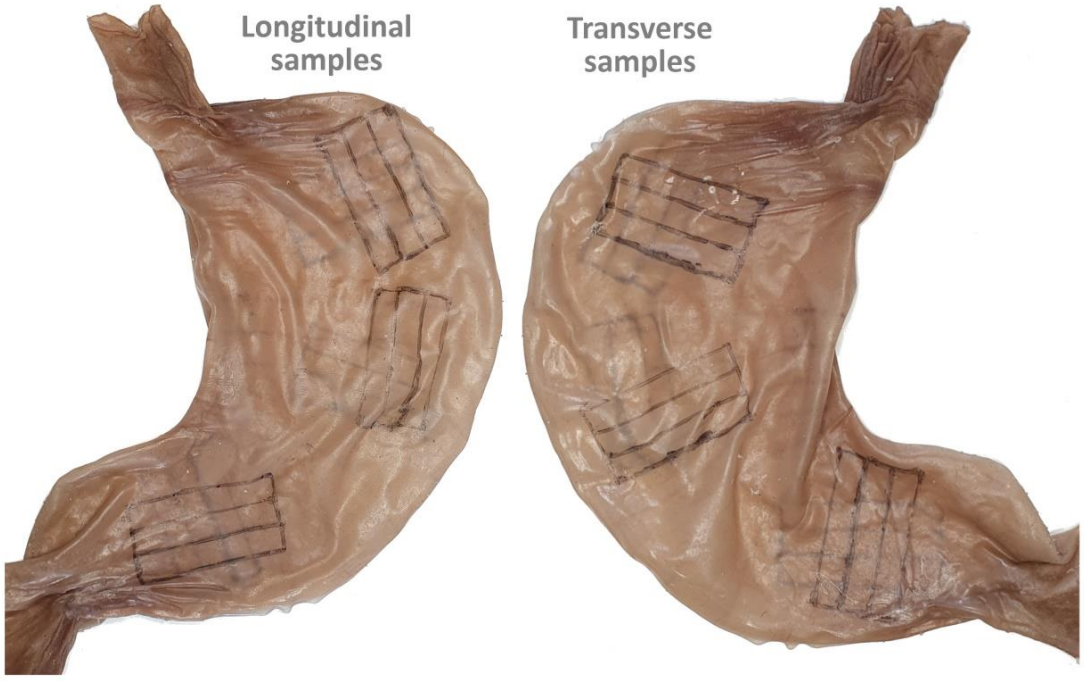

Fig. 10: Locations of the extracted artificial membrane material samples used for tensile testing.

The uniaxial tensile tests indicate that the artificial membrane material can stretch to over 200% for both longitudinal and transverse-oriented samples before showing signs of material failure (Fig. 11Fig. 12). The composite membrane material experienced a slow degradation of the knitted fibres as the strain increased. The breaking of threads within the weave of the elasticated nylon fabric could be observed as sharp dips in the stress-strain curve beginning at approximately 250% strain. The onset of thread-breaking was initiated at the compressed points of the material where it was being held in the clamps of the machine, potentially cutting through the silicone and exposing the fabric. Tearing would also begin to spread from the cut edges of the composite material where the nylon fabric had been exposed from the silicone. This suggests that the strength of the woven fabric can be improved when it is completely covered by the silicone rubber, and that stress points can be minimised in an artificial membrane by ensuring that the nylon fabric remains fully embedded within the silicone.

The difference in the amount of stress experienced between samples is influenced by the amount of pre-stretch that different regions of the nylon fabric experience prior to embedding it in silicone. This is most obvious in the transverse samples of the corpus region and the longitudinal samples of the antrum where the nylon stocking has been stretched

Table 5: Thickness measurements of the composite membrane samples

Sample location	**Fundus**		**Corpus**		**Antrum**	
	Longitudinal	Transverse	Longitudinal	Transverse	Longitudinal	Transverse
Average sample thickness (mm)	0.86	1.01	0.86	0.77	0.95	0.82

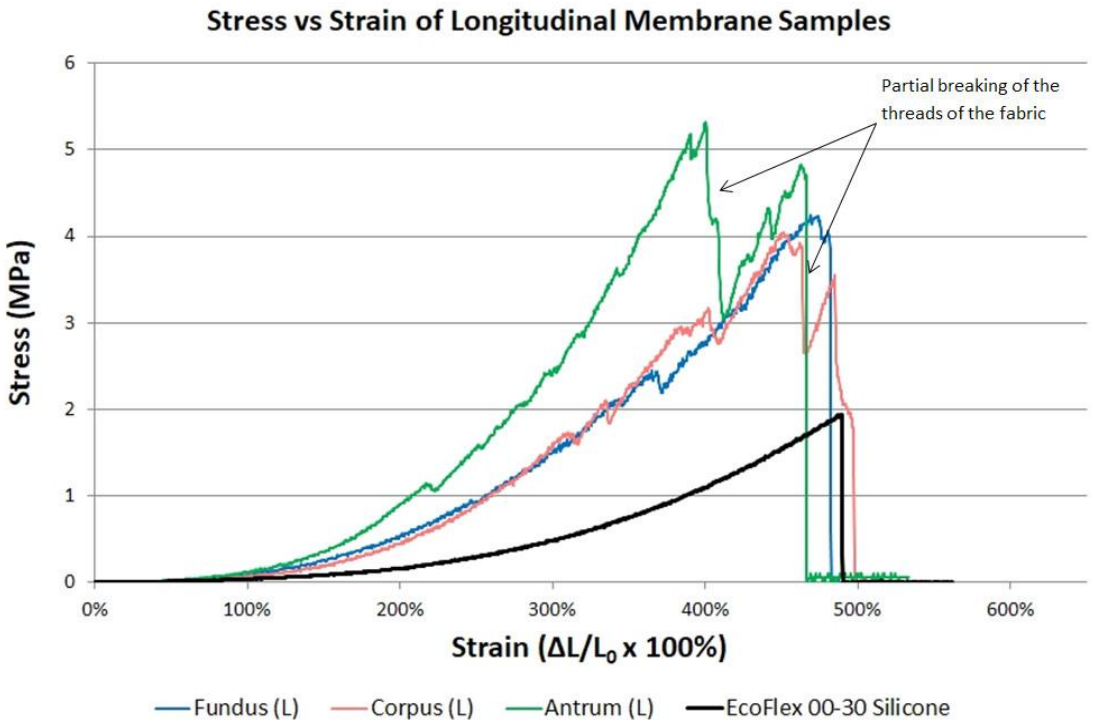

Fig. 11: Stress vs strain performance of the longitudinal composite membrane samples.

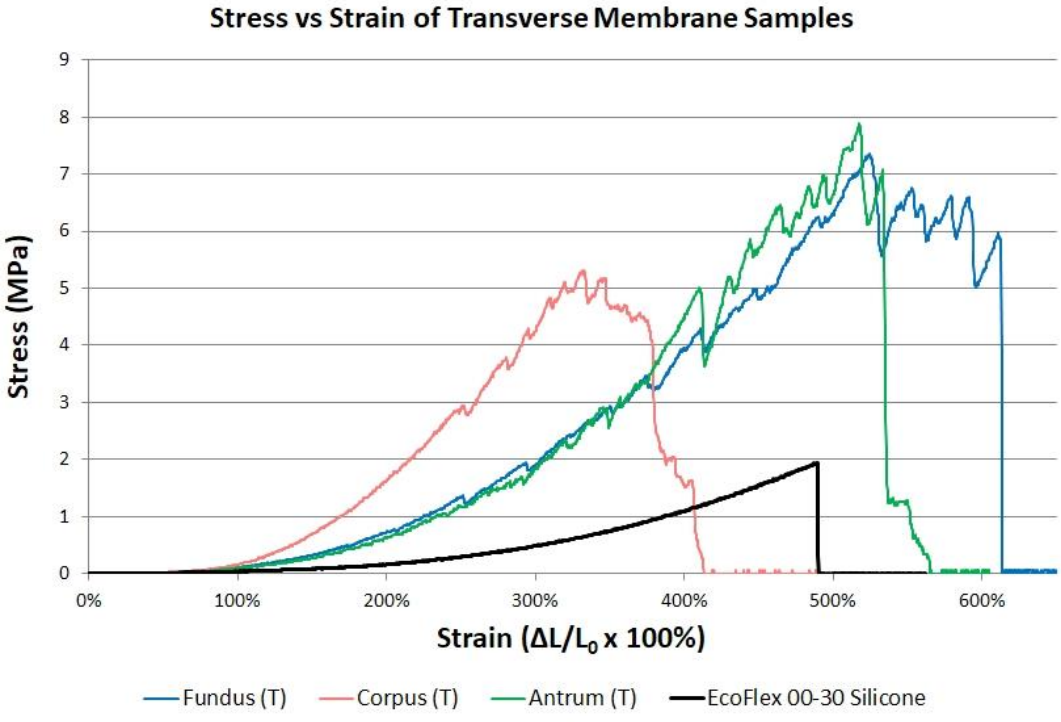

Fig. 12: Stress vs strain performance of the transverse (circumferential) composite membrane samples.

significantly when pulled over the stomach template. The ability of the membrane to withstand strain up to 200% is most important in the fundus and corpus regions of the artificial stomach as this is where most stretching activity is likely to occur, such as when simulating the gastric toning of the stomach wall and providing for the accommodation of food.

Fig. 13 shows that the composite material has good ability to provide 200% stretch over all regions of the stomach, but also that any transverse or circumferential stretching over the corpus region is likely to experience stiffer response from the material. Fig. 14 shows images of the fabricated composite membrane sac taken at various stages of filling with water; up to a 3.5 litre capacity. A greater capacity of filling is possible but not considered to be required

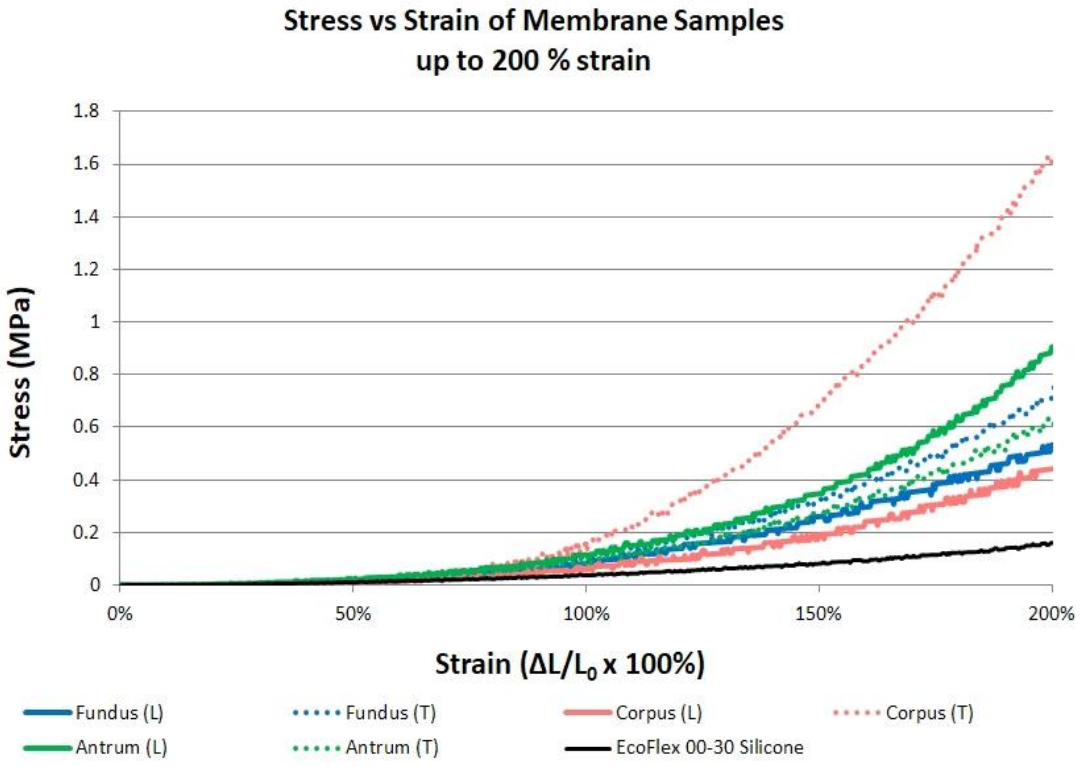

Fig. 13: Stress vs strain performance of the longitudinal and transverse composite membrane samples stretched up to 200% of their original length.

for the reactor shell as a volume of 1-1.5 litres is a typical volume for a full human stomach.

The shape and expansion of the membrane was highly influenced by where the sac was held or constrained and any contact with surrounding rigid physical objects. When freely suspended from the gastroesophageal junction the sac elongates significantly as gravity pulls down on the water mass and the elastic material stretches. The membrane material experiences longitudinal stretch mostly at the upper region of the sac, while the base tends to expand outwards where most of the water content collects. This characteristic of membrane stretch, due to gravity acting on its contents, suggests that the shape of physical bodies or boundaries surrounding the filled membrane can significantly impact how the stomach shape is formed in a bio-relevant manner.

In the biological system, the surrounding organs and tissue of the abdominal cavity act as the physical boundaries to the stomach. These anatomical boundaries are not entirely rigid themselves and can react against the expanding stomach wall as it fills with food. The liver, pancreas, spleen, and kidney are fixed in position and do not change significantly in size during the process of digestion. However, the stomach is situated above the transverse colon, which can dynamically change its shape and form as it transports digesta to the descending colon. Little is known about what effect the motions of the transverse colon or the boundary presence of a filled or empty colon may have on the biomechanical actions of the stomach wall. Therefore, the presence of a dynamic moving boundary at the lower region of the stomach may require consideration in design of an appropriate biomimetic enclosure for the stomach reactor model.

During fabrication of the membrane there is potential for pinholes to appear in the composite material from inadequate application of liquid silicone. The first layer of applied

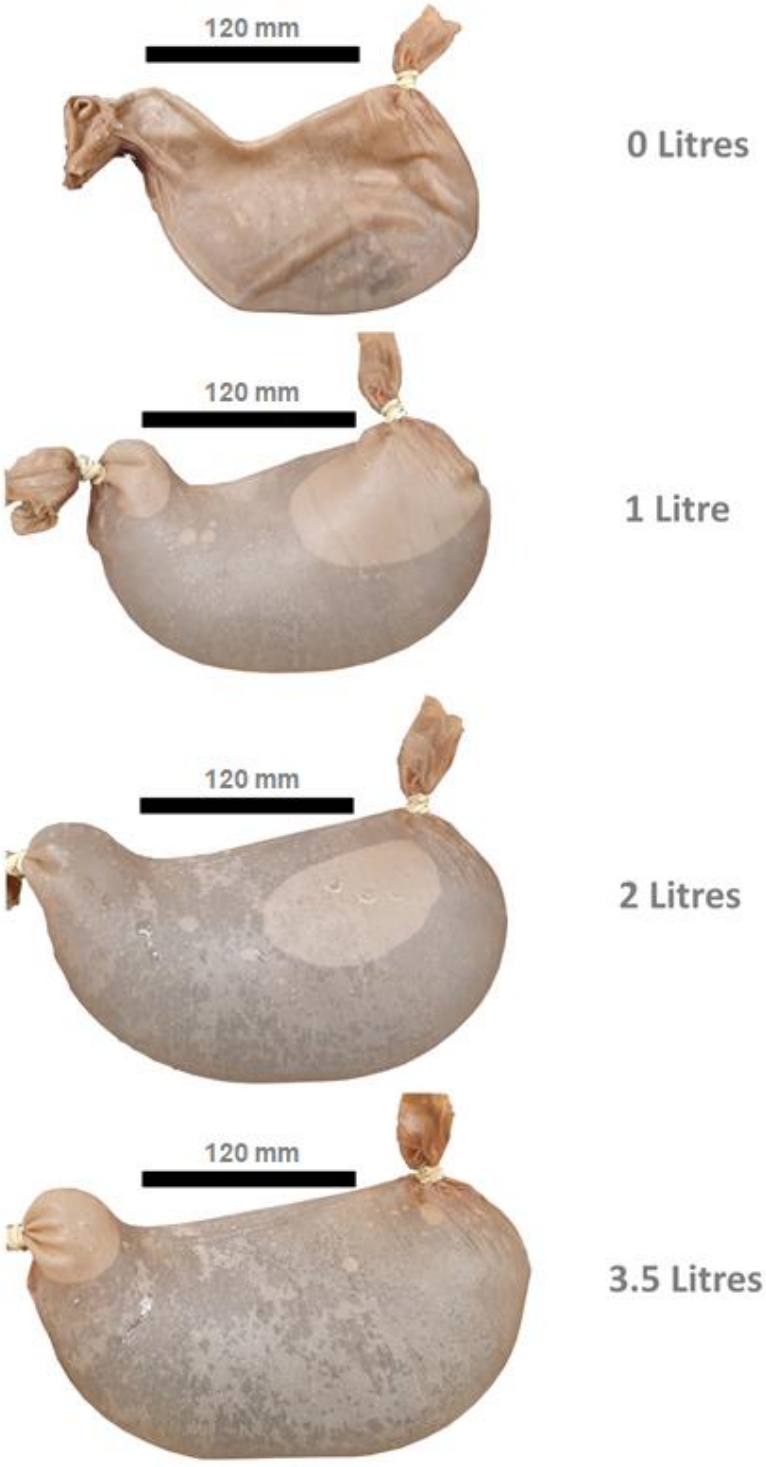

Fig. 14: Composite membrane stomach filled with up to 3.5 litres of water while placed on a flat surface.

silicone requires the greatest attention so that the fabric layer is properly 'wetted' and can provide a consistent surface for the subsequent layers of silicone to adhere to. The appearance of voids or holes within the silicone can create stress points in the composite material as it is filled, which can rupture and cause the fluid to leak out when under pressure. The appearance of voids can be reduced by degassing the liquid silicone at 90 kPa vacuum pressure in a vacuum chamber for 3-5 minutes, which releases dissolved gases within the liquid silicone so that it does not form bubbles as it cures.

If leakage is observed when filling the membrane sac, then these holes can be identified and marked so that additional plugging of the holes can be made when the sac has been emptied of water. A small amount of silicone can be applied to any marked holes and then left to cure to fully seal them. Larger holes or tears in the fabric material can also be patched with a small piece of silicone-wetted fabric if necessary, however this should be avoided if possible as it can affect the material stiffness of the membrane at these areas and cause expansion of the membrane to deform in an unknown manner.

The alternative template forms used in creating the membrane sacs, the 3D stomach form and the sheet-cut 2D form, show no significant difference in the expanded stomach shapes formed when the membrane sacs are filled with fluid. The 2D sheet-cut form is however significantly easier, cheaper, and faster to produce than the 3D stomach form and is a preferred method for membrane fabrication due to these fabrication advantages. The 2D MDF form can also be easily altered or scaled in size to create alternative stomach shapes that mimic anatomical variances in individuals e.g., scaled to a child-sized version.

With the addition of the nylon fabric the transparency of the composite material membrane becomes reduced compared to that of a mono-material silicone membrane (Fig. 15). The composite membrane remains semi-transparent, but the transparency level can alter depending on the type of elastic nylon fabric that has been used and the denier, or linear mass density of fibres, of the fabric weave. The colouring of the fabric affects the final appearance of the material. Skin-coloured knitted nylon fabric was therefore preferred for use over other coloured fabrics as they create a more natural-looking stomach.

Increasing the thickness of the membrane shell or increasing the hardness of the silicone used in the composite material increases the shell stiffness and alters its folding and buckling characteristics. The stiffness, folding, and buckling characteristics of the

Fig. 15: Transparent inflatable stomach shape made from 100% silicone rubber and filled with coloured water.

membrane material are important as to how the shell deforms when being manipulated. This influences the generation of peristaltic slow-wave contraction patterns, inner surface deformation patterns from the closure of a sphincter, and recreation of mucosal layer surface folds. As these characteristics can also differ over different regions of the gastrointestinal tract, it may be necessary to alter the membrane shell thickness at different anatomical locations for example, thickening of the membrane layer at the pyloric sphincter. Another method may be to employ the use of harder or softer silicones within the composite material.

Silicones of different stiffness can be layered on the composite material to create a range of different membrane deformation effects. For example, a softer silicone such as Ecoflex™ 00-10 (Smooth-On Inc., USA) can be layered on top of Ecoflex™ 00-30 (Smooth-On Inc., USA) that is used to encase the nylon fabric. If the membrane sac is turned inside-out to place the softer silicone on the inner surface of the sac, the softer inner surface silicone layer will come under compressive stress and wrinkle and fold as a result. This effect suggests a simple method of fabrication for the stomach folds on its inner surface, which can be observed when the stomach is un-stretched or empty but disappears when the stomach wall expands.

An improved method for the mimicry of surface layer folds, or rugae, can be achieved by expanding the stomach sac prior to the addition of a layer of soft silicone. Expansion is achieved by inflating the membrane sac to a point where the filled sac resembles that of a filled stomach and then tying the open ends closed. The sac should be turned inside-out before inflating to maintain the correct form of the stomach. The softer silicone is then layered onto the outer surface of the expanded membrane to a thickness of 2-3 mm. When the silicone is cured, the sac can be deflated and turned inside out to regain its original

form. This method of layering on a pre-expanded surface and then inverting the surfaces simulates the same effect as when a faster growing inner surface, for instance the innermost mucosal layer, is confined from expansion during cell growth by the slower-growing outer boundaries of the circular and longitudinal muscle layers.

The composite silicone and elasticated nylon fabric membrane displays encouraging physical characteristics for mimicking the properties of a biological gastric tract membrane. Reinforcement of the membrane, provided by the embedding of the elastic fabric, gives it improved tear resistance while also allowing the membrane to be constructed with a smaller thickness than would be required for a pure silicone membrane. Maintaining a thin cross-section of the membrane improves its flexibility and folding or buckling characteristics, allowing it to mimic the deformation patterns of a biological tract wall more closely. The improved tear strength of the thin membrane material also provides a suitable substrate for the direct connection of artificial muscles to the fabric-silicone composite.

3.2. Silicone sponge

Silicone sponge is silicone rubber with a cellular, sponge-like structure. The structure is formed by introducing numerous bubbles, cells, or voids within the liquid rubber as it cures. The two forms of sponge that can be created are closed-cell sponge, where the voids or bubbles are completely closed off from each other, and open-cell sponge where the cells are not closed off from each other and therefore possess an ability to draw in liquids or air into the sponge structure.

These sponge materials exhibit different mechanical properties to those of pure silicone structures as the total mass of silicone material used is reduced. The density, stiffness, and tensile properties of the sponge material are lower than for pure silicone. However, unlike

pure silicone rubber these silicone sponges are capable of elevated levels of compression as well as elastic extension, making them useful in applications where both elastic compressibility and extensibility are required. The mechanical properties of elastic silicone sponge may be useful for influencing specific artificial stomach membrane characteristics including fluid retention and absorbency, compressive folding and the forming of soft internal ridges, and acting as a conduit for secretion of gastric fluids or lubricating mucus.

Several different methods could be employed for fabricating silicone sponge [170] including direct templating, where a sacrificial solid is added to the curing silicone and removed by leaching or melting [171-176], emulsion templating [177, 178], gas foaming, phase separation and 3D printing [179]. Silicone sponges have been used in a variety of applications including soft robotic biomimicry of the human heart [180], the separation of oil from water [171-173, 178, 179], pressure and thermal sensing [174, 181, 182], electromagnetics [183], wound dressings [184] and the continuous pumping of water through a capillary action [176].

A silicone sponge was prepared using the sugar templating method [171-176] and trialled as a potential membrane layer for an artificial stomach. The sponge material was first moulded as a stand-alone membrane layer on a stomach-shaped form, while a second trial involved layering it onto an elasticated knitted nylon fabric to assess its adhesion and folding capabilities. The silicone sponge material was made using a ratio of 2:1 granulated sugar to liquid silicone, which was mixed in a container until it was evenly distributed. The ratio of sugar to silicone allowed for an open-cell sponge structure to be obtained whilst maintaining enough fluidity in the sugar-silicone mixture for it to be evenly spread over a surface without run-off occurring. The texture of the mixture resembled that of wet sand but also exhibited enough fluidity to adhere to itself without collapsing or breaking off. The level

of fluidity of the mixture also ensures that the resulting sponge structure form is completely enclosed after the curing of the silicone.

The mixture of sugar and silicone is best applied to a solid or rigid structure since it requires to be firmly pressed onto a surface. The amount of pressure to apply may vary depending on what is required to spread the mixture evenly, combine adjacent sponge mixture sections together, and achieve an adequate thickness of the final surface covering. Use of a rigid, rather than flexible, backing material helped to ensure that an even thickness of the material could be applied over the entire form.

A solid 3D stomach form was used as the backing material for the sugar-silicone mixture, the fabrication of which is described in Section 3.2. The form was covered with a layer of plastic film to help assist in the removal of the cured sponge material from the surface of the form. Sections of silicone and sugar mixture were gradually built up by hand-pressing it over the surface of the stomach form, while material thickness was periodically assessed by the insertion of a pin in various locations of the compacted mixture. A targeted thickness of 5 mm was sought over the entire stomach form, but due to variability in the applied pressure, and inconsistent smoothing of the compacted silicone and sugar surface, this result was adjusted to 7 mm ±1 mm.

A variation of a 3D stomach silicone sponge structure was created with a set of embedded expandable braid unit constrictors (Section 4.2). An initial layer with thickness of 3-4 mm was spread over the stomach form and allowed to cure. Eleven expandable-braid unit constrictors were distributed over the sponge layer by placing them in an orientation replicating that of the circumferential muscle layer, beginning from just under the gastro-oesophageal sphincter, and covering a region from the corpus down to the pyloric sphincter

(Fig. 16). A further four unit-constrictors were positioned over the fundus, above the gastro-oesophageal opening, to represent muscles in an oblique orientation. All constrictors were then covered with another 2-3 mm thick layer of silicone and sugar mix to completely embed them within the sponge structure.

Once the silicone had fully cured, the silicone and sugar mixture became rigid due to the high sugar content, making it difficult to remove the cured sponge material from the stomach form in a single intact piece. The sugar could be removed by dissolution while it is in solid form, however, it was desired that the internal surface of the sponge material first be coated with an impervious layer of silicone. To accommodate this internal impervious layer of silicone, the cured silicone-sugar material needed to be removed from the form with the sugar content intact. A cut was therefore made between the fourth and fifth unit-constrictors and angled towards the oesophageal opening so that the fundus region could be flipped back over the top of the 3D mould (Fig. 16).

When the cured sugar and silicone stomach was removed from the form, liquid silicone was poured into the internal cavity, spread over the inner surface, and left to set and create an impervious barrier on the inside of the sponge material. The entire sponge structure was then immersed in warm water with a little detergent and agitated by hand to assist in the dissolving of the sugar. The dissolution process needed to be repeated several times to ensure that as much sugar as possible was removed from the structure, at which point the sponge structure was allowed to fully dry.

To determine the tensile properties of the sponge material three sample lengths each of sponge and pure silicone (Ecoflex™ 00-30, Smooth-On Inc., USA) were subjected to uniaxial stretching on a universal testing machine (Instron 5960 Dual Column Tabletop). The samples were all 25 mm long by 10 mm wide by 7 mm thick. The testing machine was fitted with a 30 kN load cell and the sponge samples were stretched at a strain-rate velocity of 200 mm per minute. Preconditioning of the samples was undertaken by applying 3 cycles of

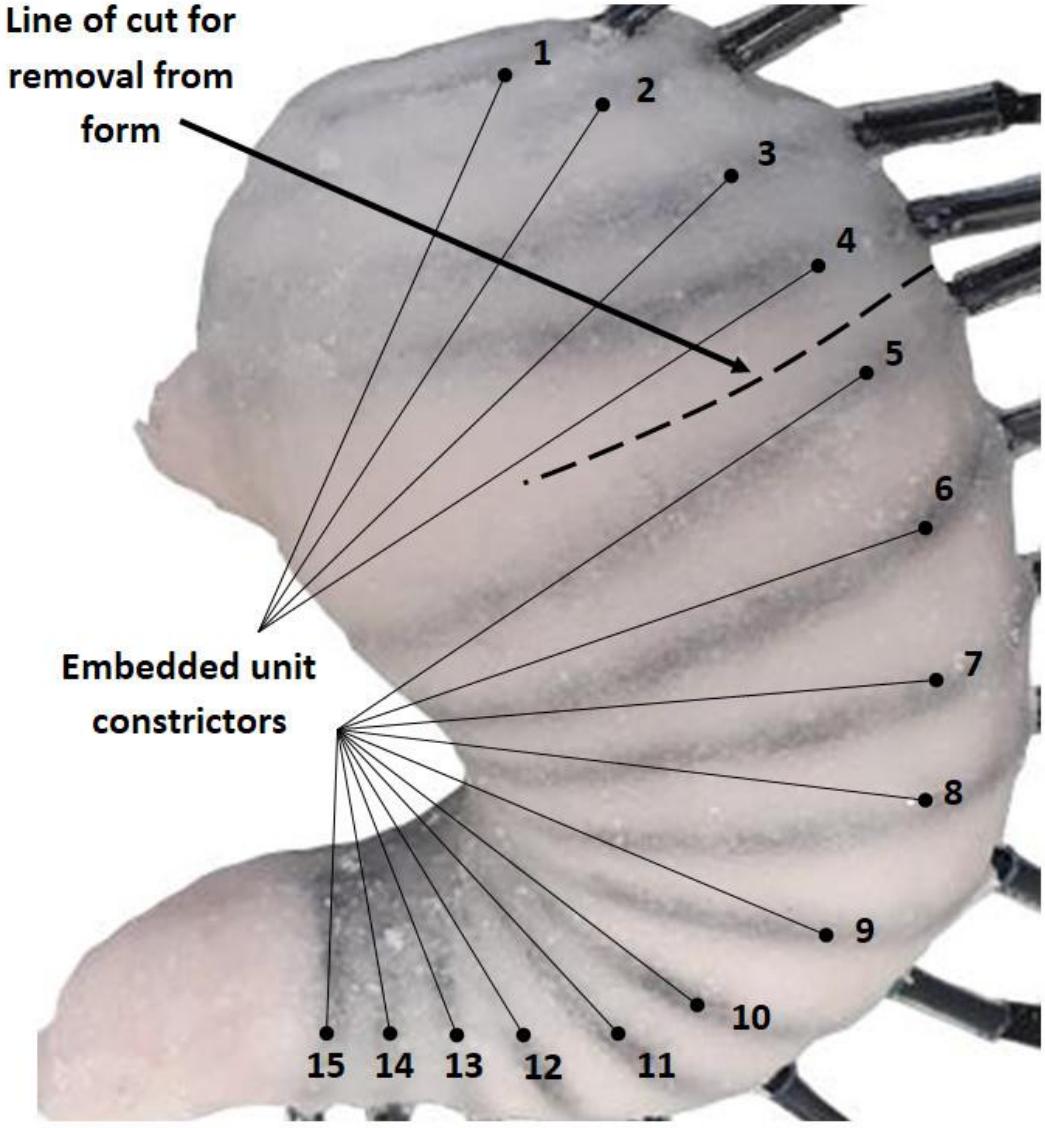

Fig. 16: A silicone-sugar mixture moulded over a 3D shape of a stomach. Expandable-braid unit constrictors are embedded within the sponge material.

stretching up to 100% strain prior to stretching the samples to their point of complete failure. No recovery period was allowed between the preconditioning cycles and final stretch.

The sponge material was capable of significant extension due to the elastic properties of the silicone (Fig. 17). An extensibility of nearly 400% was achieved by the test samples while the stiffness of the material was found to be lower than the pure silicone. However, the cellular structure of the material also causes the breaking strain of the sponge to be lower than that of pure silicone.

The direct templating method, using granulated sugar as a template filler material for the silicone, was employed due to its ease-of-use in fabrication and the low cost of the materials and process involved. An open-cell structure was desired so that the sponge material demonstrated absorbency of fluids as well as compressibility of the material. Sixty-six percent of the mass of the prepared silicone sponge material consisted of granulated sugar. Granulated cane sugar has a density of 1.59 g/cm^3 while Ecoflex™ 00-30 silicone has a density of 1.07 g/cm^3, therefore when the sugar was dissolved from the encapsulating silicone the remaining sponge structure had a potential compression ratio of up to approximately 57% of its original volume. At this compression ratio all the open cells within the structure would be compacted.

The uncured silicone-sugar mixture was found to readily adhere to elasticated nylon knitted fabric in its semi-liquid state. Once cured and the sugar dissolved, the sponge material continues to provide good adherence to the elastic fabric, even when stretched to the full extensibility of the fabric substrate. This aspect can be exploited to create a sponge-fabric composite material suitable for reinforced membrane fabrication of the stomach and other gastrointestinal sections. Adequate sealing of at least one of the inner or outer surfaces of the sponge material is required to complete the membrane to a condition where it becomes impervious to fluid and can contain fluid contents when expanding and contracting.

The silicone sponge material displays potential as a distinct tissue layer for the artificial membrane, particularly as a mucosal or inner layer of the tract because of its low stiffness

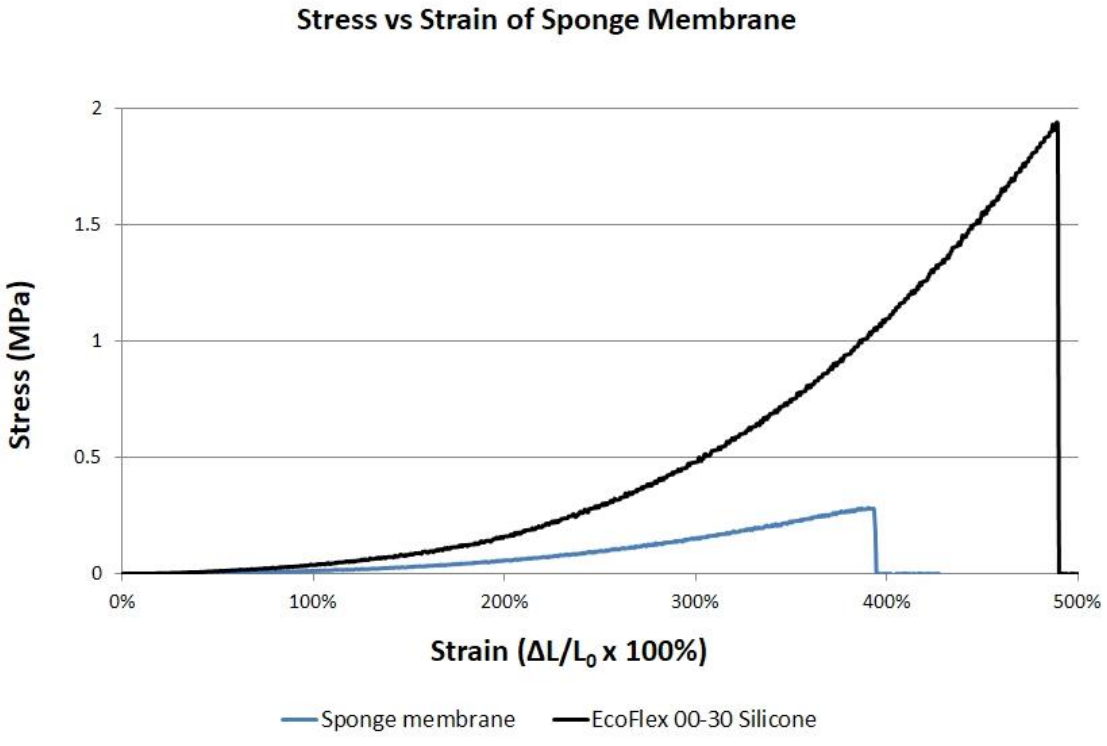

Fig. 17: Stress vs strain performance of the silicone sponge membrane.

and compressibility characteristics. A short tubular structure of the material was fabricated to investigate surface folding characteristics and contraction properties of the sponge. A 100 mm tubular length of the composite elastic membrane (Section 3.2) was first fabricated to act as base structure for the sponge material layers. Elastic nylon stocking of 7 denier (Anko, Kmart Australia Ltd.) was pulled over a 35 mm diameter length of polyvinyl chloride (PVC) tubing and sealed with liquid silicone (Ecoflex™ 00-30, Smooth-On Inc., USA). When cured, the composite elastic membrane tube was expanded over a piece of 70 mm diameter PVC tubing to pre-stress the base membrane layer prior to the application of the sponge layer.

A soft silicone (Ecoflex™ 00-10, Smooth-On Inc., USA) was mixed in with granulated sugar at a ratio of 1:2 liquid silicone to sugar by weight and spread over the base composite membrane layer at a thickness of 2-3 mm. Once the sugar-silicone mixture had cured, the artificial membrane tube was peeled from the PVC tubing and the sugar dissolved from the silicone. The two-layer membrane tube was then stretched by 100% over a length of 35 mm diameter PVC tubing and held in this position with cable ties. A final layer of liquid silicone was spread over the sponge material to seal or semi-seal the membrane tubing and create a soft, thin, surface layer.

The fully cured three-layer artificial membrane tube was then turned inside out. The process of pre-stressing the different layers of the artificial membrane by stretching them during fabrication mimics a build-up of residual stress within the membrane as found in biological gastrointestinal tract tissue layers *i.e.*, stresses that arise from the different growth rates of the tract wall layers. Turning the membrane inside-out then causes the thicker, but softer, silicone sponge material layers to fold and buckle as the (now) outer composite elastic membrane layer constrains the softer inner layers from expansion. The cutting of a

ring-section, obtained from the artificial tubular membrane, into a sector, results in the residual stress being released. When floated on top of a body of water the sector will invert and curl back against itself as the inner sponge layer is allowed to expand to its equilibrium state (Fig. 18). This result compares well with the stress behaviour of biological gastrointestinal tissue observed by Gregersen and Kassab [45].

To assess the folding capabilities of the composite material several circular rings of different internal diameter were used to act as fixed–diameter constrictors on the external surface of the artificial tubular membrane. The solid rings were laser cut (Epilog Fusion 120W) from a 4.5 mm thick sheet of MDF. Fig. 19 shows the ridges and folding that occurs on the inner surface of the membrane when constricting the external membrane surface with 40 mm, 30 mm, 20 mm, and 18 mm internal diameter solid rings. Complete closure of the internal

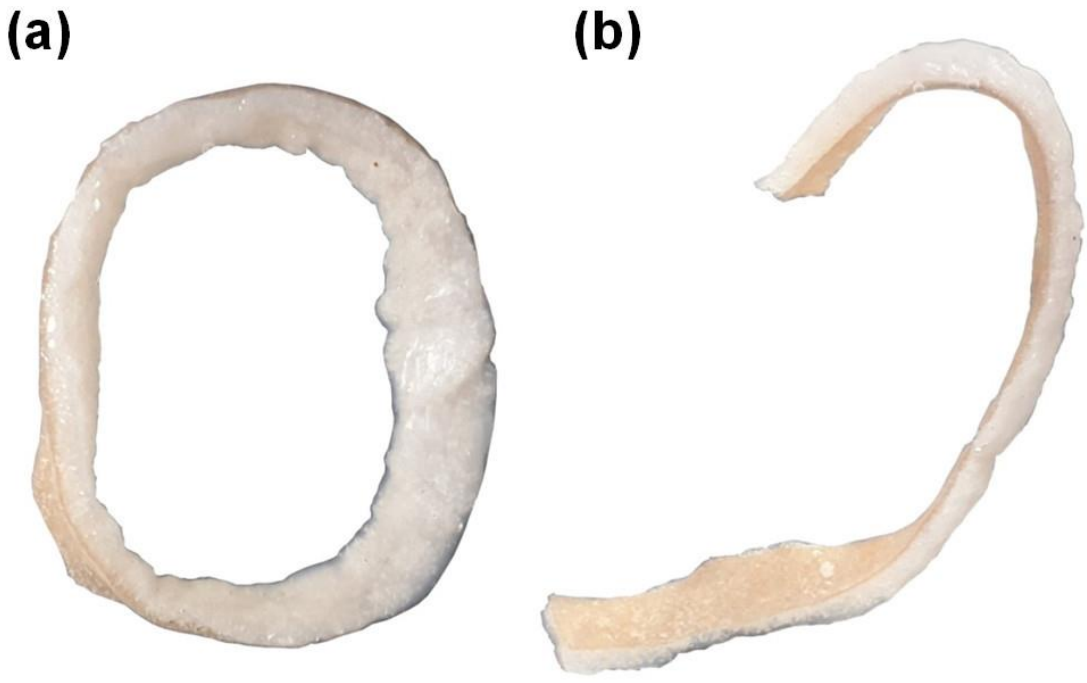

Fig. 18: (a) A complete ring section cut from the tubular multi-layer artificial membrane. (b) The same ring section cut to show the inverted curling of the section as the residual stress within the membrane is relieved.

lumen occurred at an external circular constriction of 18 mm in diameter. The folding and buckling patterns of the inner sponge soft silicone layer were intended to mimic the biological patterns observed from a human stomach.

Analysis of the images in Fig. 19 using image processing software (ImageJ, [185]) was used to calculate the internal cross-sectional area of the lumen with respect to the diameter of the external constriction. The folding of the membrane wall due to the contractions is comparable with the folds found in a human stomach, taken from endoscopic images of the closing of the pyloric sphincter. Fig. 20 shows the correlation between lumen cross-sectional area and the diameter of the external constrictions can be represented by a 2^{nd} order polynomial. This result is useful when determining the amount of external constriction that is required to contract the inner surface of the stomach by a desired amount.

The surface of the inner sponge layer develops small ridges resulting from the compression of the softer sponge material by the outer composite elastic membrane. These ridges are apparent even when the artificial membrane tubing is turned inside-out (Fig. 21). The ridges develop into deeper peaks and valleys as the constriction of the membrane tubing is increased. On further constriction the inner surface ridges begin to collide and compress into each other, occupying any available space and eventually resulting in the lumen becoming fully occluded. The occlusion capability of the sponge when fully constricted has significance for use of this characteristic at sphincter regions of the artificial tract.

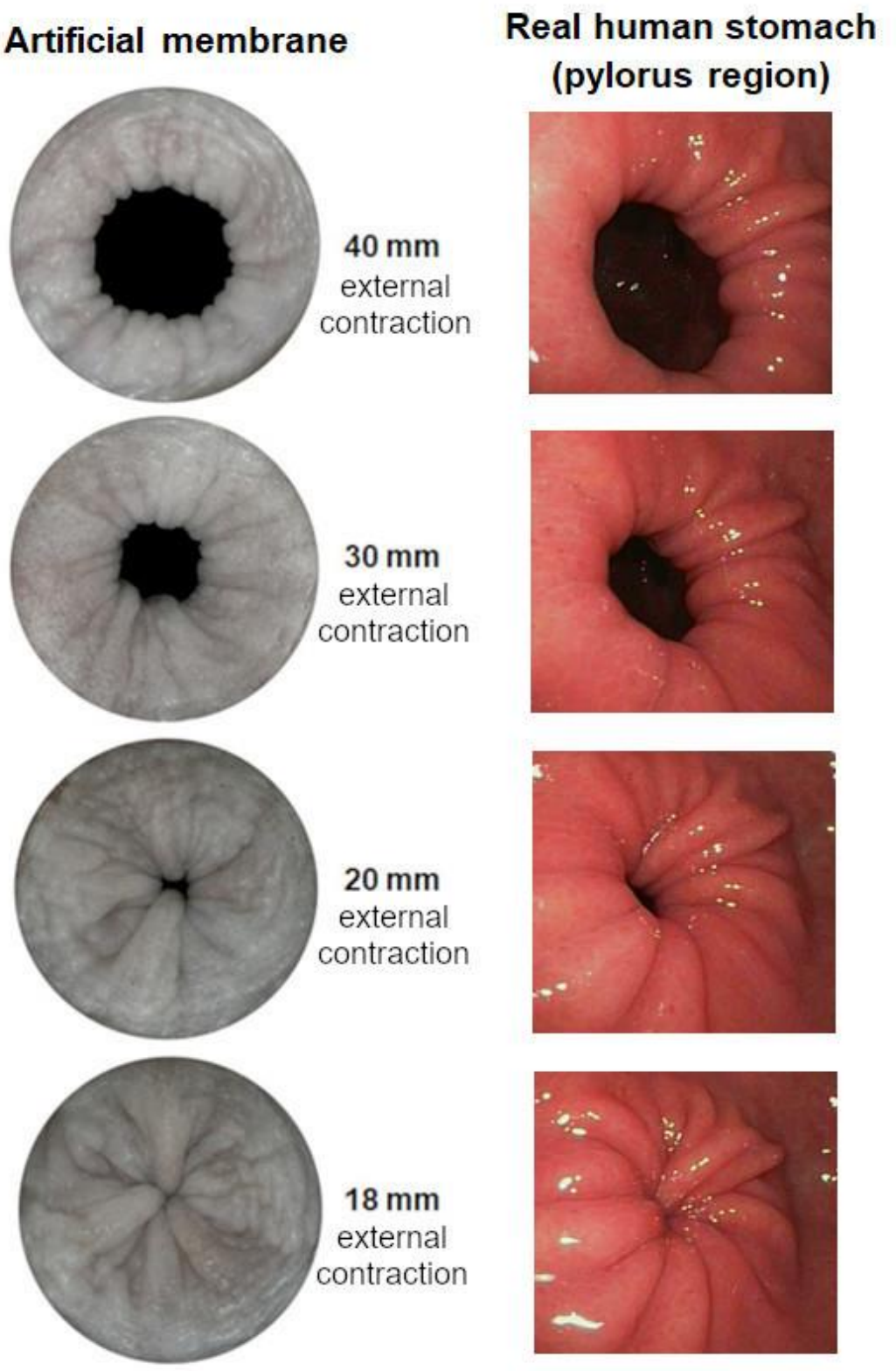

Fig. 19: Demonstration of compressive folding that develops on the inner surface of a multi-layer sponge membrane (left) when different diameters of contraction to the external membrane surface are applied. *Note*: Images of real human stomach sourced from video " Peristalsis in the stomach, endoscopy". Copyright 2023 by Science Photo Library. https://www.sciencephoto.com/media/410578/view/peristalsis-in-the-stomach-endoscopy. Reproduced by permission.

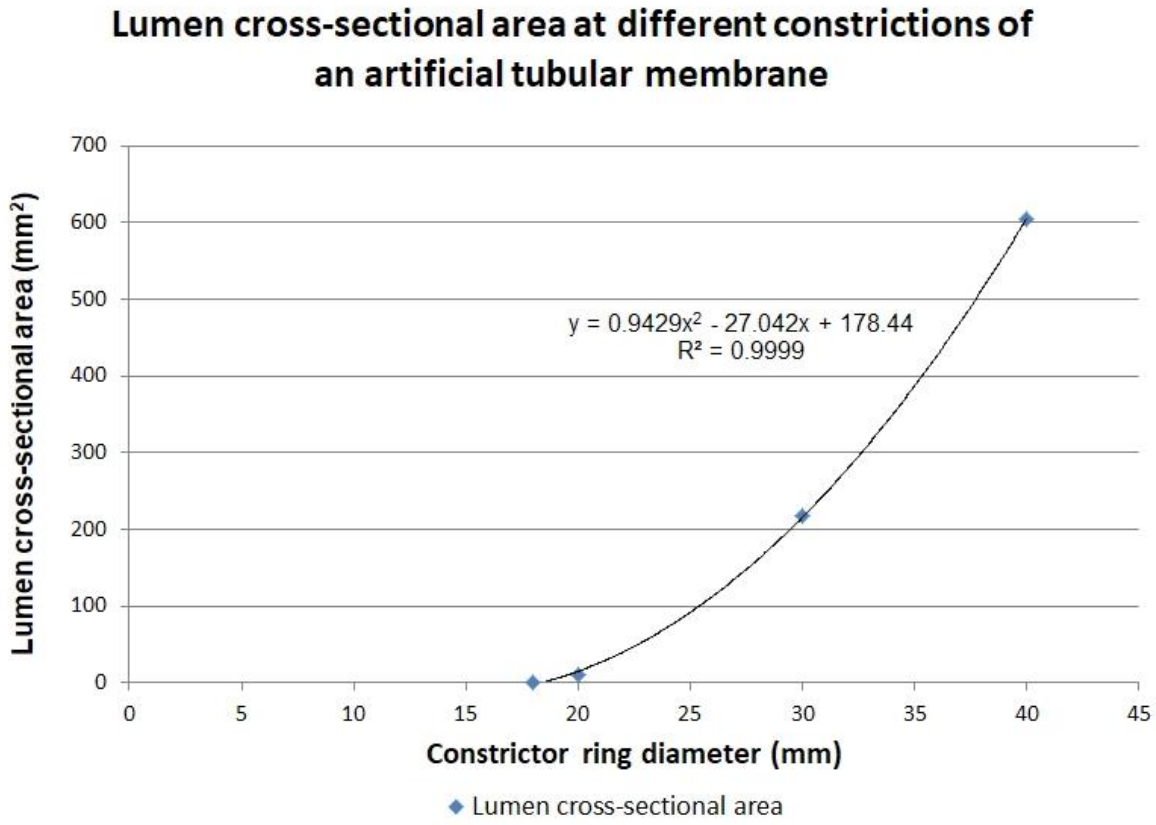

Fig. 20: Chart of the lumen cross-sectional area for an artificial tubular membrane at various external constriction diameters.

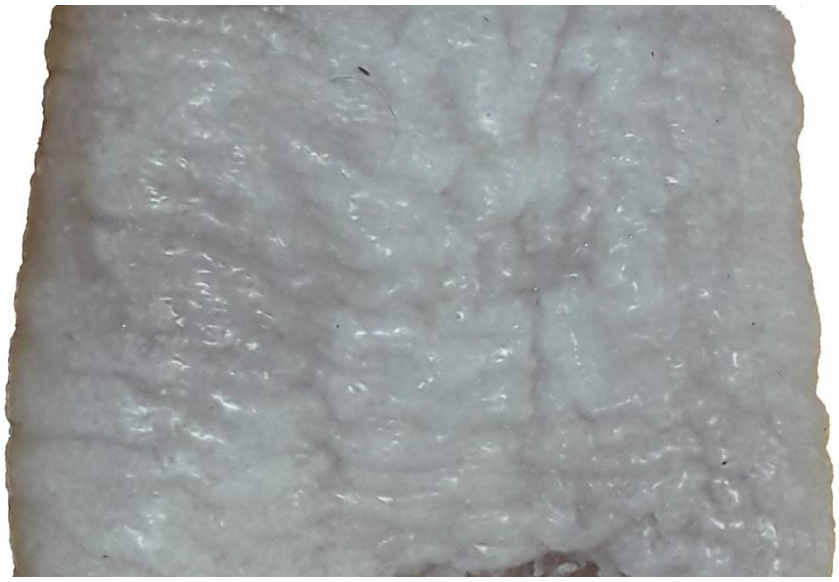

Fig. 21: The appearance of ridges and folding on the surface of the fabricated pre-stressed multi-layer artificial membrane tube prior to turning the tube inside-out.

Some types of artificial muscle or unit constrictors may be embedded directly within this type of sponge material. The main requirements are that the operation of the constrictor is not restricted in movement by the surrounding silicone sponge and that the 'muscle' remains located in its original position. This becomes apparent when the surrounding silicone sponge gets entangled within the constrictor material as it is being constricted; reducing its ability to attain its full constriction range and creating wear on the silicone material by the repetitive abrasive action from constrictor movement. Eventually the action of the constrictor may result in it cutting through the surrounding sponge material to the membrane surface, effectively dissecting the membrane as it does so.

To reduce the abrasive effects of movement from the constrictor against the silicone the constrictor could either be separated from the silicone by a protective layer, or the movement between constrictor and silicone could be minimised as much as possible. Providing a protective layer between the constrictor and silicone layers proves difficult as the protective layer was also required to expand and contract along with the silicone membrane and constrictor. Plastic films were considered but were found to degrade and rupture against abrasive action. Use of the composite elastic membrane as a surface layer, or the minimisation of any contact movement between the constrictors and the silicone layer, are viable options for reducing abrasive wear on the sponge material.

Holes or tears in the sponge material can be repaired by adding patches of uncured silicone-sugar mixture to the affected areas. The cured mixture requires dissolution of the templated sugar prior to use, but the resulting adherence of silicone to silicone is strong and the membrane will again take on the appearance of a single structure with homogenous physical properties. This ability to add sections of sponge material to itself after the sugar has been

dissolved from the original material, and that it can be applied to other surfaces such as fabrics and pure silicone, shows that the sponge material can be added to other membrane surfaces after their initial fabrication. This suggests that the sponge material could be added to silicone sponge surfaces, pure silicone surfaces, or even silicone-fabric composite membranes in a way that they can provide open-cell porous sections or pathways through a non-porous membrane structure. This suggests suitability for the material to perform as some form of artificial mucosal layer.

A disadvantage to use of the silicone sponge material as an artificial membrane layer is a reduction in transparency of the silicone due to its cellular structure. The matrix of voids within the silicone refracts visible light which causes the material to become opaque. Some amount of translucency can be regained if these voids are again filled with a clear liquid, but the level of transparency is less than that obtained with pure silicone rubber. The application of sponge material as an inner porous layer is also likely to reduce overall transparency or translucency of a multi-layered artificial membrane significantly.

The mechanical strength of the sponge material is also affected by the density of its porous structure. Silicone sponge material is softer and less stiff than pure silicone but also susceptible to increased tearing at large strain. If the sponge material is not reinforced *e.g.*, embedded with an elastic fabric, the thickness of the sponge is required to be significantly increased to achieve similar strength properties to solid silicone membranes. This material is therefore not considered to be ideal as an artificial membrane on its own but displays potential as a lining material for the inner surfaces of a composite membrane, due to its porosity and absorption capabilities as well as its compressibility and folding characteristics. Silicone sponge absorption capabilities require further investigation for its use as a liner

material in an artificial stomach, as unadulterated silicone sponge is hydrophobic but will readily soak up oils and organic solvents [171, 173].

3.3. Summary

Mimicry of the physical characteristics of a biological stomach tract wall can be achieved by using a multi-layer approach in the fabrication of a membrane for an artificial stomach reactor. One approach involves using a combination of a reinforced outer layer made from a composite of silicone rubber and elastic nylon fabric material, a compressible porous middle-layer made from silicone sponge, and an internal surface layer made from soft silicone to act as a barrier against fluids and gastric contents. The three layers demonstrate mimicry of the biomechanical characteristics of the extra-cellular matrix (ECM) and serosa, the sub-mucosal layer, and the mucosal layer of the biological tract wall, respectively. Pre-stressing of the layers, by stretching them prior to the addition of subsequent layers, can result in the appearance of contractive and folding characteristics like those of biological systems. The combination of physical characteristics and material properties contributed by each of the individual layers results in a composite material that demonstrates suitability as a biomimetic stomach membrane.

The muscles

Chapter 4 – The Muscles

Digestive tract motility is dependent on the contraction and expansion interactions occurring between the muscle layers in the longitudinal and circumferential orientations of the tract [1]. During peristaltic contractions, the longitudinal muscles relax, extending as the circumferential muscles contract. Similarly, the circumferential muscles relax as the longitudinal muscles contract. Mimicry of this basic expansion and contraction interaction between the muscle layers can be challenging to achieve in a controlled physical model.

Artificial muscles mimicking those of the stomach require physical characteristics resembling biological smooth muscle including contraction force, contraction range, flexibility, comparative size and form, connectivity to the membrane, and controllability. Several innovative designs of 'soft' actuator have been considered that attempt to simulate these muscle characteristics. They incorporate linear compressive and expansive actuation in combination with material flexibility, allowing the artificial muscle segments to flex and bend in response to external forces.

This chapter describes the development of artificial muscle actuators and their implementation including unit constrictors, deforming braided membrane structures, tendons and Bowden cables, and an exploration of aspects of reactor membrane and muscle interconnectivity. Section 4.1 involves the development of a range of individual artificial muscles, or unit constrictors. The unit constrictors are made from inexpensive nylon fishing line or expandable braided sleeve and are designed to replicate the action of separate bundles of muscle. An evaluation of potential connection methods for attachment of the artificial muscles to a flexible elastic membrane is included. Section 4.3 introduces a tubular braided membrane structure for moving and mixing materials using controlled peristaltic

deformation patterns. The remaining section (Section 4.4) investigates the use of Bowden cables for providing distanced actuation of the artificial muscles through the pulling of flexible tendons. 'Tendons' refer to the flexible line or cable that passes through the artificial muscles and hollow Bowden cables.

4.1. Unit constrictors

This section describes the development of a range of artificial muscles made from inexpensive expandable braided sleeve and nylon fishing line that effectively mimic several desired characteristics of biological smooth muscle including:

i. they provide sufficient contractive force whilst maintaining a highly flexible form
ii. they will relax back to their original unloaded length
iii. they are sufficiently small and compact in size to be embedded within, or on top of, another layer of membrane material
iv. they can maintain a layer thickness comparable to actual muscle layer thickness, and
v. they can be effectively controlled via tendons pulled by basic winding mechanisms.

Biological muscle action involves a strong unidirectional contraction only. As the muscle cells are relaxed a reciprocal muscle action, acting in another direction, is required for the muscles to extend and return to their original length. This suggests that a reciprocal pair of artificial muscles may be used to mimic the action that biological muscles display. However, the need for a reciprocating pair of artificial muscles may not be necessary if the returning action of the muscle can be carried out passively by design.

There are a variety of 'soft' artificial muscles that have potential to display characteristics and properties like those of the smooth muscle layers of the gastrointestinal tract including;

electro-active and photo-active polymers [99-102], electrically-driven hydrogels [103-107], phase-change materials [108], pneumatic or fluid-driven actuators [109-111], shape memory alloys [112], twisted nylon fishing line or thread [113-121], origami or kirigami based actuators [109, 122-124], knitted or woven textile actuators [186] and worm-like peristaltic locomotion robotic platforms [129, 131, 132, 187-197]. Many of these artificial muscles may be cost-prohibitive, difficult to effectively implement or control, or require complex fabrication methods. Some of them are only partially soft in their construction as they can require rigid or solid materials to complete their actuation capability or to contain the artificial muscle. Others may require heating or produce significant amounts of heat during operation, which could complicate temperature control of the stomach reactor.

An external or indirect force applied to the flexible surface of a membrane is a common approach for many dynamic *in vitro* gastric tract simulation models that employ some form of mechanical muscle actuation [24-28, 67, 68, 70, 71, 79]. The artificial muscles are typically not physically attached to the membrane but instead provide an external force or pressure that deforms the surface of it, therefore the membrane moves with the muscle action, but the muscles do not necessarily move with the membrane surface as it deforms elsewhere along the tract. Membrane surface deformation created from detached, externally applied contractions can result in limited ability to control the overall deformation pattern of the membrane wall.

To effectively mimic artificial smooth muscle the unit constrictors should be able to passively flex and elongate or extend along with the membrane surface. If the artificial muscles are bonded or attached to the membrane, then they will follow the stomach wall as it moves and deforms. Without this characteristic the muscles could restrict much of the

deformation that typically takes place. Fully attached constrictors can also passively provide compressive stress to the membrane that mimics the contractive and folding characteristics of actual biological gastric wall tissue when in an un-filled state *i.e.*, mimicry of the folding that results from differences in tissue growth rates between the inner mucosal layer of the wall and the muscle tissue layers [47], and the residual stress that these different growth rates create [39].

A further requisite for the effective use of simulated artificial muscle bundles is that they can be linked together in some way. The interconnected artificial muscles can then mimic a single unified layer of muscle that can be built into, and become, an integral part of the reactor membrane. A unified muscle layer made from individual unit constrictors allows for various sections of the layer to be controlled independently, and subsequently behave in a manner like that of the mimicked biological material. An example of this is the action of peristalsis, where the contraction of a series of adjoining muscle bundles are triggered in sequence, one after the other, to create a wave-like contraction pattern. Attachment of the unit constrictors directly onto a contiguous substrate or layer of elastic material would achieve the desired connectivity and interaction between each constrictor and form a layer of artificial muscle.

The unit constrictors described in this section have ability to contract and yet return to their original length upon relaxation. The returning action comes from compression of a coil or set of coils during the contraction of the unit constrictor. The stored energy of the compressed coil provides a restoring force for the unit constrictor. This allows the artificial muscle to perform constrictive actions and then return to its original un-loaded length without the need for a reciprocal set of artificial muscles. The compact design of this

artificial muscle also means that it has a small footprint on the reactor and requires few additional mechanisms to be put in place to control the muscle action.

4.1.1. Coiled nylon fishing line

Commercial nylon fishing line is a low-cost material that can come in a wide range of diameters and rated tensile strengths. Nylon line was selected because it is non-metallic, has high flexibility, and provides low a surface friction against many types of material. Coiled nylon unit constrictors were fabricated using 0.4 mm, 0.57 mm, and 0.8 mm diameter commercial nylon (polyamide 6/6) fishing line to provide actuation mechanisms for simulating the contraction of individual muscle sections or bundles of muscle tissue. The unit constrictors were designed in the form of a compressible spring by tightly coiling nylon line over a solid rod or mandrel and heat-setting the coils in place. Flexible tendons or lengths of nylon line were threaded through each coil to provide cable-driven actuation for the compression and expansion of the unit constrictor.

Nylon line from each of the different diameters were cut from rolls of fishing line and wound around mandrels made of solid steel welding rods of 1.2 mm and 1.8 mm diameter. A mandrel was inserted into a cordless electric-drill chuck along with one end of the nylon line and the chuck was closed around them so that they were held in place. Another short length of 2.4 mm steel rod was held perpendicular to the mandrel so that a consistent spacing between the formations of each rotation of the coil could be made. The drill was then slowly turned to wind the nylon line as a helical coil around the mandrel.

When a 100 mm length coil had been formed the nylon was held in place with adhesive tape to prevent it from uncurling. The nylon was then annealed by passing it over a 200° Celsius temperature source, provided via a heat-gun, so that the nylon would soften to a glass

transition state and the residual stress energy formed in the coiling process could be released. Once it had cooled to room temperature the same annealing process was repeated two more times to ensure that all residual stress was removed from the nylon and that the coil would not unwind when removed from the steel mandrel. To complete the coil as a unit constrictor a length of flexible line was threaded through each of the prepared nylon coils to act as a contractive tendon or cable (Fig. 22).

4.1.2. Expandable braid

Expandable braided sleeve is commercially available as a cable management product and is made from numerous thin flexible thermoplastic filaments that are woven to create a hollow tubular strip of intertwined helical coils. Manufacture of the expandable braid is undertaken

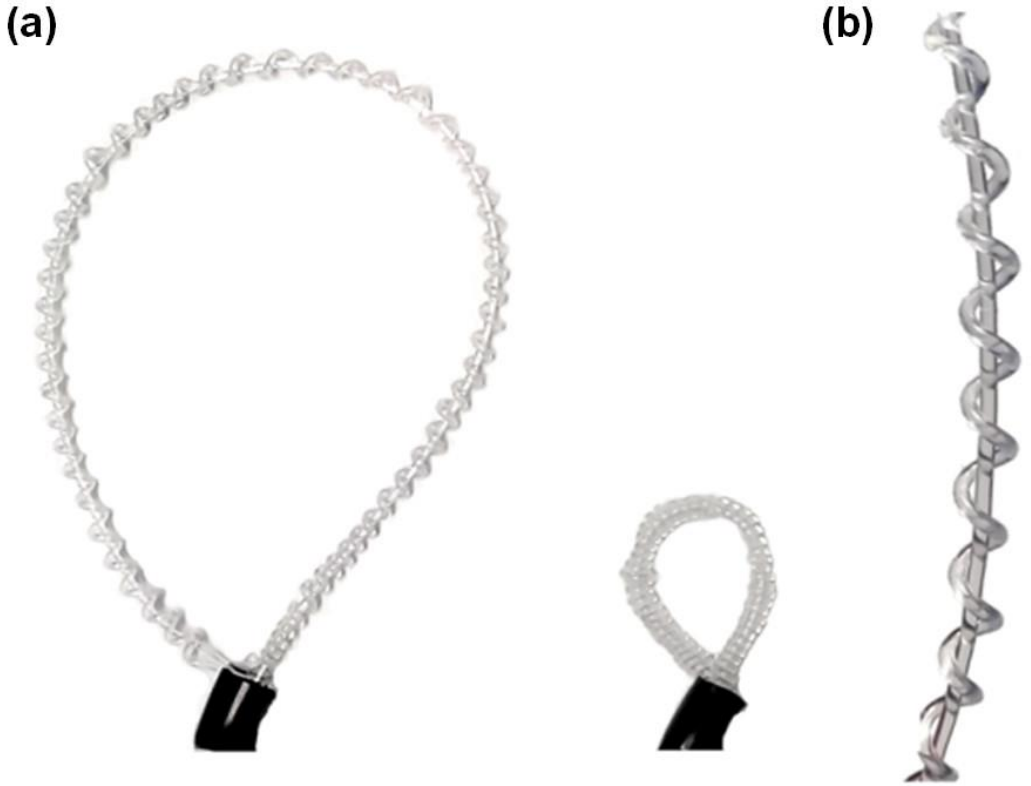

Fig. 22: (a) Looped nylon spring coil unit constrictors in both an expanded and contracted state. (b) A close-up image of the nylon coil showing the tendon threaded through it.

via complex mechanical rotary braiding machines known as 'maypole' braiding machines [198] and similar expandable braid materials have been used with pneumatic balloons in McKibben-type artificial muscle actuators [199, 200]. As this braid is constructed from numerous helical coils it has similar spring-like attributes to that of a single coil spring, however the intertwined helices of the braid threads are orientated in both clockwise and anti-clockwise directions which cause the braided material to form a tubular shape that will expand transversely as the tube is constricted longitudinally.

Lengths of 3 mm diameter expandable braid, left in the unexpanded state, were cut using a hot knife to prevent the ends from fraying. A flexible nylon tendon was threaded through the centre of each length of braid to provide a means for constriction of the expandable tubing. Loops of artificial muscle can be created by connecting the two ends of braided tubing together and providing a single outlet point for the nylon tendon. Expandable braid is made from fine threads of polymer that exhibit spring-like characteristics like those of the coiled nylon line. The braid also displays a similar ability to self-return to its original unloaded length when in a relaxed state (Fig. 23).

4.1.3. Unit constrictor contraction force tests

Contraction ratios were obtained from unit constrictor samples by dividing the change in circumference, or perimeter, for each constrictor ($P_i - P_f$) by the unit constrictors' initial circumference (P_i) and multiplying the result by 100% (Eqn. (4-1)). A negative contraction ratio would therefore indicate that expansion has taken place.

$$contraction\ ratio = \left(\frac{P_i - P_f}{P_i}\right) \times 100\% \qquad (4\text{-}1)$$

Where: P_i = initial looped unit constrictor circumference, P_f = final looped unit constrictor circumference

The tensile and contraction tests were undertaken on a universal testing machine (Instron 5960 Dual Column Tabletop) at a velocity of 250 mm per minute using a 30 kN load cell. The tests involved attaching the nylon coil type unit constrictors to the universal testing machine grips and contracting the coils. A 1.0 mm diameter rigid brass rod was used to act as a tendon for the constrictors so that they would not buckle out of axis as they were being contracted. One end of the brass rod was looped to prevent it from pulling through the spring-coil or braided tubing. Contraction tests required a custom-made rig that held each constrictor in place at the lower testing machine grip while the solid brass rod, acting as a tendon, ran through the centre of the constrictor and was connected to the upper grip of the testing machine. The solid rod was displaced by the upper testing machine arm so that the force used to contract the unit constrictor could be measured.

The maximum contraction ratio that can be achieved differs between nylon spring coils depending on the original helix angle provided during their fabrication. To minimise any

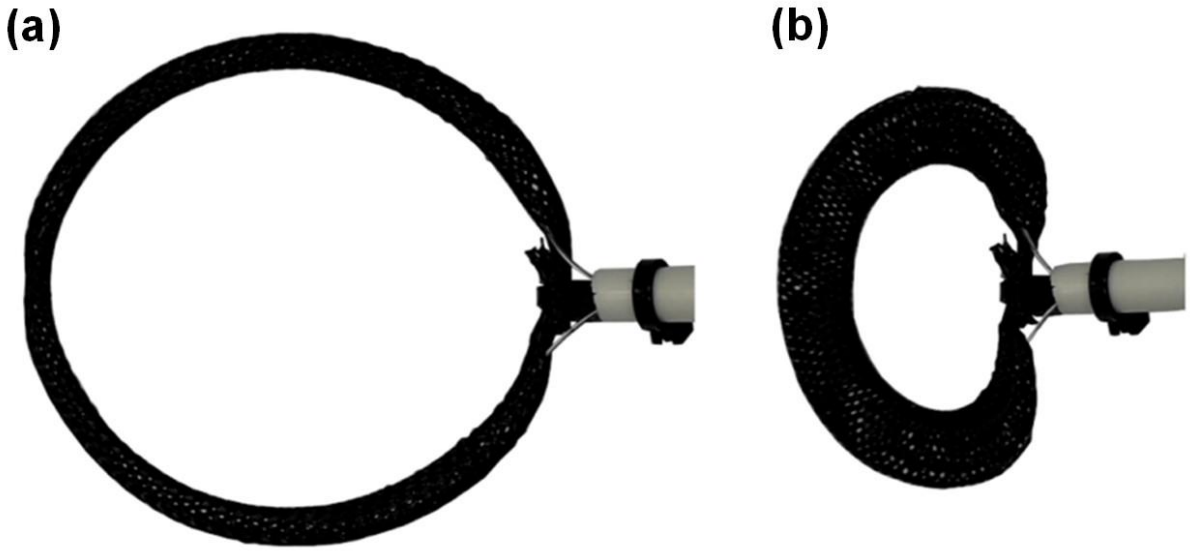

Fig. 23: A loop of expandable braid tubing being contracted from its relaxed state (a) to its fully-constricted state (b).

differences in the resulting contraction ratio all nylon spring coil samples were given an initial helix angle of 45°.

Testing of the coiled nylon line unit constrictors indicate a linear stiffness during the linear contraction and extension tests (Fig. 24 and Fig. 25). The contraction ratio of the coiled nylon line unit constrictors, when the coil was turned end-to-end into a loop, can reach over 60% from its original unloaded or 'relaxed' length (Fig. 26). The contraction ratio of the braid can reach also reach over 60% of its initial extended length, which is on par with the maximum contraction ratios exhibited by the coiled nylon. The stiffness of the monofilament nylon coils appears to increase as the diameter of the nylon used is increased. Looped and linear forms of the expandable braid unit constrictors showed non-linear stiffness during contraction (Fig. 27).

Various nylon line coil constrictor widths can be created by changing the diameter of the nylon line and the internal diameter of the spring as set by the diameter of mandrel used for winding of the spring-coil. Fig. 28 shows two unit-constrictors of different widths, 3.4 mm, and 1.2 mm. Altering the width of the unit constrictors can be useful when attaching them to a smaller or larger size of the artificial stomach shell, the number of 'muscle bundles' that can potentially be placed over a specific region can be increased when the unit constrictors are of smaller or narrower width. For example, the fabrication of a stomach reactor to mimic a child's stomach would benefit from use of narrow unit constrictors due to the smaller surface area available over the stomach wall.

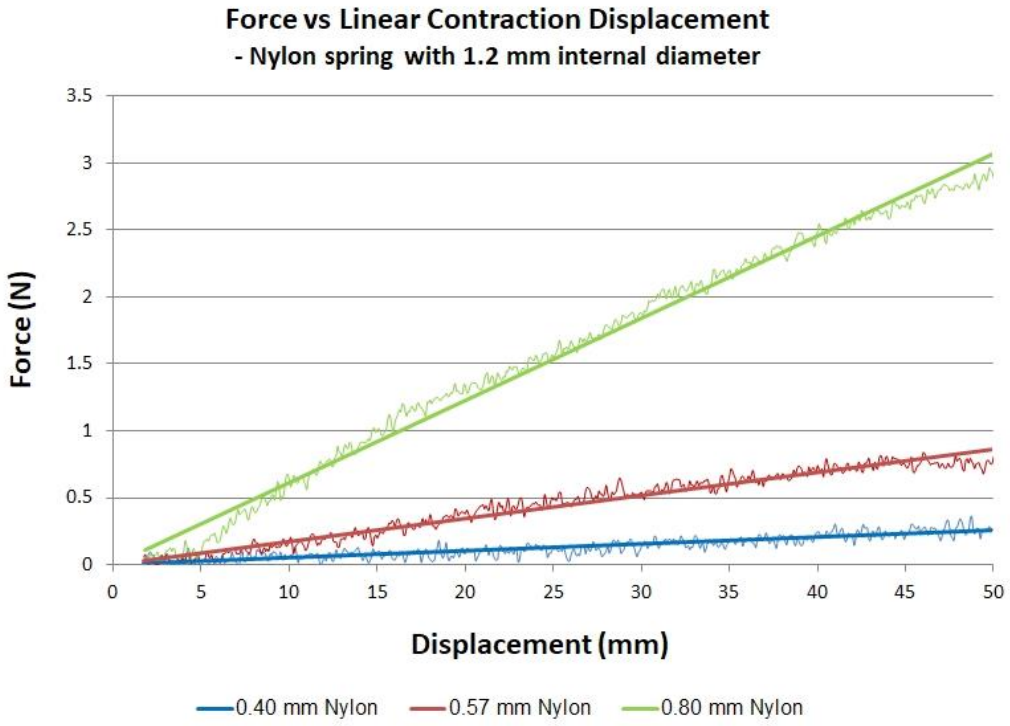

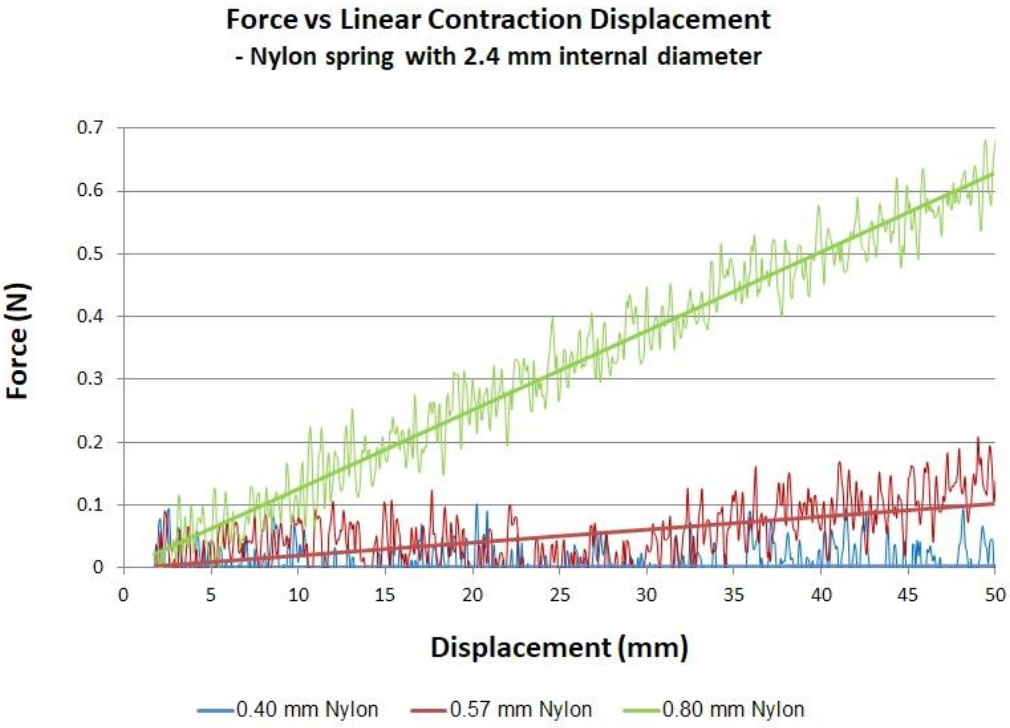

Fig. 24: Compression test results of 0.4, 0.54, and 0.80 mm monofilament (a) Nylon springs made with 1.2 mm internal diameter and (b) 2.4 mm internal diameter.

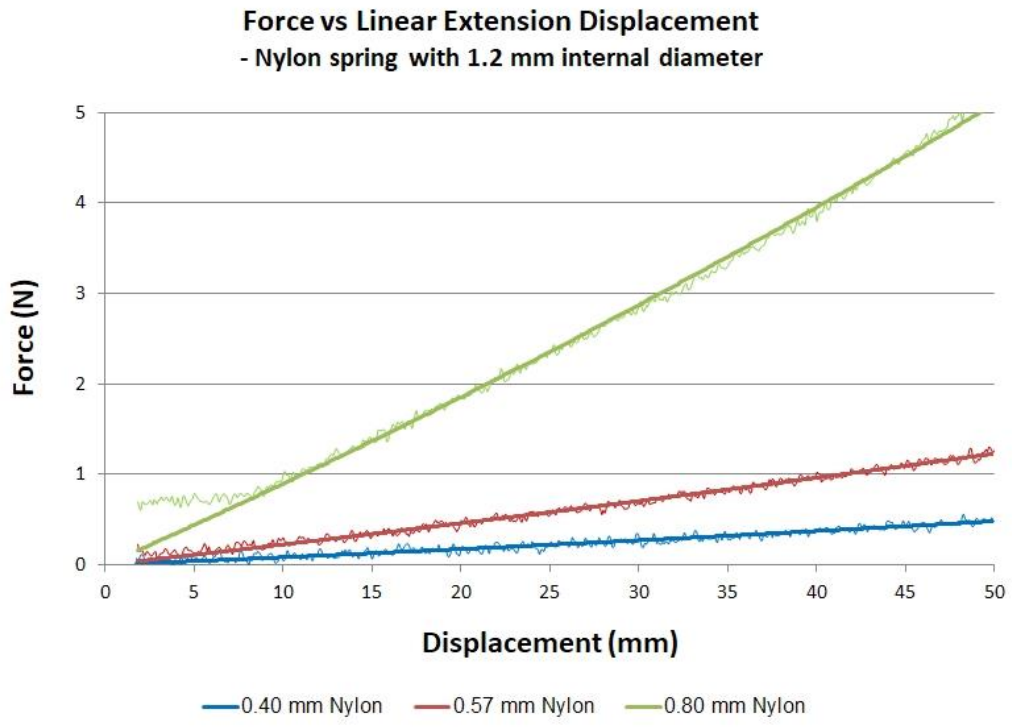

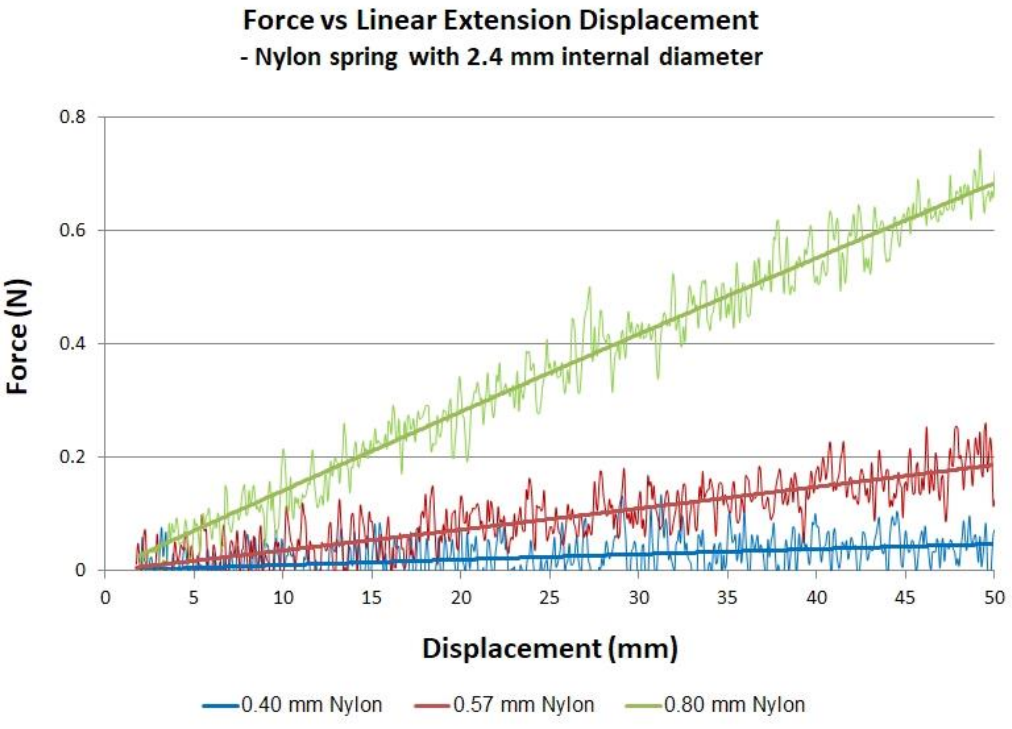

Fig. 25: Extension test results of 0.4, 0.54, and 0.80 mm monofilament Nylon springs made with (a) 1.2 mm internal diameter and (b) 2.4 mm internal diameter.

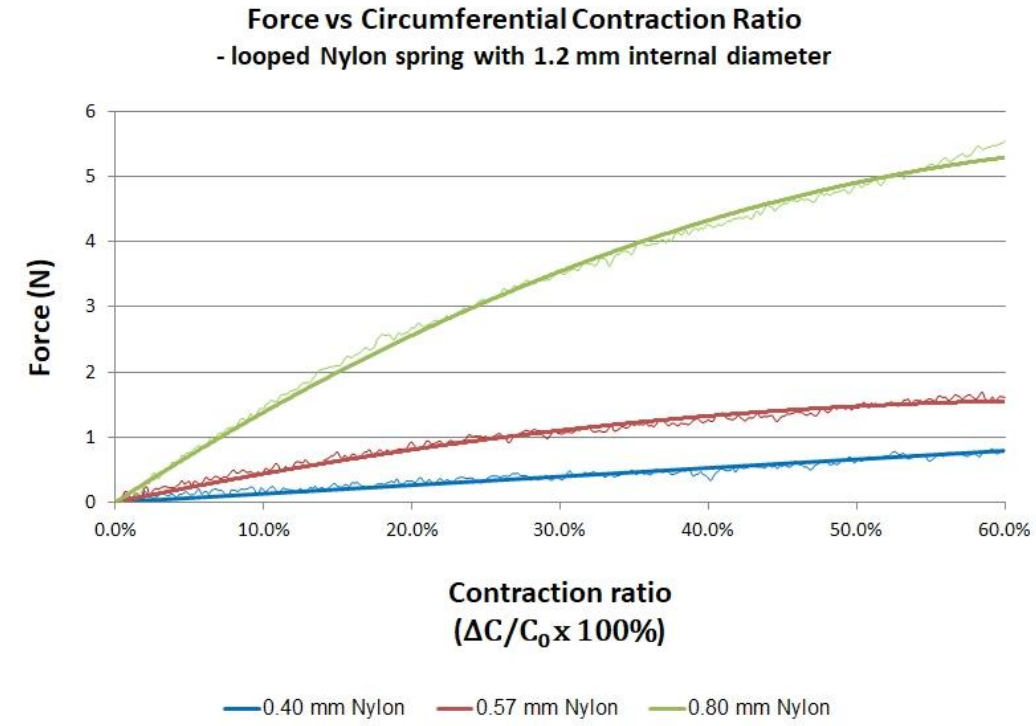

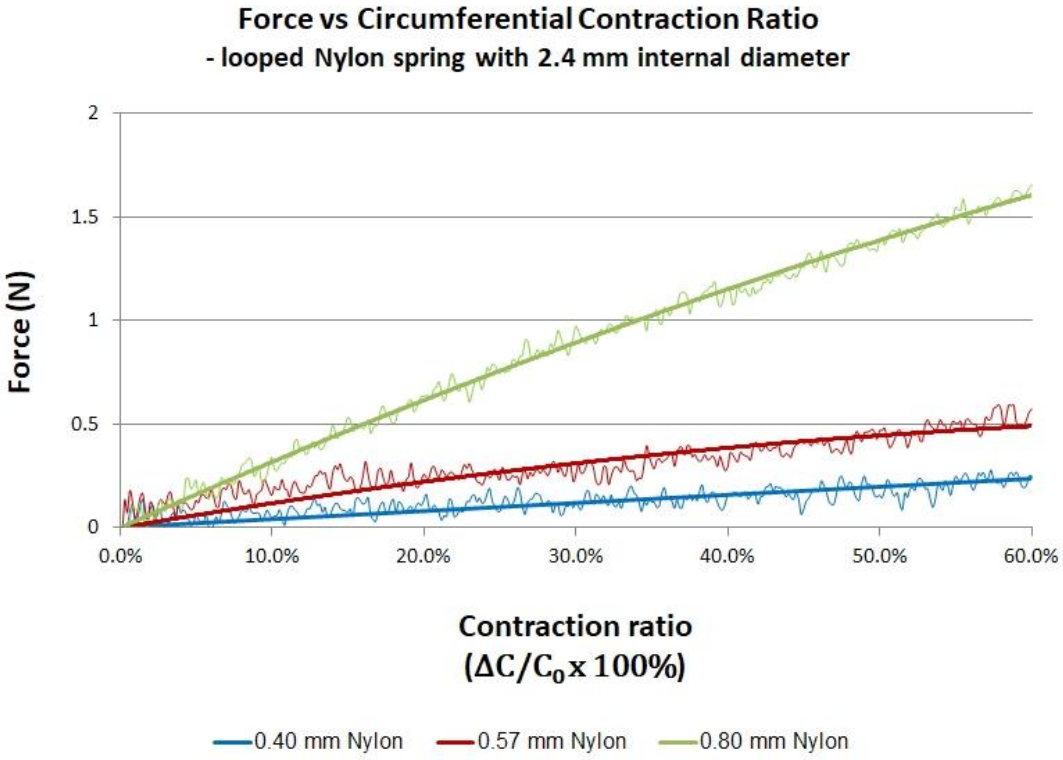

Fig. 26: Force versus contraction ratio test results of looped monofilament nylon springs made with (a) 1.2 mm internal diameter and (b) 2.4 mm internal diameter.

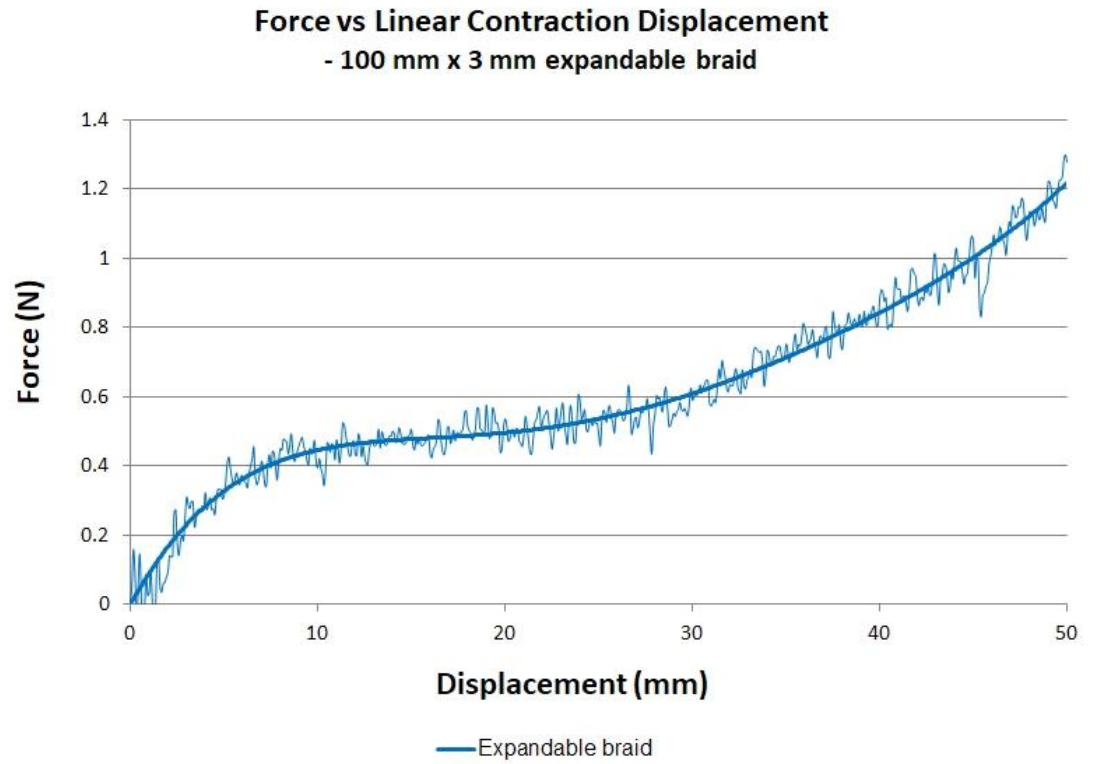

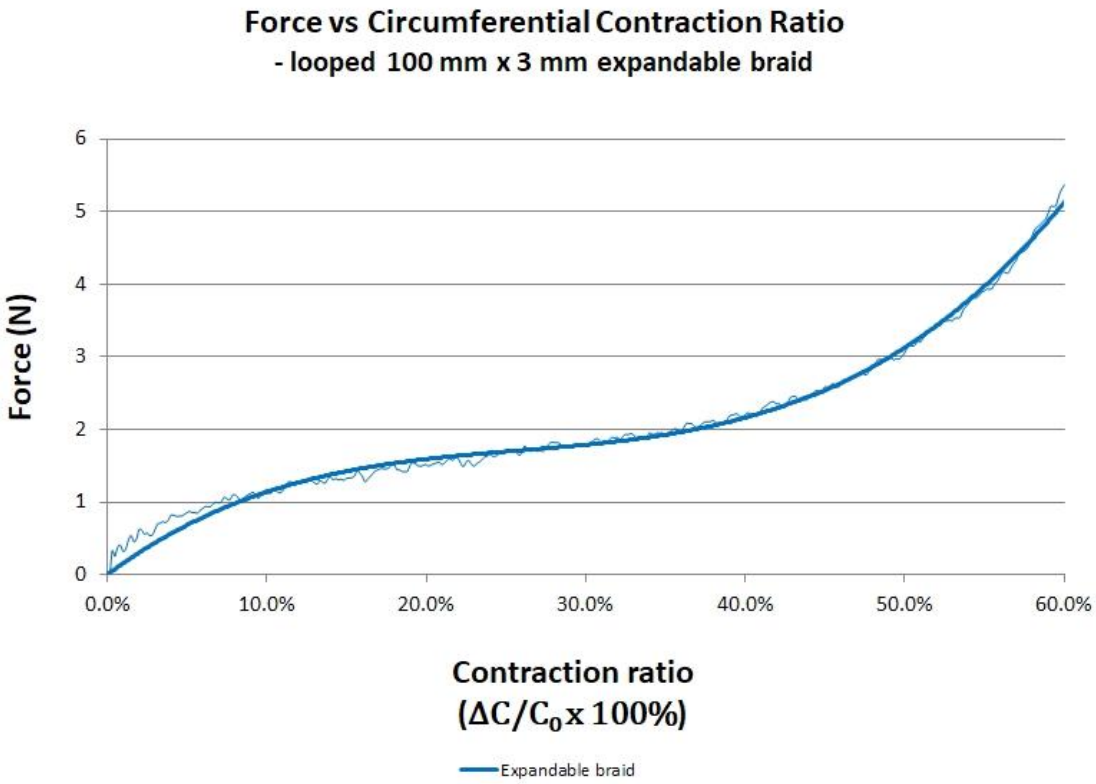

Fig. 27: (a) Force versus compression and (b) force versus looped contraction ratio test results of expandable braid.

4.1.4. Connecting unit constrictors to a membrane

Several different methods for interconnecting the two types of unit constrictors to a membrane were explored including embedding the constrictors within multiple layers of membrane material, attachment of the expandable braid via flexible intermediary materials that adhere to silicone, and the sewing or tying of the nylon coils directly to the embedded fabric material of the membrane. Individual constrictors made from lengths of expandable braid can be combined into a structure of interconnected longitudinal and circumferential artificial muscles that can be 'morphed' (Fig. 29). A model was fabricated from expandable braided tubing lengths that were measured to match the dimensions of a 150% scaled

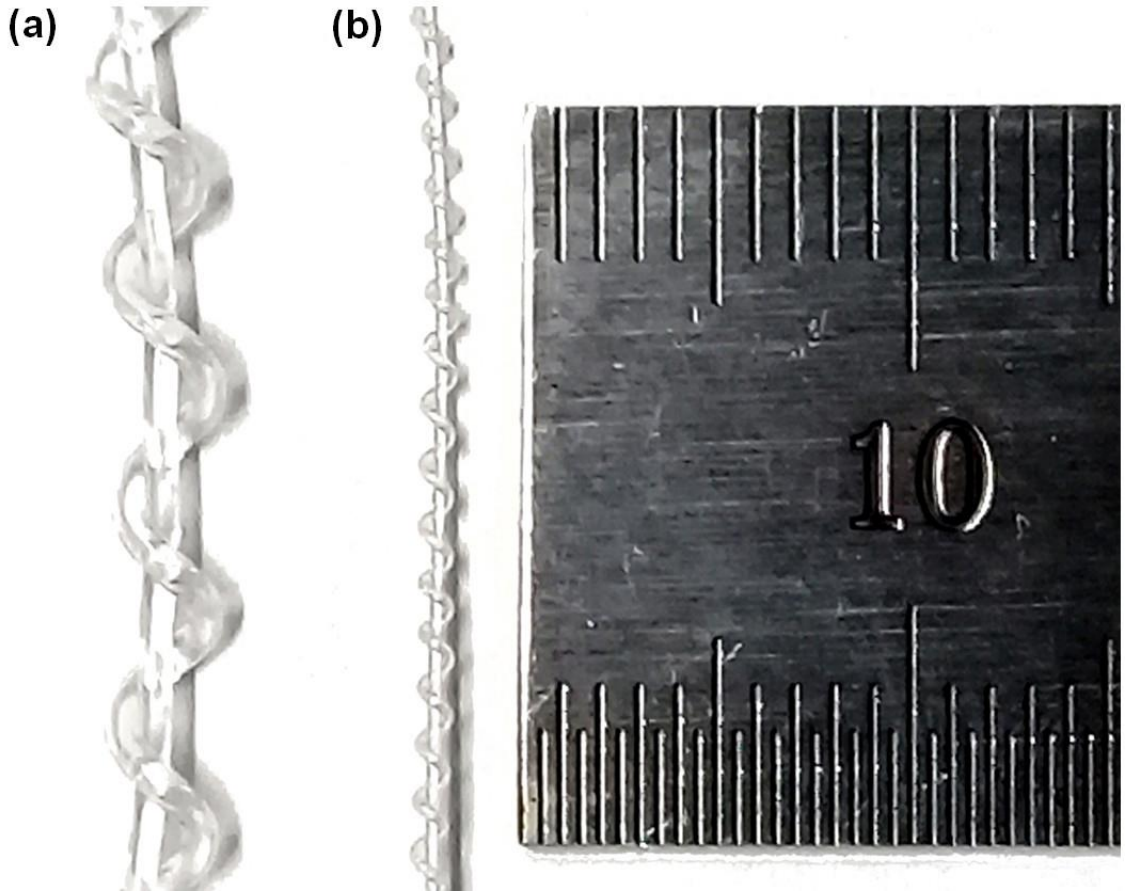

Fig. 28: Coiled nylon unit constrictors of (a) 3.4 mm and (b) 1.2 mm width. The scale is shown in millimeters.

version of an actual stomach derived from a three-dimensional CAD model of a scanned human stomach (BodyParts3D, © The Database Center for Life Science licensed under CC Attribution-Share Alike 2.1 Japan). The network of artificial muscles can have the expandable braid unit constrictors independently actuated to morph various regions of the structure and return it to its original structural form when they are relaxed. Peristaltic operation of the constrictors remains possible even when the structure has been morphed to an entirely new form and the stomach has taken on a new shape.

The structure of the morphing interconnected expandable braid tubes maintains a good correlation to the general form of a stomach. Actuation of the individual constrictors also allowed for changes in the overall shape to be made or for a sequence of peristaltic contractions to occur. However, connecting a membrane to the muscle structure proves difficult. The braided tubing does not adhere well directly to silicone surfaces and loosens from the membrane material after multiple contractions of the constrictors. The braided

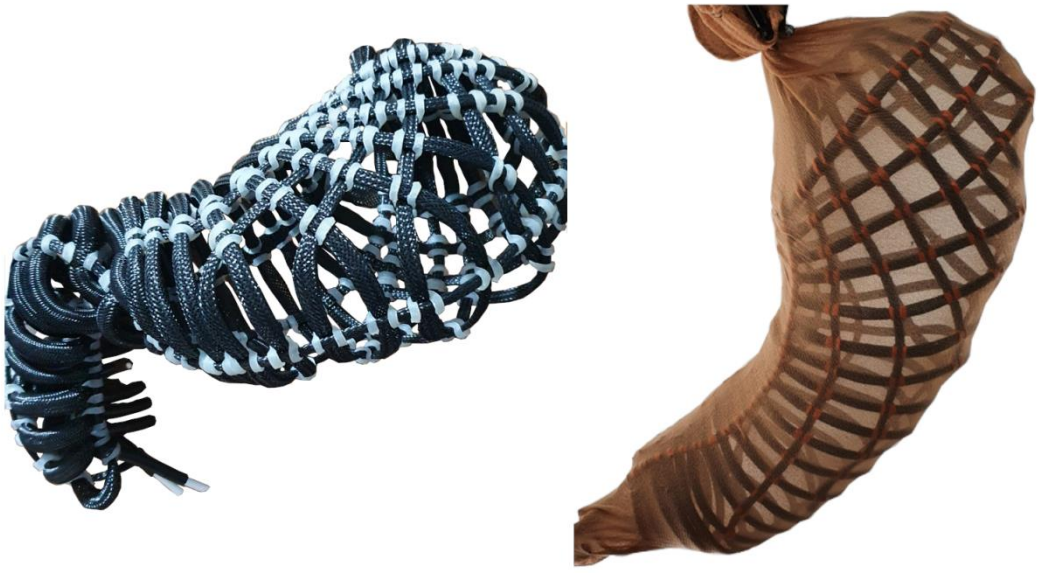

Fig. 29: Examples of interconnected expandable braid artificial muscles forming a 'morphing' stomach shape.

tubing also tends to twist and buckle when undergoing contractions, causing it to pull away from the material it is attached to. Another disadvantage was the expandable braids' inability to extend sufficiently. The braid unit constrictors could initially be heat-set at a semi-constricted length to provide some additional allowance for extensions to take place, but the overall range of extension and contraction of the expandable braid was more limited than that displayed by the coiled nylon spring unit constrictors.

One method explored to maintain connection between the expandable braid tubing and the membrane was to use an intermediary material. The material would need to adhere well to silicone while still being connected to the braid, allowing the unit constrictors to flex and move more freely when actuated. This intermediary material would mimic the extracellular matrix (ECM), a layer composed of collagen and elastin tissue that connects the various layers of the gastric wall. A soft silicone sponge strip, with holes in it to allow the threading of the unit constrictor through it, was used for testing this method of connection (Fig. 30). The sponge strips can be bonded directly to a silicone membrane layer at various points along their length. Solid silicone strips were initially trialled but were found to be much stiffer than the silicone-sponge material, required a significantly greater force for achieving actuation, and caused the membrane to buckle in an uncontrollable manner when contractions were applied.

Another connectivity approach was to embed the unit constrictors within multiple layers of membrane material. This approach mimicked the multi-layered structure of the biological gastric wall. Unit constrictors were placed as a separate layer over the artificial membrane and then covered with another layer of membrane material (Fig. 31). The constrictors were able to contract within the layers they were embedded in and remained in a fixed location

on the membrane. Single unit constrictors were able to be effectively embedded, but challenges were experienced with the side-by-side embedding of multiple constrictors.

It was difficult to create an adequate bond between the inner and outer membrane layers so that adjacent unit constrictors were kept apart. The multiple layers also increased overall stiffness of the membrane. The increased stiffness of the membrane caused excessive buckling and folding to occur over the artificial gastric wall. It also created torsional deformation of the embedded unit constrictors when they were contracting, and a larger tension force was required when pulling the tendons during actuation of the artificial muscles.

Fig. 30: An example of expandable braid unit constrictors threaded through flexible silicone sponge strips and placed over a silicone stomach shape.

Nylon spring-coil constrictors can be directly tied onto the surface of an artificial composite membrane. Tying onto the membrane is best done while the membrane is placed over a rigid form, as in the flat wooden template form described in Section 3.2 (Fig. 9). Using a rigid form as a backing material makes it easier for positioning the unit constrictors into their correct locations. The spring-coils were pre-stressed by extending them by 20% before attaching them over the form. A 0.25 mm diameter nylon line, thread through the membrane material with a needle, was used to tie each of the spring-coil constrictors to the

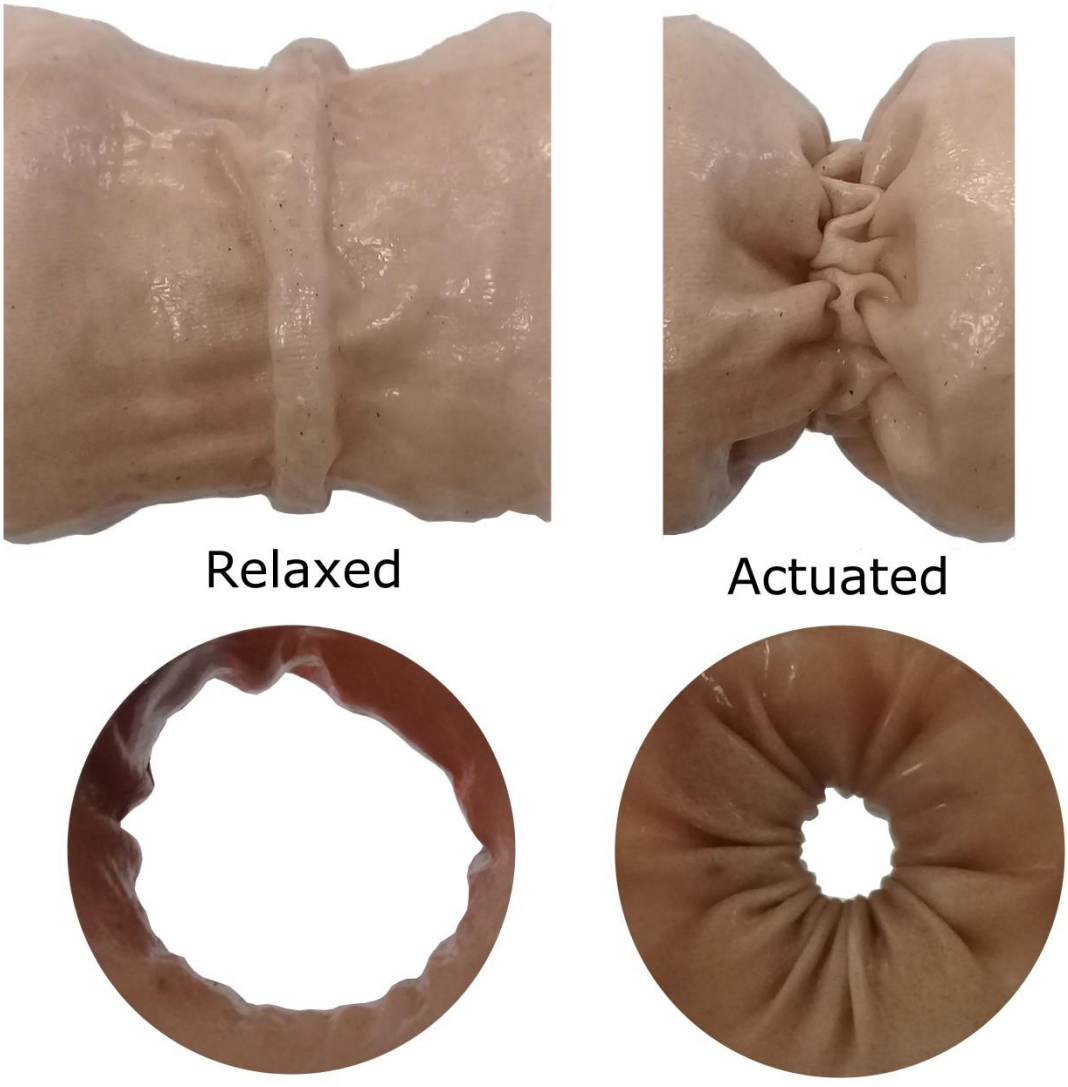

Fig. 31: Unit constrictors embedded within layers of artificial membrane.

nylon fabric layer of the membrane at regular intervals. After tying all the constrictors, the entire membrane was removed from the form and turned inside out so that a layer of silicone could be applied to the inner surface. Upon curing, the additional layer of silicone assisted in resealing the membrane once more to a watertight condition.

In a relaxed state the constrictors would contract a small amount, due to the amount of pre-stressing of the coils prior to attachment, and a visible pattern of folding of the silicone-fabric membrane could be observed (Fig. 32). This folding was created to mimic formation of the rugae folds that appear on the inner surface of the biological stomach wall when it is in an un-expanded state. The observed pattern of folds correlates with the locations on the membrane where the constrictors are physically tied with nylon line. Changing the number of, or distance between, the tied locations of the constrictors can therefore affect the folding pattern forming over the membrane surface.

The unit constrictor type of artificial muscle show good potential for mimicking and simulating the muscular biomechanics of the stomach wall and exhibit several beneficial properties including:

i. They provide a contractive force that can be controlled through applied tension to a flexible tendon.
ii. The amplitude of the contraction can be controlled by the displacement of the tendon.
iii. They maintain a highly flexible form that follows the deformation of the elastic membrane material they are attached to.
iv. They return to the original length and form of the artificial muscle when tension on the tendon is removed.

v. They are small and compact.

vi. They can be embedded within a layer of membrane material or attached close to the surface of an artificial membrane and create 'layers' of artificial muscle tissue.

vii. They have a thickness like that of biological muscle layer thicknesses.

These types of unit constrictor actuators are highly flexible with a controllable contraction rate that can be maintained even when they twist out-of-plane. However, there are some differences between the coiled spring and expandable braid unit constrictors. The maximum contraction ratio achievable by the expandable braid was found to be 70% compared to 80% for the coiled nylon spring unit constrictors. The transparency of the unit constrictors made

Fig. 32: Direct tying of nylon spring coil unit constrictors onto an artificial membrane surface.

from the expandable braid was also reduced due to the number and colour of the threads it was made from and the interlocking weave of the braided tubing.

Contraction of the expandable braid results in a transverse expansion of the tubing material during axial contraction of the coils. Less torsional twisting of the expandable braid would occur compared to the coiled nylon springs, but an increase in twisting of the expandable braid loops is noticeable when the loop diameter was increased in size. The widening of the expandable braid tubing from constriction gives the braided unit constrictors a muscle-like appearance during contractions, as bundles of biological muscle fibre will also thicken as they contract.

The unit constrictor artificial muscles contain no metal or rigid parts, and are remotely actuated via flexible tendons, so they eliminate any need for electrical or thermal operation mechanisms to be placed directly onto, or close to, the reactor membrane. This aspect improves controllability over temperature regulation of the reactor shell, while also allowing for the potential use of magnetic tracing techniques without interference occurring from nearby metal components.

4.2. Braided structures

Some braided structures have shown an ability to deform in a peristaltic manner. An example is the expandable braid material used for creating unit constrictors in Section 4.1. The spiral geometry of the interweaved threads has been applied in creating the peristaltic motion displayed in locomotion of worm-robots [129-132], and in the design of gastrointestinal stents [133].

A method for contracting the braided structure in a patterned peristaltic manner was investigated by deforming a tubular braided structure with constricting flexible tendons (Appendix A). In this way, the controllable contraction patterns that were created have the potential for being used in the moving and mixing of food materials within the internal cavity of the structure. This method has applicability in mimicking the transport of a bolus of food through the oesophagus and is described further in Section 5.1.2 where it is used in the design of a linear peristaltic pump.

One aspect of the commercially available expandable braid tubing used to create the tubular structures described in Appendix A and Section 5.1.2 is that the braid exhibits a limited extent to which it can be expanded and contracted. Limit to contraction meant that full closure of the lumen was not possible without addition of a thick inner tube, made of silicone, being placed inside the braid. However, a significant amount force is then required to contract both the braided structure and the thick inner silicone tubing. The thickness of the required inner silicone tubing also alters the peristaltic deformation of the structure and flattens out the peristaltic contractions. As a result, a method for increasing the maximum contraction limit of the braided structure was considered.

Increasing the maximum contraction limit of the braided tubing would mean that a thinner and more deformable inner tubular sleeve of silicone could be used. A complete closure of the lumen can then be achieved with improved deformation properties and less constrictive force being applied by the tendons. Complete occlusion of the lumen can be approached by increasing the spacing between the braided threads or by reducing the total number of threads the structure is constructed from. A hand-made braided tube was created using 1.0 mm diameter nylon line that was thread in an over-under pattern along a 50 mm diameter tube of polyvinyl chloride (PVC) (Fig. 33). The hand-made braid was capable of complete closing of an inner membrane when constricting it with circumferential nylon tendons. The

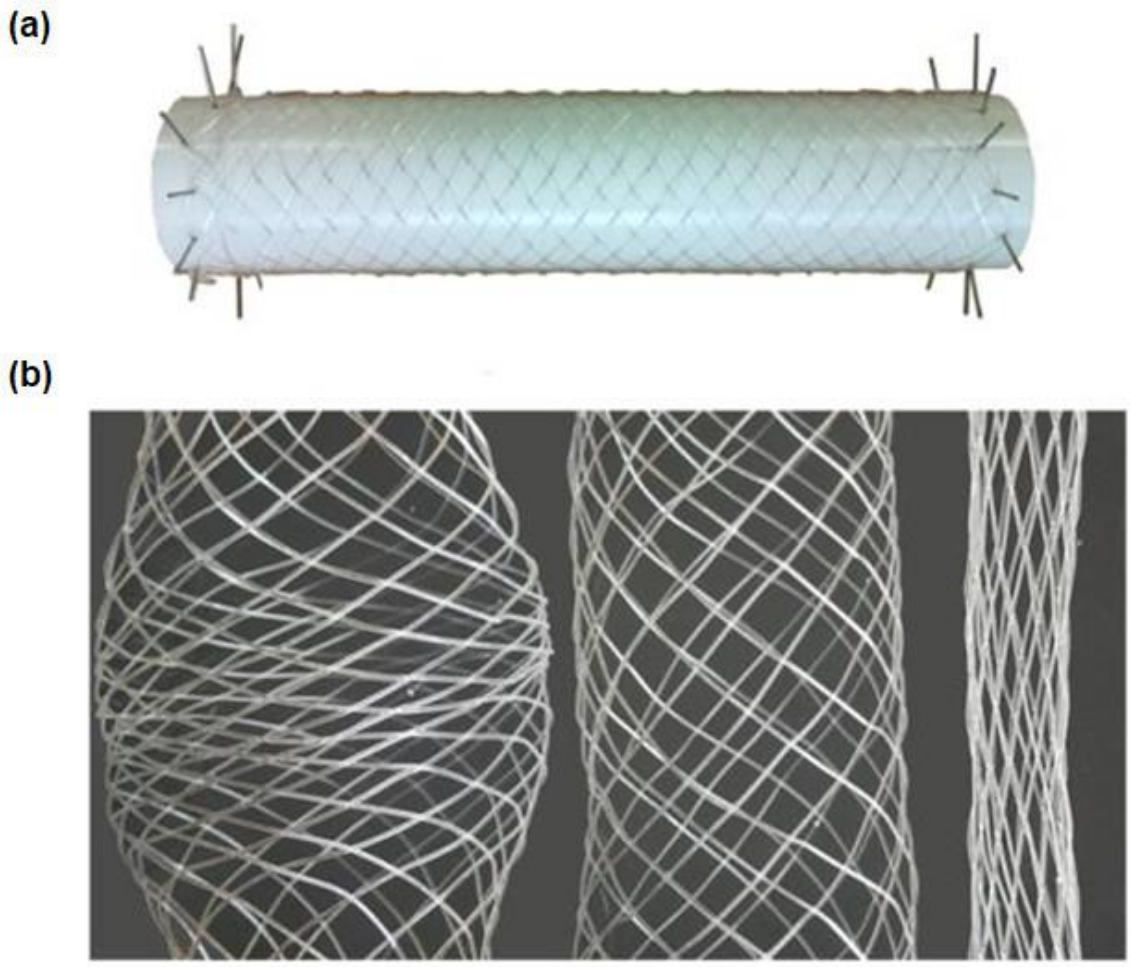

Fig. 33: (a) A braided tube constructed with nylon line. (b) The same nylon line braided tube displaying different levels of expansion and contraction.

hand-made braided structure also displays considerable radial expansion capabilities when the axial length of the braided tube is contracted.

4.3. Tendons and Bowden cables

Flexible Bowden cables allow for remote actuation of an end-effector to take place, in this case the drawing and releasing of a unit constrictor tendon (Fig. 34). Bowden cables are hollow, flexible cables that are used to transmit mechanical force or energy by the displacement of an internal tendon relative to the outer housing. The cables may incorporate a composite structure using a tightly coiled helix with a flexible plastic outer coating. Some Bowden cables also have an inner lining made of PTFE (polytetrafluoroethylene) or similar material to assist in lowering frictional contact with the moving tendon.

The Bowden cable acts as a conduit for the displacement of the tendon while the actual

Fig. 34: Bowden cables running unit constrictor tendons from a braided tube.

pulling force behind the tendon displacement can be located at some distance from the unit constrictor. This allows the artificial muscles to be near to or directly on the reactor membrane without the need for a driving mechanism or pulley system to be placed directly alongside them. The ability to free up space around the actuating artificial muscles allows the membrane to deform more freely without colliding into other objects.

Polyvinyl chloride (PVC) or polypropylene (PP) flexible tubing was initially employed to act as a basic Bowden cable, but flexibility was limited and surface friction with the movement of the nylon tendon was significant. Friction would increase as the bending angle of the Bowden cable increased, which resulted in a larger pulling force being required to draw the tendon through the cable. Curtain wire, which was narrower, more flexible and exhibited lower friction, was investigated, but it had an intrinsic stiffness to it due to the steel coil it was comprised of. Use of a nylon coil for the Bowden cable was considered for improving the overall flexibility and reducing friction against the nylon tendon.

As no nylon Bowden cable could be commercially sourced it was fabricated to specification. A length of nylon line was taped to one end of a steel rod 1.8 mm in diameter. The rod and nylon line were placed into a cordless drill chuck and the nylon line was slowly wound around the rod while ensuring that the coils were packed tightly together. This was continued until a desired length of the Bowden cable was achieved, at which point the loose end of the nylon line was attached to the rod by a piece of adhesive tape to prevent the coil from unwinding.

The coil was then heated while on the steel rod using a heat gun at a temperature setting of 200° Celsius. The heat was passed over the coil in a reciprocating manner from one end to the other while slowly rotating the rod at the same time. Several passes were made over the

rod before removing the heat and allowing the nylon coil to cool. This process was repeated two or three times to ensure that the coil was set in place and would not unwind when released from the rod.

Before removing the coil from the rod, a length of 3 mm diameter heat-shrink tubing was placed over the nylon coil and heated with a heat gun to shrink the tubing in place and further ensure that the coil could not unwind. When cooled, the covered nylon coil (Fig. 35) was removed from the rod using a gentle twisting action and the ends of the fabricated Bowden cable trimmed with a pair of scissors.

The internal diameter of the cable should be at least 1.5 times the diameter of the tendon or tendons passing through it. This reduces the amount of surface friction that the tendon encounters as it moves through the Bowden cable. Two 0.4 mm diameter tendons can pass through a 1.8 mm internal diameter Bowden cable easily and with little resistance.

Bending of the Bowden cable causes increased friction between the tendon and cable to occur [201-203]. Maintaining as small a bending angle as possible reduces the amount of friction encountered when pulling the tendon. However, the purpose of the Bowden cable is to allow as much freedom of action for the end-effector or unit constrictors as possible. A

Fig. 35: A nylon coil Bowden cable with a pair of nylon tendons running through it. Part of the outer plastic sheath has been removed to expose the nylon coil.

small increase in friction through increased bending angles can be justified by allowing the unit constrictors a greater freedom of movement.

The type of material used for the flexible tendons of the artificial muscles is required to exhibit limited stretch when placed under tension. This is because a stretching tendon affects the amount of displacement of the tendon taking place during a unit constrictor contraction. This in turn affects the calculation of the contraction ratio that is achieved. Three types of flexible tendon material, nylon monofilament (Maxistrike, 15 lb, 0.40 mm), fluorocarbon monofilament (Black Magic Tough Fluorocarbon, 20 lb, 0.40 mm), and polyethylene braid (Black Magic Hyperglide 13x Braid, 50 lb, 0.405 mm), were tested using a universal testing machine to determine the amount of stretch – strain - of the tendons when placed under increasing level of tensile force (Fig. 36). The polyethylene braid showed the

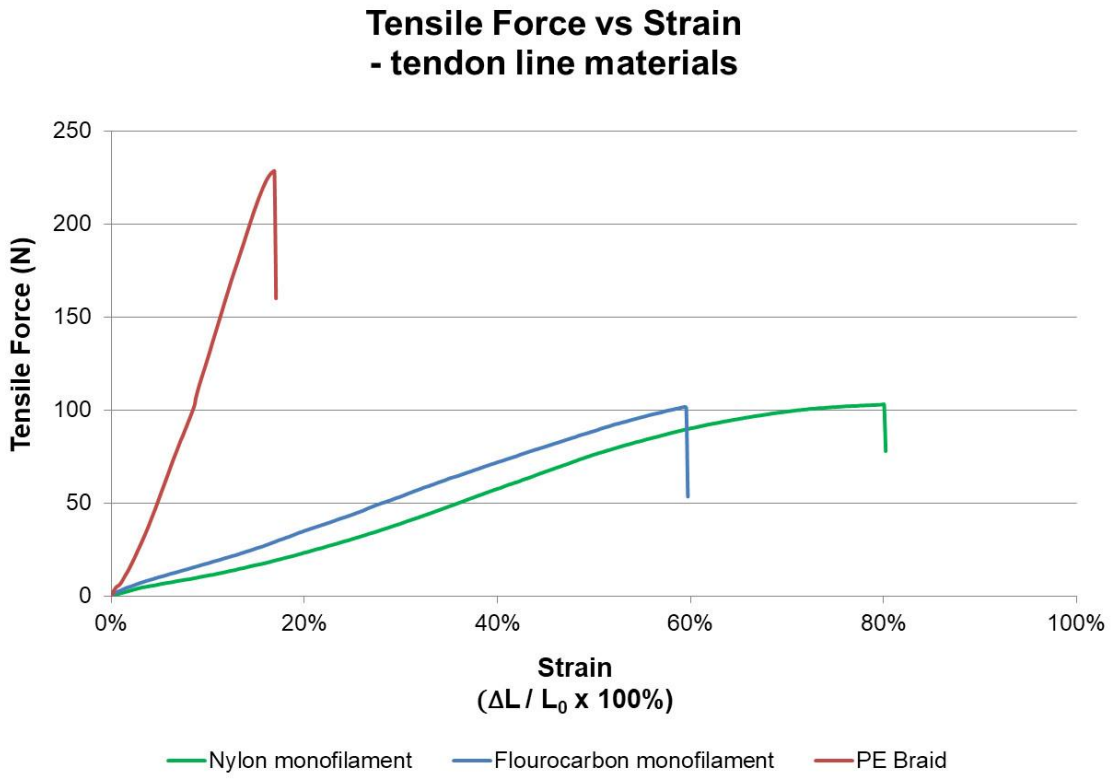

Fig. 36: Tensile force test results of three different tendon line materials.

least amount of stretch when placed under tension and is the most suitable of the three types of flexible line to use as a unit constrictor tendon.

4.4. Summary

This chapter explored the use of three diverse types of artificial muscle for deforming the flexible membrane of an artificial gastric tract. The first of the artificial muscles were unit constrictors made from coiled nylon line and an expandable braided sleeve, the second involved contraction of the surface of an expandable braided tube. The artificial muscle systems investigated involved the pulling of tendons to control their contractive action. Tendon actuation was found to be a highly controllable method for obtaining a desired contraction force and amplitude of contraction for the artificial muscles. Flexible fabricated nylon Bowden cables were developed to decouple the artificial muscles from a tendon pulling system and provide the constrictors with greater freedom of movement over an attached membrane.

Unit constrictors made from coiled nylon line and expandable braid (Section 4.2) display high flexibility and controllability within a compact form. Both forms of unit constrictors had similar maximum contractive ratios of 60-70% of their initial length. However, the coiled nylon line also had the ability to extend or expand beyond its initial length and displayed better flexibility. The unit constrictors can be connected to create a layer of artificial muscle by attaching them onto a flexible elastic substrate material. Connected artificial muscle layers made from unit constrictors exhibit a good ability to mimic the mechanical characteristics of biological smooth muscle layers. The shape of the membrane the unit constrictors can be attached to may be complex and irregular, such as the shape of a stomach, and may involve substantial expansion. The high flexibility of the coiled nylon line

unit constrictors allows them to closely follow the surface deformation and folding of complex membrane shapes.

Expandable braided tubing forms a tubular structure made from many fine intertwined coils that display a smooth, wave-like deformation of the tubular surface when placed under controlled contractile activity. Contractive tendons can be threaded through the braided tubing to constrict the structure at specific points and create peristaltic deformation patterns. The expandable braid can be placed as a sleeve or sheath over an elastic tube and act as an artificial layer of muscle. This type of artificial muscle layer may best be used in mimicking contractive actions over long tubular sections of the gastric tract *e.g.*, the oesophagus.

Chapter Five

Actuation of the muscles

Chapter 5 – Actuation of the muscles

Actuate means to put into motion or action. Control over the mechanical deformation of a simulated gastric tract membrane involves actuating the artificial muscles at a specific time and location, depending on the biomechanical deformation pattern being mimicked. Deformation patterns can differ significantly between anatomical regions and digestion phases. To successfully mimic the biological system, consideration should be given to the diverse types of membrane deformation patterns that occur and appropriate mechanisms or methods of actuation that can be used to obtain these patterns.

The major anatomical regions of the human gastric tract of interest in this study are the oesophagus, stomach, and the proximal region of the duodenum. The stomach is sub-divided into four anatomical regions; the fundus, corpus, antrum, and pylorus (refer Fig. 2, Section 1.1). However, functional regions may span the anatomical boundaries and are where specific digestive functions take place. For example, the gastric reservoir functional region includes the fundus and corpus sub-regions of the stomach and is where tonic contractions take place to provide for the accommodation of ingested food. Tonic contractions create a continued muscular tension and occur at the lower oesophageal and pyloric sphincters which manipulate the entry and emptying of contents within the stomach. The gastric pump functional region is where phasic contractions such as peristaltic waves occur. Phasic contractions can span the corpus, antrum, and pylorus sub-regions of the stomach depending on the type and extent of gastric pumping taking place.

Receptive, adaptive, and feedback mechanisms can trigger deformations which promote the gastric relaxation of the stomach wall. Receptive stomach mechanisms involve a brief relaxation of the gastric reservoir during chewing and swallowing actions. The act of

swallowing stimulates mechanoreceptors in the pharynx and oesophagus and prepares the stomach for an incoming bolus of food. As it fills, intragastric pressure within the stomach body increases which triggers an adaptive mechanism to expand the stomach volume [204]. The sensing of the presence of gastrin, a hormonal control chemical, is a feedback mechanism that triggers the stimulation of additional gastric juice secretions [3]. Sensing of nutrients in the chyme within the small intestine causes additional relaxation of the gastric reservoir, delaying emptying of the stomach and allowing more time for the intestine to process the available nutrients [3].

The function of the gastric reservoir is to store and empty the stomach contents. The emptying process is carried out by two mechanisms: tonic contraction of the reservoir and small peristaltic waves moving over the upper corpus region of the stomach. Mixing and evacuation of the contents typically only involves a superficial layer of chyme that has been diluted by gastric juices [3]. During this process, pH level remains high within the stomach and the digestion of starch by amylase continues to occur within the middle region of the stomach.

The gastric pump process involves the creation of peristaltic waves that begin mid-way over the stomach region and propagate toward the pylorus. The peristaltic waves occur 2 to 3 times per minute - every 20-30 seconds - and are triggered by electrical waves originating within the stomach wall. The electrical waves are initiated by the interstitial cells of Cajal (ICC) which produce electrical potential signals and act as pacemakers for the triggering of the peristaltic muscle contractions [205]. The frequency and propagation velocity of the peristaltic slow waves are determined by these pacesetter potentials. The pacesetter potentials are always present but may not always trigger a peristaltic contraction wave due

to the electric potential being below a necessary threshold level for actuation. Upon reaching the threshold level, excitatory neurotransmitters, one of the most prominent being acetylcholine, are released and induce an electro-mechanical coupling [3]. However, the findings from Hocke et al. [206] suggest that minute slow-wave contractions still occur even when the pacesetter potential threshold has not been reached.

The stomach emptying mechanism of the antral pump involves a deep contraction of the muscles towards the lower region of the stomach as the peristaltic waves reach the antrum. Gastric pumping involves three phases: propulsion, emptying and mixing, and retro-propulsion and grinding. The phase of propulsion involves waves moving over the antrum and propelling chyme into the terminal antrum. The emptying and mixing phase, which is associated with the gastric sieving effect, is where the pyloric sphincter opens slightly, and small amounts of chyme are swept into the duodenum from waves occurring over the middle of the antrum. Duodenal contractions are inhibited during this emptying and mixing phase. The retro-propulsion and grinding phase involves contraction of the terminal antrum and a closing of the pyloric sphincter. This action prevents flow of the contents from the pylorus into the duodenum and propels the digesta back into the middle antrum region of the stomach, causing some mixing and grinding to occur with the contents.

The rate of gastric emptying is dependent on several factors: the relaxation of the reservoir, the depth of antral wave constriction, the amount of pyloric opening, the receptive relaxation of the duodenal bulb, and the contractive pattern of the duodenum [3]. The pylorus and pyloric sphincter act as an electric isolator to the stomach pacesetter potentials, rendering the duodenum as a separated region of activity. However, the motility of the duodenum is strongly related to that of the stomach. The duodenal pacesetter potentials

occur at a higher frequency with 3 to 4 contractions appearing during a single antral contraction of the stomach. During the emptying phase, the duodenal bulb is relaxed, and contractions are inhibited, allowing the duodenum to passively accept digesta transferred from the stomach. Duodenal contractions are more likely to occur during the antral pump phase of retro-propulsion, where the pyloric sphincter is closed, and can sometimes occur during the antral phase of propulsion.

This chapter introduces methods that provide actuation of the artificial muscles for an artificial stomach and allow for the simulation of many forms of deformation that occur in the biological system. Included are mechanical actuation methods for creating multiple constrictions from a single rotating mechanism, and a pulley-driven actuation system for driving individual unit constrictor contractions.

5.1. Independent actuation of individual unit constrictors

A range of dynamic contraction patterns is obtainable from the independent actuation of the artificial stomach muscles. Independent control over individual unit constrictors should be considered when the contraction amplitude or actuation sequencing varies over time, or the deformation activity patterns change due to feedback from sensors or other control mechanisms. The deformation patterns of the stomach exhibit highly dynamic and variable behaviour during the entire process of digestion; contractions change in amplitude during both the fed and fasting states, the stomach stretches and contracts to accommodate contents, and the pyloric sphincter opens and closes creating a sieving and retro-propulsive grinding effect on food particles. Implementation of independent actuation methods are therefore considered for the artificial muscles attached to the artificial stomach membrane.

Independent actuation of the tendon-driven unit constrictors involves the ability of the actuation system to contract and expand each unit constrictor on demand. This means that each unit constrictor tendon is pulled and released by controlling the direction and speed of a winding spindle and motor. Although this form of control over the unit constrictor actuation provides for basic contractile activity of the artificial muscle it does not necessarily mean that the muscles are being activated in a manner that is biologically relevant. To achieve muscle actuation that mimics that of a biological system more advanced control methods for the constrictor actuation are required.

Controlling the correct amount of individual unit constrictor contraction is complex and requires consideration of several factors including:

i. Monitoring the absolute length of tendon that is being retracted or released and the time required to complete the operation so that a specific contraction ratio and speed of contraction can be achieved.
ii. Providing a pulling force capable of fully retracting the unit constrictor tendon and deforming the reactor shell and its contents. This includes overcoming any surface friction created through tendon contact with the Bowden cables and the attached membrane.
iii. Provision for changes in speed or direction of the winding motors in response to feedback signals received from various sensors or control sources.

Other considerations for the motor control system include: the total number of unit constrictors requiring actuation, the physical size and electrical characteristics of the motors, the diameter of the winding spindles or pulleys, and the type of tendon line material being used. The total number of unit constrictors that are to be independently actuated

determines the total number of winding motors required. The physical size, electrical characteristics, and number of winding motors required influence the physical footprint and power requirements of the motor control system. The diameter of the winding spindles affects the rate of contraction that can be achieved at various motor speeds - large diameter spindles can create faster winding rates but take up more space. The type of flexible tendon material used should be capable of continuous winding and unwinding on the spindles or pulleys without developing line memory. Line memory occurs when a flexible line is curled around a spool or spindle for an extended length of time and will re-coil itself when it is unwound from its spindle.

5.1.1. Creating peristaltic waves in the stomach

Before determining the mechanical requirements for unit constrictor actuation the generation characteristics of the peristaltic slow wave patterns need to be defined. These characteristics include the amplitude of the contractions that occur over the different regions of the stomach, the velocity of the peristaltic slow wave as it travels over the greater curvature of the stomach and the frequency of peristaltic slow wave activity within a specified period. Each characteristic influences the actuation timing of the unit constrictors, the amount and rate of winding or displacement required for each of the unit constrictor tendons, and the mechanical power required for actuation of the unit constrictors.

A peristaltic slow wave contraction pattern is maintained over the artificial stomach surface by timed sequential actuation of the independent unit constrictors. The period and frequency of the generated peristaltic slow waves are determined by sequentially delaying the actuation timings of adjacent unit constrictors. Actuation timings are also influenced by

the physical separation between adjacent unit constrictors over the artificial stomach surface.

To maintain continuous slow-wave contractions over a region of the stomach membrane requires at least three adjacent unit constrictors to be actuating in a specific pattern (Fig. 37). Initially, all unit constrictors are in a relaxed state (Fig. 37(a)) with minimal tension applied to the unit constrictor tendons. The first constrictor (C1) then contracts towards its programmed contraction ratio (Fig. 37(b)). Once C1 reaches its programmed contraction ratio it holds this contracted state while the second constrictor (C2) begins contracting to its programmed contraction ratio (Fig. 37(c)).

When both C1 and C2 have reached their programmed contraction ratios (Fig. 37(d)) C1 then expands in diameter and returns to its initial relaxed state while C3 begins to contract (Fig. 37(e)). Upon C3 reaching its programmed contraction ratio (Fig. 37(f)) C2 will then expand and return to its initial relaxed state. This process continues sequentially throughout the entire series of unit constrictors, from the corpus region towards the antrum, until the contraction wave reaches the pyloric sphincter.

Actuation timings

During the generation of each peristaltic wave the unit constrictors attached to the artificial stomach membrane undergo three sequential states of actuation:

i. Contraction period: the contraction period (t_c) begins with a unit constrictor at its starting contraction ratio or resting state. The tension on the tendon is then increased and the unit constrictor contracts until a programmed ratio of contraction is reached.

ii. Holding period: the holding period (t_h) maintains the contracted state of a unit constrictor without further contraction or expansion taking place. It occurs when a unit constrictor has reached its desired or maximum contraction ratio.

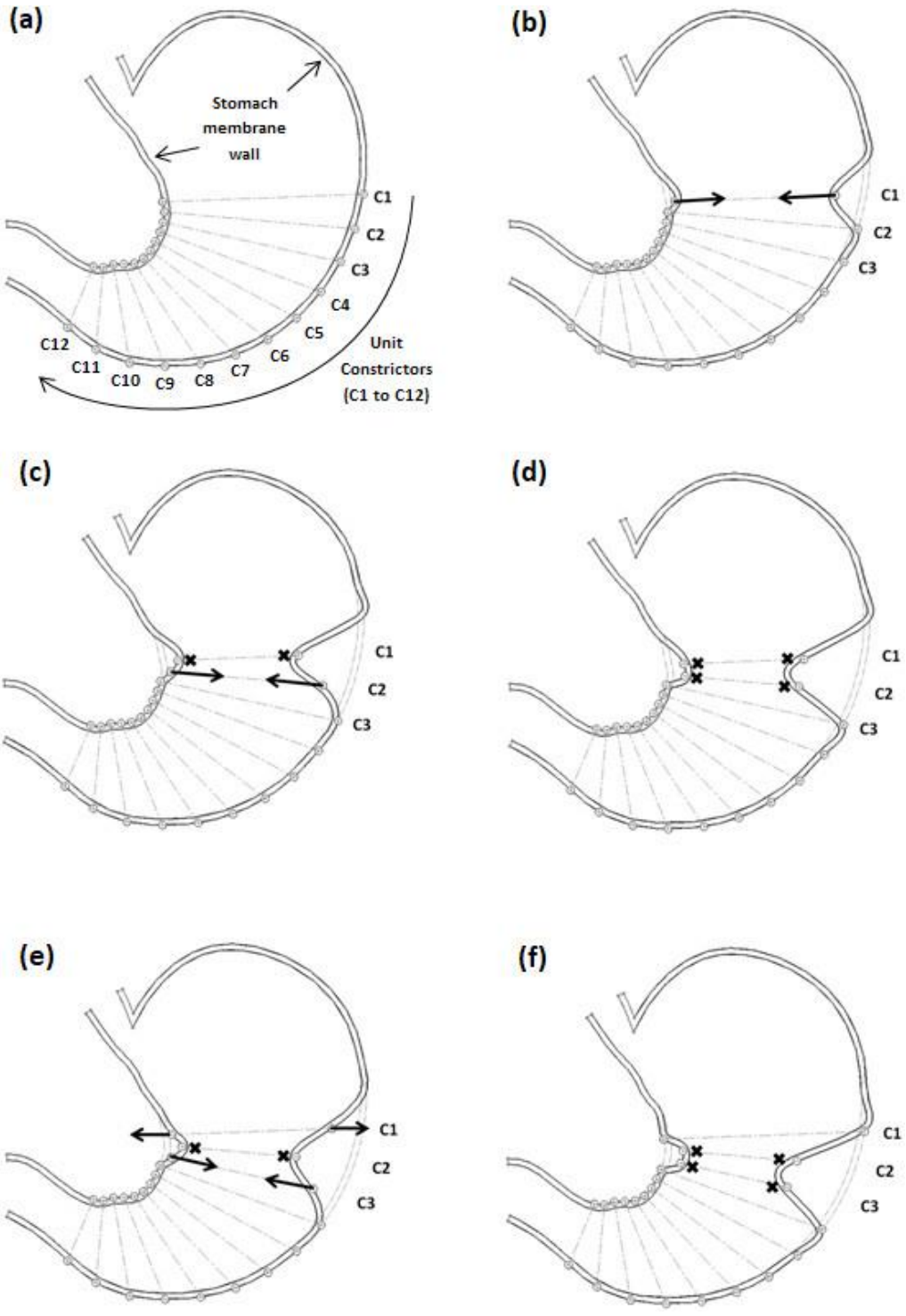

Fig. 37: Sequence of actuation states for adjacent unit constrictors. Contraction amplitudes have been exaggerated for clarity.

iii. Expansion period: the expansion period (t_e) occurs when tension on the unit constrictor tendon is decreasing, causing the unit constrictor to expand in diameter from its contracted state until it reaches its starting contraction ratio or relaxed state.

Fig. 38 shows a timing diagram representing the different actuation states of two adjacent unit constrictors attached to the artificial stomach. The complete actuation time (t^i_{full}) for a single unit constrictor during the generation of a peristaltic wave is found by adding the timings of the contraction, holding, and expansion states that it passes through (Eqn.

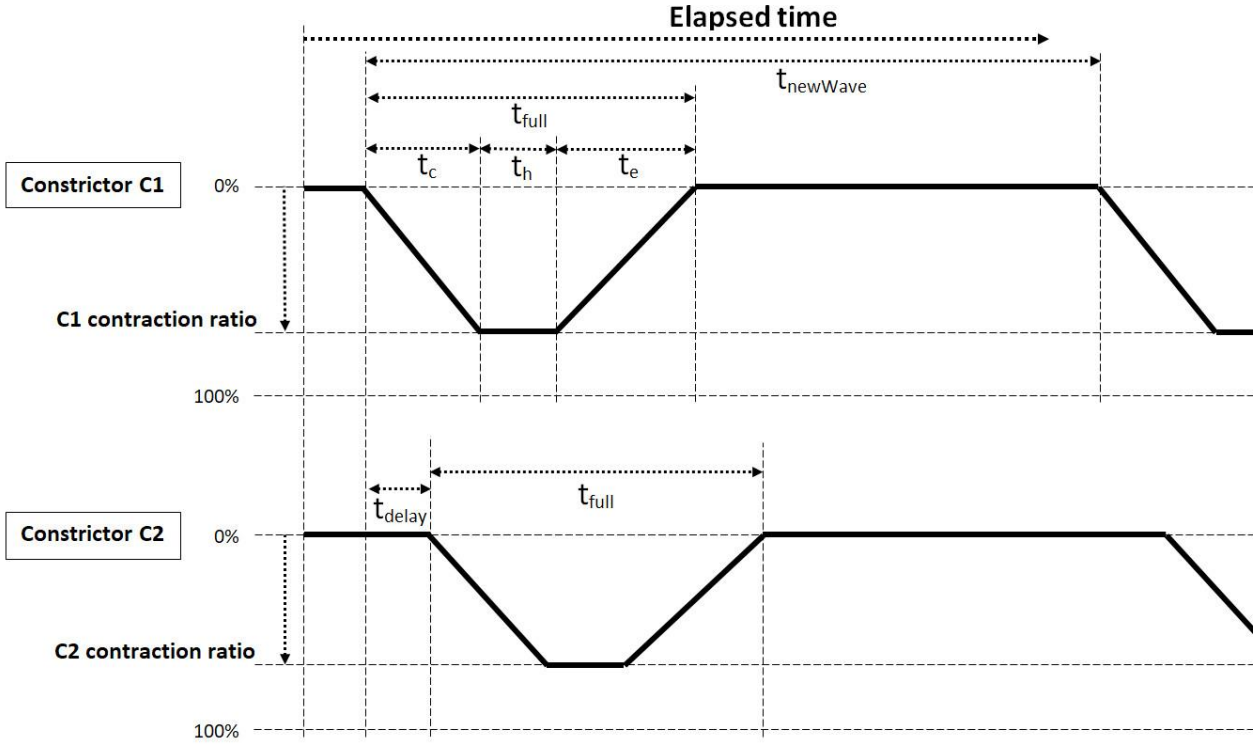

$t_{newWave}$ – time before the generation of a new peristaltic wave
t_{full} – actuation time of a unit constrictor
t_c – contraction time
t_e – expansion time
t_h – holding time
t_{delay} – time delay before the next adjacent unit constrictor begins to actuate

Fig. 38: Example timing diagram for two adjacent unit constrictors during peristaltic slow wave generation.

(5-27)).

$$t_{full}^{i} = t_{c}^{i} + t_{h}^{i} + t_{e}^{i} \quad (5\text{-}1)$$

A time delay (t_{delay}) occurs from the start of a contraction actuation of one constrictor and the start of contraction for the next adjacent constrictor. This delay mimics the delayed contraction pattern of muscle bundles that form the layers of circumferential smooth muscle in a human stomach. The velocity of the peristaltic wave travelling over the stomach is controlled by varying the delay timing between adjacent unit constrictors.

The velocity of a peristaltic wave travelling over the surface of the greater curvature of the stomach reaches between 3 to 8 mm s^{-1} [207]. The velocity of the wave varies depending on the region of the stomach that it is passing over. O'Grady et al. [207] used high resolution electrophysiology mappings of the propagation of peristaltic wave pacemaker electrical signals, measured over the greater curvature of the stomach, and recorded the velocity of the travelling signal as being in the range of 5.2-5.4 mm s^{-1} within the antral region, and 3.0-3.3 mm s^{-1} in the corpus region. These measurements provide a basis from which the unit constrictor delay timings can be estimated for specific regions of the stomach.

The minimum and maximum timing delay between adjacent unit constrictor actuations are calculated from the maximum and minimum velocities of the travelling peristaltic wave. The average distance between adjacent unit constrictors over the greater curvature of the stomach (refer to Fig. 2, Section 1.1) is 18 mm so the time delay between actuation of adjacent unit constrictors when the peristaltic wave is travelling at 8 mm per second would be 2.25 seconds (Eqn. (5-2)).

$$t_{delay}(minimum) = \frac{distance}{velocity} = \frac{18\ mm}{8\ mm.s^{-1}} = 2.25\ seconds \quad (5\text{-}2)$$

When the peristaltic wave is travelling at 3 mm per second the time delay would be an average of 6 seconds between adjacent unit constrictors (Eqn. (5-3)).

$$t_{delay}\ (maximum) = \frac{distance}{velocity} = \frac{18\ mm}{3\ mm.s^{-1}} = 6.00\ seconds \quad (5\text{-}3)$$

The total time for a peristaltic wave to propagate from the corpus to the pyloric sphincter (t_{wave}) is found from the summation of the time delays for unit constrictors from C2 through to C12 (Eqn. (5-4)).

$$t_{wave} = \sum_{i=2}^{12} t_{delay}^{i} \quad (5\text{-}4)$$

In a healthy human stomach there are 2.83 ± 0.35 contractions beginning every minute [207]. This would mean that the timing delay between the start of one peristaltic wave and the initiation of the next wave ($t_{newWave}$) would range between 27.5 and 40.5 seconds (Eqns. (5-5) and (5-6)).

$$t_{newWave}\ (minimum) = \frac{60\ s}{(2.83+\ 0.35)-1} = 27.5\ seconds \quad (5\text{-}5)$$

$$t_{newWave}\ (maximum) = \frac{60\ s}{(2.83-\ 0.35)-1} = 40.5\ seconds \quad (5\text{-}6)$$

The contraction ratio or contraction amplitude for unit constrictors varies between the corpus and antrum regions of the stomach. Smaller contraction amplitudes are found in the corpus region compared to the antrum. Magnetic resonance imaging (MRI) scan

measurements conducted by Lu et al. [208] found that contractions in the antrum reach an amplitude of 5.18 ± 0.24 mm and 3.30 ± 0.16 mm in the corpus. However, data from the literature is limited as to how quickly these contractions reach these amplitudes so contraction timings for the unit constrictors (t_c) could vary considerably. Winding motor velocity and torque therefore need to accommodate rapid contraction rates of the unit constrictors if required.

Table 6 shows the minimum and maximum timing parameters of the unit constrictors during the generation of a peristaltic wave over the artificial stomach. Each unit constrictor can use its own unique parameters or use parameters common to the regions of the stomach that the unit constrictor is attached to. For example, unit constrictors in the corpus region (C1 – C6) may all use parameters of t_{delay} = 5.6 seconds, t_c = 4.0 seconds, t_h = 4.0 seconds, and t_e = 5.0 seconds, while unit constrictors in the antrum region (C7 – C11) may have parameters of t_{delay} = 3.4 seconds, t_c = 3.0 seconds, t_h = 3.0 seconds, and t_e = 4.0 seconds. Pairing these timings with progressively increasing unit constrictor contraction amplitudes - starting from

Table 6: Minimum and maximum values for peristaltic wave timing parameters.

Parameter	Minimum value (s)	Maximum value (s)
$\mathbf{t_{newWave}}$	27.5	40.5
$\mathbf{t_{delay}}$	2.25	6.00
$\mathbf{t_c}$	> 0 (dependent on winding motor max. speed)	$t_{newWave} – (t_h + t_e)$
$\mathbf{t_h}$	0	$t_{newWave} – (t_c + t_e)$
$\mathbf{t_e}$	> 0 (dependent on winding motor max. speed)	$t_{newWave} – (t_c + t_h)$

the corpus and towards the antrum – would result in an example set of parameters as shown in Table 7. Fig. 39 shows the corresponding timing diagram for the example parameter. The period between generation of a new peristaltic wave ($t_{newWave}$) in Fig. 39 has been set to 28.5 seconds, meaning that a new peristaltic wave is started at a rate of 3.1 times per minute.

5.1.2. Determining mechanical power required for actuation

Several steps are involved in determining suitable motor specifications for the pulling of the unit constrictor tendons. The first step involves determining the maximum speed, or displacement per unit time, for the retraction of the unit constrictor tendon. The second step is to determine the tensile force that is applied to the tendon to achieve a desired constriction of the unit constrictor. Power requirements for the winding motor can then be calculated by using Eqn. (5-7) for translational motion or Eqn. (5-8) for rotational motion, depending on whether a linear or rotational measurement system is used.

Table 7: Example timing parameters and contraction ratios for unit constrictor actuation on the artificial stomach.

Constrictor	Region	Contraction Ratio (from starting circumference)	t_{delay}	t_c	t_h	t_e
C1	Corpus	20%	0	4.0	4.0	5.0
C2	Corpus	25%	5.6	4.0	4.0	5.0
C3	Corpus	30%	5.6	4.0	4.0	5.0
C4	Corpus	35%	5.6	4.0	4.0	5.0
C5	Corpus	35%	5.6	4.0	4.0	5.0
C6	Corpus	35%	5.6	4.0	4.0	5.0
C7	Antrum	40%	3.4	3.0	3.0	4.0
C8	Antrum	45%	3.4	3.0	3.0	4.0
C9	Antrum	50%	3.4	3.0	3.0	4.0
C10	Antrum	55%	3.4	3.0	3.0	4.0
C11	Antrum	60%	3.4	3.0	3.0	4.0
C12	Pylorus	60%	3.4	3.0	3.0	4.0

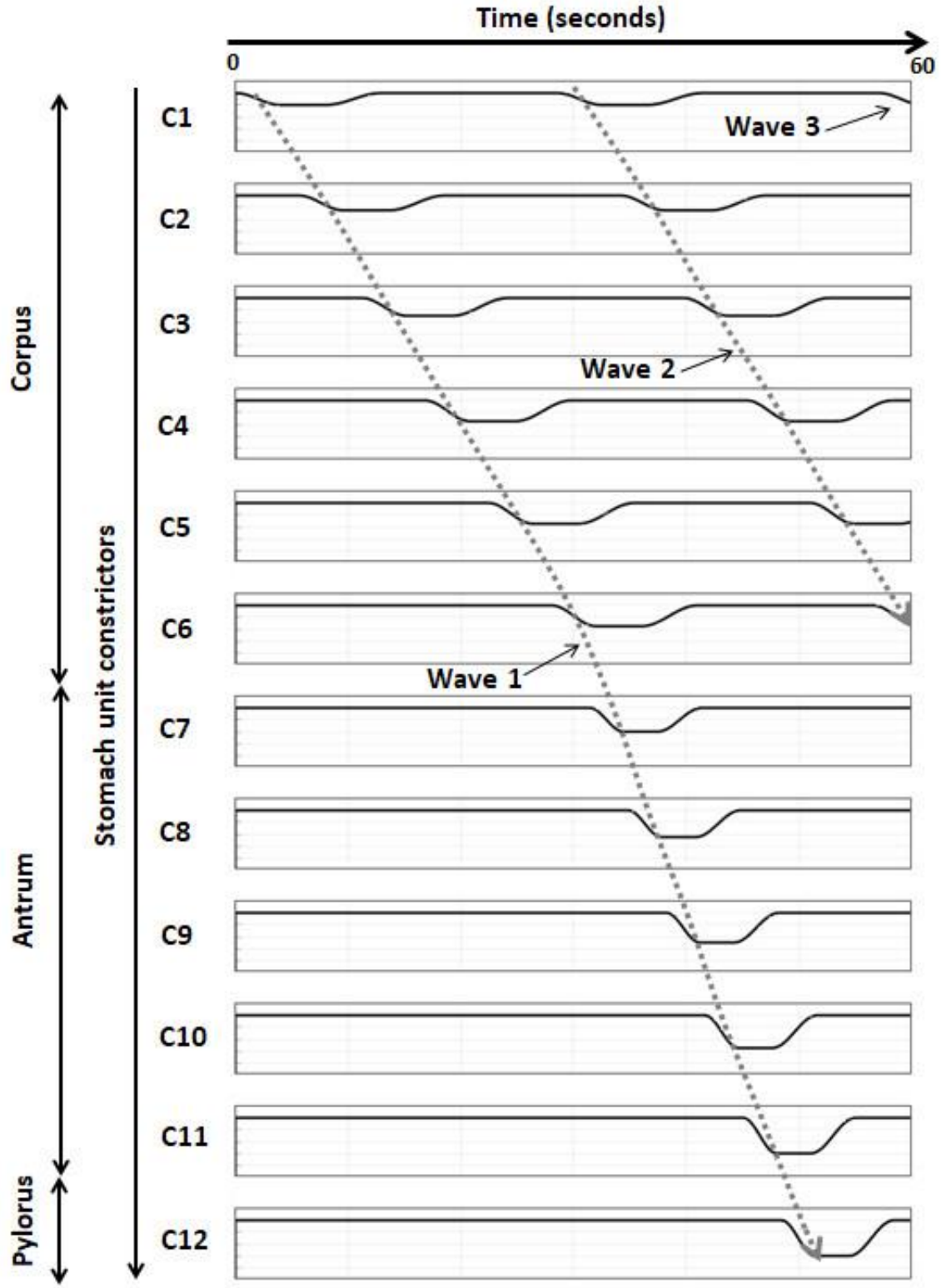

Fig. 39: Example timing diagram using parameters from Table 7 for the actuation of unit constrictors attached to the artificial stomach.

$$Power\ (translational) = force\ \times\ distance\ per\ unit\ time \tag{5-7}$$

$$Power\ (rotational) = torque\ \times\ angular\ velocity \tag{5-8}$$

Tendon displacement and unit constrictor contraction

The nylon coil unit constrictor described in Section 4.1 uses the displacement of a looped tendon running through the nylon coil to contract the constrictor. A tendon loop is formed by threading a braided polyethylene fishing line (Black Magic Hyperglide 13x Braid) through a Bowden cable and then through the constrictors' nylon coil before returning through the Bowden cable (Fig. 40(a)). The Bowden cable is assumed to be an incompressible hollow tube that maintains a constant length when under compression (refer Section 4.3). When the ends of the tendon lines are pulled through the Bowden cable the tendon loop reduces in circumference and contracts the nylon coil of the unit constrictor (Fig. 40(b)). The displacement of the tendon from this contraction action can be calculated from the change in length of the tendon lines exiting the Bowden cable (Eqn. (5-9)).

$$displacement\ of\ tendon = x = x_f - x_0 \tag{5-9}$$

Where: x = displacement or change in length of the tendon lines
x_o = initial tendon line length
x_f = final tendon line length after pulling or releasing of the tendon

Total tendon displacement during unit constrictor contractions is dependent on the required contraction ratio or contraction amplitude to be achieved and the circumference of the unit constrictor before contraction takes place. The total length of the tendon lines

being pulled through the Bowden cable is equal to the reduction in the circumference of the tendon loop. Because two ends of the tendon line are being drawn through the Bowden cable at the same time (Fig. 40(a)) the total length of line being pulled through the cable is twice the measured displacement of the tendon (Fig. 40(b)). The final circumference of the unit constrictor (P_{final}) can then be calculated by subtracting twice the displacement of the tendon line (2x) from the starting circumference of the unit constrictor (P_{start}) (Eqn. (5-10)). A contraction ratio for the contraction action can be calculated from the initial and final unit constrictor circumferences using Eqn. (4-1) (refer Section 4.1).

$$final\ unit\ constrictor\ circumference = P_{final} = P_{start} - 2x \qquad (5\text{-}10)$$

The amount of tendon displacement – or length of tendon retraction - required to reach a specified contraction ratio is dependent on the initial circumference of the individual unit constrictor, which in turn depends on where it is attached on the artificial stomach membrane. The contraction ratio refers to the external unit constrictor circumference and not the internal surface perimeter of the contracting lumen. Calculation of the contraction ratio for the internal lumenal surface is more complex than that of the unit constrictor contraction ratio because the inner membrane surface will fold and buckle under compression (refer Fig. 19, Section 3.2). The ratio of contraction for the lumen is dependent on the thickness of the membrane material at the point of constriction; a thicker membrane will occlude more of the lumen under unit constrictor contraction than a thinner membrane.

Angular displacement of the winding motor shaft

Electric motors attached with winding spindles are used for winding the unit constrictor tendons. The displacement of the unit constrictor tendon is calculated from the radius (r) of the winding spindle or pulley that the tendon is wound on to and the angular displacement ($\Delta\Theta$) of the shaft of the winding motor (Eqn. (5-11)), where the angular displacement is in radians. The rate of unit constrictor contraction and expansion can thus be changed by

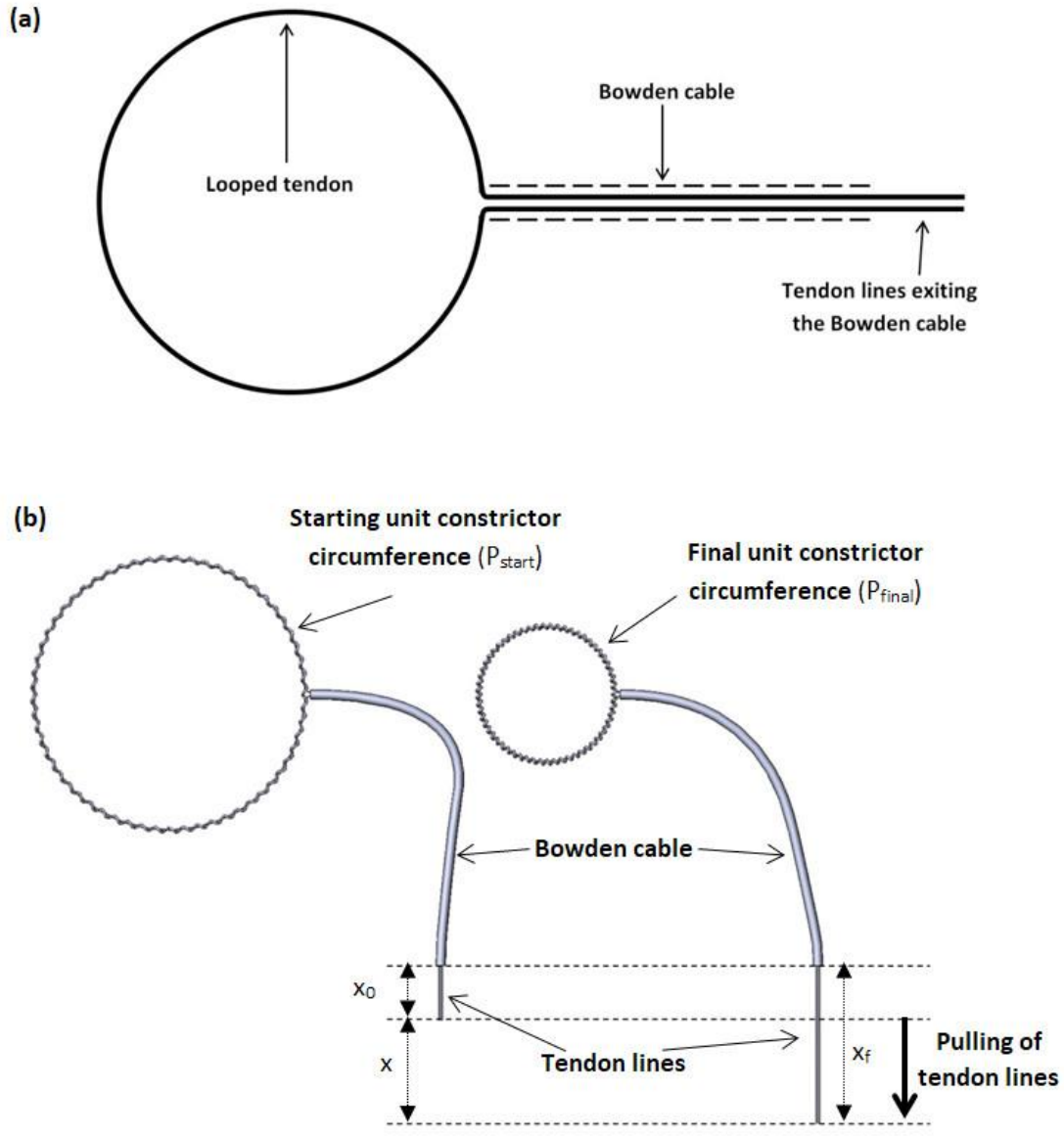

Fig. 40: Looped tendon displacement during contraction of a unit constrictor.

altering the rotational speed of the winding motor.

$$displacement\ of\ tendon = x = r\Delta\theta \tag{5-11}$$

Eqn. (5-12) provides the total angular displacement of the winding motor shaft during the contraction of the unit constrictor.

$$total\ angular\ displacement = \Delta\theta = \frac{x}{r}\ radians \tag{5-12}$$

Angular velocity and revolutions per minute of the winding motor

Maximum mechanical power is required when the unit constrictors contract at their maximum rate. The rate of unit constrictor contraction is dependent on the velocity of the travelling peristaltic wave as it travels over the stomach surface. The minimum actuation time delay between two adjacent unit constrictors is 2.25 seconds (refer Table 6, Section 5.1.2) and the rate of contraction of the unit constrictor should at least match this minimum timing. Thus, a minimum unit constrictor contraction time (t_c) of 2.5 seconds was selected for estimating the maximum velocity of the unit constrictor contractions.

Eqn. (5-13) gives the average angular velocity (ω) of the winding motor shaft from the angular displacement (ΔΘ) divided by the time taken for contraction (t_c). This can then be converted into average revolutions per minute (RPM) of the winding motor by multiplying the angular velocity by 60 seconds and dividing by 2π (Eqn. (5-14)).

$$average\ angular\ velocity\ (radians\ per\ second) = \omega = \frac{\Delta\theta}{t_c} \tag{5-13}$$

$$average\ RPM = \omega \times \frac{60\ seconds}{2\pi} \tag{5-14}$$

Measurement of the tensile forces required for pulling of unit constrictor tendons was obtained by attaching the looped tendon of a unit constrictor to a universal testing machine (Instron 5960 Dual Column Tabletop) and pulling the tendon through a 300 mm long Bowden cable (Fig. 41). A 0.405 mm diameter braided PE (polyethylene) fishing line (Black Magic Hyperglide 13x Braid) with 22 kg (50 lb.) rated breaking strain was used as the tendon for the unit constrictors due to its low-stretch characteristics (refer Section 4.3). The tendon lines exiting the non-constrictor end of the Bowden cable were fed through a 2 mm hole made in a rigid holding rig. The holding rig was clamped into the lower jaws of the testing

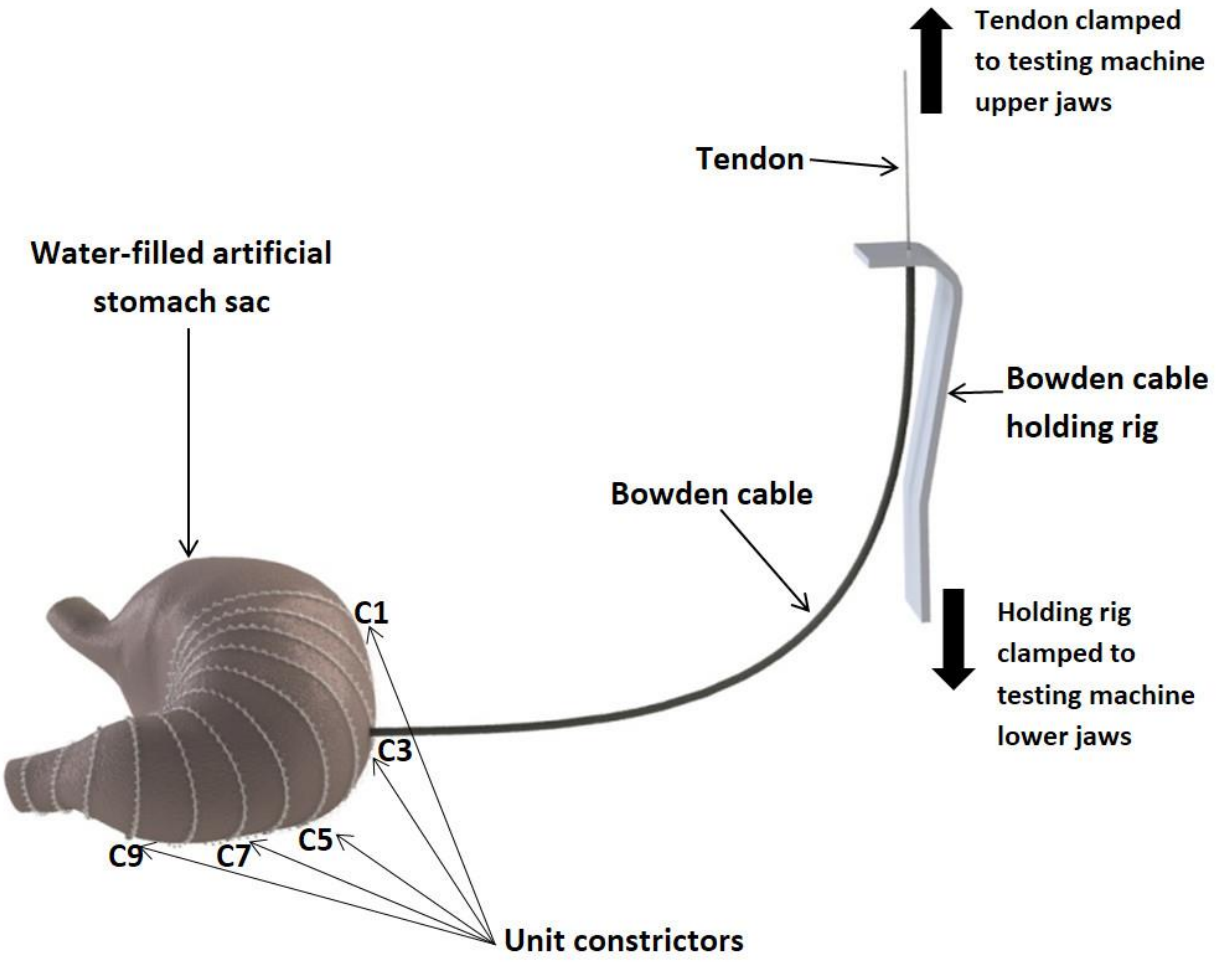

Fig. 41: Testing setup for unit constrictor tendon applied tensile force.

machine while the loose ends of the tendon were clamped into the upper jaws using a cable-tension clamp. The Bowden cable was laid out to maintain a 90° bending angle between the tensile machine and the unit constrictor. An extension rate of 1000 mm/minute was used on the tensile machine for pulling the tendon.

An initial trial was undertaken to determine the volume of the water-filled artificial stomach that produced the highest tensile forces during unit constrictor contraction. A single unit constrictor – C1 – was tested against stomach volumes of 0, 0.5, 1.0 and 1.5 litres of water. Fig. 42 shows the tensile force applied to the unit constrictor tendon as it was pulled. At 1.0 and 1.5 litre volumes the unit constrictor began its contraction in an initially expanded state – a negative contraction ratio, having been stretched by the expansion of the artificial stomach membrane when filled with water. Tests at 0 and 0.5 litre volumes of the stomach started with the unit constrictor at its initial contraction ratio of 0% - where no initial stretching of the artificial membrane was evident. A volume of 1.5 litres for the artificial stomach exhibits the highest levels of tensile force being applied to the unit constrictor throughout the contraction period. At a volume of 1.5 litres the unit constrictor also achieved the highest contraction ratio – approximately 90% - when contracted to a 50 N tension force. During the expansion phase, when the unit constrictor returns to its starting contraction ratio, the tension force initially drops rapidly and then continues to remain under 5 N.

Tests were then carried out for each individual unit constrictor – C1 to C11 – at a filled stomach volume of 1.5 litres, with no additional tensioning being applied to any of the other unit constrictor tendons during the test. Pulling of the tendon continued until the applied tension force reached 50 N. Each of the tested unit constrictors began their contraction in an expanded form relative to their initial circumference of P_0, which is noted in Fig. 43 as a negative contraction. Fig. 43 shows the applied tension force recorded during the pulling of the tendon was similar amongst all unit constrictors tested. A 60% contraction ratio was typically achieved before any significant increase in tension force was encountered.

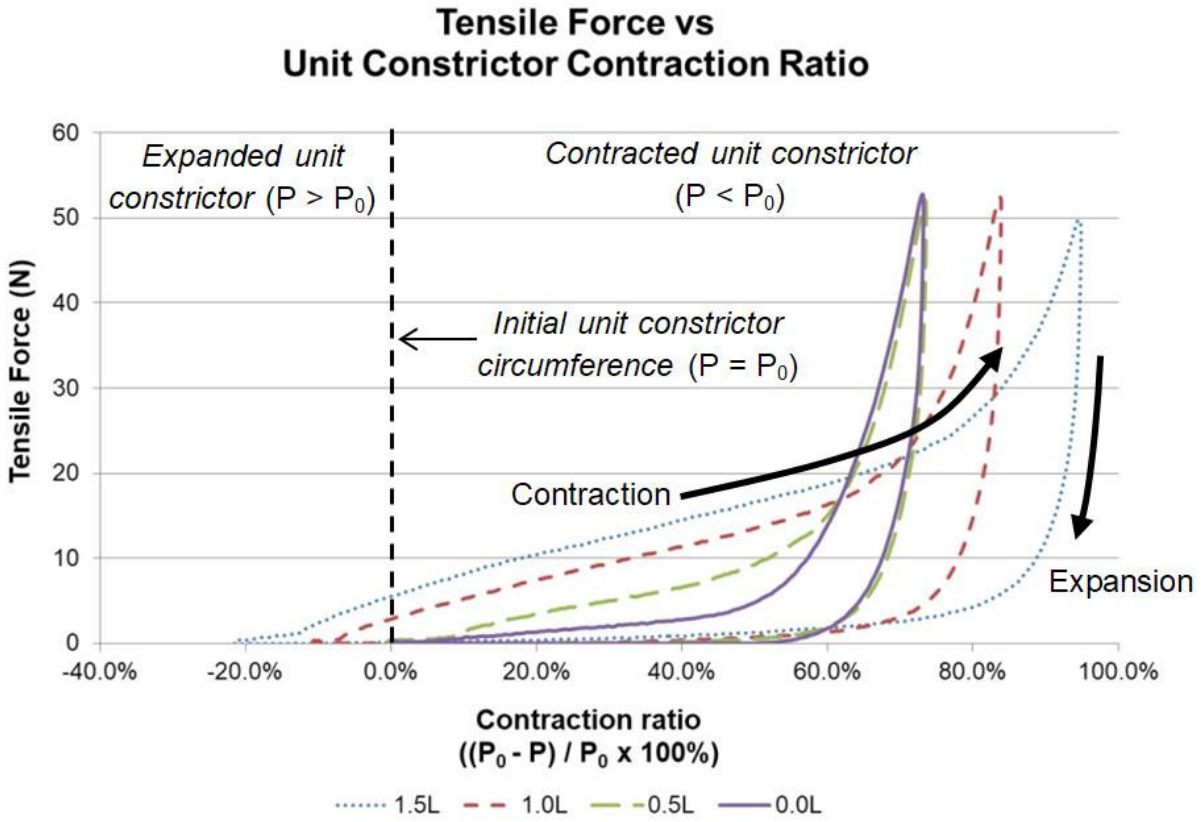

Fig. 42: Chart of tensile force encountered during the actuation of unit constrictor C1 at different water-filled volumes of the artificial stomach.

The applied tension force remains linear to 50-70% contraction ratio for each of the looped unit constrictors. Above 70% contraction ratio the applied tension force encounters significant increase. This occurs as the nylon coil of the unit constrictor begins to self-collide and the flexible artificial membrane that the unit constrictors are attached to begins to fold and press against itself. The results also suggest that a 70-90% contraction ratio should be a maximum amount of contraction applied to the unit constrictors to prevent excessive tensile forces damaging them. The coiled nylon unit constrictors and artificial membrane showed no signs of damage during any of the tests up to 50 N.

The tension force measured was taken from the tensioning of a single unit constrictor

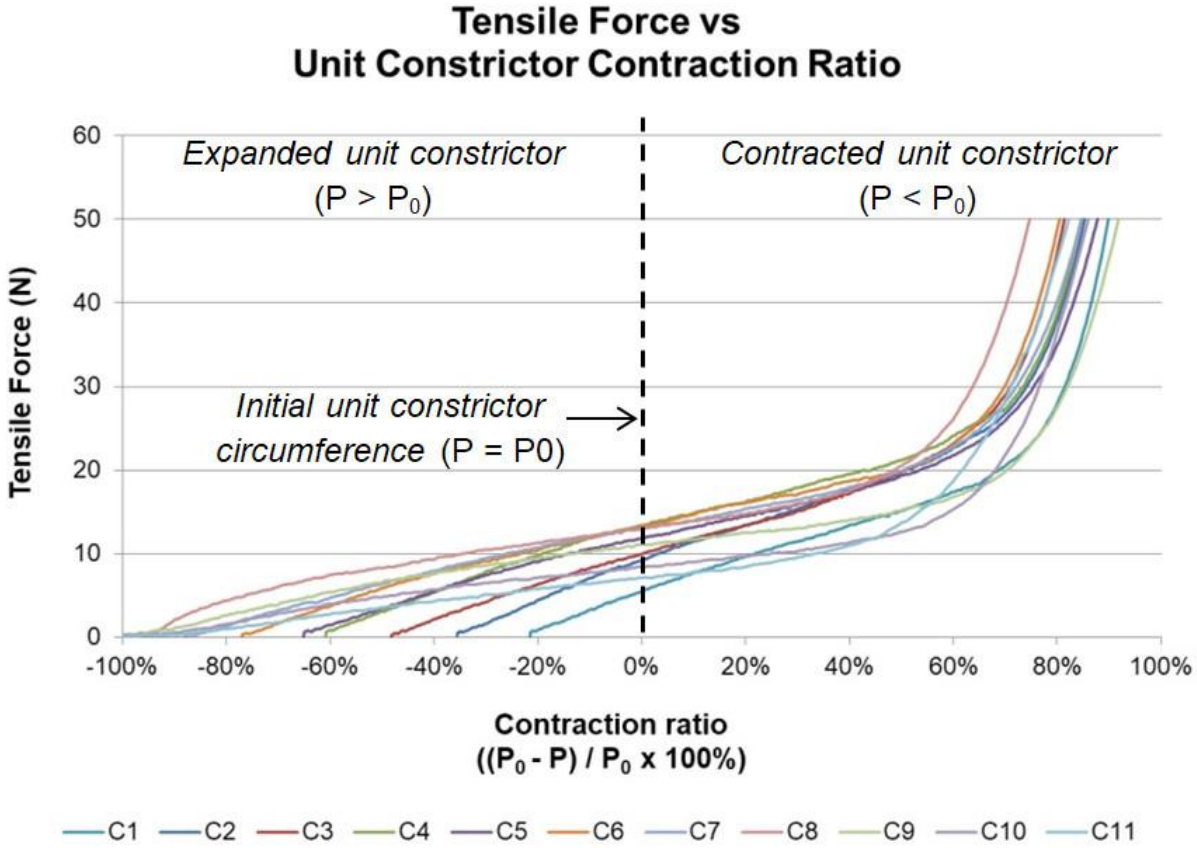

Fig. 43: Chart of tensile force experienced during contraction of unit constrictors C1 to C11 on an artificial stomach filled with 1.5 litres of water.

tendon with no other unit constrictor tendons being tensioned at the same time. When multiple unit constrictor contractions occur at the same time, as happens during the progressive propagation of peristaltic slow wave contractions along the stomach wall, the determination of force required for contraction of the tendons becomes complicated. As the initial contraction begins, starting in the region of the stomach corpus, the constrictors adjacent to the initial contraction begin to contract after a specified delay, and so on with subsequent unit constrictors onwards towards the pylorus. This suggests that during peristaltic slow-wave contractions the tension force being applied to the unit constrictor tendons is not solely concentrated on any one constrictor but is spread over adjacent constrictors presently undergoing actuation. However, determining the tensile force required for contraction of individual unit constrictors allows for an estimate of the maximum mechanical power required to complete a contraction.

Determining the mechanical power and winding motor speed-torque requirements

Table 8 shows the parameters used for calculating the power requirements of the winding motors from contraction of the unit constrictors (c1 to c11) attached to the artificial stomach membrane. C12 was completely closed off. A progressively increasing contraction ratio, from 20% of the starting circumference of unit constrictor C1 to 60% of the starting circumference of unit constrictor C11, was applied to the unit constrictors from the corpus region to the pylorus. These parameters provide total or average values calculated over the contraction period and not instantaneous values over the actuation time.

Eqn. (5-9) and column 9 of Table 8 provide the total displacement of the tendon during the contraction time. However, displacement of the tendon over the full contraction period is not constant. Acceleration and deceleration of the winding motor causes the winding

spindle to speed up at the beginning of the contraction and slow down as it approaches the end. To allow for this, the instantaneous displacement of the tendon (Eqn. (5-15)) was modelled following a sinusoidal-wave to simulate the acceleration and deceleration, where the variable (t) is the time between zero and the total contraction time (t_c).

$$instantaneous\ displacement = s(t)$$

$$= (\sin(\frac{t}{t_c}\pi + \frac{3}{2}\pi) + 1) \times x \qquad (5\text{-}15)$$

Fig. 44 shows the displacement of the tendons for unit constrictors C1 to C11 when Eqn. (5-15) is used to calculate tendon displacement over a 2.5 second contraction period. Each constrictor is separated by a delay time (t_{delay}) of 2.5 seconds between the actuation of each subsequent unit constrictor. The holding and expansion periods of unit constrictor actuation are not shown in Fig. 44 as the power requirements for these actuation states are decreasing or negligible compared to the contraction period.

Table 8: Parameters used for power calculations for unit constrictor contractions.

Constrictor	Contraction time	Initial circumference	Starting circumference	Starting contraction ratio	Contraction ratio from starting circumference	Final contraction ratio	Final circumference	Tendon displacement	Winding spindle radius	Winding motor - angular displacement	Winding motor - angular velocity (average)	Winding motor - revolutions per minute
	t_c	P_0	P_{start}	CR_{start}	CR	CR_{final}	P_{final}	x	r	$\Delta\Theta$	ω	RPM
	s	mm	mm	%	%	%	mm	mm	mm	rads	rads/s	
C1	2.5	251	305	-22%	20%	2.8%	244	31	7.5	4.1	1.6	15.5
C2	2.5	239	324	-36%	25%	-1.7%	243	41	7.5	5.4	2.2	20.6
C3	2.5	226	335	-48%	30%	-3.8%	235	50	7.5	6.7	2.7	25.6
C4	2.5	212	341	-61%	30%	-12.6%	239	51	7.5	6.8	2.7	26.1
C5	2.5	195	322	-65%	35%	-7.3%	209	56	7.5	7.5	3.0	28.7
C6	2.5	178	315	-77%	40%	-6.2%	189	63	7.5	8.4	3.4	32.1
C7	2.5	162	307	-90%	45%	-4.2%	169	69	7.5	9.2	3.7	35.2
C8	2.5	148	292	-97%	50%	1.4%	146	73	7.5	9.7	3.9	37.2
C9	2.5	139	277	-99%	55%	10.3%	125	76	7.5	10.2	4.1	38.8
C10	2.5	129	261	-102%	60%	19.1%	104	78	7.5	10.4	4.2	39.9
C11	2.5	108	218	-102%	60%	19.3%	87	65	7.5	8.7	3.5	33.3

The mechanical power required for the winding of a tendon and contraction of a unit constrictor can be calculated from the product of the angular velocity of the motor shaft and the applied motor torque (Eqn. (5-8)). The required winding motor torque (τ) is the product of the radius of the winding spindle (r) and the tensile force (F) (Eqn. (5-16)).

$$required\ torque = \ \tau = rF \tag{5-16}$$

Force calculations were based on the tendon displacement over time as provided by Eqn. (5-15) and then matched against the applied tension force per tendon displacement as found during the tensile tests for each unit constrictor. The instantaneous torque required for each

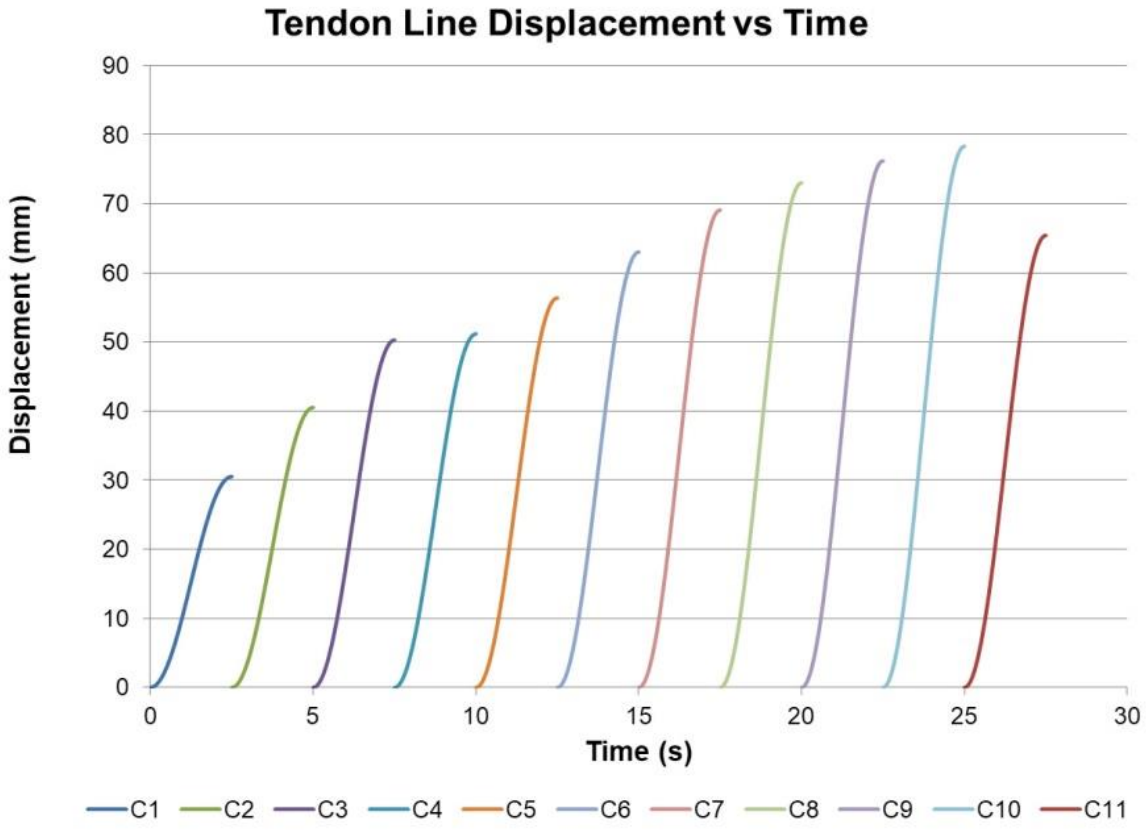

Fig. 44: Chart of the displacement of unit contraction tendon lines during contraction on a 1.5 litre volume artificial stomach. C12 was closed off.

unit constrictor contraction was then calculated by multiplying the required force by a winding spindle radius of 7.5 mm.

The required mechanical power during the contraction period, per unit constrictor, was determined using Eqn. (5-8) for rotational power calculation and is plotted in Fig. 45. The required power for unit constrictor actuation increases from unit constrictor C1 to C8 – from the corpus to the mid-antrum – and then begins to decrease for unit constrictors C9 to C11 – from the mid-antrum to the pylorus.

A winding motor required speed versus required torque chart is shown in Fig. 46. Included in the chart is the speed-torque characteristic of a 0.5 Watt GA12-N20-100 metal gear motor. The GA12-N20-100 motor was considered for use as a possible winding motor for the unit constrictors due to its small size (12 mm x 10 mm x 35 mm). Fig. 46 shows that the speed-torque requirements for the winding of the unit constrictors cannot be provided by the speed-torque characteristics of the GA12-N20-100 metal gear motor *i.e.*, the speed-torque curves of the unit constrictors do not all fall completely underneath the speed-torque curve of the GA12-N20-100 motor. Larger motors with improved speed-torque characteristics can potentially be used to individually drive the unit constrictor contractions, but this would increase the overall footprint and cost of the motors. Addressing this problem led to rethinking of the approach taken and the development of a capstan mechanism for providing mechanical advantage in the winding of the unit constrictor tendons.

5.1.4. Creating mechanical advantage with a capstan mechanism

The power and size of the motors required for the contraction of the unit constrictors can be reduced through the application of mechanical advantage. This also reduces the overall cost

and physical footprint of the motors, particularly if the number of motors required for driving the individual unit constrictors is substantial. The capstan mechanism creates mechanical advantage by amplifying a small input tension into a much larger output tension force. This section describes how a tendon and pulley system can implement use of the capstan mechanism to gain mechanical advantage.

The principle of the capstan mechanism involves a constantly rotating spindle producing a large amount of torque, around which a flexible tendon or rope is coiled. A small tension force applied to one end of the tendon, and in the same direction that the capstan spindle is rotating, will produce a larger tension force on the tendon on the other side of the capstan spindle [209, 210]. The increase in applied tension force from the input tension to the output

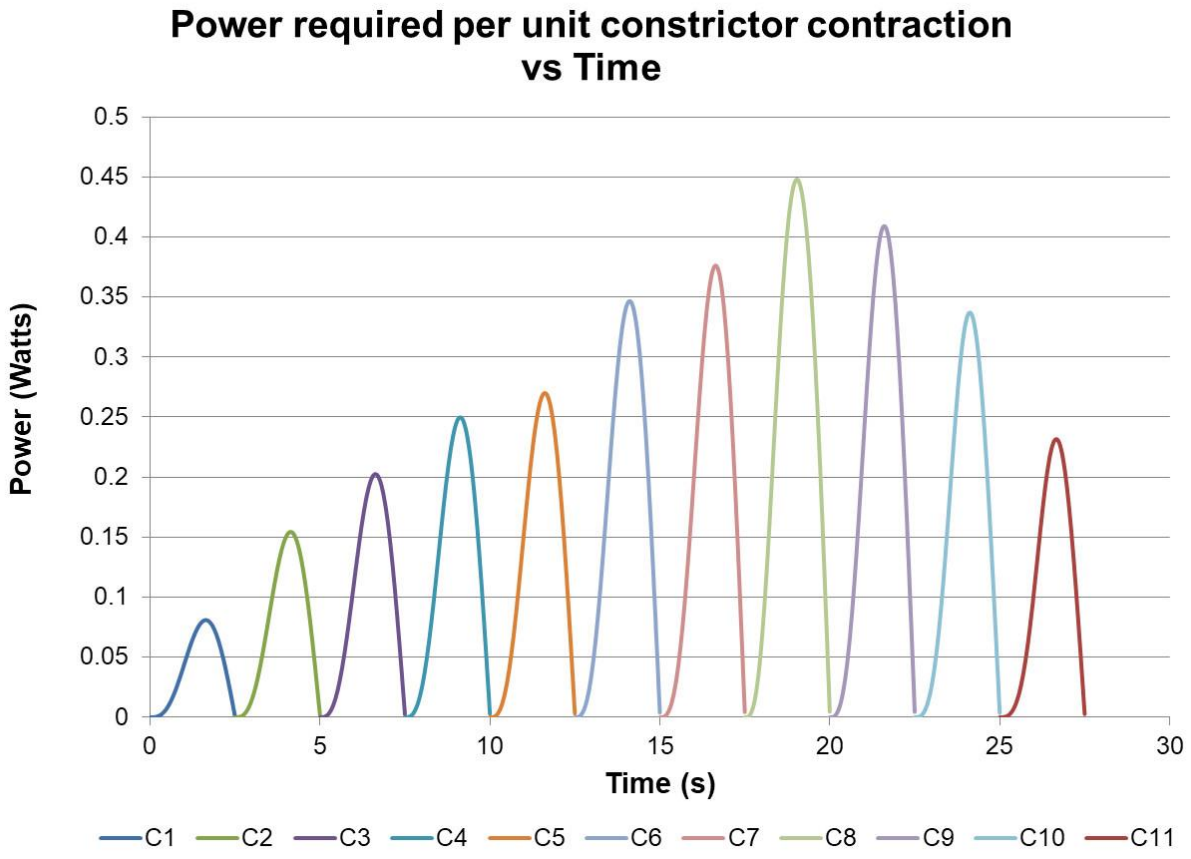

Fig. 45: Power requirements for unit constrictors C1 to C11 during a contraction time of 2.5 seconds per unit constrictor. C12 was closed off.

tension depends on the amount of friction contact occurring between the capstan spindle and the tendon. The amount of contact friction between the tendon and capstan spindle can be altered by changing the number of turns or coils that the tendon makes around the capstan spindle. Increasing the fractional number of turns of the tendon around the capstan spindle therefore increases the output tension achieved by the mechanism (Eqn. (5-17)) [209].

$$T_2 = T_1 e^{\mu\beta} \tag{5-17}$$

Where:
T1 = input tension
T2 = output tension
μ = friction coefficient between spindle and tendon
β = angle (in radians) in which the tendon is in contact with the spindle (fractional number of turns or coils)

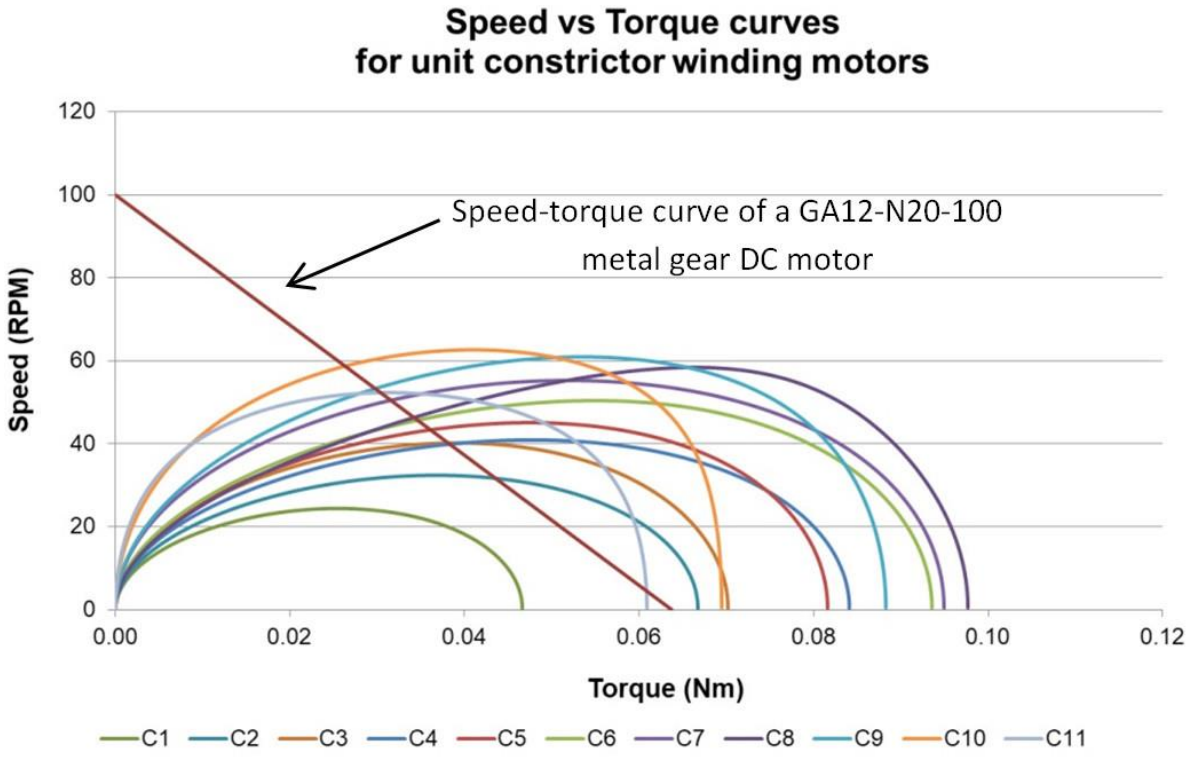

Fig. 46: Required speed-torque characteristics for the winding spindles of unit constrictors C1 to C11 compared against the speed-torque capability of a 0.5 Watt GA12-N20-100 metal gear DC motor.

The coefficient of friction for braided polyethylene line (Black Magic Hyperglide 13x Braid, 50 lb, 0.405 mm) when wrapped around mild steel tubing was determined experimentally by measuring the output tension force obtained from a capstan mechanism setup. A capstan motor and spindle was placed underneath a universal testing machine with one end of the braided polyethylene line gripped in its upper jaws. A 1 Newton mass was suspended at the other end of the braided line to act as the input tension to the capstan mechanism. The braided line was wrapped around the capstan spindle before suspending the 1 N mass from it. The number of turns of braided line wrapped around the capstan spindle was increased from 1 turn to 9 turns in 1 turn stages and the results of the measured output tension force obtained is shown in Fig. 47.

A coefficient of friction (μ) of 0.065 was obtained by fitting an exponential curve to the experimental data and rearranging Eqn. (5-17). This coefficient is comparable with that obtained by Dhouibi et al. [211] when investigating the friction behaviour of high-density polyethylene (HDPE) against 304L stainless steel. Increasing the number of turns of tendon around the capstan spindle can provide significant magnification of the output tension. However, the output tension force is constrained to an absolute maximum level by the speed-torque capability of the capstan motor that is being used. The advantage obtained here is that the input tension force applied by the winding spindle can now be reduced by the level of force magnification provided by the capstan mechanism - this means that smaller motors with lower torque capabilities can be used to drive the input tension from the winding spindles.

If the continuous rotational velocity of the capstan spindle drops to an insufficient rate, then the mechanical advantage obtained by the capstan mechanism may be lost. The rotational velocity of electric motors has an inverse relationship to the amount of torque provided by the motor. As the torque increases, the velocity reduces. Selection of a capstan motor with sufficient power to handle the required speed and torque characteristics, along with an appropriate choice for the capstan spindle diameter, can prevent this problem from occurring.

For mechanical advantage to be maintained the capstan spindle needs to rotate at least as fast as the maximum rate of draw that is being applied to the tendon. The angular velocity (ω) and diameter (D) of the capstan spindle determine the maximum potential winding rate

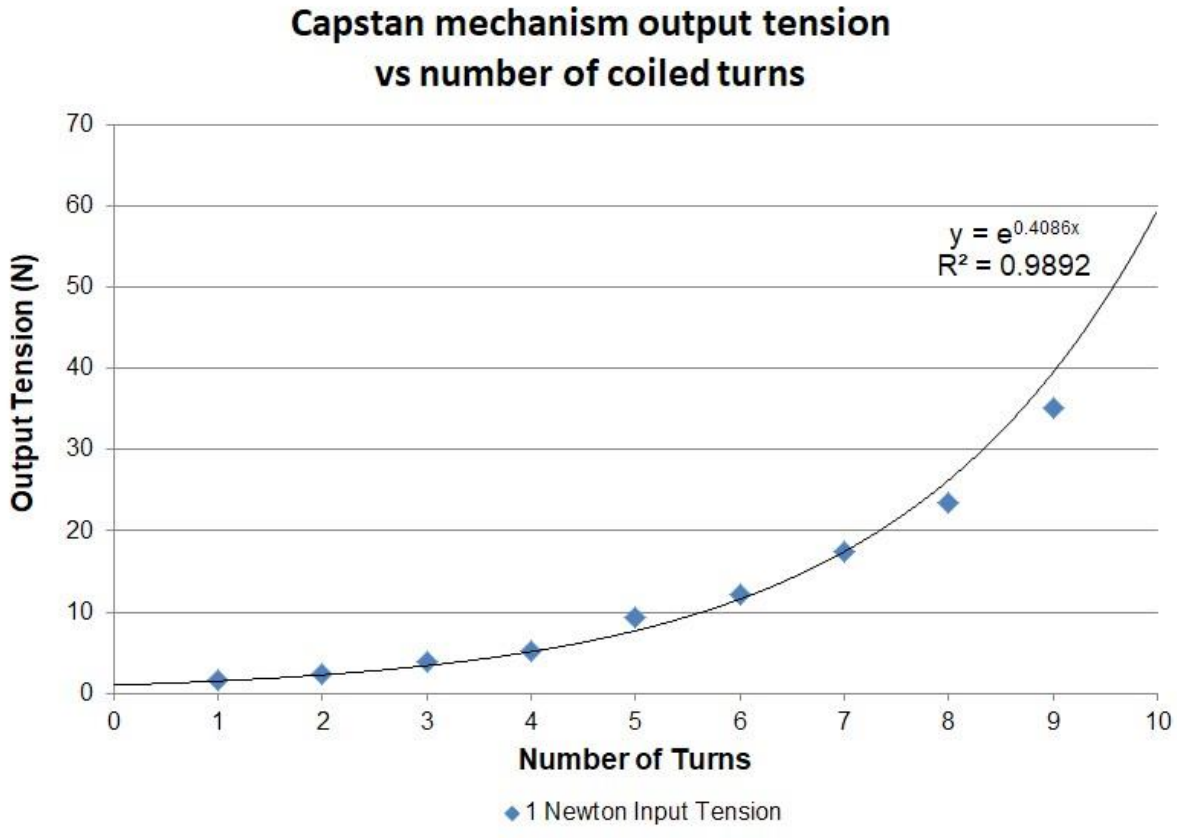

Fig. 47: Range of output tension obtained from a capstan mechanism when a 1 Newton mass was suspended on a polyethylene braided line wrapped around a mild steel tube capstan spindle.

of the tendon as defined by Eqn. (5-18). The angular velocity of the motor shaft varies depending on the load being applied to the motor at any one time, but if the capstan spindle's rotational velocity always exceeds the maximum required amount of tendon draw then the capstan mechanism will continue to provide mechanical advantage.

$$maximum\ rate\ of\ tendon\ draw = \frac{\omega}{2\pi}\pi D = \frac{\omega D}{2} = \omega r \qquad (5\text{-}18)$$

Where:
ω = angular velocity
D = diameter of the capstan spindle
r = radius of the capstan spindle

A proof-of-concept model was constructed for a tendon actuation system using mechanical advantage obtained by the capstan mechanism. Fig. 48 shows a basic configuration diagram of a capstan mechanism being applied to the contraction of a unit constrictor. The tendon lines from a unit constrictor are passed through a 2 mm hole in a fixed wall or plate to prevent the unit constrictor's Bowden cable from moving when tension force is applied to the tendon, therefore allowing the looped unit constrictor to contract as a result. The tendon is coiled around a capstan spindle several times and attached to a winding spindle powered by a small, geared, DC motor. The capstan spindle is continuously rotating in the same direction as the uptake direction of the winding motor and driven by a motor with larger power capabilities. To mechanically amplify the contraction force in pulling the tendon the winding motor and spindle should be winding on the tendon in the same rotational direction as the capstan spindle is rotating. The input tension to the capstan spindle is then transformed by the mechanism to an amplified output tension to the unit constrictor tendon.

Initial trials of the capstan mechanism indicated deficiencies in the take-up and release of the input tension of the tendon. Friction contacts of the tendon arising between the winding spindle and capstan spindle (Fig. 49) affected the input tension being applied to the capstan spindle and caused a small delay to occur between winding spindle activation and the contraction of the unit constrictor.

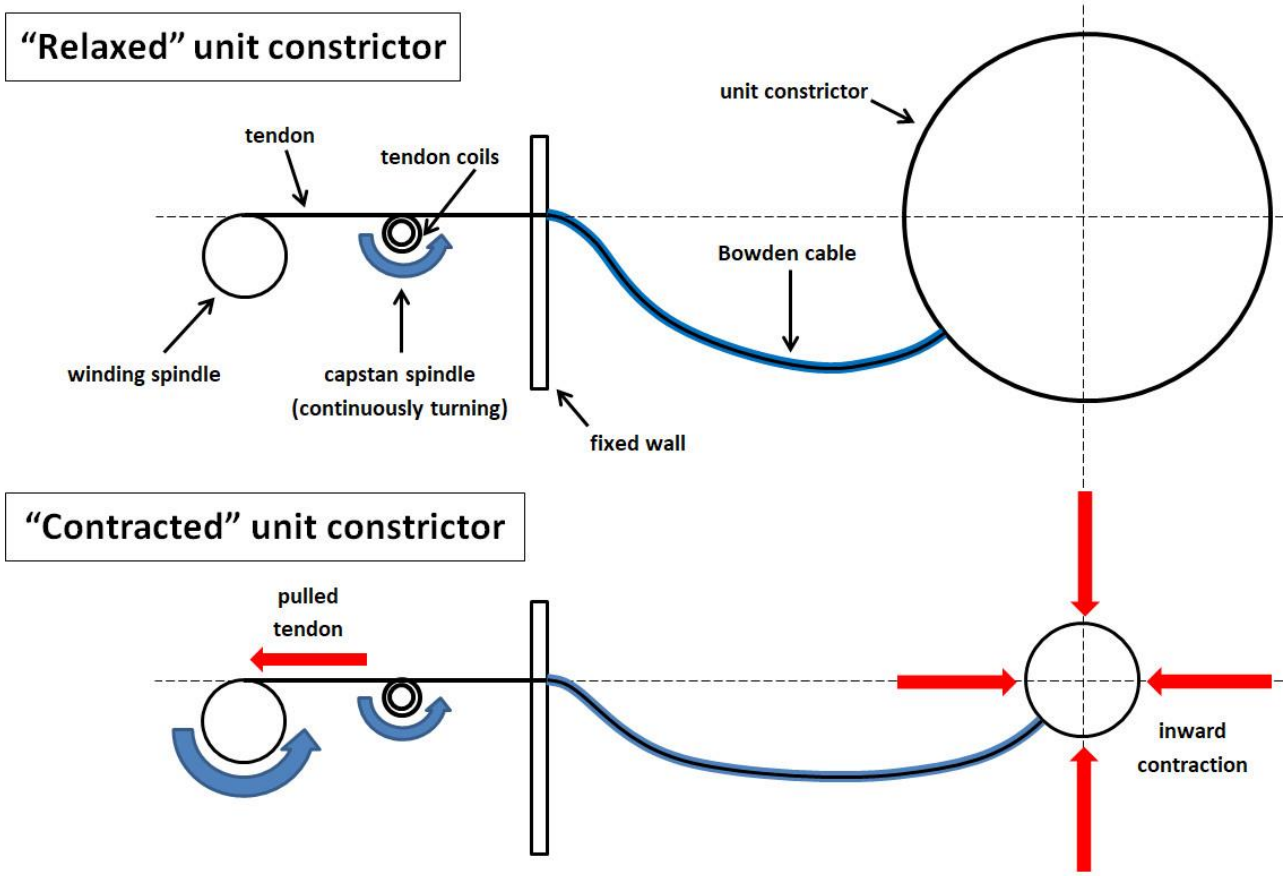

Fig. 48: Diagrammatic example of the contraction of a unit constrictor employing a capstan mechanism.

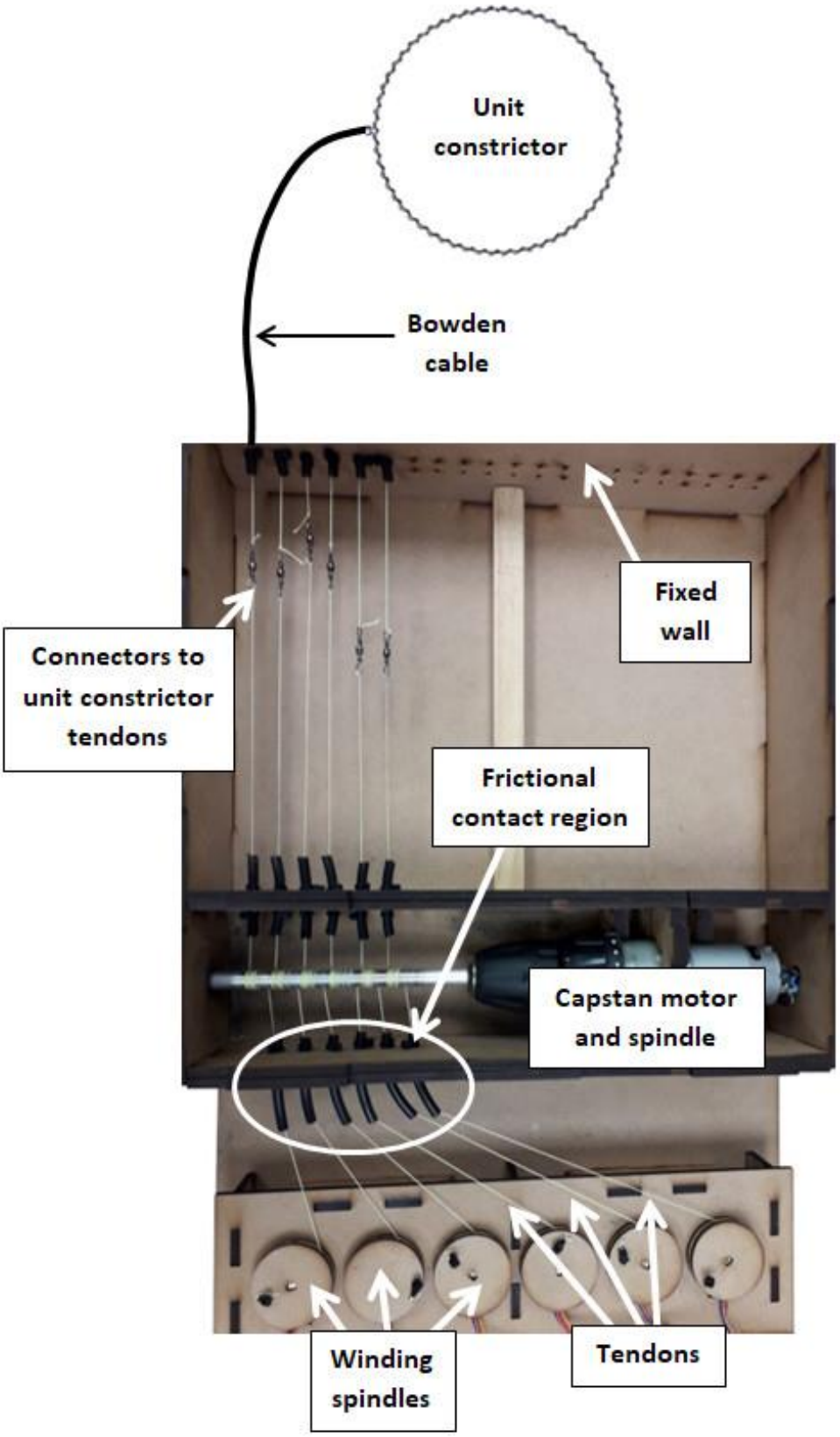

Fig. 49: Proof-of-concept prototype model of the winding control system using a capstan mechanism.

This was because displacement of the tendon needed to overcome static friction before a sufficient input tension was able to be provided to the capstan spindle. If the amount of static contact friction to overcome is significant then the initial rate of change in the input tension can be dramatically affected. As a result, the contraction of the unit constrictor may visibly respond with an initial sudden jump in contraction. This situation can occur on both take-up and release of the input tension of the tendon.

Minimising friction effects on the input tension may be achieved by ensuring a direct line of feed of the tendon from the winding spindle to the capstan spindle, or by introducing a pulley in between the winding and capstan spindles to reduce frictional contact through rotational redirection of the tendon. However, if the amplification provided at the output tension side of the mechanism is large then even small disturbances in the input tension side can cause the unit constrictor to rapidly contract in an uncontrollable manner. These disturbances can arise from overcoming the static friction of a connected pulley, from loose fastenings of the winding motor bracket or spindle, or from backlash from the winding motor shaft.

Feeding the tendon from a perpendicular direction to the capstan axis prevents it from drifting along the capstan spindle, which can cause a loose tendon to wrap over its own coils. If a tendon begins to wrap itself over its coils, it can prevent the tendon line from smoothly uncoiling off the capstan spindle and result in an uncontrollable, and at times catastrophic, contraction of the unit constrictor to take place. To mitigate this problem both the input and output sides of the capstan spindle should have the tendon approach it perpendicularly.

The flexibility of the type of tendon line material used for the capstan mechanism can also develop memory of curvature after repeated winding and unwinding around a spindle or pulley. This can add to the problem of the line wrapping over itself during operation of the capstan mechanism. To minimise tendon stretch and the potential for memory of curvature developing in the tendon line a braided polymer fishing line (Maxistrike Braid – 30 lb) was used as the winding tendon instead of a monofilament nylon line.

The capstan mechanism only produces force amplification of the tension in a single direction. Reversing the direction of the winding spindle reduces the tendon input tension force being applied to the capstan spindle. As the input tension force reduces, the contact friction of the tendon coils on the capstan spindle decreases, allowing the tendon to relax, pass back through the Bowden cable, and expand the unit constrictor. Because the capstan spindle is continuously rotating in a single direction it then acts as a brake when the winding spindle is releasing tendon [210], preventing further extension of the unit constrictor until the input tension is again reduced.

A lack of tendon tension on either side of the capstan spindle can also create a problem. This problem can occur when the winding spindle is releasing tension on the tendon and there is insufficient tension force being taken up at the output side of the capstan spindle. For example, assume a unit constrictor was undergoing a contraction by increasing the input tension on the tendon lines via the winding spindle. If the winding spindle reverses direction, and the unit constrictor was unable to extend in response, the tendon tension on both the input and output sides of the capstan spindle becomes slack. A slack tendon on the winding spindle can cause the tendon to slip off the winding spindle entirely. A slack tendon on the capstan spindle can cause the tendon coils to loosen and unwind, potentially

wrapping over themselves in a haphazard manner. If the winding spindle then increases the input tension the self-wrapped coils on the capstan spindle may not unwind properly, and the constantly rotating capstan spindle will continue to wrap more tendon around itself until the unit constrictor is fully contracted and either the tendon breaks, or the winding or capstan spindles seize - potentially damaging or destroying the motors.

A linear slider was trialled in the tendon control system to mitigate potential catastrophic failure of the tendon resulting from insufficient input and output tensioning. The slider was positioned between the capstan spindle and the tendon coming from the unit constrictor (Fig. 50(a)). Movement of the linear slider was created by using the capstan mechanism for both forward and reverse direction of the sliders' motion (Fig. 50(b and c)). The winding spindle produces input tension to the capstan spindle while movement of the slider creates tension on the output side during both the winding and unwinding actions, therefore minimising potential for the tendon coils on the capstan spindle to go slack. The tendon coming from the unit constrictor is directly connected to the linear slider which then allows the slider to regulate the amount of contraction being applied to the unit constrictor.

The winding spindle consists of two separate take-up sections to pull the linear slider in both forward and reverse directions (Fig. 50 (d)). One of the take-up sections is winding on as the other take-up section is winding off. This reciprocal winding action prevents the tendon line from becoming slack and spreading uncontrollably over the capstan spindle during the winding process.

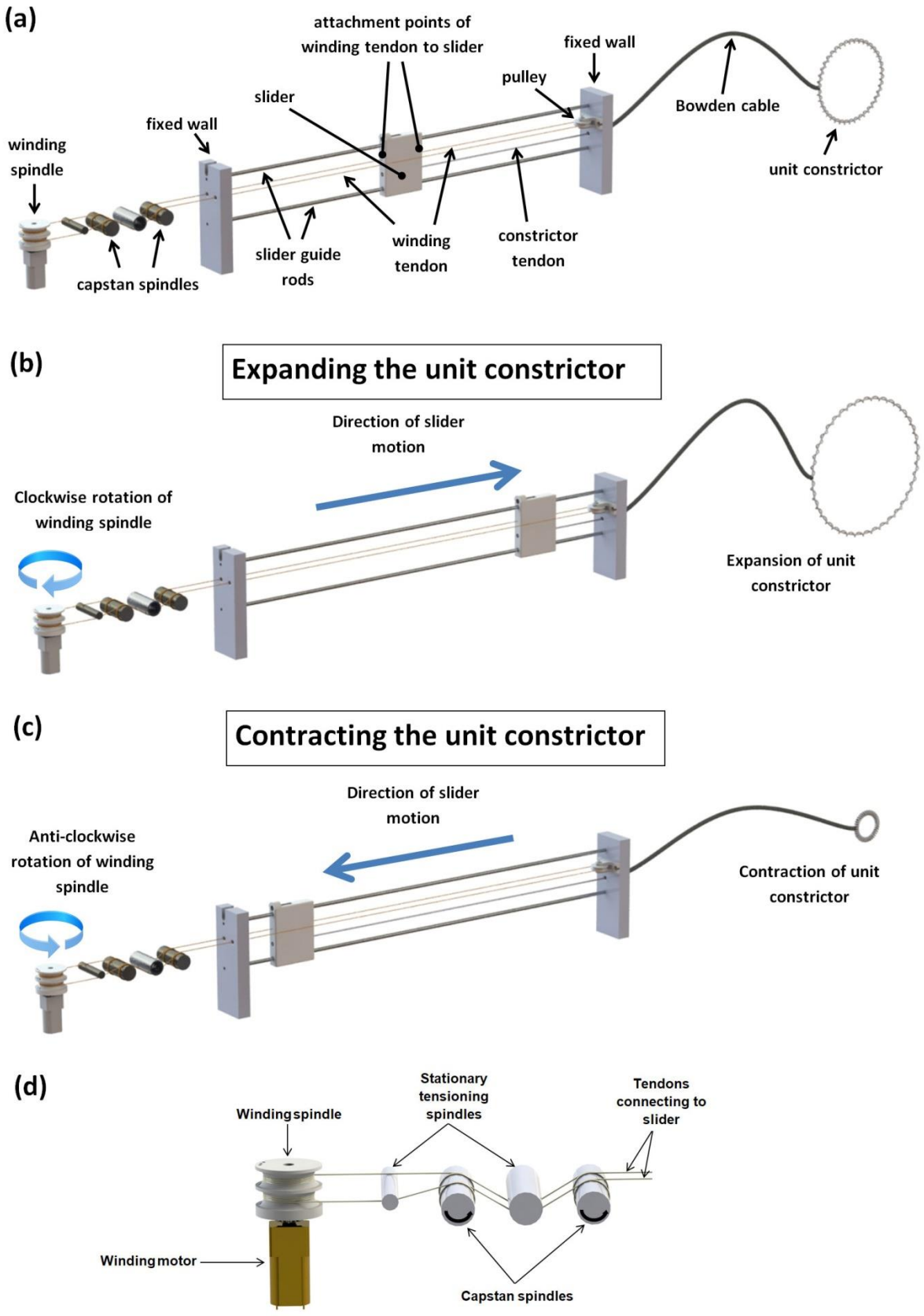

Fig. 50: (a) Rendered image of the parts of the linear slider and capstan mechanism trial setup. (b) Expansion of the unit constrictor. (c) Contraction of the unit constrictor. (d) View of the tendon line coiled around the winding spindle and two capstan spindles in series.

Capstan mechanisms can be placed in series so that the output from one capstan spindle becomes the input to another (Fig. 50 (d)). This further reduces the input tension force required from the winding motors and redistributes the power burden for actuation over multiple capstan motors. Additional tensioner spindles can be placed to assist in reducing axial wandering of the tendons over the capstan spindle surface and redirect the tendon lines to the upper or lower take-up sections on the winding spindle.

The speed-torque requirements for the unit constrictor winding motors calculated in Section 5.1.1 (Fig. 46) showed that an unassisted GA12-N20-100 metal gear DC motor, intended as a typical motor size for the winding of the tendons, was incapable of providing sufficient power for the task. Combination of low-torque winding motor with a capstan mechanism employing a high-torque geared DC motor and ten turns of the braided polyethylene tendon line over the capstan spindle, results in torque requirements for the winding spindle of the unit constrictor tendons being reduced by approximately 60 times (Fig. 51). With the subsequent reduction in torque requirements the low-torque winding motors now have capability to suitably drive the winding of the tendons. This is shown in Fig. 51 by the speed-torque requirement curves of the unit constrictor contractions falling completely within the speed-torque output curve of the low-torque motor.

Sensing the amount of tendon winding taking place

Quantifying the amount of displacement that the tendons undergo is accomplished by measuring either the rotary displacement of the motors and spindles, or the linear displacement of sliders (Section 6.1). Rotary displacement involves measuring the angular rotation of the winding motor shaft and then calculating the length of tendon that subsequently wraps or unwraps around the winding spindle perimeter. This calculation is

dependent on the diameter of the winding spindle and in maintaining continuous measurement of the angular rotation that is carried out by the motor shaft. Alternatively, sensing of the linear displacement of the slider can be an absolute measurement, meaning that continuous incremental sensing of the sliders' position may not be necessary and that measurements need only be carried out when required. Tendon displacement feedback mechanisms for the actuation control system are explained in more detail in Chapter 6.

5.2. Continuous actuation of multiple unit constrictors

The ability to actuate multiple constrictions over the tract wall from a single controllable mechanism can reduce the cost and complexity of a physical simulation model. Some of the gastric tract deformation patterns that occur are cyclic and repetitive, which suggests that

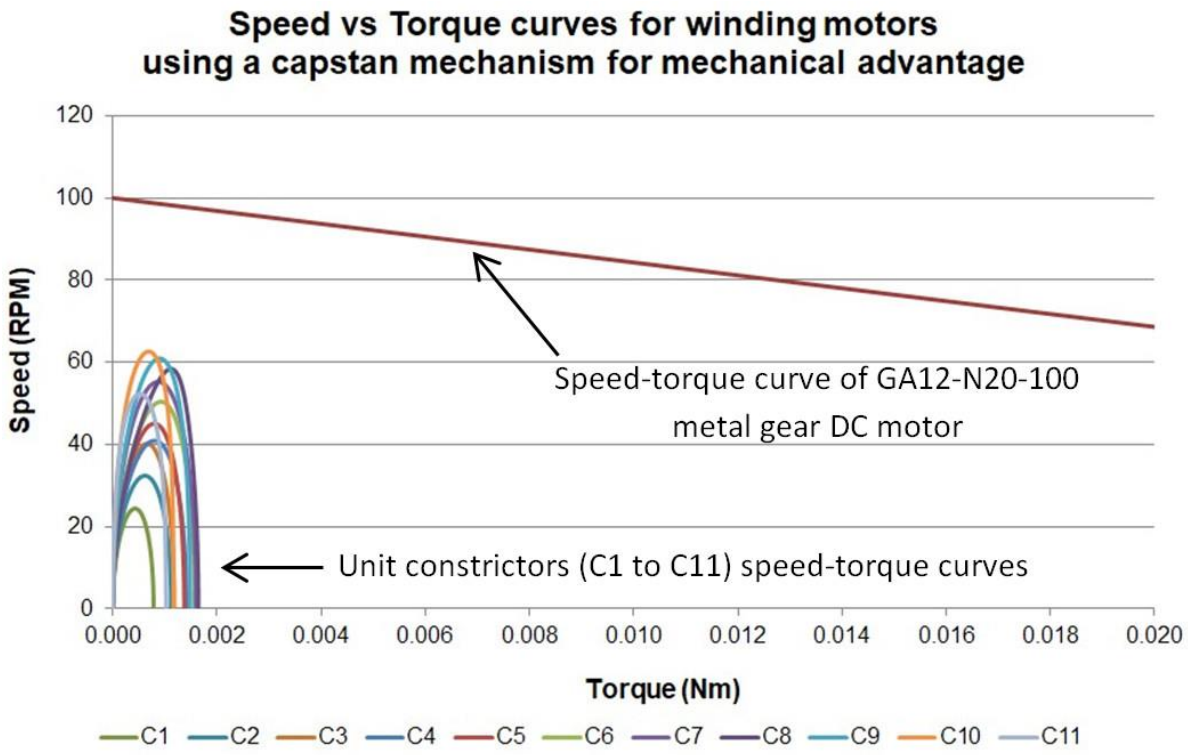

Fig. 51: Reduced unit constrictor speed-torque characteristics achieved through the implementation of a capstan mechanism delivering mechanical advantage to the winding of tendons.

the contraction pattern may be automated by mechanical means. This type of deformation control mechanism applies to situations where the amplitude of the constrictions is consistent over time, or the deformation pattern is not subject to alteration from feedback mechanisms. An example of the type of deformation pattern deemed suitable for single mechanical actuation control is the action of swallowing a bolus of food by the oesophagus.

The oesophagus can be treated as a simple tubular section of the gastric tract that produces a steady, consistent peristaltic wave that propels the tract contents towards the stomach. In this way the oesophagus acts as an effective pump for boluses of food. A series of unit constrictors positioned along a length of artificial membrane tract can be used to provide contractions that mimic the circular contractions of the oesophageal tract wall. However, to actuate each of these artificial muscles individually along the entire length of oesophageal tract would require a substantial number of motors. Reducing the total number of motors required to control these multiple constrictions can be cost-effective and achievable using innovative mechanical actuation systems.

5.2.1 Rotating disc mechanism

A rotating disc mechanism was developed for pulling multiple unit constrictor tendons through the rotation of a single electric motor (Fig. 52 (a-d)). Multiple circular discs were attached to an axle that was driven by a geared direct-current (DC) electric motor. Tension pins were inserted between adjacent discs at an offset distance from the central axis (Fig. 52 (a)). The discs were separated from each other by an eight-millimetre gap to allow for the tendons to pass between the discs (Fig. 52 (b)). The role of the tension pins was to create a tension on the unit constrictor tendons as the disc was being rotated, causing the unit constrictors to contract from tensioning of the tendon (Fig. 52 (d)).

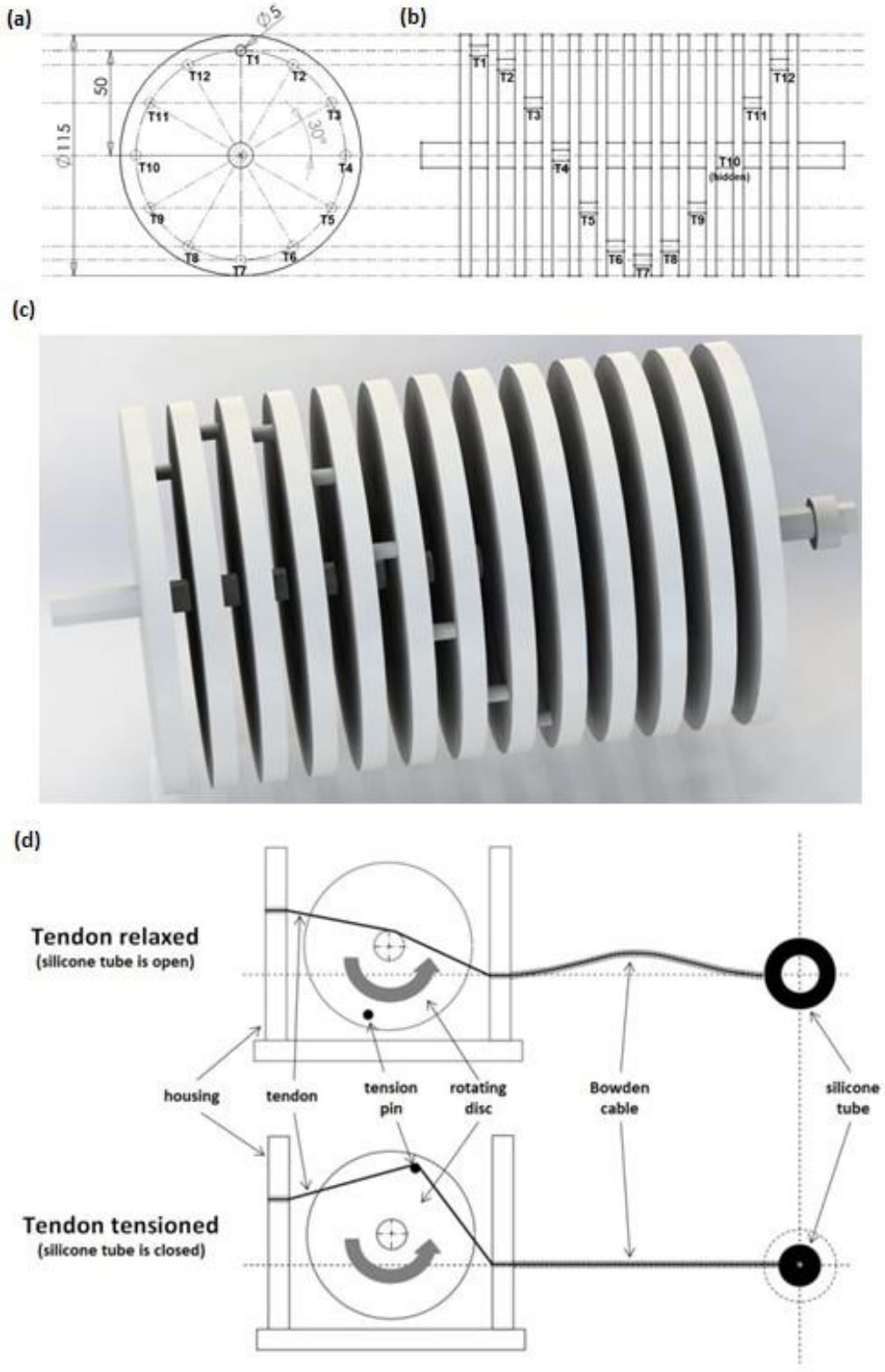

Fig. 52: (a) End view and (b) side view diagram of rotating discs with tension pins offset from each adjacent pin by an angle of π/6. (c) Rendered image of the rotating discs configuration. (d) Diagrammatic representation of the tension applied to unit constrictor tendons by a rotating disc with an attached pin.

Each tension pin is offset from its adjacent tension pin by a specified angle, creating a spiralling configuration of the pins along the length of the disc mechanism. This offset provides sequential actuation of the unit constrictors as the discs rotate. To actuate a series of twelve consecutive unit constrictors within a single rotation of the discs would require the tension pins to be offset from each other by an angle of $2\pi/12$ or $\pi/6$ (30°) (Fig. 52 (a)). As the discs rotate, the tendons are placed under tension by the pins and the unit constrictors are contracted one after the other, simulating a peristaltic contraction of the artificial muscles that is repeated each time the set of discs completes a full revolution.

The offset distance of the tension pin from the central axis (see Fig. 52 (a)) determines the amount of displacement being placed on the constrictor tendons, and thus the amplitude of the contraction or contraction ratio achieved by the unit constrictor. The diagram in

Fig. 53 shows the notation and geometry involved with the displacement of the tendons as the discs rotate. Calculation of the length of displacement of the unit constrictor tendon begins from obtaining the angle of the discs' tension pin with relation to the horizontal axis (θ).

When a disc rotates and the tension pin travels below the horizontal axis the tension pins will not be in contact with the tendon and the unit constrictor is placed in a relaxed state. This means that tensioning of the tendon occurs during only one half of the revolution period of the discs. During the other half-rotation, the tendon has no contact with the tension pin and therefore no tension is being applied to it (Fig. 52 (d)). Calculation of the amount of tendon displacement when it is in contact with the tension pin is based upon the angle of the tension pin with respect to the central axis (θ). The horizontal (x) and vertical

(y) distances of the tension pin from the central axis is obtained from Eqns. (5-19) and (5-20).

$$x = r_{offset}\cos(\theta) \tag{5-19}$$

$$y = r_{offset}\sin(\theta) \tag{5-20}$$

Using Pythagoras' theorem, the distance to the axis of the tension pin from the tendon entry point (A) and the fixed point of the tendon (B) can be obtained (Eqns. (5-21) and (5-22)).

$$A = \sqrt{(C - x)^2 + y^2} \tag{5-21}$$

$$B = \sqrt{(C + x)^2 + y^2} \tag{5-22}$$

The length of tendon (A`), beginning from the tendon entry point and ending tangent to the surface of the tension pin, can also be obtained using Pythagoras' theorem where A is the hypotenuse and the radius of the tension pin (r_{pin}) is the other known length of the right triangle (Eqn. (5-23)).

$$A` = \sqrt{A^2 - {r_{pin}}^2} \tag{5-23}$$

Similarly, the length of tendon from the surface of the tension pin to the fixed point of the tendon (B`) can be obtained using Eqn. (5-24).

$$B` = \sqrt{B^2 - {r_{pin}}^2} \tag{5-24}$$

To calculate the length of tendon that is in contact with the tension pin (P_{arc}) first requires obtaining angles (e), (f), (a`) and (b`) (Eqns. (5-25) to (5-28)).

$$e = \cos^{-1}\left(\frac{C-x}{A}\right) \tag{5-25}$$

$$f = \cos^{-1}\left(\frac{C+x}{B}\right) \tag{5-26}$$

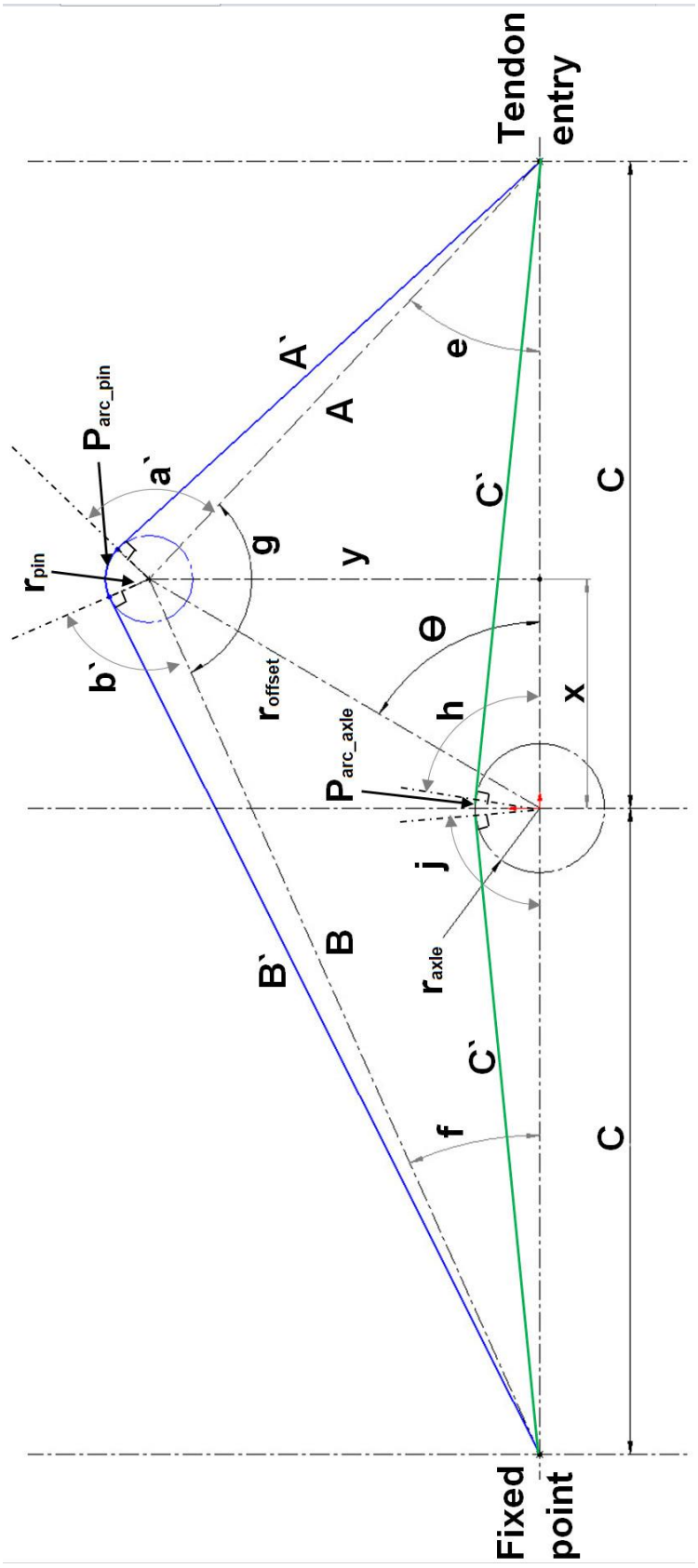

Fig. 53: Notation diagram of the geometry involved with the rotating disc method for tendon displacement.

$$a` = \cos^{-1}\left(\frac{r_{pin}}{A`}\right) \quad (5\text{-}27)$$

$$b` = \cos^{-1}\left(\frac{r_{pin}}{B`}\right) \quad (5\text{-}28)$$

Subtracting (e) and (f) from π gives (g) (Eqn. (5-29)), which is then used with angles (a`) and (b`) in Eqn. (5-30) to provide the arc length of tendon that is in contact with the tension pin.

$$g = \pi - (e + f) \quad (5\text{-}29)$$

$$P_{arc\_pin} = r_{pin}(2\pi - (g + a` + b`)) \quad (5\text{-}30)$$

The length of tendon when the tension pin is at angle (ϴ) to the horizontal axis is obtained by adding the lengths A`, B`, and P_{arc} (Eqn. (5-31)).

$$length\ of\ tendon\ at\ angle\ (\theta) = A` + B` + P_{arc\_pin} \quad (5\text{-}31)$$

When the tendon is not under tension it simply rests on top of the central axis. By using Pythagoras' theorem to obtain length C` (Eqn. (5-32)) and calculating angles (h) (Eqn. (5-33)) and (j) (Eqn. (5-34)) to get P_{arc_axle} (Eqn. (5-35)) we can calculate the length of tendon in its resting state (Eqn. (5-36)).

$$C` = \sqrt{C^2 - {r_{axle}}^2} \quad (5\text{-}32)$$

$$h = \cos^{-1}\left(\frac{r_{pin}}{C}\right) \quad (5\text{-}33)$$

$$j = \cos^{-1}\left(\frac{r_{pin}}{C}\right) \quad (5\text{-}34)$$

$$P_{arc\_axle} = r_{axle}(\pi - (h + j)) \quad (5\text{-}35)$$

$$length\ of\ tendon\ at\ resting\ state = 2C` + P_{arc\_axle} \quad (5\text{-}36)$$

The change in length of tendon when placed under tension by the tension pin – the total tendon displacement (Eqn. (5-37) - is then obtained by subtracting the length of tendon in its resting state (Eqn. (5-36) from the length of tendon when placed under tension (Eqn. (5-31)).

$$total\ tendon\ displacement = A` + B` + P_{arc\_pin} - (2C` + P_{arc\_axle}) \qquad (5\text{-}37)$$

The maximum displacement of the tendon occurs when the disc pin is 90° from the horizontal axis. For a tension pin of 2.5 mm radius (r_{pin}) with an axial offset (r_{offset}) distance of 35 mm, an axle radius (r_{axle}) of 7 mm, and a total distance between the tendon entry and its fixed point (C + C) of 130 mm, the length of displacement of the tendon line passing over the tension pin when the tension pin is rotated to 90° about the horizontal ($\Theta = \pi/2$) would be 20.4 mm. This would result in a total reduction of the unit constrictor circumference of 2 x 20.4 mm = 40.8 mm as there are two tendon lines coming from the looped unit constrictor passing over the tensioning pin. If the outer sleeve of the expandable braid tubing (refer Section 4.1.2) has an initial relaxed diameter of 25 mm, then applying Eqn. (4-1) (Section 4.2) for the braid contraction ratio would result in a contraction ratio of (1 – ((π x 25 mm – 40.8 mm) / (π x 25 mm))) x 100% = 52.0%. This translates to a final contracted braid diameter of 25 mm x (1 – 0.52) = 12.0 mm. A contracted diameter of this magnitude is sufficient to completely close an artificial tract tube of soft rubber that has an initial relaxed internal lumen diameter of 10 mm and a wall thickness of 7 mm.

5.2.2. Linear peristaltic pump

The rotating disc mechanism can be employed to drive a series of unit constrictors to sequentially squeeze a flexible tube or tract and therefore behave as a linear peristaltic pump. To demonstrate the pumping ability of such a mechanism an expandable braided tube was fitted over an inner soft silicone tube constructed from Ecoflex™ 00-30 (Smooth-On Inc., USA), with an internal diameter of 10 mm and thickness of 7 mm, to act as the tract of an artificial oesophagus. Flexible braided polymer tendons (Maxistrike Braid 30lb, Maxistrike, New Zealand) were threaded through the expandable braid and run through Bowden cables to the rotating disc mechanism (Fig. 54). Lengths of 6 mm internal diameter

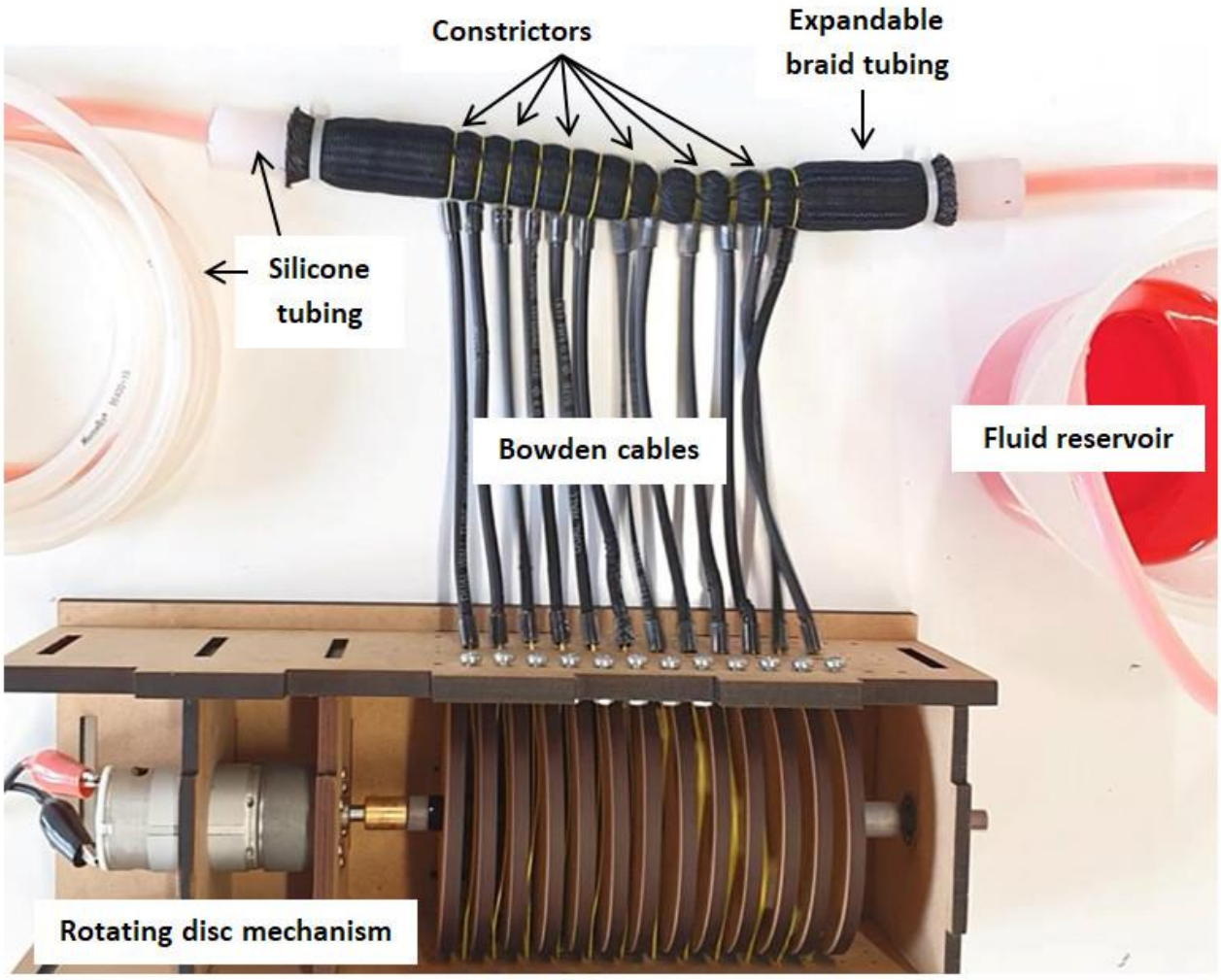

Fig. 54: A linear peristaltic pump showing a proof-of-concept prototype of the rotating disc mechanism connected to an expandable braided tube with attached tendons for actuation.

silicone tubing were attached to the ends of the tubular pump to transport the trialled fluids to and from the pump.

The experimental setup involved peristaltic pumping of water and glycerol (99.5%) to specified heights and measuring the volumetric flow rate or capacity that was achieved. The fluid filled a weir that was connected to the pump via a length of 6 mm internal diameter silicone tubing. The total static head achieved by the pump was calculated by subtracting the height of the static suction head from the height of the static discharge head (Fig. 55).

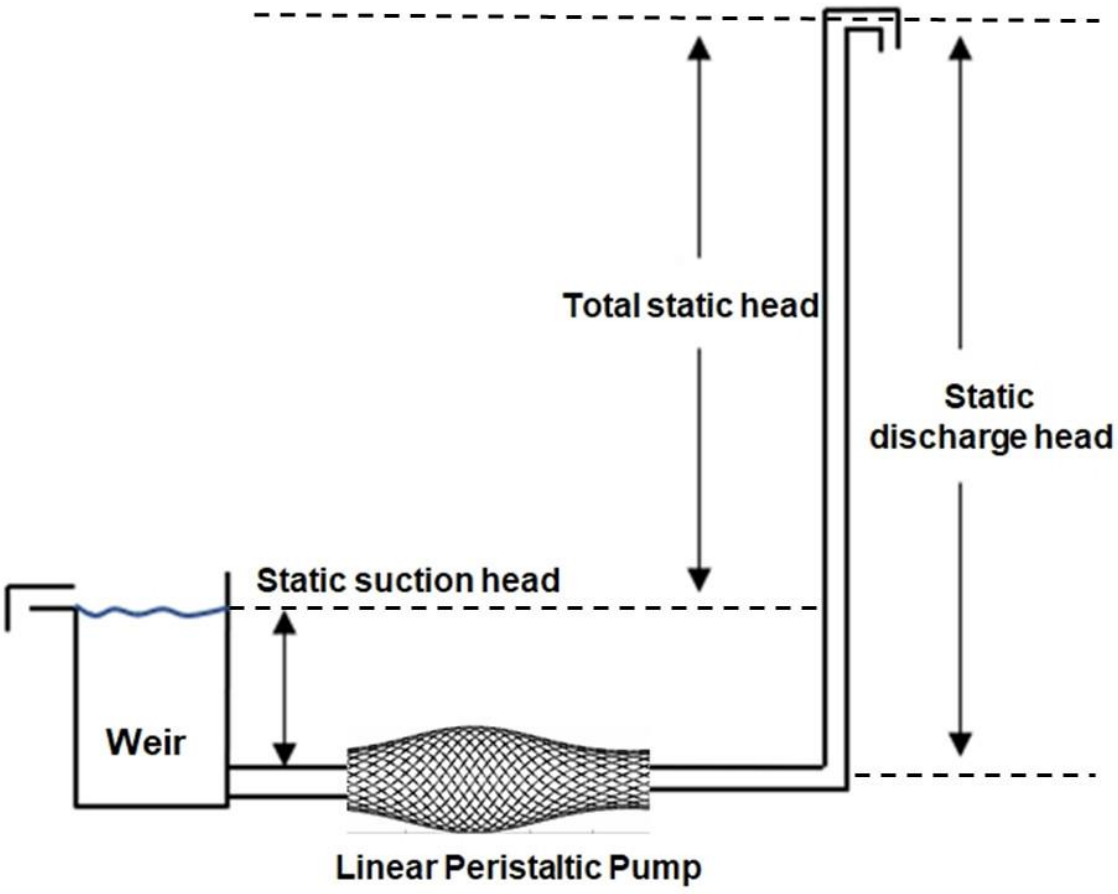

Fig. 55: Setup of measurement trial of linear peristaltic pump performance.

Initially the pump mechanism used a pattern of tension pin placements that created a sinusoidal contraction of the unit constrictors, which allowed for two contractions of the tract to be performed per single revolution of the discs. The tension created on the tendons was capable of entirely closing the tract tubing but was not capable of completely relaxing the tubing when the tendons were relaxed. This resulted in a sub-optimal volumetric capacity being achieved by the pump (Fig. 56 – ▲ green triangle) as the lack of expansion of the tubing prevented a larger volume of fluid from being transported during each peristaltic contraction.

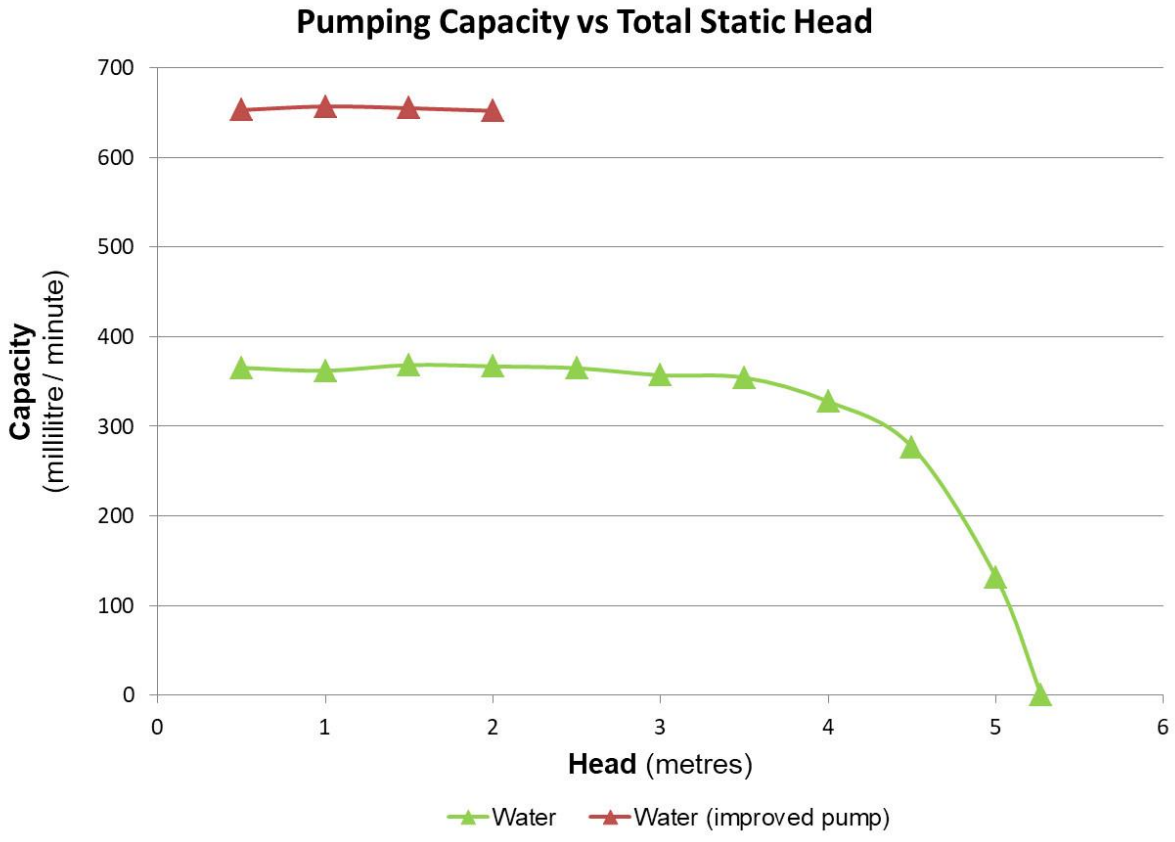

Fig. 56: Chart of linear peristaltic pump performance for the pumping of water at 22° C.

An improved version of the pump was developed where only a single contraction of the series of unit constrictors was created for every revolution of the discs. The relaxation period of the tendons was extended during each revolution to allow the tract to expand significantly between contractions and draw more volume of fluid into the tubing. Although the trial using the improved pump covered a static head of only up to 2 metres the capacity was twice that obtained by the original pump (Fig. 56 – ▲ red triangle). Fig. 57 shows the peristaltic pumping of 99.5% pure glycerol at 22°C resulted in a lower capacity of only 9-11 millilitres per minute because the glycerol was significantly more viscous when compared to water at the same temperature, as is shown in Table 9 [212].

The peristaltic transport of higher-viscosity fluids was affected by the increased friction the

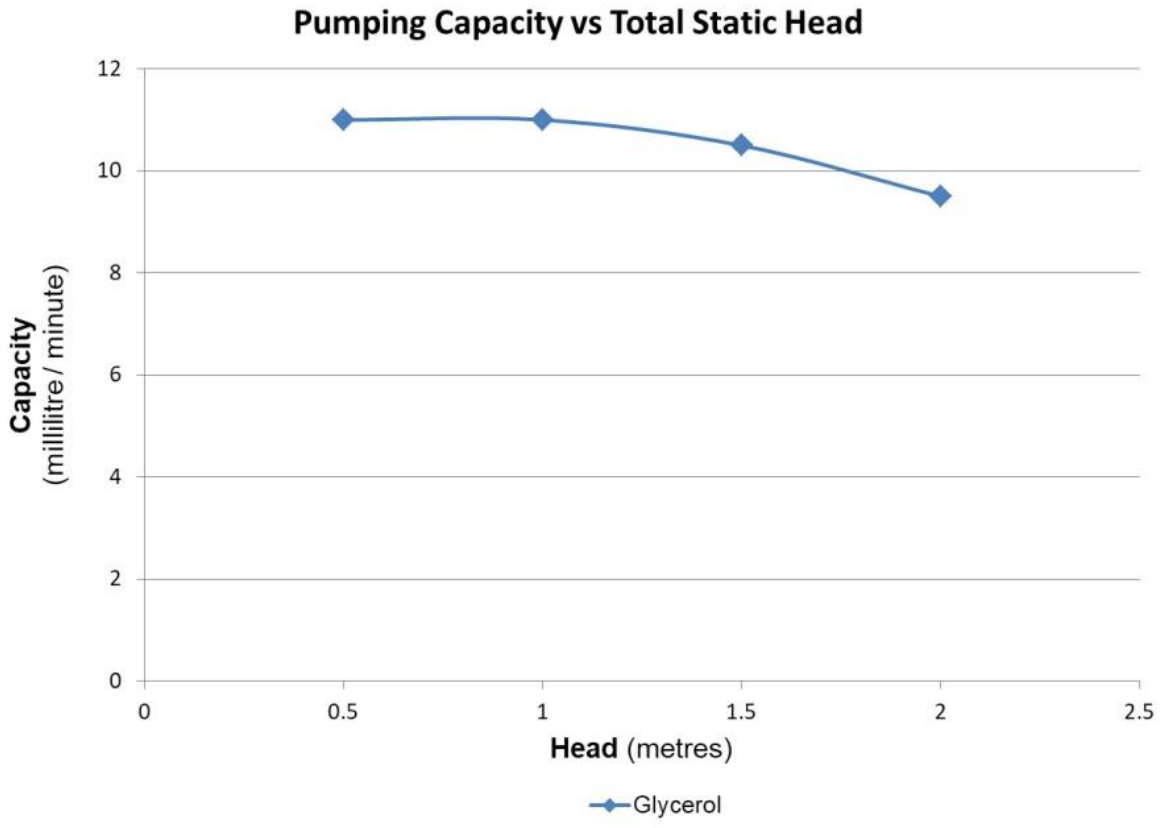

Fig. 57: Chart of linear peristaltic pump performance for pumping of glycerol (99.5% pure) at 22° C.

fluids experience against the surface of the tubing that it is travelling through. High-viscosity fluids therefore take more time to be drawn into the inlet of the pump tubing which decreases the ability of the tubing to expand to its original relaxed diameter. The volume of fluid being pumped through the tubing during each peristaltic wave is reduced compared to the volume being pumped through with a less viscous and therefore less frictional fluid.

The effects of high viscosity fluids on pumping capacity could be overcome by priming the pump inlet with a small volume of the viscous fluid prior to the initiation of the contractions. A volume of the fluid is therefore pushed or injected into the inlet, expanding the tract as it does so, and creating an initial volume of material upon which the peristaltic contractions can contract against. Some surface friction from pump contents could also be present throughout the entire length of tubing, but this could be mitigated by introduction of a surface lubricant to the inner lining of the tubing. Application of a tract surface lubricant may then assist in the same way as saliva and mucus secretions 'lubricate' the oesophageal tract to effectively propel a bolus of food.

The rotating discs mechanism provides a constant contraction ratio to the unit constrictors it is attached to so may prove to be more suitable for controlling the contraction of longer uniform lengths of tract for example, the oesophagus and intestinal segments. The reduced

Table 9: Viscosity (in centipoise) of water and glycerol at different temperatures. Sourced from: Gregory, S. (2018). Physical properties of glycerine. In Glycerine (pp. 113-156): CRC Press.

	0°C	**10°C**	**20°C**	**30°C**	**40°C**
Water	1.792	1.308	1.005	0.8007	0.656
Glycerol	9420	3090	1150	500	235

number of motors required to control the entire number of contractions suggests that this method provides a cost-effective means for simulating this form of membrane deformation. However, control over the constriction pattern must be predetermined and set into the mechanism prior to its operation.

The capstan mechanism described in Section 5.1.2 can be used in conjunction with the rotating disc mechanism. This reduces the amount of torque required by the motor in the tensioning of the unit constrictor tendons as the discs revolve. This combination is useful if the tension pins have a large offset from the central axis, causing the moment arm of the tension force to be large. If the tension force from tendons acting on the tension pins becomes large, then the central axis experiences significant unidirectional stress, which in turn places the rotating disc motor and its mounting brackets under stress and potential damage of the motor. Addition of a capstan mechanism would assist in reducing the stress placed on the central axis, the rotating disc motor, and associated mounting brackets.

5.3. Summary

This chapter introduced two unique methods of actuation for the artificial muscles of the biomimetic gastric tract simulator. The first method involved the pulling of individual unit constrictor tendons with dedicated winding motors to create independent actuation over the artificial muscles. Independent actuation of the artificial muscles can provide a wide range of potential contraction patterns for the artificial gastric tract shell.

The second method was a novel mechanism using a series of rotating discs with attached pins to coordinate the tensile pulling of the unit constrictor tendons. This method demonstrates capability for actuating multiple unit constrictors using just a single electric

motor. The addition of a capstan mechanism and motor to the rotating disc mechanism allows for improved capability in tensioning of the unit constrictor tendons.

A capstan mechanism and linear slider was demonstrated as a means for reducing the required power and size of the winding motors, therefore providing a cost-effective solution for the actuation of the artificial muscles.

Chapter Six

Feedback and Control

Chapter 6 – Feedback and Control

This chapter describes methods of feedback relating to controlling a biomimetic *in vitro* gastric tract simulation model. This includes measurement of applied force for the contraction of the artificial muscles, internal pressure sensing, and the sensing of membrane stretch. Techniques are discussed for measuring the force applied to artificial muscle contraction, and measuring changes in intra-luminal pressure as the gastric wall is being deformed during the process of digestion. Sensing of membrane stretch, and measurement of membrane shell deformation investigates the development of novel stretch-sensing materials and their potential for determining the amount of stretch taking place over an elastic membrane. Finally, the potential application for using feedback measurements in the virtual visualisation and mapping of the deforming artificial gastric tract is introduced.

6.1. Feedback and control of muscle actuation

Maintaining control over the contractions of the unit constrictors requires at least two sensing and feedback mechanisms to be put in place on the motor control system. The first involves obtaining feedback on the displacement of the unit constrictor tendons so that the contraction ratios of the looped constrictors can be constantly monitored. The second feedback mechanism is measurement of the tension force applied to the unit constrictor tendons so that the tension of each constrictor is maintained within a specified range. Both feedback mechanisms can be used for calculating the necessary direction and speed of the winding motors over a specific period. In this way all the unit constrictors should operate synchronously to dynamically deform the membrane shell with the desired patterns of contraction and expansion.

6.1.1. Constrictor contraction

Controlling constrictor contraction involves measurement of the length of tendon that is pulled from the unit constrictor loop. The circumference of the constrictor loop reduces as the tendon is pulled and increases as the tendon is released or returned (refer Fig. 40 (b), Section 5.1.2). The length of tendon pulled from the end of the Bowden cable is termed as the displacement of the tendon. Tendon displacement is used to calculate the contraction ratio of the unit constrictor as it is actuated, which is the ratio of the final circumference of the constrictor over its initial circumference. The initial circumference is the fabricated circumference of the unit constrictor when the stomach is empty. The starting circumference of the constrictor is its circumference before a contraction takes place, which in turn is dependent on the total volume of the stomach as it accommodates food. A near-empty stomach will therefore have smaller starting circumferences of the unit constrictors whereas a full stomach will have larger starting circumferences.

Determination of unit constrictor tendon displacement can be made by measuring either the linear displacement of the tendon as it is being pulled or released, or from the rotational displacement of the winding spindle as it winds or unwinds the tendon lines. Linear displacement measurements determine the distance an object has travelled in a straight line from a predefined reference point. With respect to the unit constrictor, this means measuring the change in length of the tendon lines that exit the Bowden cable (refer Fig. 40, Section 5.1.2). Rotational displacement measurements determine the angular displacement of a motor shaft or winding pulley as it turns. The linear displacement of the unit constrictor tendon can be determined from the total angular displacement of the winding shaft and the radius of its winding spindle as in Eqn. (5-11) (Section 5.1.2).

Angular displacement of a motor shaft

Sensors and feedback mechanisms that could be used for measuring the rotational displacement of the winding spindle are commercially available. However, the first consideration should be the type of motor employed for the winding of the tendons; options are stepper, servo, or geared DC motors. The type(s) of motor used dictate whether additional feedback mechanisms or support electronics are necessary for accurate measurement of the amount of tendon displacement taking place.

Stepper motors

Stepper motors rotate in steps. A control signal is sent to the stepper motor driver that determines when a step is to be taken and in what direction the motor is to turn. The generation of a step signal to the motor allows for counting of the number of steps made and an evaluation of the total shaft rotation. However, even though a step signal has been sent to the stepper motor, the motor may not always make that step. This can occur when the motor provides insufficient torque for the load it is bearing and the motor stalls, resulting in a misstep. The result of these missteps is that the calculated amount of motor shaft rotation may not always match the actual amount of rotation that has occurred.

To minimise or eliminate the possibility of missteps during operation requires the stepper motor to be properly sized for its application. Alternatively, the open-loop control of the stepper motor may be converted into a closed-loop control system by adding a rotary encoder to the stepper motor shaft [213]. The rotary encoder senses incremental physical changes in the motor shaft rotation which can be accumulated and compared with the number of step pulses that have been sent to the stepper motor. This form of closed-loop control system allows for a more accurate calculation of the rotational displacement.

Geared DC motors and servo motors

Geared DC motors provide little control over the positioning of the motor shaft. Rotary encoders must be fitted for measuring the amount of motor shaft rotation taking place. Although the degree of shaft rotation can be sensed and measured, these motors are more difficult to control for precise rotational positioning and angular velocity. However, they tend to be cheaper than stepper or servo motors, can be much smaller, and can also be combined with additional control systems to convert them into servo motors with rotational ranges extending beyond those of standard servo motors.

Servo motors are geared DC motors with built-in control electronics allowing them to operate with closed-loop control over the rotational position of the motor shaft. A pulse-width modulated (PWM) signal is provided to the servo motor that dictates the absolute positional angle of the motor shaft. Servo motors can provide substantial amounts of torque and the closed-loop control system allows for accurate rotational positioning of the motor shaft.

However, most standard servo motors have limited rotational range, typically up to only 180° rotation of the motor shaft. Due to this limited rotational range these standard servo motors require attachment of a large diameter winding spindle to the motor shaft to fully displace the tendons of the unit constrictors. A drawback to this approach is that the available torque from the motor diminishes as the diameter of the attached winding spindle increases.

Customised servo motors

Customised servo motors can be constructed by physically coupling a rotary potentiometer to the shaft of a geared DC motor. The changing resistance of the rotating potentiometer provides an absolute measure of the angular position of the motor shaft. Gears connecting

the motor shaft to the shaft of the potentiometer allow for multiple turns of the motor shaft to be sensed, rather than limiting it to the 180° rotational action of a standard servo motor. The ratio of the gears used determines the fractional number of turns of the motor shaft that can be sensed by the turning of the potentiometer shaft.

Fig. 58 shows an example of a rotary potentiometer shaft coupled to a small, geared DC motor shaft with a set of spur gears. The gear ratios were achieved using a pair of 2:1 gears driving a pair of 3:1 gears, which creates a final reduction gear ratio of 6:1 from the motor shaft to the potentiometer shaft. The potentiometer shaft therefore rotates one complete turn to every 6 turns of the motor shaft. This arrangement allows the winding motors to use a small diameter winding spindle to fully wind the unit constrictor tendons while preserving most of the available torque of the winding motor. However, some torque is still lost in driving the gearing and potentiometer shaft.

Linear displacement of a slider on a track

The tendon winding system described in Section 5.2.2 uses a system of pulleys and a linear slider on a track to couple the winding motors to the unit constrictor tendons. The use of a slider on a linear track provides opportunity for tendon displacement to be determined by the linear displacement of the slider. Two low-cost methods for achieving measurement of the displacement of a linear track slider have been investigated; the first involves feedback from the extension of a stretch sensor attached to the slider, while the second measures force feedback from the extension of a spring.

Feedback from stretch sensor extension

A silicone tube filled with a conductive ionic liquid was employed as a stretch-sensing feedback device for obtaining the absolute position of a linear slider on a track [214]. This

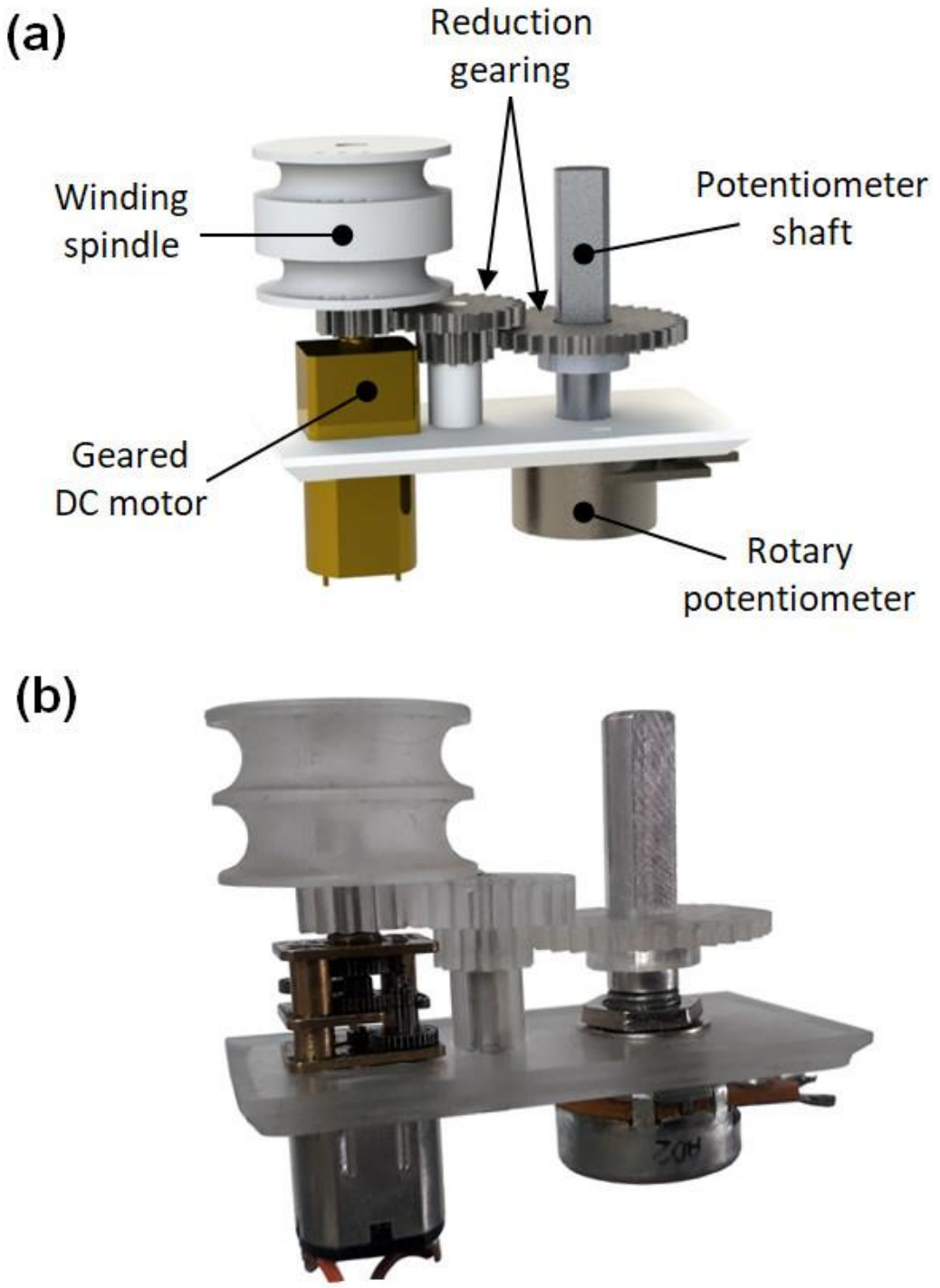

Fig. 58: A rotary encoder that uses a potentiometer driven by gears to determine the angular displacement of the winding motor shaft. (a) Identification of the component parts. (b) Image showing a physical prototype with 3D printed winding spindle and gears.

stretch-sensing device is fully described in the conference paper reproduced in Appendix B. A saline solution was used as the ionic liquid within the silicone tubing while the ends of the tubing were terminated with stainless steel electrodes that also kept the liquid contained. When stretched, the cross-sectional area of the conductive channel would decrease while the distance between the stainless steel electrode terminals increased. This would result in a measurable change in resistance between the two terminals.

A 3.3 volt, 10 kHz alternating current input signal was passed through a series circuit combining the stretch sensor and an additional carbon resistor of known value. The resulting circuit acted as a potentiometer when the stretch sensor was stretched. An alternating current was used to prevent electrolytic breakdown of the aqueous ionic fluid from developing bubbles at the electrode terminals. The change in resistance provided from the feedback of the sensor was used by a microcontroller to control the speed and direction of a winding motor, and thus alter the position of the slider. The stretch-sensor provides the absolute position of the linear slider so the microcontroller can maintain accurate control over the slider's position on the track.

However, the stretch-sensor used in the prototype model described in Appendix B presents a challenge as the saline water tends to diffuse out of the silicone tubing over time. This is due to silicone having a high permeability for water vapour [215-218]. The permeability of water vapour through silicone is influenced by the chemical composition of the silicone, the thickness of the silicone material, and environmental factors such as relative humidity, temperature and pressure [215, 217]. Over time, the aqueous solution contained in the channel of the stretch sensor tubing develops bubbles that disrupt the conductive pathway

and change its electrical characteristics. This eventually causes the sensor to become inoperable.

To mitigate the effect of water permeating through the silicone tubing, an ionic liquid with a lower permeability was investigated. An example of an alternative ionic liquid to use is an aqueous solution of sodium chloride and propylene glycol as demonstrated by Zhang et al. [219]. Propylene glycol has reduced capacity compared to water for permeating through a silicone material. The use of a conductive glycerol as an ionic fluid also shows promise as a means for retaining the conductive pathway within the silicone tubing, and significantly extending the operating lifetime of the stretch sensor. Glycerol has a lower vapour pressure than water at the same temperature, and thus the glycerol will diffuse through silicone tubing at a lower rate than water.

A conductive glycerol was developed by heating 90 grams of glycerol (99.5% pure, Ajax-Finechem, Univar) and 10 grams of sodium chloride (NaCl) to 80° C for 30 minutes. The glycerol-salt solution was stirred constantly as it was heated to assist in the dissolution of the salt. Increasing the concentration of sodium chloride in the glycerol results in increased conductivity of the solution (Fig. 59), until the concentration of sodium chloride exceeds approximately 7% of the total weight of sodium chloride and glycerol and the conductivity does not increase further. This occurs as the glycerol becomes saturated with sodium chloride, shown by the dotted line in Fig. 59.

When initially put into the silicone tubing the conductive glycerol has very low water content (< 0.5%) and hygroscopic characteristics – it readily absorbs moisture. As a result, the glycerol begins to gradually absorb moisture from the surrounding atmosphere by the permeation of water vapour through the silicone tube wall. This is the opposite of what occurs when using a saline solution as the ionic liquid and water vapour begins to leave the tubing by permeating out of the tubing to the external atmosphere. The conductivity of the glycerol solution will change depending on how much water is absorbed or released through the silicone tubing. According to Gregory [212] , the surface layer of glycerol will equilibrate to the relative humidity of the surface it is in contact with, resulting in a glycerol-water mixture. Therefore, the conductivity of the glycerol solution in the silicone tubing is

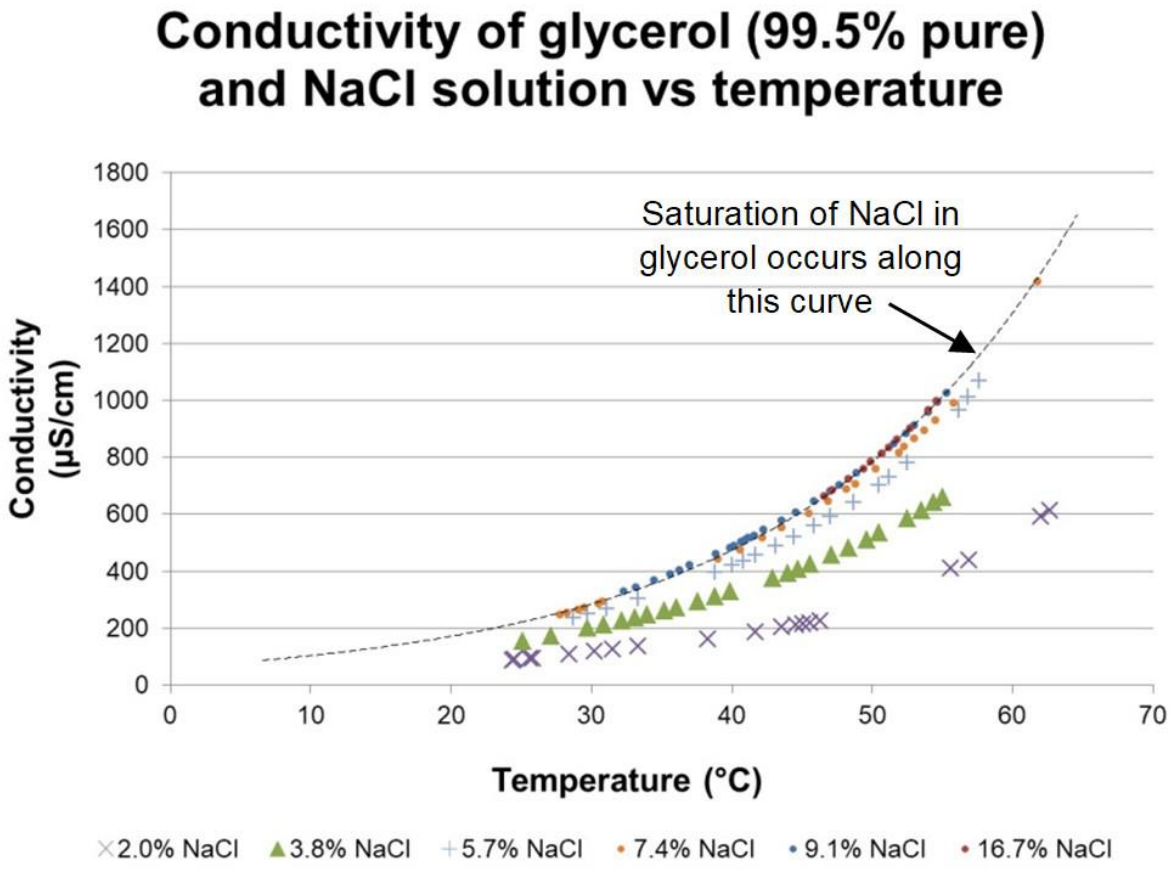

Fig. 59: Conductivity of glycerol (99.5% pure) and sodium chloride (NaCl) solutions with different concentrations of NaCl over a range of temperatures.

dependent on the humidity of the external atmosphere as well as the temperature of the solution.

A Wheatstone bridge should be used to counter effects on the conductivity of the ionic liquid sensor from any changes in temperature or atmospheric humidity. An appropriate Wheatstone bridge configuration can be made from three 'dummy' sensors (R_1, R_2, R_3) connected to an active stretch sensor ($R_{Stretch}$) [220] and supplied with a constant excitation voltage (V_{EX}), as shown in Fig. 60. The voltage reading obtained across V_o is used to calculate the change in resistance of the sensors connected to the bridge. It is important that the 'dummy' sensors have the same dimensions and geometry as the active stretch sensor so that they all change in resistance at the same rate. As the temperature or atmospheric humidity changes, each of the four sensors will change in resistance proportionately, leaving V_o unchanged. However, any time the stretch sensor ($R_{Stretch}$) is stretched, and the resistance between its terminals changes with respect to the amount of stretch, the voltage across V_o will reflect this change and a true measure of the resultant stretch can then be taken.

Feedback from linear extension of a spring

An alternative to the use of an ionic liquid stretch sensor for measuring the displacement of a linear slider is to use a basic spring-force sensor. A proof-of-concept physical model was developed for measuring the force required for the displacement of a spring over a linear distance. The model used a steel spring attached to a load-cell at one end and to a linear slider at the other (Fig. 61 (a)). A load cell is a transducer that converts force into an electrical signal which changes as the amount of deformation of the load cell changes [221]. Measurements of the force applied by the steel spring as it was extended by the linear slider were obtained by converting the analogue load-cell signal to a digital reading with a

microcontroller, and calculation was made of the extension displacement of the spring by using Hooke's law (Eqn. (6-1)).

$$F_s = kx \tag{6-1}$$

Where: F_s = spring force (N); x = spring displacement (m); k = spring constant (N/m).

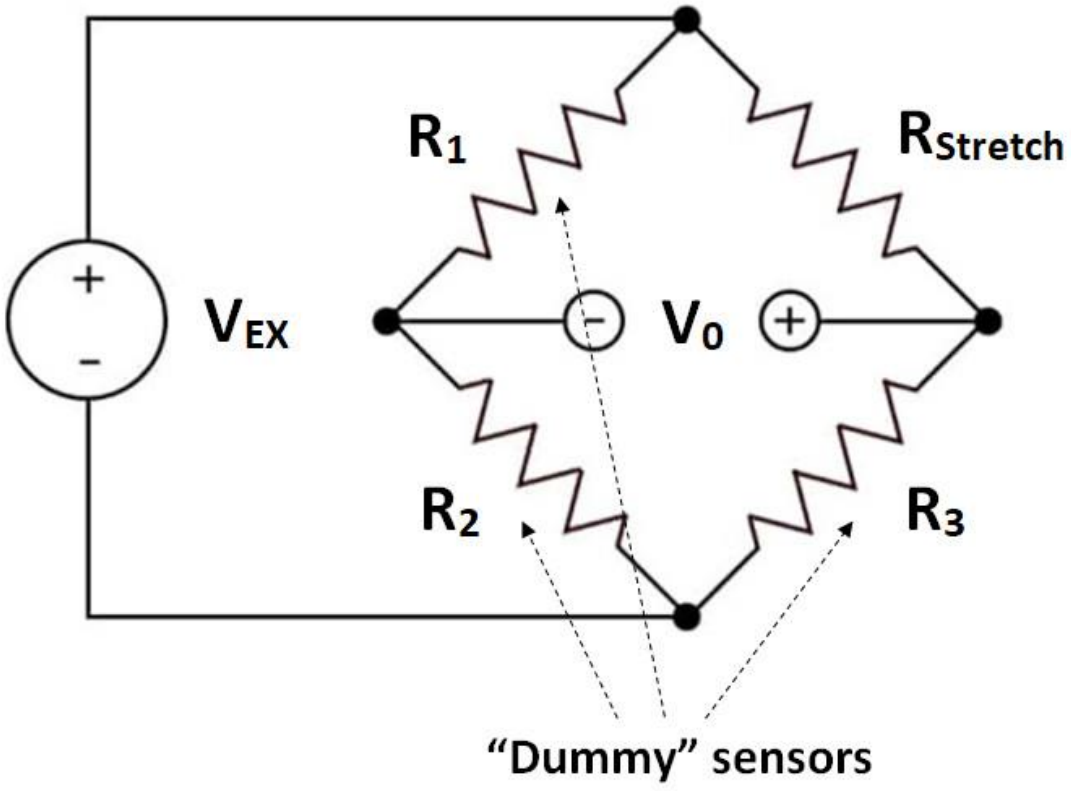

Fig. 60: Wheatstone bride setup for the stretch sensors.

Measurement of the force required to displace a steel spring enables linear correlation between force and spring displacement. This force-displacement correlation is less susceptible to changes in environmental temperature or humidity than the ionic liquid

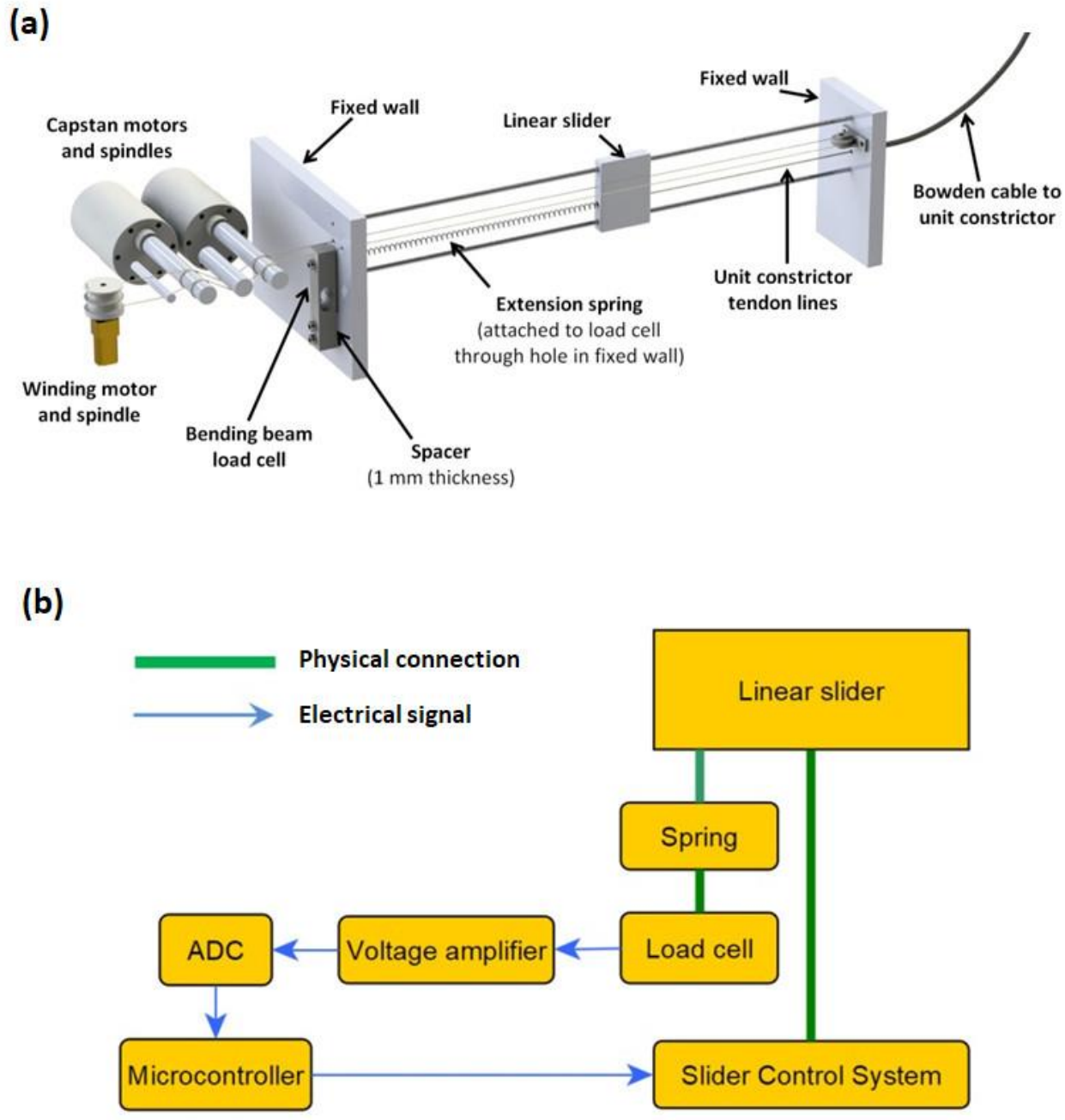

Fig. 61: (a) Physical layout of the spring extension components used for measuring the displacement of a linear slider. (b) Component block diagram for load cell measurement of a spring attached to a linear slider.

stretch-sensor method described above. It therefore could provide more repeatable and reliable means of calculating the displacement of the linear slider. However, using the spring extension method for determining linear displacement is complicated by the need for additional support electronics to convert the load cell analogue electrical output to a readable digital output.

The electrical output of a standard load cell is typically in the range of millivolts or microvolts, so voltage amplification is required to increase the load cell output reading to a more detectable range. The amplified output voltage can then be converted from an analogue to a digital reading using an ADC (analogue to digital converter). Each unit constrictor would thus require a load cell, voltage amplifier, and ADC directly interfaced with the load cell bridge sensor for measuring the linear displacement of its slider (Fig. 61 (b)).

6.1.2. Tension force applied to unit constrictor tendons

Monitoring the tension force applied to the tendons of the unit constrictors can indicate when a constrictor tendon has become slack or when the tension applied during contraction exceeds a specified limit. This feedback is useful when stomach contents are being emptied, or when unit constrictors are approaching contraction beyond their design requirement. Removal of slack from unit constrictor tendon lines is also useful when slack in the lines is created from movement of the artificial stomach membrane. This movement of the membrane is typically caused by the contraction action of adjacent unit constrictors.

A slack tendon should show negligible or no tension force measurement from the tension sensor and result in triggering the retraction of the tendon. Retraction of the tendon occurs until a minimum tension force initially becomes sensed, at which point the slack will have

been removed from the tendon lines and the unit constrictor will be considered to have reached its starting contraction ratio. When the sensed tension force in the tendon lines reaches a maximum specified limit the unit constrictor contraction action should be halted or reversed *i.e.*, the tendon is no longer pulled or is released to decrease the amount of tension being applied to the tendon lines.

Load cells

One method that can be used to assess applied tension force to the unit constrictor tendons is to attach one end of the Bowden cable, furthest from the unit constrictor, to a bending beam type load cell. Fig. 62 shows such a system. The system contains a load cell that is used to assess tension forces by sensing change in resistance from the deflection of an array of strain gauges attached to the load cell surface. As the tendon of the unit constrictor is pulled, and the constrictor contracts, a reaction force is created along the axis of the incompressible Bowden cable which acts upon the load cell. An estimate of the applied tendon tension force can be calculated from the amount of deflection of the load cell caused by this reaction force.

The force measured by the load cell is an estimate because it includes contact forces occurring between the tendon surface and the internal surfaces of the Bowden cable, and contact forces at the tip of the Bowden cable where the tendon exits and spreads out to loop around the unit constrictor. These contact forces can vary depending on the amount of bend incurred by the Bowden cable and the amount of inward-directed radial force that the looped tendon of the unit constrictor applies to the artificial tract. The presence of additional contact forces can be mitigated by minimising the length of Bowden cable used, decreasing the bend angle the Bowden cable develops during a contraction action, and

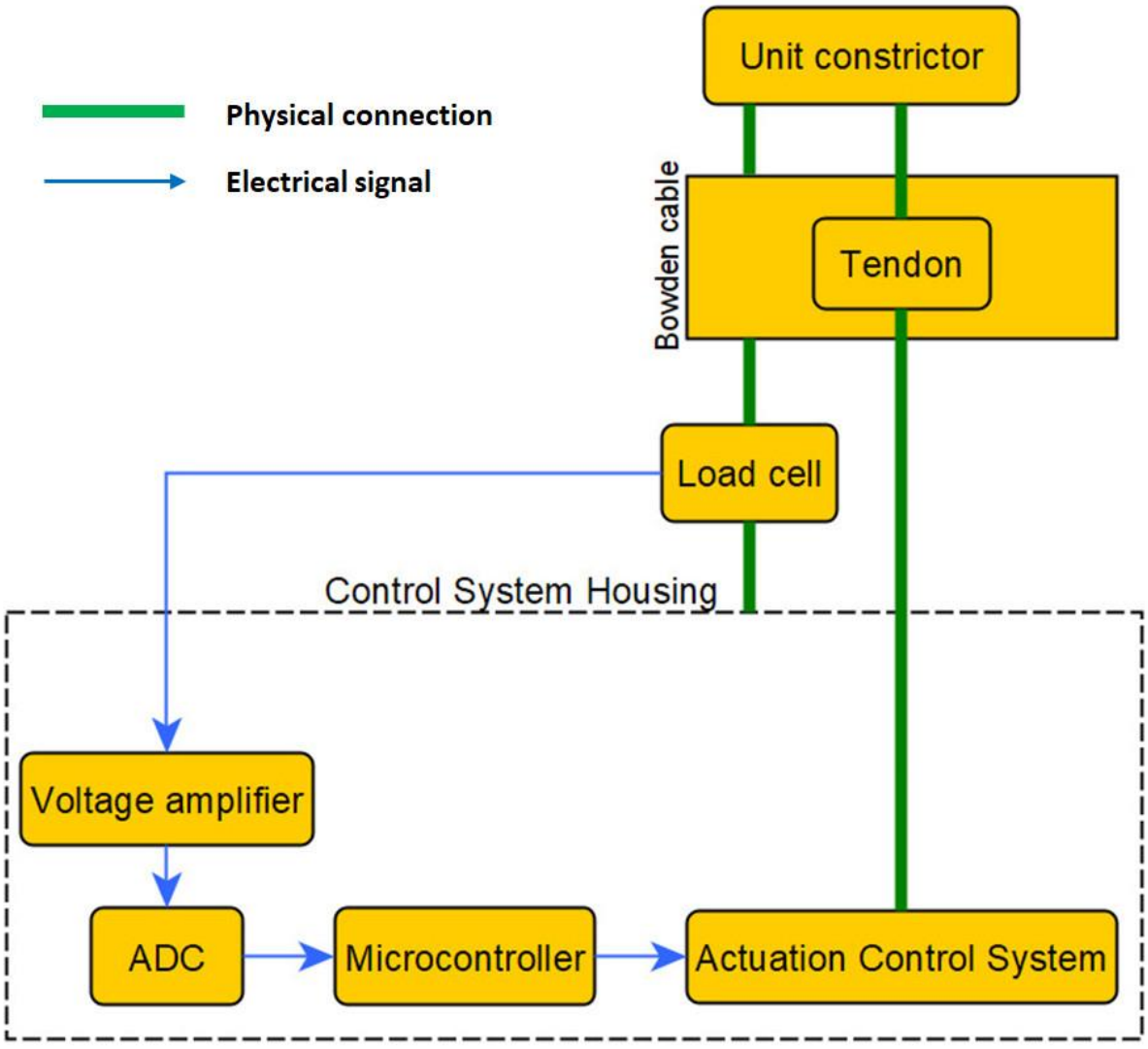

Fig. 62: Component block diagram connections for measuring tendon tension with a load cell.

minimising contact friction occurring at the tip of the Bowden cable *e.g.*, by introducing roller bearings at the tips to reduce friction on the tendons as they exit the Bowden cable.

Changes in measured reaction force originating from the bending of the Bowden cable can be mitigated by deliberately introducing a single 360° loop in the Bowden cable. Introduction of a 360° loop maintains a consistent contact friction force between the tendon lines and the inner surface of the Bowden cable throughout actuation of the unit constrictor. This approach for maintaining a constant contact friction force between the Bowden cable and tendon was demonstrated by Jeong and Cho [202]. However, deliberately increasing the friction force by introducing a 360° loop in the Bowden cable needs to be accounted for when evaluating the motor power requirements for actuating unit constrictors. Also, for this method of friction compensation to effectively work the total bend angle of the Bowden cable should not deviate from 360°, which can occur if the unit constrictor is moved away from its original position with respect to the Bowden cable.

Compression of a piezo-resistive polymer film

Another approach for obtaining feedback from the reaction force of the Bowden cables can be achieved through the compression of a film of piezo-resistive material as the Bowden cable presses upon it. The piezo-resistive effect occurs when a change in electrical resistance is caused by mechanical strain being applied to a piezo-resistive material. Velostat (Desco Industries) is a low-cost, carbon impregnated, polyethylene film used for protecting items or devices from electrostatic discharge. Velostat as a piezo-resistive material has been explored for use in a variety of sensing purposes including pressure measurement [222-226], force measurement [227, 228], posture recognition [229-231], gesture recognition [232, 233], and impact detection [234]. The electrical resistance characteristics of the conductive polymer

film decrease as the material is compressed and compacted, allowing for measurement of the change in resistance in the material to be made from an applied compression force.

A small compression sensor was fabricated using Velostat, copper plates, and 3D printed plastic parts to monitor the tension force being applied to tendon lines running through Bowden cables (Fig. 63). A circular piece of Velostat film was placed between two circular copper plates that act as electrodes for measuring the resistance of the polymer sheet (Fig. 63 (a)). Rigid 3D printed plungers connected to the ends of the Bowden cable press the copper plates against the piezo-resistive film (Fig. 63 (b)). When tension is applied to the tendon lines running through the centre of the sensor (Fig. 63 (c)) the ends of the Bowden cables react with compressive force that causes the copper plates to compress the piezo-resistive film. A voltage potential is obtained from the two copper electrodes using a bias resistor and a regulated voltage supply to create a voltage divider circuit. The DC voltage that is sensed depends on the amount of compression being applied to the piezo-resistive material. This voltage is then converted from an analogue signal to a digital reading by a microcontroller.

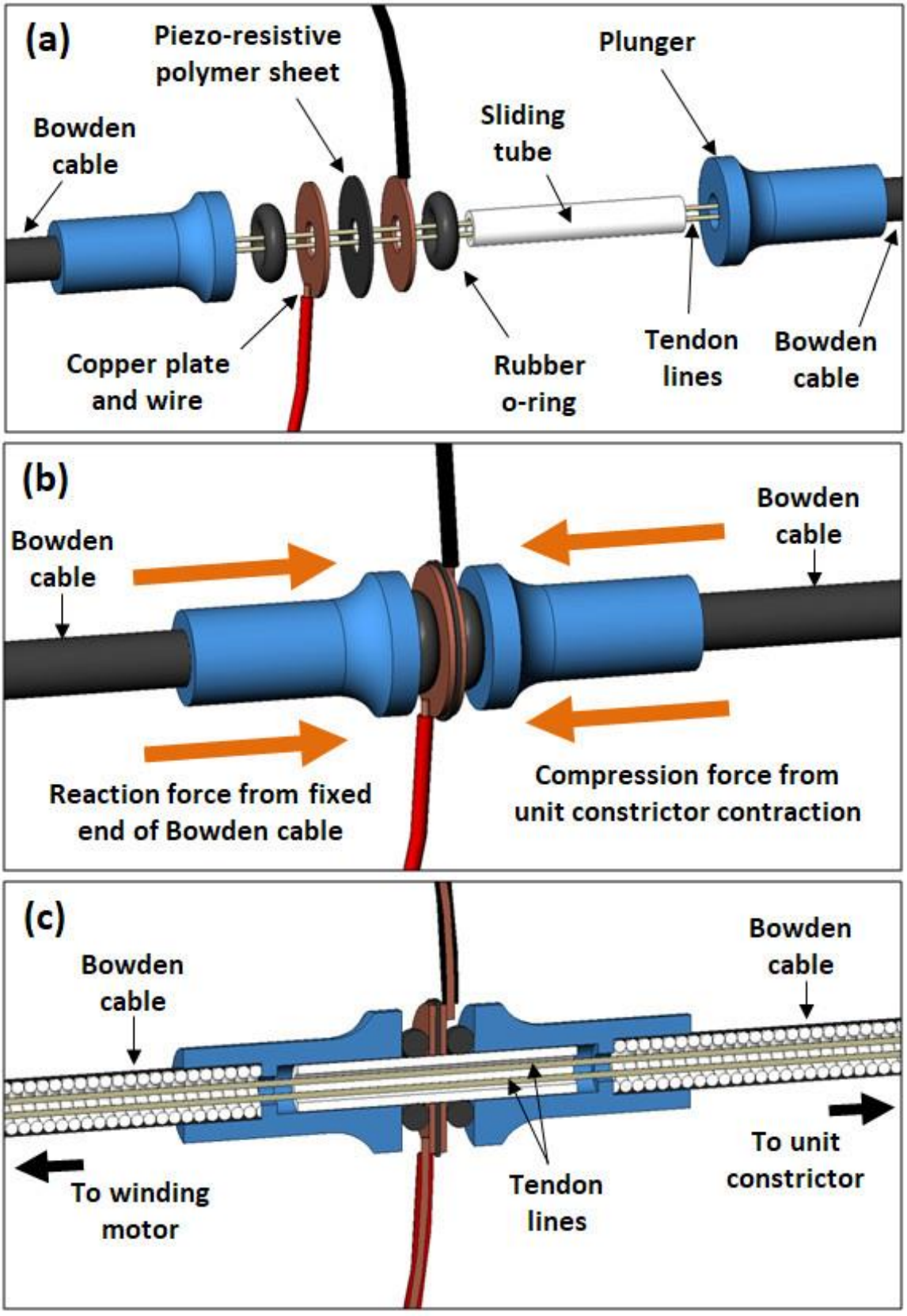

Fig. 63: Tension sensor developed for measuring change in tension force applied to the tendon lines during actuation of a unit constrictor. (a) Exploded view of sensor components. (b) Direction of forces applied during tendon tensioning. (c) Cross-sectional view of the tension sensor showing the tendon lines running through it.

Fig. 64 shows the resistance feedback response of the fabricated tension sensor when an applied force compressing the piezo-resistive polymer film is increased from 0 to 55 Newtons (N). The loading and unloading sensitivity of the sensor differs due to hysteresis because of polymeric characteristics of the piezo-resistive sheet and the rubber O-rings used to spread the compression force against the copper electrodes. The highest sensitivity of the sensor occurs between 0 to 10 N of applied compression force where the feedback from the sensor remains linear. The sensitivity of the sensor at levels of applied force below 10 N suggest that it can be useful for sensing when the tendon lines have become slack and an increase in tendon tension is required.

The sensor is placed in-line with a Bowden cable to sense the tension force applied to the

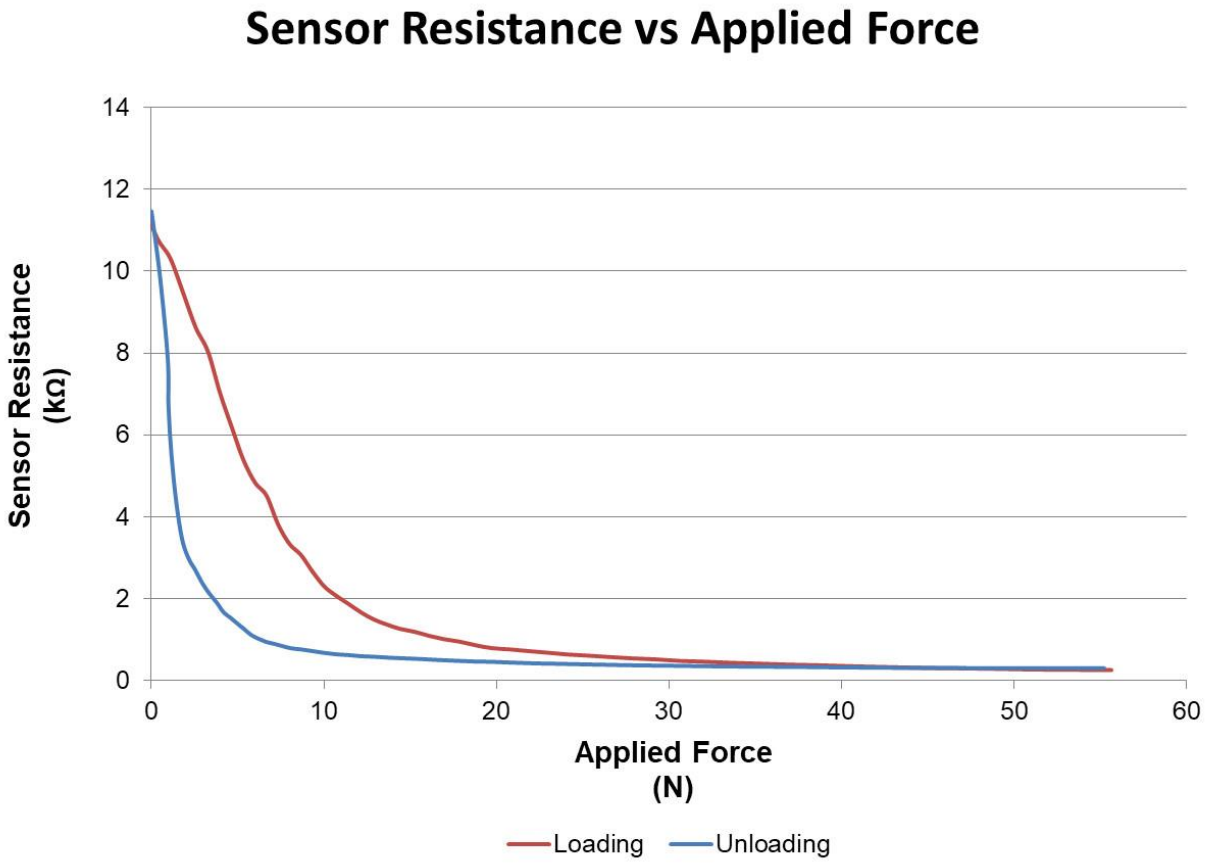

Fig. 64: Resistance of a piezo-resistive tension sensor versus applied compression force.

tendon lines during contraction of a unit constrictor. The sensor is low cost, easy to fabricate, lightweight, and compact. It requires minimal support electronics for providing feedback of the tension of the tendon lines to the analogue-to-digital converter (ADC) of a microcontroller. Placement of the piezo-resistive tension sensor in-line with a Bowden cable also means that it does not require a fixed mounting point, which would be required if using a bending beam load cell as a tension force sensor.

6.2. Other feedback and control mechanisms for the artificial stomach

In vitro measurements of intragastric pressure and the deforming geometry of the gastric tract membrane would be useful when integrating the requirements of the *in vitro* physical model with observed *in vivo* measurements. Feedback mechanisms indicating the deformation of the membrane provide information for regulating and controlling the contraction or expansion actions that are needed to achieve desired deformation patterns. Temperature, pH, and humidity sensors can also be useful for monitoring simulations concerning the digestion of food materials. Measurements obtained by the feedback devices can also assist in reconstructing a virtual map of the deformation, pressure, and other physical changes occurring throughout the stomach during simulation.

6.2.1. Membrane stretch

Sensing and measuring the amount of stretch that occurs over the elastic membrane of a simulated gastric tract reactor has two potential uses. The first is to sense the amount of stretch occurring in the fundus region of the stomach and using this feedback to trigger adaptive relaxation of the constrictors, thus adapting the stomach volume to better accommodate its contents. This is applicable during runtime operation of the physical *in vitro* model to ensure the stomach expands appropriately when food enters. The second use

is to measure unidirectional change in the membrane surface for mapping of the tract geometry. These measurements can be recorded and used to provide information about how the stomach mechanically deforms during digestion.

The fundus region of the stomach is of specific interest for sensing membrane stretch. This is because the fundus is less constrained by surrounding organs compared to other regions of the stomach and does not undergo peristaltic wave deformations. Fig. 65 shows the region of the fundus where the placement of stretch sensors is proposed. Membrane stretch sensed in this area would indicate an increase in volume of the stomach from the input of food via the oesophagus or stretch from food contents being pushed back into the fundus region from the corpus and antral contractions.

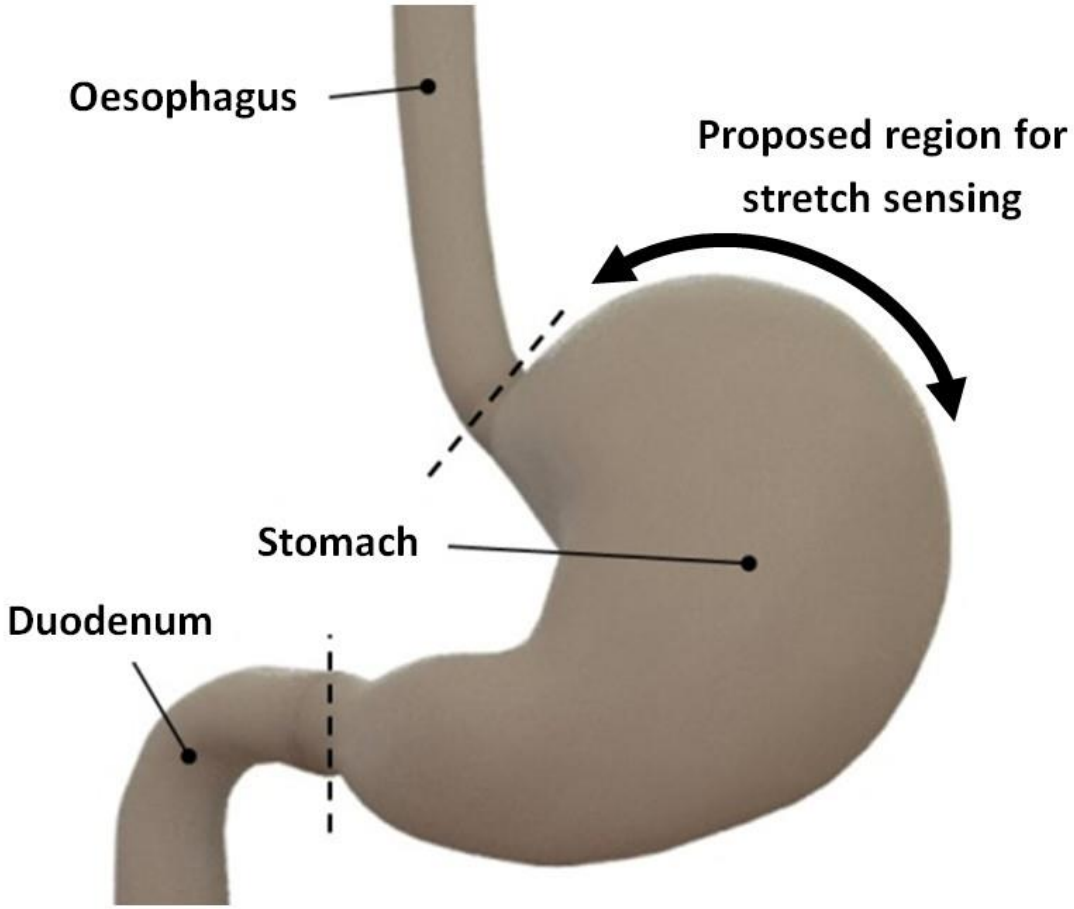

Fig. 65: Proposed region for stretch sensing on the fundus of the artificial stomach.

The stretch sensors need to be able to deform along with the gastric wall membrane they are attached to without significantly altering the membranes' deformation characteristics. Stretch sensors are designed to stretch and return to their original form when relaxed. Because of this elasticity, a sensor therefore requires some force to be applied to stretch it and this force should be negligible in comparison to the force acting to stretch the membrane material of the gastric model. Otherwise, stretching of the sensor will prevent the membrane from deforming in the manner intended in its design.

A preliminary investigation into fabricated stretch sensors was carried out to determine if a suitable solution could be found for the attachment of a sensor to a flexible elastic silicone membrane. The preliminary investigation is fully described in the conference paper reproduced in Appendix C. The investigation led to the development and testing of a novel conductive rubber composite material which is fully described in the conference paper reproduced in Appendix D. The conductive rubber uses change in electrical resistance for measuring stretch on an artificial stomach wall. The low-cost, easy-to-make conductive rubber is made from a conductive gel embedded within a silicone (polydimethylsiloxane) elastomer tube and can be fabricated as part of or within the artificial stomach or gastric tract wall membrane.

However, a disadvantage of the gel-embedded silicone composite sensor was the gradual evaporation of the hydrated ionic gel from within the silicone structure. Moisture retention of the ionic conductive material was required for the sensor to maintain functionality during prolonged usage. The conductive glycerol used for the silicone tube stretch sensor described in Section 6.1.1 was considered as a candidate for further enhancing the material properties of the gel-embedded silicone sensor.

The glycerol-gel sensor was made using a premix of 3.0 grams of saturated conductive glycerol (refer Section 6.1.1.2) and 0.5 grams of guar gum powder. To the premix was added 3.0 grams of deionised water and 3.0 grams liquid detergent (Palmolive® Original, Colgate-Palmolive, USA), which was then stirred at 300 RPM for two minutes. The glycerol-gel mixture was combined with a platinum cure silicone (EcoFlex™ 00-30, Smooth-On Inc., USA) at a ratio of one part glycerol-gel mixture to two parts of the liquid silicone. The silicone and glycerol-gel mixture was stirred at 600 RPM for three minutes and then placed in a vacuum chamber and degassed at a gauge pressure of negative 90 kPa, for a further five minutes.

The uncured glycerol-gel and silicone mixture can be spread as a continuous layer over a silicone membrane that has been laid on a flat surface, poured or injected into moulds, or injected into a length of vinyl tubing to form cylindrical shapes for the stretch sensor. Unlike the silicone-tube stretch sensor described in Section 6.1.1 a glycerol-gel sensor can be used in its cured form without requiring an external sealing layer. This increases the variety of sensor forms that can be fabricated. Lengths of stretch sensor can also be cut directly from flat sheets of the cured material.

Resistance readings obtained from the sensors are highly dependent on their dimensions and geometry. This is because the conductivity of the sensor is directly related to the cross-sectional area of the conductive tracts formed by the embedded ionic gel. Multiple sensors should therefore be made with the same dimensions and geometry if they are to maintain uniformity in resistivity. However, distribution of the ionic gel within the silicone structure may not always be consistent between sensors and readings could still vary considerably.

Further investigation into methods of fabrication that improves the uniformity of resistivity for this type of sensor material is recommended.

The glycerol-gel sensors are sensitive to changes in temperature and humidity. A Wheatstone bridge can be used to compensate for temperature or humidity changes if these environmental conditions are likely to fluctuate. An alternative to using a Wheatstone bridge is to measure the temperature and humidity that the stretch sensors are exposed to, and then numerically compensate for the stretch sensor readings accordingly. As the glycerol-gel sensor material is sensitive to temperature and humidity, it could be used in the measurement of these environmental conditions. Temperature levels can be sensed by an un-stretched glycerol-gel sensor material if it is kept inside an impermeable seal, while unsealed sensor material will react to changes in both temperature and humidity. An advantage of using the glycerol-gel stretch sensor for monitoring temperature and humidity fluctuations, rather than using standard temperature and humidity sensors, is that changes in resistance of the sensor material will occur at the same rate for all the sensors.

6.2.2. Intragastric pressure, temperature, pH and humidity

Intragastric pressure is the pressure within the stomach cavity. The stomach expands to accommodate incoming food by relaxing the muscles in the fundus region [165]. In doing so the stomach tends to maintain a stable intragastric pressure as it fills. However, levels of intragastric pressure can vary between the different regions of the stomach and can also be affected by various other factors including external pressure being applied to the abdomen, respiration, voluntary contraction of the abdominal muscles, and posture [81]. *In vivo* measurements of intragastric pressure can prove useful in indicating dysfunction or disturbances from normal stomach biomechanical activity.

A basic gastric balloon catheter can be inserted into the *in vitro* stomach model by using a 3 mm outer diameter polyvinyl tube with one end terminated by a small rubber balloon. The other end of the catheter is attached to the positive input of a digital pressure sensor while the negative input of the sensor is left open to the external atmosphere to act as a reference pressure. A 30 mm length of polyvinyl tubing, with 3 mm internal diameter, can be used as a tube entry point for the catheter. The tube entry point penetrates the fundus region of the artificial stomach shell, close to the lower oesophageal sphincter, so that it does not interfere with the peristaltic operation of the unit constrictors. The catheter can then be inserted into the stomach cavity through the tube entry point with minimal interference to the digestive contractions. When not being used, the tube entry point can be plugged or closed to prevent contents escaping from the stomach.

Temperature and pH probes can be inserted into the *in vitro* stomach cavity in a similar manner to the gastric balloon catheter. Although they are not considered essential elements for demonstrating the mimicry of biomechanical action of the stomach, they are mentioned here for potential use in future *in vitro* model simulations. Temperature and humidity control or monitoring inside of the reactor containment unit, but outside of the artificial stomach shell, may also be a viable means for obtaining reliable readings from the glycerol-gel stretch sensors (Section 6.2.1). If humidity and temperature control can be maintained in the physical model, the need for a Wheatstone bridge or numerical compensation for the stretch sensor readings would be redundant.

6.3. Control of the biomimetic gastric tract simulator

Control of the artificial stomach model is centred on the use of a programmable microcontroller unit (MCU) for sending instructions to the motor controllers and for

processing the feedback obtained from various sensors. The MCU is provided with timing and contraction parameters for the unit constrictors as described in Section 5.1.1. These parameters are used for determining the required angular position of the winding motor shafts over time so that the unit constrictors contract in an orchestrated pattern that simulates the biomechanical activity of the gastric tract.

Fig. 66 shows a top-level schematic diagram of the connections for the control components of the physical *in vitro* gastric tract model. Customised servo motors (refer Section 6.1.1) were selected as the type of motor to be used for the winding motors. Customised servo motors were chosen because they require only a single pulse-width modulated (PWM) signal to move the winding motor shaft to its required angular position. Each winding motor has servo control electronics that align the angular position of the winding motor shaft with the PWM signal that it has been sent. The PWM signal the motor receives changes over time to match the required angular position of the motor shaft at that specific time.

The motor controller for the winding motors uses two daisy-chained PWM driver boards or dedicated microcontrollers, each capable of providing 12-bit resolution PWM signals to control up to 16 individual servo motors. The PWM controller boards communicate with the main MCU through the I2C serial communication protocol. The required position of the winding motor shafts is calculated by the MCU at each time step of the simulation of the *in vitro* model and converted into 12-bit PWM outputs. The PWM outputs for all winding motors are passed to the PWM driver boards via the I2C interface, converted into independent PWM signals, and connected to their respective servo motors as the position input for the motor shaft.

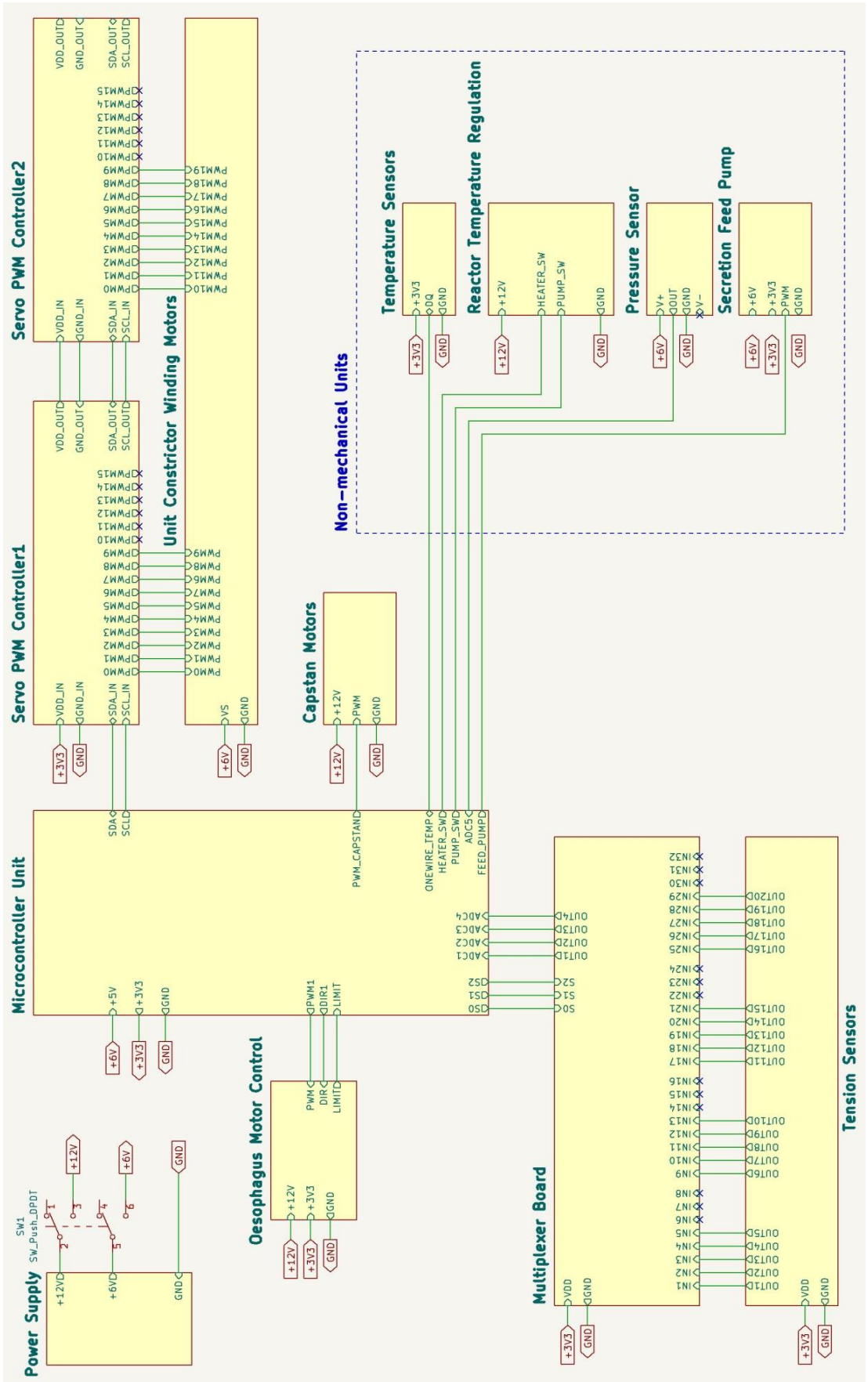

Fig. 66: Top-level schematic overview of electrical components for control of the physical artificial stomach model.

The capstan motors and motor for the linear peristaltic pump are also controlled by PWM signal. The PWM signal is used to control the speed of the DC motors. The linear peristaltic pump has another digital input that determines the direction of rotation of the motor. A digital signal from a limit switch placed on the linear peristaltic pump motor shaft is used to provide feedback for the simulated oesophagus. This feedback signal is used to indicate when a full swallowing action has been completed and the pump motor is to be turned off.

Analogue voltage feedback signals from the tension sensors are relayed to a multiplexer board. The MCU switches through the inputs to the multiplexer board to sequentially pass the analogue voltages from the tension sensors on to four analogue-to-digital converters (ADC) and recorded. The converted digital values of the tension sensors are used in determining whether a particular constrictor has reached its minimum or maximum level of contraction for its tendon lines. Readings from the tension sensors can also be useful for tracking the force of contraction being applied over time by any unit constrictor.

The MCU also provides inputs and outputs to monitor and control several environmental feedback and regulatory components. These components are to be incorporated into prospective versions of the *in vitro* stomach model and include sensing of the containment temperature, regulation of the environment temperature, intra-luminal pressure sensing, and control over the release of gastric juices into the stomach. Temperature and pressure sensor outputs are treated as analogue inputs to the MCU and converted to digital values before being recorded with a time stamp. Temperature regulation involves the control of a water heater and pumping system driven by feedback from the temperature sensors. Timed actuation of a motor connected to a peristaltic pump provides control over the introduction

of gastric juices into the artificial stomach, via tubes inserted through the stomach membrane.

6.4. Virtual feedback

Information obtained from the various sensors employed on the *in vitro* physical model can provide information for recreating a visual or virtual representation of the *in vitro* models' deformation. Measurement data obtained by pressure, stretch, tendon displacement, and tension force feedback sensors can be used to reconstruct temporal three-dimensional virtual reconstructions of the simulated gastric tract. With use of the finite element method (FEM) and 3D virtual simulation software, approximations of the intragastric pressure distributions, applied forces and deformation of the surfaces of the biomimetic *in vitro* model can be visually mapped and recorded. This not only allows for the biomimetic *in vitro* model to be compared against observed *in vivo* data on gastric wall activity and force distributions but also provide comparison of the actual deformation occurring on the *in vitro* model with the intended, or programmed deformation of the model.

Measurements obtained by the stretch sensors and tendon displacement feedback of the unit constrictors provide information on the expansion and contraction deformations of the artificial membrane over different regions of the artificial gastric tract. Tendon tension forces indicate the amount of hoop tension that the looped unit constrictors experience and can be used for estimating the inward surface pressure applied by contractions. The estimated surface pressures from the constrictor contractions can be correlated against intragastric pressure measurements taken from different regions of the artificial tract.

A preliminary investigation was undertaken into how sensor feedback measurements could be used for generating a visual representation of the deformation of the artificial tract. The

open-source software SOFA (Simulation Open Framework Architecture) was selected as a candidate for three-dimensional reconstruction of the artificial tract, due to its specific focus on real-time medical simulation and ability to model rigid, viscoelastic, or fluid bodies with non-linear FEM algorithms [235-239].

A 3D mesh model of a cylindrical tube, with 50 mm outer diameter and 5 mm wall thickness, was constructed using tetrahedral FEM elements as a basic shape for an artificial tract. The looped unit constrictors were modelled using circumferential stiff springs placed at equidistant locations over the length of the cylindrical mesh. The circumferential springs were provided with differing values of spring tension to elicit a range of contractive actions over the FEM mesh (Fig. 67 (a)). Gravity and changes in internal surface pressure were also applied to the virtual mesh model to provide visual feedback on how these forces affect the deformation of the simulated tract (Fig. 67 (b)).

A more sophisticated version of the gastric tract virtual simulation was developed and involved using more complicated 3D mesh models derived from magnetic resonance imaging (MRI) scans of the human abdomen (BodyParts3D, © The Database Center for Life Science licensed under CC Attribution-Share Alike 2.1 Japan). The mesh models of the abdominal organs included the oesophagus, stomach, duodenum, liver, pancreas, spleen, left kidney, transverse colon, and an oval vessel for containment of the organs (Fig. 68).

The improved version of the simulation model accounts for collisions of the deforming stomach with its surrounding organs. The collisions use physics-based algorithms for calculation of the contact responses between the stomach and the surrounding organs. A

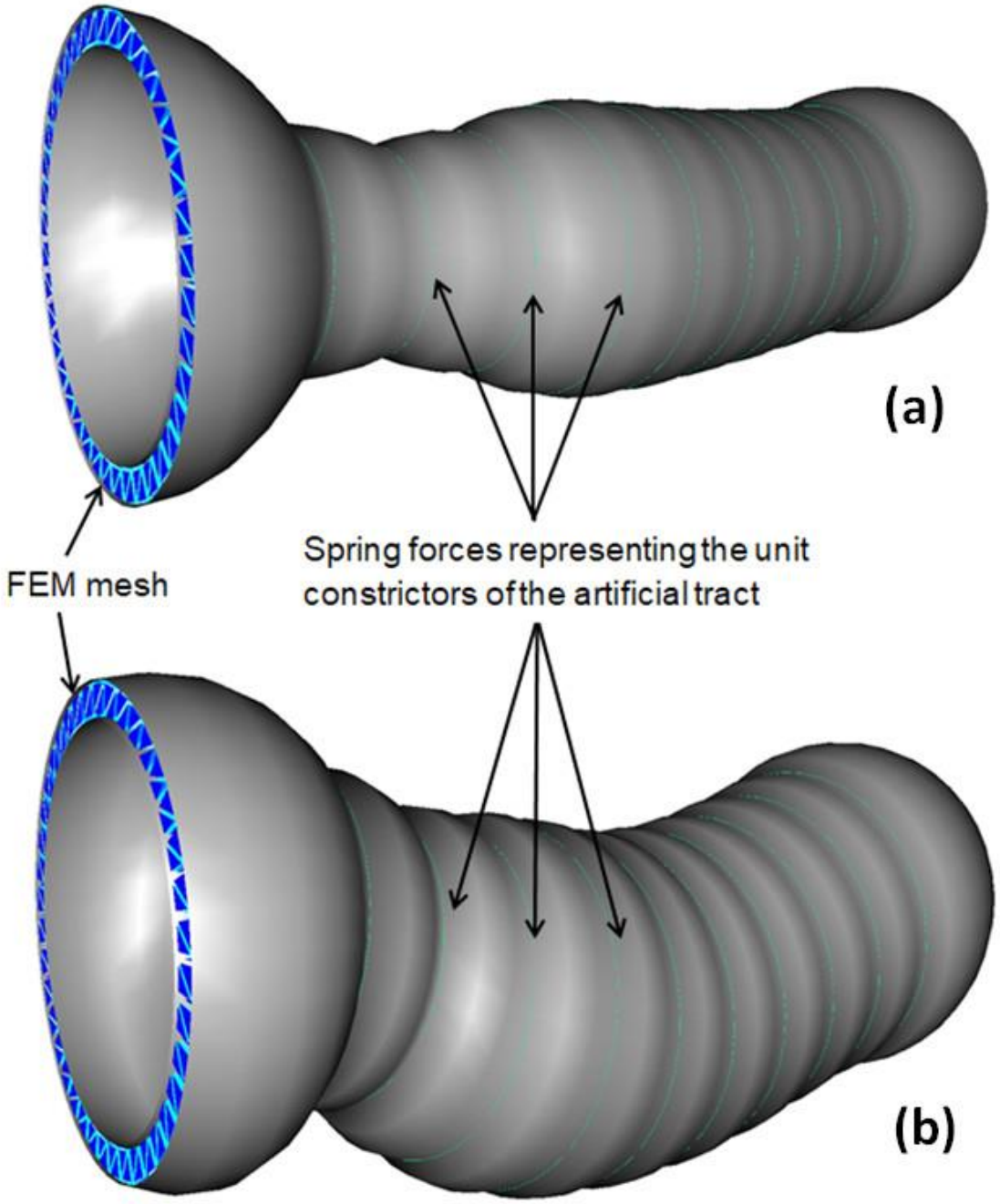

Fig. 67: (a) Example 3D FEM reconstruction of a soft-bodied cylindrical tube tract modelled in SOFA, with the contraction of looped unit constrictors represented by stiff spring tension forces. (b) The same 3D model showing the effects of gravity and an internal surface pressure being applied to the FEM mesh.

graphics processing unit (GPU) is used to handle most of the physics and graphics calculations so that the frame rate of the simulation remains above 25 frames per second, which is sufficient for providing the updating of the simulation in real-time.

These preliminary results indicate potential for deriving a reconstructed 3D visual model of gastric tract deformations from feedback measurements obtained by the physical *in vitro* gastric tract model. This would allow for comparisons to be made between the desired and actual deformations of the artificial stomach, which can then be used in adjustment of the

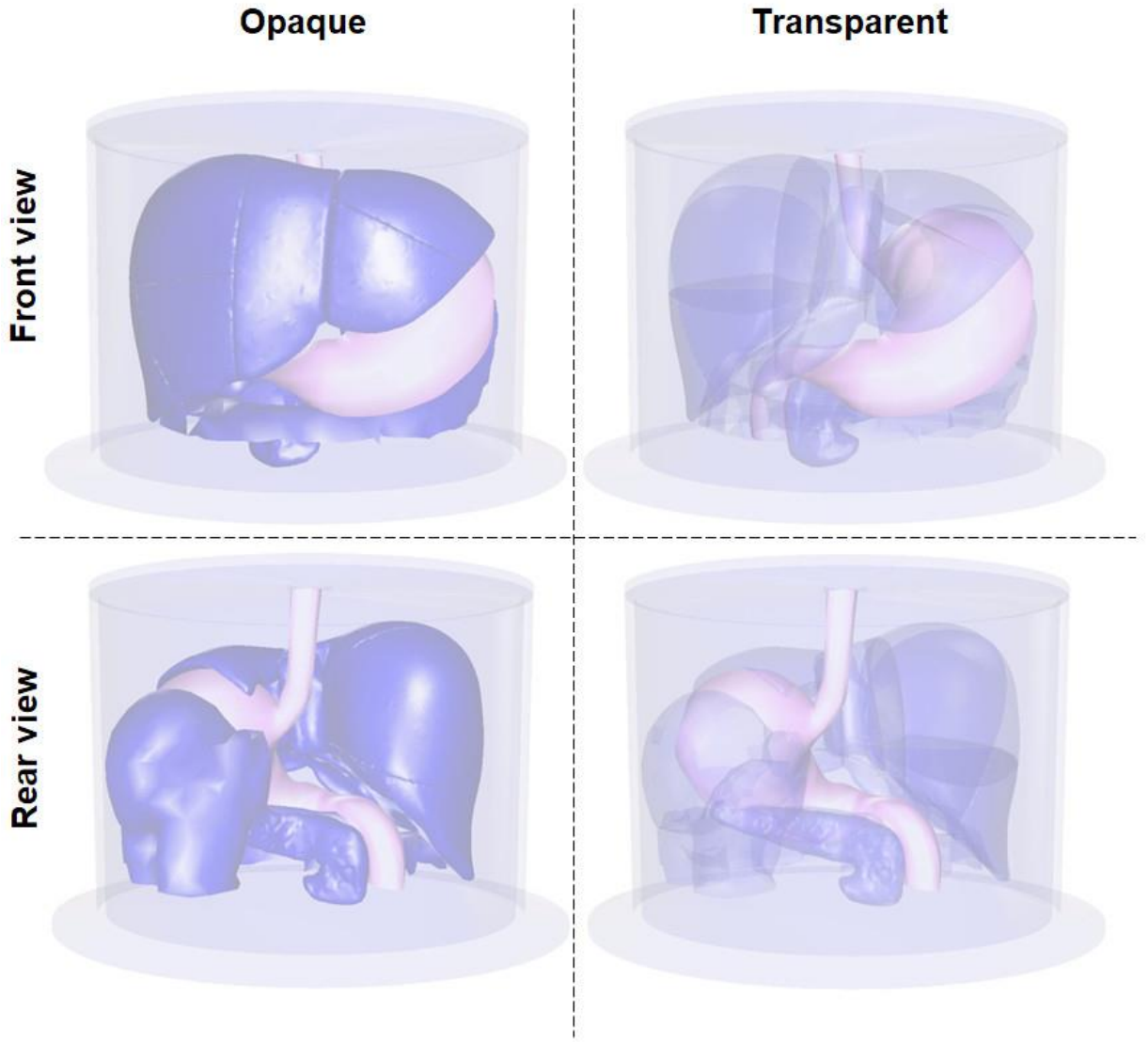

Fig. 68: Virtual mesh models of the gastric tract (pink) and surrounding organs (purple) placed in a transparent oval containment vessel.

operating parameters to achieve different simulation conditions. However, the ability of the virtual reconstruction software to accurately represent the actual deformation of the physical model remains to be verified, and beyond the scope of this thesis.

6.5. Summary

This chapter discussed methods, techniques, and devices that could be used for providing feedback and control of the artificial gastric tract simulator. Feedback and control of the muscle actuation system includes taking measurements of the displacement of unit constrictor tendons and sensing the tension force created in the artificial muscle tendons during contraction actions. Measurement of tendon displacement was demonstrated by sensing changes in the winding motor shaft positions, and from feedback of the changing position of a linear track slider driven by the tendon winding motors. A geared potentiometer attached to the shaft of a winding motor shows good potential as an appropriate low-cost, customisable means for providing accurate feedback on the displacement of the tendons.

Tension sensors were also developed for providing an estimate of the amount of tension force experienced by the tendons of the unit constrictors. This was achieved by obtaining feedback of the reactive compression force from the Bowden cables when the unit constrictor tendons were pulled through them, either from measurement of the deflection of a bending beam load cell or from the amount of compression applied to a piezo-resistive polymer film. The compression of a piezo-resistive film suggests a low-cost, easy-to-implement, lightweight, and compact method for sensing the pressure force being applied by the reaction of the Bowden cables.

The use of stretch sensors for measuring the amount of stretch occurring over the stomach wall was investigated. A novel stretch sensor material, derived from embedding a conductive gel in silicone, was developed and adapts the sensing material as an integral part of the elastic surface of the stomach shell. However, the sensor material exhibits sensitivity to temperature and humidity and would require some form of measurement compensation, or environmental control. Further research into the uniformity, accuracy, and suitability of the developed stretch sensor is therefore suggested prior to its consideration as a feedback mechanism for the *in vitro* model.

Virtual simulation of the gastric tract model provides means for visualising the various forms of feedback received from the physical model. Comparisons could then be made between the desired and actual outcomes of the deformation patterns actuated on the physical model. The ability to approximate gastric shell deformation outputs in a near real-time, virtual environment provides visual feedback for a user interface and numerical modelling of the physical phenomena involved with simulating gastric tract motility.

Chapter Seven

Biomimetic gastric tract simulator

Chapter 7 – Biomimetic gastric tract simulator

This chapter discusses general integration and configuration of the core components of the artificial gastric tract including the membrane (Chapter 3), artificial muscles (Chapter 4), implementation of a full actuation system (Chapter 5), and operational feedback and control aspects (Chapter 6). The objective is to provide an integrated design for the biomimetic *in vitro* physical gastric tract model that mimics the contractive and expansive actions of the membrane and muscle layers found in the biological gastric tract wall. The proposed *in vitro* model demonstrates controllable contraction of the unit constrictors via motor-driven tendons and programmable control over deformation patterns applied to the stomach reactor membrane. Biomimicry of the smooth muscle contractions, both in form and function, provide it with an ability to demonstrate controllable peristaltic motility.

The various stages involved in the digestion of food suggest that different types and forms of control mechanisms may be required to be put in place. In general, the stages of digestive activity within the gastric tract include:

i. mastication of a food bolus
ii. swallowing of the bolus and transportation of it to the stomach
iii. accommodation of the food within the stomach body
iv. breakdown and mixing of the accommodated food with digestive juices in the stomach
v. the passing or emptying of the digested food from the stomach to the duodenum and small intestine

For an *in vitro* physical model, each of these processes may make use of different forms of control mechanism to actuate the muscle contractions and manipulate them in a manner suitable to the type of deformation pattern involved.

Control of artificial gastric tract muscle contractions can be divided into two types:

i. multiple contractions controlled by a single mechanical mechanism, and
ii. independent muscle contraction controllers that respond to feedback mechanisms and programmable activity

Contractions of the oesophagus involve a consistent wave-like contraction pattern along the entire length of the oesophageal tract that propels a bolus of food to the stomach. Each circumferential muscle along the oesophagus contracts until complete closure of the tract lumen occurs; suggesting that there is no change in the amplitude, or maximum contraction ratio, of the contractions involved. This means that the oesophageal form of contraction action can be mimicked using muscle contractions controlled via a single mechanism *i.e.*, driving each of the artificial muscles to a constant contraction ratio or amplitude, and along the length of tubular tract in a periodic wave-like manner.

Contractions of the stomach and proximal duodenum require a more sophisticated approach to mimicry of the biological contractile activity. This is because stomach and duodenal contractile motility patterns can vary considerably. Motility patterns of the biological stomach depend on numerous biomechanical, bioelectrical, and biochemical feedback mechanisms that are initiated from various systems including the endocrine, gastrointestinal, and nervous systems [3]. Biological feedback mechanisms can also be influenced by various factors including the volume of contents within the stomach, the stage of digestion, and pH or nutrient levels of the digesta. As these feedback mechanisms are

related to the temporal generation of specific contraction patterns, rather than the control over biomechanical action, their inclusion in the *in vitro* model is beyond the scope of this thesis. However, their importance in influencing stomach muscle contractile activity means that the artificial stomach muscles of the *in vitro* physical model need to be able to respond to these feedback signals with independent variable control over the individual unit constrictors.

Fig. 69 shows a block diagram configuration of the connections between the core *in vitro* gastric tract components, including the control systems and feedback components. The tension control unit for the artificial stomach unit constrictors is based on the individual tendon control system described in Section 6.3. Feedback of tendon tension is provided via tension sensors (Section 6.1.1.2) that are connected in series with the unit constrictor Bowden cables (Section 4.4), stretch sensors for measuring membrane stretch over the fundus region of the stomach (Section 6.2.1), temperature sensors for regulation of the enclosure temperature, and pressure sensors measuring the intragastric pressure inside the stomach reactor (Section 6.2.2).

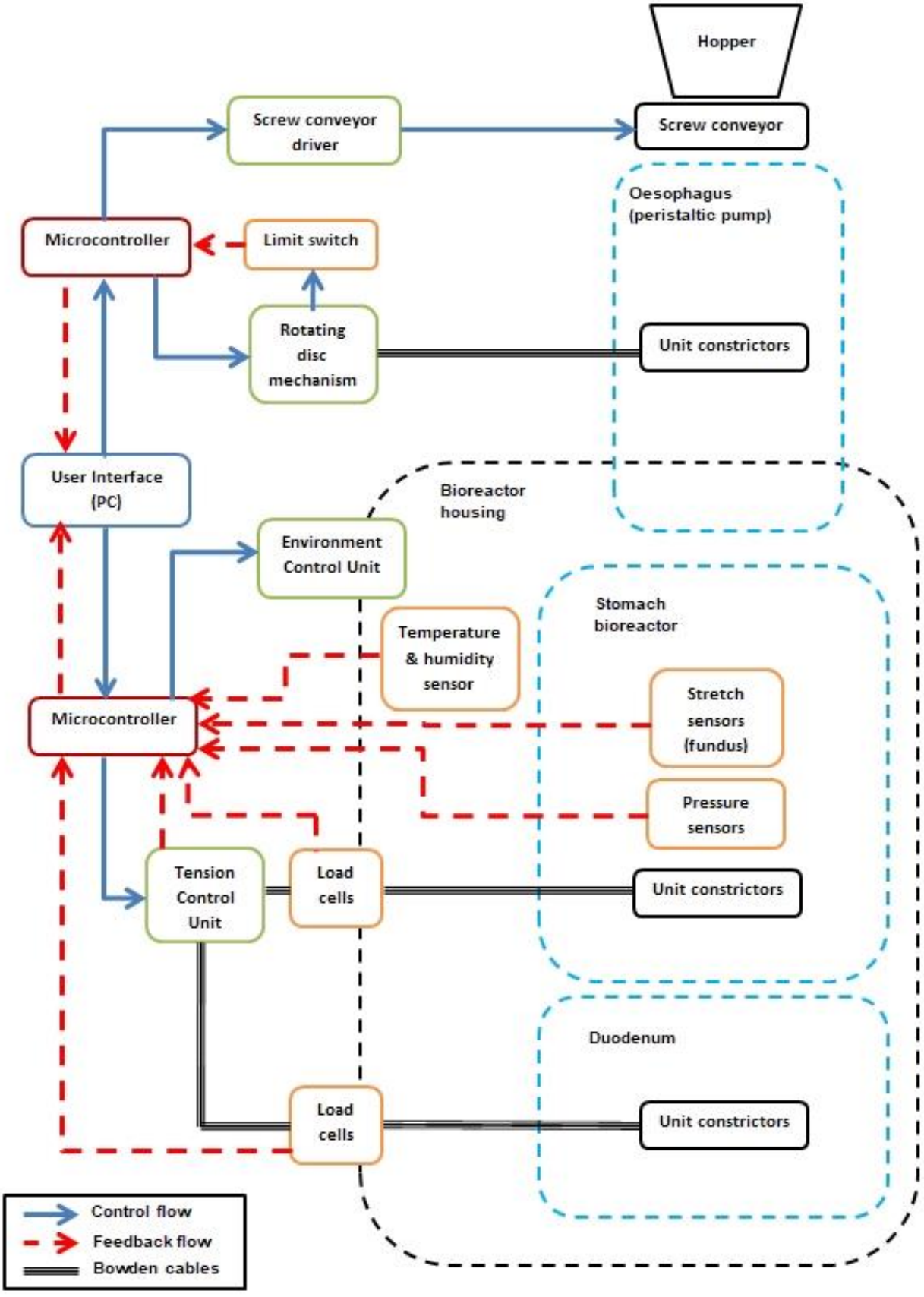

Fig. 69: Block diagram of the proposed *in vitro* gastric tract control system and feedback components.

7.1. Components of the oesophagus

The first stage of digestion involves the mastication, or mechanical disintegration, of food particles in the mouth. The processes involved with the mastication stage are beyond the scope of this thesis but are necessary for the preparation of a bolus of food prior to its transportation to the stomach. The physical or mechanical process of mastication is combined with the secretion of saliva; consisting of a salivary amylase that assists in the breaking down of carbohydrates, and a lingual lipase for breaking down triglycerides [240]. The masticated food also gains additional lubrication from the saliva, which assists in the process of swallowing and propelling the bolus of food down the oesophagus and into the stomach.

Swallowing of masticated food in a liquid, semi-solid or slurry form first involves it being loaded into a hopper or receptacle with a mechanism for priming the oesophageal tract with a bolus-sized amount of food. One possibility is to introduce a motor-driven screw conveyor positioned at the base of the hopper. Alternatively, the priming of the food bolus in the oesophagus could be carried out using an automated plunger system or similar mechanism that delivers a set volume of masticated food. The type of priming system used is irrelevant if the amount of food primed into the entry point of the artificial oesophagus can be constantly controlled and contained. The output of the priming unit feeds into the beginning section of the artificial oesophagus, which is made using the linear peristaltic pump device described in Section 5.1.2.

Adjustment to the feed rate of the priming unit can alter the volume of food material that is pushed into the artificial oesophagus before it is pumped into the stomach. However, the internal diameter of the artificial oesophageal tract is the dominant factor that determines

the limit to the volume of food that can be transported during a swallowing action. The expandable braid used in the linear peristaltic pump has a minimum contracted diameter of 10 mm and a maximum expanded diameter of 25 mm, while the inner silicone tube has an outside diameter of 20 mm and a thickness of 3 mm. Increasing either the maximum expanded diameter of the braided tube, or the length of tract that is relaxed during peristalsis can increase the volume of food that can be transported during a single swallowing action.

Modifications could also be made to the priming unit so that a small amount of air is introduced with the food bolus during each simulated swallow. This type of alteration may enhance the biomimetic characteristics of the *in vitro* gastric tract simulator. However, this could result in a significant volume of air accumulating within the artificial stomach reactor over time unless an outlet mechanism for venting the trapped air is installed. In a biological system, air inside the stomach is released when the diaphragm presses down on the fundus region and the trapped air is then forced back up the relaxed oesophagus, resulting in a belching action [241].

Once the tract is primed with a bolus of food, the constrictive action of the oesophagus propels the food bolus down the tract. In this manner the oesophagus behaves like a biological pump and flexible conduit for the transport of food to the stomach. Control over constriction of the artificial oesophagus is carried out using a rotating disc mechanism (Section 5.1.1). Uncontrolled drop-through of the material down the oesophageal tract can occur if the tract is fully opened and the material is fluid and of low viscosity. To avoid this, the artificial oesophagus should always have a section of tract that remains in a contracted state, closing off the silicone tubing and preventing drop-through from occurring. The

peristaltic movement of the contracting constrictors propels the bolus of food forward with controlled velocity down the entire length of the artificial oesophagus (Fig. 70).

The contraction pattern applied to the artificial tract needs to maintain closure of the tubing at its base region when a swallowing action is not occurring. This mimics the closure of the lower oesophageal, or cardiac, sphincter of the gastric tract. Closure of the cardiac sphincter is required to retain food contents within the stomach during digestion and prevent chyme and gastric juices from travelling back up the oesophagus. The stomach contents can be forced back up the oesophagus if the sphincter is not kept completely closed due to pressure caused by the stomach contractions. Only during a swallowing action should the sphincter

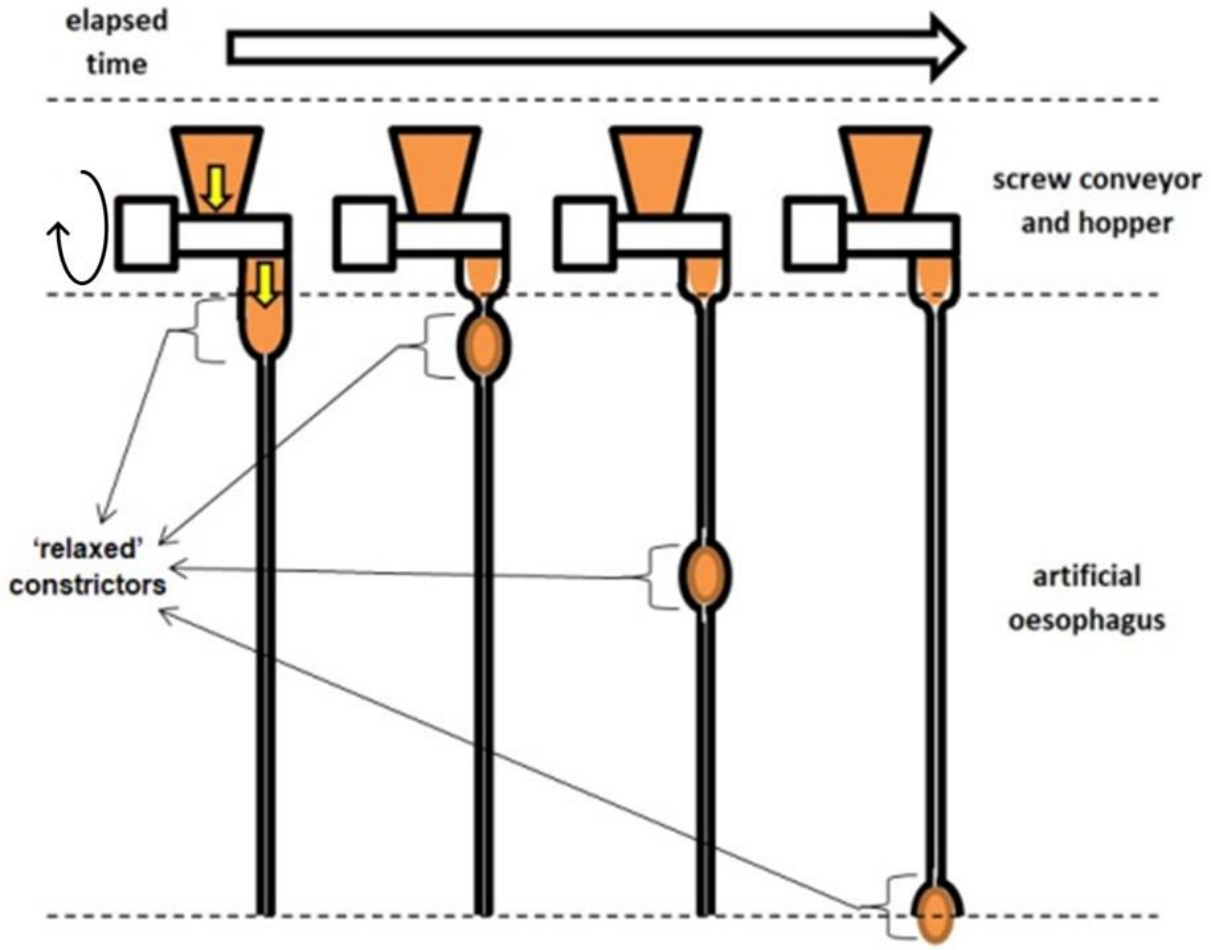

Fig. 70: Basic diagrammatic example of peristaltic formation and propulsion of a bolus of food down the artificial oesophagus to the stomach.

be opened to allow passage of the food bolus towards the stomach.

A capstan mechanism (Section 5.3.2) can be added to the rotating disc mechanism to assist in reducing the torque required from the motor when tensioning the unit constrictor tendons. Introducing a capstan mechanism to the rotating disc mechanism reduces the load being placed on the rotating disc motor, allowing for improved control over the rotational velocity of the discs. The tension required to contract the unit constrictor tendons on the artificial oesophagus can vary depending on the properties of the food material being passed down its tract. Solid or semi-solid food materials and highly viscous fluids require larger tension forces to completely close the constrictors and artificial tract than do low viscosity liquids. The creation of larger tension forces requires more torque being generated from the rotating disc motor, which results in slowing the motor down and therefore also reducing the speed of the simulated swallowing action. Wrapping the unit constrictor tendons around a capstan spindle, which is rotated by a high-torque motor, will help to maintain constant propulsion velocity of the food bolus.

An *in vivo* study of bolus velocity during oesophageal transit to the stomach by Nguyen et al. [242] suggests that bolus velocities can range between 4 and 15 cm/s in the oesophagus and that body posture can also impact the speed of the swallowing action *i.e.*, whether the body is upright or supine [242]. A 15 cm length of artificial oesophagus tract, with unit constrictors being placed along the entire length of the tract, would require a 360° rotation of the discs to be completed within 1 to 4 seconds to maintain a bolus velocity of between 4 and 15 cm/s. A limit switch, attached to the rotating disc mechanism, is triggered when the discs have completed one full revolution and signals to the controller when the peristaltic

contractions of the unit constrictors have traversed the entire length of the oesophageal tract.

7.2. Components of the stomach and proximal duodenum

Components of the stomach and proximal duodenum include the membrane and muscle layers of the tract shell, Bowden cable connections, and various control and feedback devices for sensing and measuring tendon tension, membrane stretch, and intragastric pressure.

7.2.1 Layers of the reactor shell

The biological gastric tract wall is comprised of several layers including mucosal and submucosal layers, muscle layers, and an outer serosa or protective layer. An extracellular matrix provides elastic structural support between the layers, joining them together. The reactor shell of the artificial gastric tract has been developed to mimic some of these layered tissue structures of the biological gastric wall. This section outlines a suggested approach to configuration of the layers of the wall, or shell, of the artificial *in vitro* stomach reactor.

A 1 mm thick reinforced composite membrane layer was made using the method described in Section 3.2. The reinforced composite silicone layer mimics the serosa by providing a protective outer layer that dictates the overall shape of the stomach. It also plays the role of the extracellular matrix of the biological tract wall, acting as an elastic structural support between the artificial mucosal and muscle layers.

The inner mucosal and sub-mucosal layers of the artificial stomach are mimicked by a 3-5 mm thick layer of soft silicone rubber fabricated as an open-cell sponge structure using the dissolvable template method (Section 3.3). The sponge silicone layer is applied to the reinforced composite membrane layer by first pre-stressing the membrane layer in the

longitudinal and circumferential directions. This approach mimics the appearance of mucosal folds on the inner layer of the stomach tract that gradually disappear as the stomach membrane is expanded (Section 3.3).

A layer of artificial muscles is attached directly to the reinforced composite silicone layer. The muscle layer consists of coiled nylon fishing line unit constrictors (Section 4.2), hand-sewn onto the composite silicone surface (Fig. 71), and actuated by pulling the nylon 'tendons' threaded through each of the coils. The artificial muscle layer may need to be attached to the reinforced composite layer prior to the addition of the silicone sponge mucosal layer. This is because sewing of the constrictors onto the reinforced composite

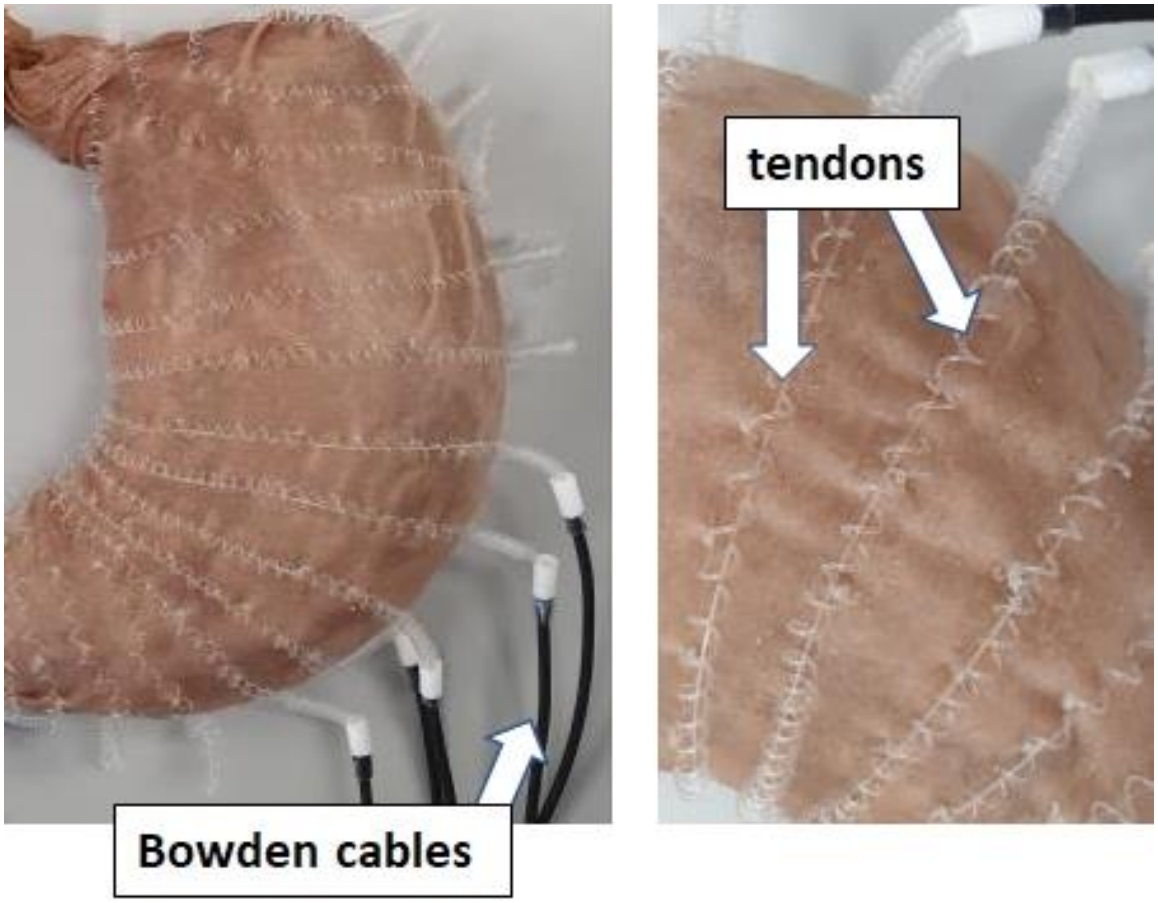

Fig. 71: Coiled nylon line unit constrictors sewn on an artificial membrane with nylon tendons running through them.

silicone layer penetrates the silicone, and the resulting holes need to be plugged. Curing a thin layer of silicone over the holes seals them and keeps the membrane shell watertight.

The size, number, orientation, and distribution of the artificial muscle unit constrictors over the membrane surface can be altered to suit different simulation requirements. Fifteen unit constrictors were attached along the artificial stomach membrane from the mid-corpus region down to the pyloric sphincter to simulate basic slow wave peristaltic deformation over the stomach. The unit constrictors have a separation of 20 mm between them along the line of greater curvature and were spaced evenly apart around the remaining circumference of the stomach. This distance of separation between the constrictors allows for smooth contraction deformation of the stomach shell surface to occur using a minimal number of unit constrictors.

A further five unit constrictors are attached from the pyloric sphincter down the proximal duodenum to provide the duodenum with the ability to contain and move chyme emptied from the stomach. Placement of unit constrictors over the fundus region of the stomach in an oblique orientation was not considered necessary for this simulation model. This was due to this model only being used for the demonstration of peristaltic deformation, and not for demonstration of the adjustment of the stomachs' overall volume.

7.2.2 Bowden cable connections

Bowden cables are used as a conduit for running unit constrictor tendons to a tension control unit. The tension control unit adjusts tension on the tendon lines which causes the unit constrictors to contract or expand. The terminal ends of the Bowden cables connecting the unit constrictors attached to the stomach are positioned along the greater curvature of the stomach. The layout of the conduit cables is configured so that they track along the

same anatomical pathway as that of the greater omentum. The greater omentum is an apron-like fold of peritoneal connective tissue that provides connection of nerves and blood supply to the stomach [6]. This placement of the Bowden cables is appropriate as the greater omentum also acts as a flexible connection point for the stomach with the rest of the biological body and influences the degree to which the stomach membrane can freely move about and deform.

Bowden cables coming from the unit constrictors on the stomach membrane connect to tension sensors to gauge the amount of tension force being applied to each unit constrictor tendon. The setup for the Bowden cable to tension sensor connections is explained in more detail in Section 6.1.2. Ideally, the transmission lengths of the Bowden cables between the tension control unit and unit constrictors should be kept to a minimum. Bends in the Bowden cable between the tension control unit and unit constrictors should also be minimised. This is to avoid the addition of tendon-to-Bowden cable contact friction forces affecting the accuracy of tension force measurements (see also Section 4.3).

7.2.3 Control and feedback mechanisms

Several feedback mechanisms are used for monitoring and adjusting the tension applied to the unit constrictor tendons and in turn determining the overall deformation shape of the reactor shell. Displacement sensors in the tension control unit (Section 6.1.1) measure the absolute length of tendon displacement and subsequently provide for calculation of the contraction ratio being applied to each unit constrictor. Other feedback mechanisms measure tendon tension, membrane stretch, and intragastric pressure of the artificial stomach reactor during the deformation of its shell. These mechanisms serve an integral part in maintaining control over the simulated digestive motility patterns.

Tendon tension

Tension sensors provide an estimate of the tension force applied to the tendons of the unit constrictors by measuring the reaction force created on the Bowden cables that encase the tendons. The tension force readings can be affected by surface friction between the internal surface of the Bowden cables and the nylon tendon lines, as well as frictional forces where the nylon tendons exit the Bowden cables. Despite the additional friction forces that may be involved, the measurements provided by the tension sensors indicate relative change in tendon tension as the unit constrictors' contraction ratios change. This is useful when limits to the contraction of the unit constrictors are reached *e.g.*, if the closure of the unit constrictor encounters a significant resistance such as a solid object or objects during their contraction. The tension sensors also indicate when the tendons have become slack and therefore no tension force is present *e.g.*, when the tendons retract to a point where they are no longer in contact with the unit constrictors.

Tension sensor feedback can be used to trigger unit constrictor actions. If contraction of a unit constrictor reaches a predefined tension force measurement upper limit, then that contraction, or series of contractions, can be halted or reduced to limit the contraction force exerted by the artificial muscle. Similarly, if the measured tension force being applied to a unit constrictor falls below a specified measurement level, then this can trigger an action to contract the tendon until the tendon begins contraction of the unit constrictor again. This can apply to situations where the stomach is either empty, or emptying its contents, and the stomach shell needs to be contracted to adjust the stomach to the reduced volume of contents.

The applied tendon tension force that is required to produce a certain pressure from the internal surfaces of the unit constrictors can be determined experimentally. Experimental methods may include the measurement of compression force required to crush calibrated agar gel beads, or the compression of a hollow rubber ball or balloon connected to a manometer. Results from these experimental methods can be used to relate the contraction of a unit constrictor to the amount of pressure it exerts on the food contents of the stomach.

Membrane stretch

Stretch sensors located on the fundus region of the stomach provide measurements of the amount of stretch occurring during expansion of the stomach shell. Although estimated measurements of shell circumferential deformation can be obtained from the individual unit constrictor contraction ratios, they do not necessarily indicate the true state of stretching that may be occurring over the entire shell surface. Stretch sensors can be used to determine membrane stretch in orientations other than that provided from the layout of the unit constrictors, or in areas where no unit constrictors have been placed.

Feedback from sensing membrane stretch in the fundus region of the stomach can trigger the adaptive relaxation or increased tone of the stomach wall, by relaxing or contracting unit constrictors and adjusting the stomach volume to better accommodate its contents. Combining the measurements of membrane stretch and contraction ratios of the unit constrictors also provides useful information for reconstructing three dimensional (3D) virtual views of the deformed shape of the stomach. These views can be reconstructed by mapping the feedback measurements taken from the physical *in vitro* stomach model onto a 3D virtual image reconstruction application (Section 6.3).

Intragastric pressure

Pressure sensors placed at various locations within the stomach shell cavity measure the intragastric pressure, relative to a reference pressure, and gauge the differences in pressure between different regions of the stomach. These sensors may be used in conjunction with the membrane stretch sensors to trigger adaptive relaxation of the stomach or determine whether overall stomach volume should be increased or reduced.

A basic, flexible gastric balloon catheter, inserted into the fundus region of the stomach model and close to the lower oesophageal sphincter, can provide feedback on changes in intragastric pressure (Section 6.2.2). The location of the sensor within the stomach cavity can be altered by extending or retracting the catheter. The use of this form of pressure sensor within the *in vitro* simulation model may be considered optional as they are an invasive device and could influence the gastric motility and mechanical action of the stomach shell.

7.3. Reactor housing and environment

Biomimicry of the gastric tract should include a recreation of the surrounding physical environment and conditions within which the biological organs of interest operate. In this case the stomach and duodenum lie within the abdominal cavity and are surrounded by other organs such as the liver, pancreas, kidney, spleen, and transverse colon. Fig. 72 shows a rendered image of the biomimetic gastric tract as it appears when surrounded by the organs. The Bowden cables of the *in vitro* model track along the greater curvature of the stomach, as it is an area that is unimpeded by the surrounding organs and allows for the cables to flex within the reactor with minimal interference.

The stomach, as it appears in Fig. 72, is shown in a distended state representing the typical volume of an adult stomach when filled with food. The volume of the stomach is 0.8-1.0 litres. At this volume only the regions around the greater curvature and fundus appear unconstrained by the surrounding organs. What is not shown in Fig. 72 is that the greater

Fig. 72: Rendered CAD image of the biomimetic gastric tract and anatomical locations of the surrounding organs.
(This work includes rendered derivatives of BodyParts3D, © The Database Center for Life Science licensed under CC Attribution-Share Alike 2.1 Japan: https://dbarchive.biosciencedbc.jp/en/bodyparts3d/lic.html)

curvature is constrained by the front of the abdominal cavity, and the upper fundus region of the stomach lies beneath the diaphragm. However, it is typically the proximal fundus region and region of greater curvature where the stomach is least constrained by surrounding surfaces, and where the most expansive deformations of the stomach shell can occur.

Representation of the anatomical shapes of the surrounding organs can be constructed by 3D printing full-size organ shells in a dissolvable or sacrificial material, then coating the shells with a 4-5 mm layer of silicone rubber before dissolving the sacrificial material away. The rubber organ shells are filled with water and placed within the transparent container in their anatomical positions. The temperature of the rubber organ shells is regulated by pumping water through flexible hoses that connect the organ shells to a temperature-controlled reservoir.

A basic confinement vessel for the stomach reactor can be created by using a transparent oval container to mimic the abdominal walls, and transparent bags filled with water to represent the surrounding organs and tissue (Fig. 73). The transparent water-filled bags provide support for the reactor, with one bag being placed under its base and another covering it from above. The water temperature within the bags is maintained at a constant temperature of 37°C to simulate temperature inside the human body. Holes placed in the top and base of the container allow for access to the upper oesophageal tract at the top of the reactor container, and an exit point for the proximal duodenum at its base.

The artificial gastric tract can be rotated to mimic the inclination of different body positions. Alteration to the orientation of the artificial gastric tract model can be achieved by attaching

the containment vessel to a gimbal rig (Fig. 74). This allows for the reactor orientation to be changed at any time during the simulations for study of the effects of posture on digestion.

A change in orientation or inclination alters the gravitational effect on the stomach reactor contents, which can result in changing the dynamics of its motile activity. Suspended support of the stomach, provided by the water-filled transparent bags, prevents it from shifting about the containment vessel when the models' orientation is altered. However, Bowden cables from the containment vessel to the tension control unit may experience significant bending from the containment vessel being placed in a certain orientation, resulting in fluctuations to the mechanical power required for actuating the unit constrictors.

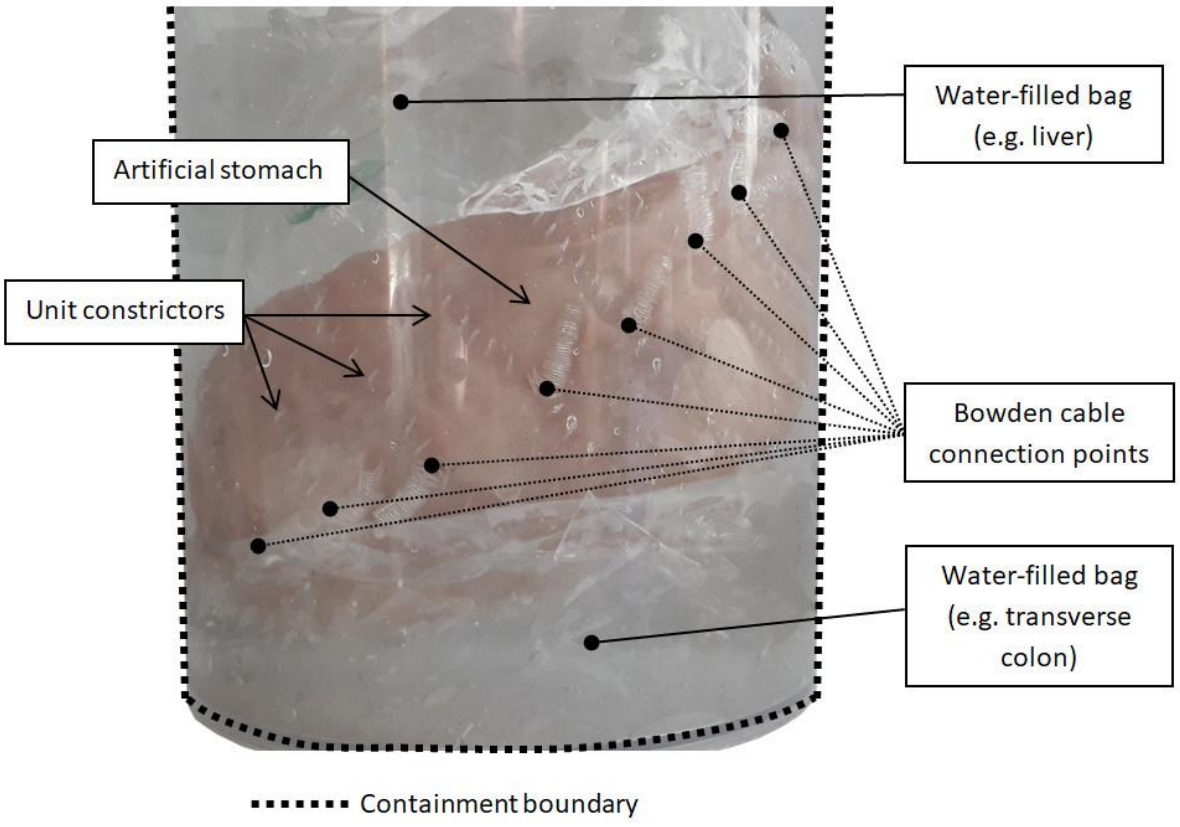

Fig. 73: Partially filled artificial stomach suspended between two plastic bags of water and placed inside a transparent container.

7.4. Simulator operation

Core operational aspects of the *in vitro* biomimetic gastric tract simulator include the implementation of a user interface, initialisation of the model for simulation, simulation of gastric tract motility, the collection of sample materials, and cleaning and maintenance of the unit.

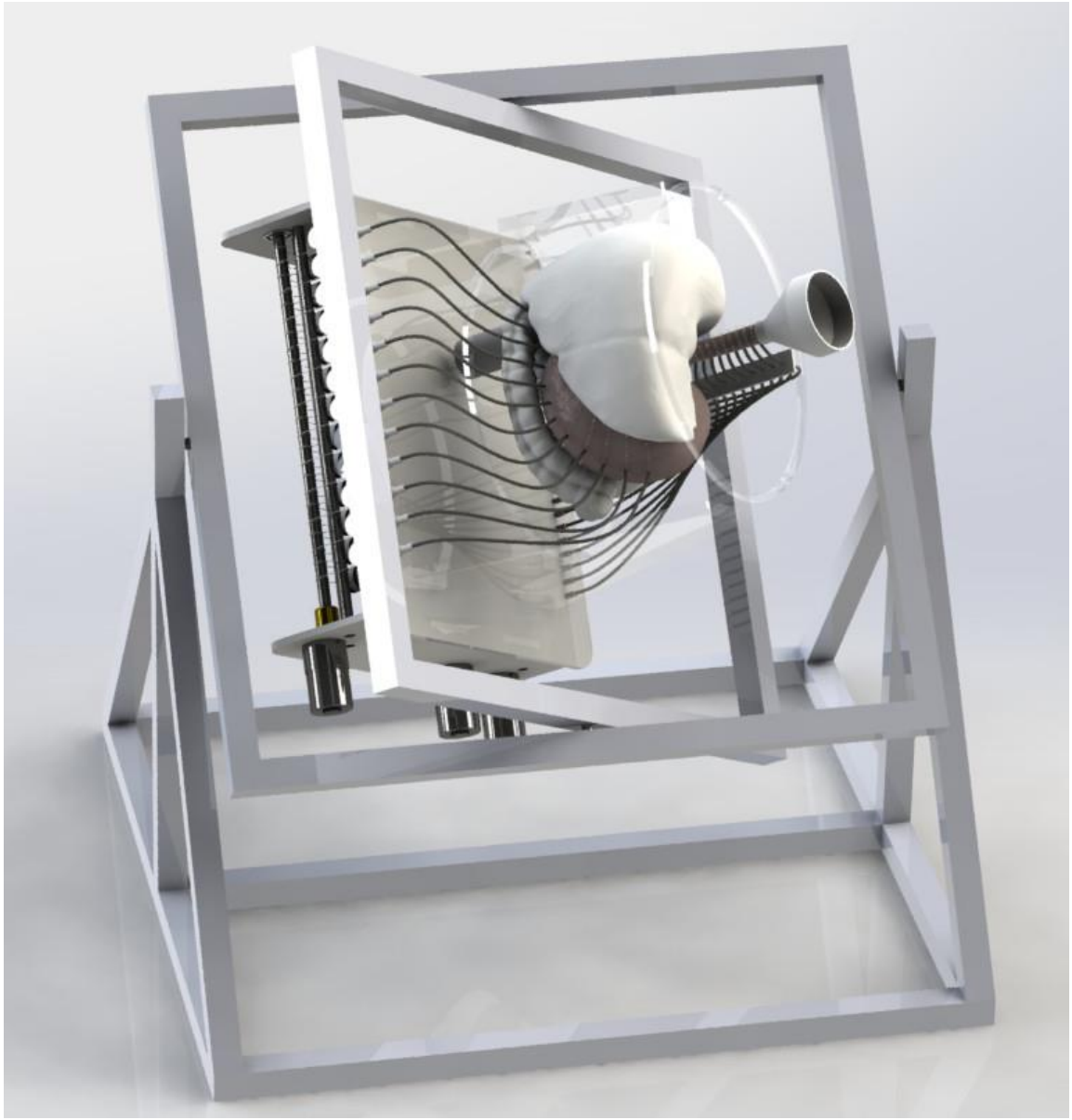

Fig. 74: Rendered example of a proposed gimbal support rig for the gastric tract containment unit.

7.4.1. User interface

The *in vitro* model is controlled via microcontrollers and a computer based graphical user interface (GUI). The design of the GUI is an essential part of the *in vitro* simulator as it provides the user with an easy-to-use tool for manipulating the operation of the models' components, and controlling the wide variety of contraction patterns that are possible during simulation. The GUI is the main user-control interface for the *in vitro* simulator and passes actuation instructions to the microcontrollers for controlling the tendon tensioning systems and unit constrictor contractions. Data collected from various feedback sensors are also passed back to the GUI interface from the microcontrollers so that adjustments can be made to the actuation of the gastric tract contraction patterns.

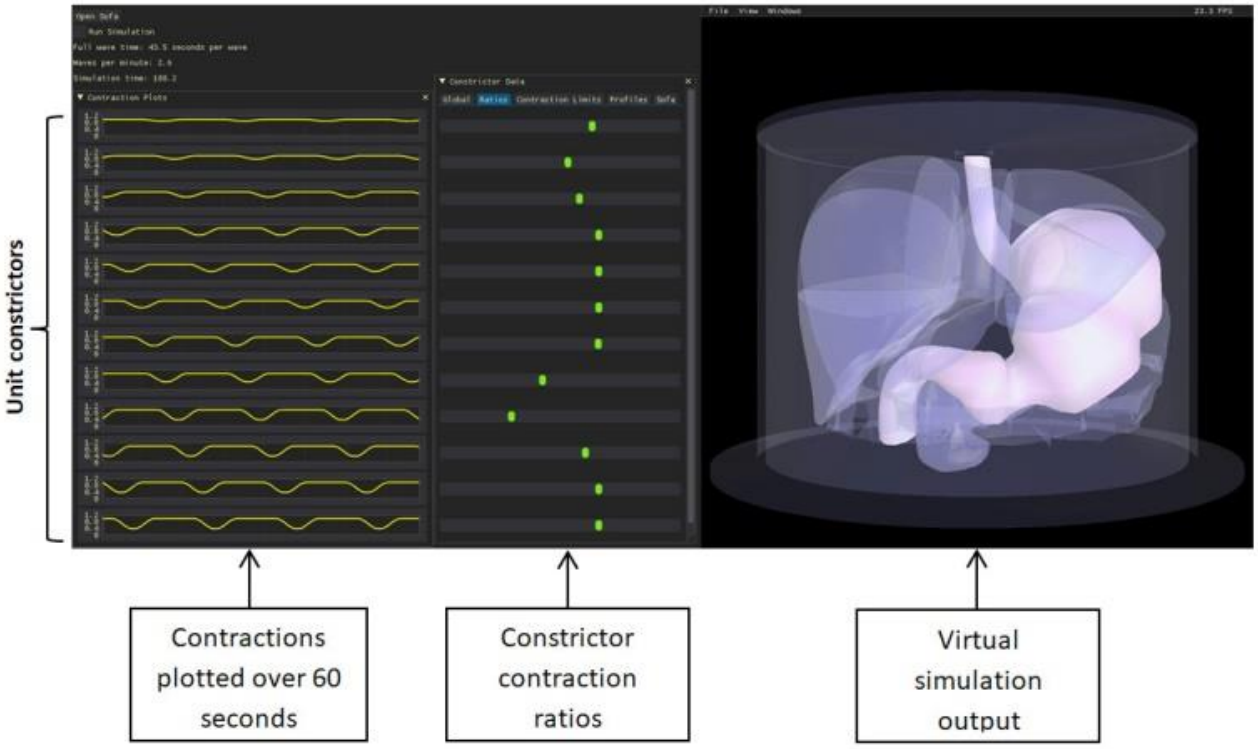

Fig. 75: A basic graphical user interface layout demonstrating the operational control over the *in vitro* gastric model.

A prototype design for the GUI accepts user input for controlling the models' operation and outputs visual representations of the intended contractions that are to be applied, as well as actuation instructions for the microcontrollers (Fig. 75). The user can input a variety of unit constrictor contraction pattern details including applied maximum contraction ratios for each constrictor, the time delay before starting the next sequential unit constrictor actuation, constrictor contraction period, constrictor holding period, constrictor expansion period, and the time delay before the start of a new peristaltic wave. Each of these input variables are used for calculating the required, or targeted, unit constrictor contraction ratios at any specific point in time. The targeted contraction ratios are sent to the specific microcontroller that controls the tendon tensioning unit, which then actuates the tendon winding motors so that the unit constrictors are contracted or expanded to match these contraction ratios.

The prototype GUI also provides visual representations of the operational state of each of the unit constrictors using a moving slider control, with each slider representing the current contraction ratio of an individual unit constrictor. The position of the control sliders in the GUI indicates the current absolute position of the linear sliders in the tendon actuation unit (Section 5.2.2); the slider positions can be considered as a snapshot of the contractive activity. A real-time, stacked plot of the changing contraction ratios for each unit constrictor over a 60 second period displays the temporal progression of successive constrictor contractions. These plots provide visual information on how the successive unit constrictor contractions relate to each other, how they propagate into a flowing slow-wave contraction pattern along the stomach shell and the frequency of the generated slow-waves over a specific period.

Two sets of control sliders or plots can be used, one for representing the targeted contraction ratios of the unit constrictors over time and the other showing the contraction ratio that is taking place. This is because the targeted contraction ratios may be affected by information collected from the feedback mechanisms. For example, if the tension measured on a unit constrictor tendon reaches a maximum or minimum limit, as set by the user, then the amplitude of the contraction can be stopped, reduced, or increased. Some unit constrictors may also be placed in a feedback monitoring state during operation so that they actuate when a reflexive or adaptive relaxation pattern is required to increase the stomach volume.

7.4.2. Initialising the model

A general approach for initialising the gastric tract model involves the tract being set to an empty state *i.e.*, without any food being present in the system. The pyloric sphincter remains open while the stomach unit constrictors contract, one-by-one, starting from the fundus and continuing down to the corpus. Opening the pyloric sphincter causes any remaining air or contents in the stomach to be expelled while the membranes' shell contracts. The tendons of the unit constrictors are contracted until the tension sensors measure a rise in tension. This indicates that all slack has been removed from the tendons and the stomach shell has adjusted to adopt a minimum volume. At this point the unit constrictors' contraction ratio can be set to 1 as they have reached a state of minimum contraction.

7.4.3. Simulation of gastric tract motility

Various patterns or sequences of contraction are programmed into the tension control units via the graphical computer interface (GUI). This includes patterns that simulate swallowing of a food bolus, peristalsis and mixing, relaxation of the fundus for accommodation of

incoming food, and control of the pyloric sphincter for the emptying of stomach contents. During simulation, the amplitude of each individual contraction or expansion within a specific motility pattern or sequence can be influenced via the monitoring of various feedback sensors.

Swallowing – the entry of food

Food material is passed into the stomach reactor by the triggering of a swallowing action. Activation of the swallowing mechanism is sent via a signal from the PC interface to the microcontroller controlling the rotating disc mechanism. Once a signal is sent, the rotating disc mechanism completes one full rotation of its discs, which actuates the full constriction pattern of the artificial oesophagus and propels a bolus of food into the stomach. The timing and frequency of signals sent to the artificial oesophagus is controlled via input at the user interface or GUI. This allows for a specific volume of food material to be transported into the stomach at any time specified during the simulation.

Adaptive or receptive relaxation

Once a swallowing action begins the tensions on the unit constrictors on the stomach membrane are continuously monitored to determine whether relaxation or expansion of the constrictors is required. As measured tension from the tendons increases the unit constrictors can be gradually relaxed or expanded in length, beginning with those covering the fundus region of the stomach and then, if necessary, progressing sequentially down to the corpus and the antrum. These adaptive relaxation actions have the potential to occur at any point where swallowing activity increases overall volume of food entering the stomach cavity, or when pressure measurements indicate that the intragastric pressure in the stomach rises above a pre-determined level. In doing so, the artificial stomach simulates

gastric expansion, which allows it to better accommodate the volume of food entering the stomach and to maintain a stable intraluminal pressure.

Gastric peristalsis

Peristaltic motility of the stomach can occur at any stage, but the amplitude and frequency of the contractions may vary depending on the physical structure, viscosity, and volume of the contents, feedback received from various biomechanical and biochemical mechanisms, and the digestive action or stage of migrating motor complex that is taking place. Independent control over the unit constrictors provides a versatile mechanism for adapting the artificial muscle contractions to suit wide variations in amplitude and frequency.

Peristalsis is a series of consecutive muscle contractions and expansions that begins in the corpus of the stomach and progresses down to the pylorus. A peristaltic slow wave pattern can be simulated by designating one unit constrictor in the corpus region to initiate the pattern. The constrictor adjacent to the initiating constrictor then begins to contract after a specified time delay, and then the next, and so on. In this way a peristaltic wave propagates at a constant velocity along the wall of the stomach (Fig. 76).

For example, if constrictors are placed 20 mm apart and it is desired to generate a slow wave at a constant velocity of 20 mm per second along the stomach wall, the time delay between each constrictor actuation would be one second. If the total distance over the greater curvature from the first to the last unit constrictor is 200 mm, then the peristaltic wave will complete its travel in approximately 20 seconds.

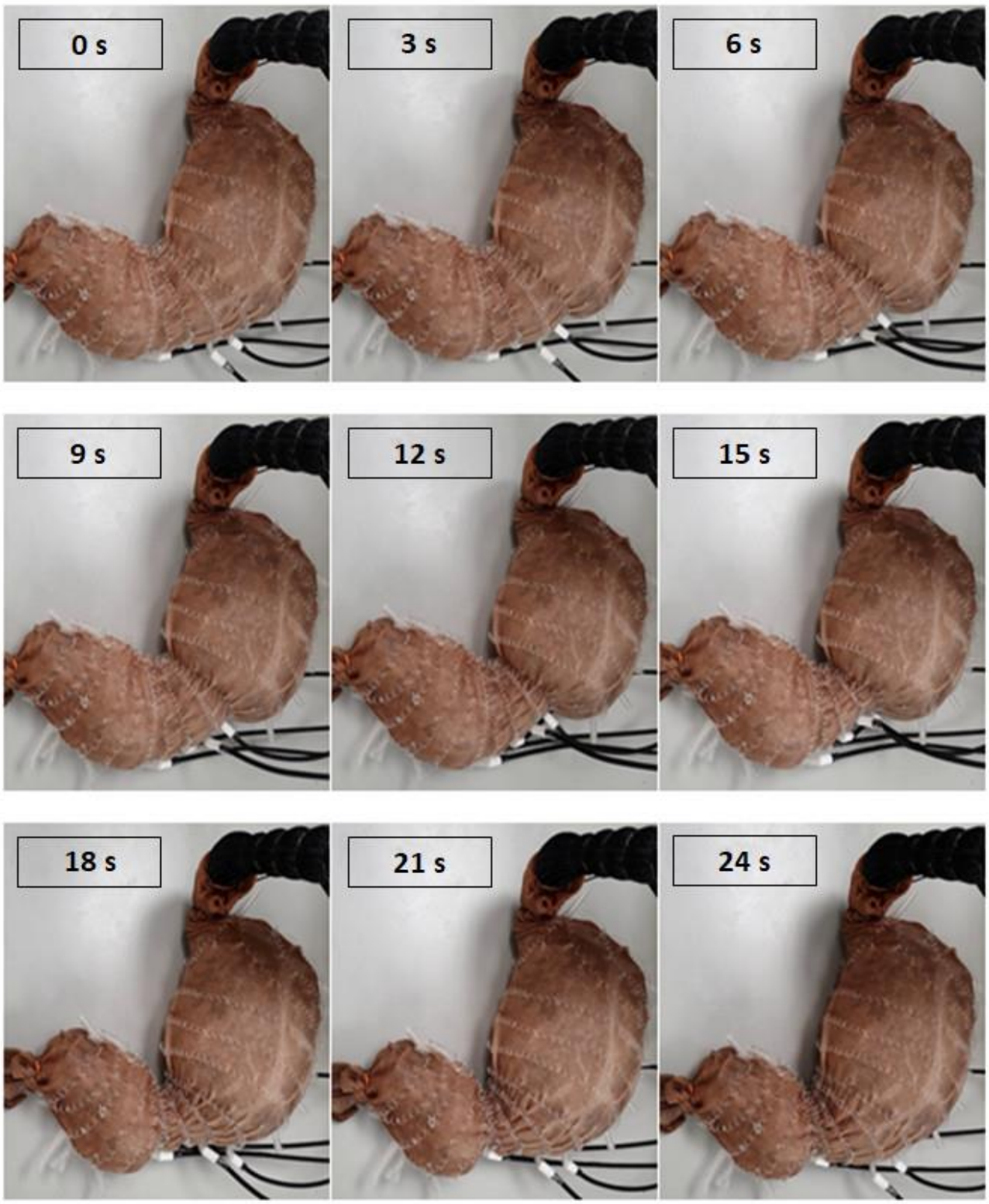

Fig. 76: A series of time-lapse images demonstrating the artificial stomach undergoing a partial peristaltic contraction pattern over the lower corpus region towards the antrum.

Although the time delay between unit constrictor contractions may not differ significantly, the speed of the contraction for each of the constrictors is more likely to be different. This is because the amplitude and applied force of the contractions differs between stomach regions and constrictors. The corpus contractions are typically shallow and initiate the movement of the stomach contents. As the wave approaches the antrum the contractions become deeper and stronger with the strongest contractions occurring nearest to the pylorus. Manipulation of the contraction amplitude and force within the antrum region can lead to the contractions creating a retro-propulsive, jet-like motion. This retro-propulsive motion rapidly forces the stomach contents back towards the corpus region of the stomach, mixing and grinding the contents as it does so.

Gastric emptying

Unit constrictors operating the pyloric sphincter perform a different role to those covering the body of the stomach. The pyloric sphincter constrictors perform strong tonic contractions that cause the section of the wall to act as a valve between the stomach and the duodenum. The sphincter prevents larger particles of the stomach contents from passing through to the duodenum during peristaltic contractions. Only particles smaller than 0.5-2 mm diameter are typically able to pass through the sphincter during most of the gastric emptying stage. However, the opening of the sphincter may increase significantly during the housekeeping stage of the migrating motor complex so that larger indigestible objects may be cleared from the stomach. Controlling the contraction ratio of the constrictors involved with the sphincter dominates as a control mechanism over the adjustment of the tension force being applied.

On exiting the stomach and pyloric sphincter the semi-digested contents, or chime, then enter the duodenum, a C-shaped intermediary section of the gastric tract that prepares the chyme for further digestion by the small intestine. Bile and digestive enzymes are added to the chime and bicarbonate and mucus are released to bring the chyme back to a more neutral pH level. Hormones released by the presence of fats and acids in the chyme regulate the rate of gastric emptying, so chemical responses from the duodenum act as a feedback mechanism for the motility of the stomach. Although such chemical feedback mechanisms play a significant role in triggering motility patterns of the stomach and duodenum they are out of scope of this thesis and have not been included as a part of the *in vitro* model.

The proximal duodenum has been included as a component within the biomimetic model of the gastric tract to partially regulate the rate of gastric emptying from the stomach reactor. As gastric emptying takes place the presence of contents within the duodenum can impede the ability of the chyme to pass rapidly through the pyloric sphincter. As contents within the duodenal tract build up, they eventually require to be moved on so that the stomach can empty. Constrictors placed over the duodenal tract recreate two types of motility pattern, peristalsis for moving of the contents further along the tract to the small intestine, and segmentation. Segmentation motility patterns do not tend to move the contents along the tract but perform a mixing action of the contents in place.

7.4.3. Sample collection

Digested material samples can be collected from a removable receptacle located at the outlet of the duodenal section of the artificial tract. A small plastic jar is screwed onto the base of the containment housing where the duodenum exits the container to capture the

sample material, or chyme, emptied by the artificial stomach through the pyloric sphincter during gastric emptying of the stomach reactor. Constrictors at the base of the duodenal tract initially prevent the chyme from dropping directly into the receptacle. When they are expanded, they can regulate the release of the contents of the duodenum into the receptacle for sample collection. Periodic release of chyme into the receptacle from the duodenum is controlled via the user interface.

Samples collected from the internal cavity of the stomach present a challenge as providing direct access to the contents may rely on dissection of the stomach membrane layers. This approach is similar in effect to surgical incisions, where the membrane is unable to immediately heal and close itself and its physical and mechanical characteristics may be irreversibly altered. This suggests that provision of sealable access points for collecting samples of the internal contents should be built into the stomach wall layers. The sealable access points are created during the fabrication of the membrane to avoid the membrane losing its physical and biomechanical characteristics.

The method for providing sealable access points to the internal contents of the stomach during membrane fabrication was to insert 40 mm lengths of 10 mm diameter cylindrical dowel into the rigid stomach template described in Section 3.2. The protruding lengths of dowel were placed at locations over the stomach body that were considered relevant for obtaining specimen samples during digestion. One was placed in the antrum while another was placed between the fundus and corpus regions of the artificial stomach. When the nylon elasticated fabric was stretched over the template, the fabric was held against the surface of the dowel by tying it at its base. A layer of liquid silicone was then applied to the entire

template which, when cured, left a short protrusion of the composite membrane material over the dowel.

The dowel was then removed from the template by cutting open the composite membrane at the top of the protrusion and pulling the dowel out. This resulted in a short tubular protrusion of the membrane to remain at the access point locations. For gaining access to the internal stomach contents the protruding membrane can be expanded by hand and kept open by stretching the material around a 40 mm diameter piece of rigid tubing. During operation of the simulator, the protrusions of membrane can be kept sealed by wrapping rubber bands around their bases. Sealing the protrusions with elastic bands allows the remainder of the stomach membrane material to expand and contract as required, but at the same time keeping the contents fully enclosed within the stomach. There is also potential for this form of access to the stomach internals to be used as entry points for the pumping of gastric juices to the stomach, or as insertion points for sensor probes to provide additional feedback measurements, such as pH levels.

7.4.4. Cleaning and maintenance

Cleaning of the tract components is recommended while the components are left in the containment vessel. Flushing of the tract while it is still placed in the containment vessel and connected to the actuation systems is easier than having to dismantle the tract components from their containment and disconnect the unit constrictor tendons and Bowden cables. It also allows for contraction actions to be activated as the reactor is *in situ* to assist in the flushing and removal of remaining digested materials. However, dismantling of the full gastric tract system may be required periodically for more thorough inspection, maintenance, and cleaning of the artificial membrane.

Use of thin, flexible, disposable liners was considered, but this would affect ability to introduce gastric juices into the stomach cavity during simulation. This disadvantage can be mitigated by design of a temporary, removable liner, which has openings over the liner surface at positions where the gastric fluids are pumped into the stomach. The openings would need to be able to seal the contents within the stomach during simulation to avoid leakage. However, there would still be some difficulty involved in the removal and replacement of a temporary liner between simulations. The liner may also move about the stomach cavity during deformations, which could affect the motility and mechanical breakdown of the food contents.

7.5. Summary

This chapter discussed configuration of the core components for the *in vitro* gastric tract simulator including design of the gastric shell layers for the oesophagus and stomach, actuation systems for simulating biomechanical motility, housing and containment of the gastric tract reactor, and operational aspects related to the model. The biomimetic model can be divided into two regions delivering distinct functional activity:

i. The oesophagus; where food material is entered into the system and the swallowing and transport of a bolus of food to the stomach is carried out.
ii. The stomach and proximal duodenum; where the accommodation of food, gastric peristalsis, and gastric emptying of the stomach contents take place.

The model incorporates two different types of actuation system; a rotating disc mechanism for driving oesophageal swallowing actions, and a tendon tensioning unit for providing independent control over the stomach and duodenum unit constrictors. Operational aspects of the simulations were discussed and included initialisation of the simulation model, a

suggested user interface layout, the role of various feedback devices on the model, and a framework for simulating various gastric tract motility actions during digestion. Sample collection and the cleaning and maintenance of the model were also discussed.

Layout of the gastric tract containment vessel involves the placement of surrounding organs, fabricated to resemble the structures of the liver, transverse colon, pancreas, spleen, and left kidney. Placement of Bowden cables along the greater curvature of the stomach minimises their contact with these surrounding organs, allowing the cables to flex when contractions take place. The surrounding organs are designed to act as water-filled shells that suspend the gastric tract and maintain constant temperature for the gastric tract environment. The containment vessel is also fitted onto a rotating gimbal rig system, allowing for re-orientation of the model into various body positions during simulation.

Chapter Eight

Conclusions

Chapter 8 – Conclusions

An advanced dynamic *in vitro* physical model of the human gastric tract was developed using low-cost, flexible materials and soft robotics to actuate and mimic human gastric tract motility in a bio-relevant manner. The physical model consists of an artificial oesophagus demonstrating pumping ability through a sequence of peristaltic contractions, and an artificial stomach shell with controllable flexible artificial muscles attached to its surface. The stomach shell demonstrates expansive and contractive action of the stomach membrane and can expand from empty to up to 5 litres in volume. The artificial muscles attached to the stomach shell are independently programmable and can provide a wide range of motility patterns mimicking those found in the human stomach and proximal region of the duodenum.

This thesis explored the development of a biomimetic gastric tract simulator through the investigation of suitable biomimetic materials, methods and techniques, their implementation into a physical gastric tract model, and integration of the physical model with the requirements of a biomimetic gastric tract simulator. Biomimicry of the biomechanical and physical properties of the membrane and muscle layers of the gastric tract wall provide a novel and demonstrable approach to simulating the biomechanics of the human gastric tract. Flexible artificial muscles, attached to an elastic artificial membrane and actuated and controlled through a series of motors and feedback mechanisms, demonstrate deformation of the artificial gastric tract wall in a biomimetic and bio-relevant manner.

Several core components were identified as required for the development of an effective biomimetic gastric tract simulator. These core components are: (1) an artificial membrane or

reactor shell to contain the food material (Chapter 3), (2) artificial muscles to create deformation of the surface membrane or shell (Chapter 4), (3) a system of actuation for the artificial muscles to produce the contractive and expansive deformation patterns (Chapter 5), and (4) appropriate feedback and control mechanisms for initiating, maintaining, and altering the desired deformation patterns (Chapter 6). Successful integration of these components into a single, combined working system is essential in creating an effective biomimetic gastric tract simulator, and these requirements were systematically presented in Chapter 1.

The membrane

An artificial membrane layer made from soft silicone rubber reinforced with elasticated nylon fabric (Chapter 3) provides the shell of the stomach reactor. The elastic silicone composite membrane material proves to be strong, thin, flexible and watertight. It is readily fabricated to a stomach shape by stretching the elastic nylon fabric over a rigid form made to anatomical dimensions of the human stomach and sealing it with layers of liquid silicone. Tubular forms of the composite material are used to replicate the shells of the oesophagus and duodenum.

A soft, porous, silicone sponge layer is pre-stressed by evenly spreading its uncured form directly onto the surface of a composite silicone-nylon fabric membrane that has been stretched out. When the stretched composite membrane is relaxed, a layer of surface folds appears on the inner surface of the artificial stomach, mimicking the mucosal folds and rugae of the biological gastric wall. Constricting a section of the tubular stomach membrane shell to complete closure of its lumen causes the artificial mucosal layer to display similar

deformation patterns to the surface folding of the biological gastric wall during peristaltic wave contractions.

The artificial membrane shell and mucosal layer that was constructed can expand up to 5 times its initial volume. It is highly flexible and durable with a thickness of 3-4 mm. Some *in vitro* models use a purely silicone shell of greater thickness, typically 5-7 mm, to prevent the membrane from tearing when being manipulated or deformed, while others enclose a thin elastic membrane within a rigid structure. The increased thickness or rigid surrounds of other models' membranes reduces their flexibility and expansive capabilities, therefore limiting the ability of these models to effectively mimic the adaptive relaxation of the fundus region for the accommodation of increasing volumes of food.

The layered structure of the biomimetic *in vitro* model presented here uses membrane layers formed under various levels of strain, mimicking the different cellular growth rates and pre-stressed properties of biological stomach layers, and causing the innermost mucosal layer to buckle and fold increasingly as the membrane shell is constricted. These fold structures, or rugae, formed by the inner mucosal layer of the biological stomach, are overlooked by most dynamic *in vitro* models. Those that have incorporated some form of folds on the gastric tract have moulded them directly onto the inner surface of the stomach shell; they are therefore set-in-place and are not randomly formed from the different deformation characteristics of the multiple layers that make up the tract wall.

The ability of the artificial membrane to fold in a bio-relevant manner allows it to mimic closure of the pyloric sphincter, representing the closure of mucosal folds that occur in the biological human stomach (Fig. 19, Section 3.2). No other *in vitro* model mimics the closure of the pyloric sphincter in this way. The closure of the pyloric sphincter at the terminus of

an antral peristaltic wave plays an important role as to how gastric sieving of digestive contents occurs during gastric emptying. Replicating pyloric sphincter closure in a bio-relevant manner provides understanding of the biomechanical role in the emptying of stomach contents during digestion.

The muscles

The biomimetic gastric tract simulator makes use of highly flexible artificial muscles, or unit constrictors, to create contraction patterns (Chapter 4). The flexibility of the unit constrictors, made from coiled nylon line, means they can bend in and out-of-plane, allowing them to follow along with the moving membrane shell that they are attached to as they contract and expand, and adjust their shape to form around surrounding objects or boundaries that may constrain their movement. This flexibility mimics the movement characteristics of the muscle layers of the biological gastric wall. Not only are these artificial muscles capable of contraction, by the pulling of a flexible tendon through the coil, but they are also capable of extending beyond their initial length as the tendons are given slack. This allows them to extend or expand along with the membrane shell when the volume of contents in the stomach increases. Other *in vitro* models that use a flexible membrane for the stomach attempt to deform the gastric wall by using artificial muscles that are typically fixed in place, detached from the membrane shell or wall, and provide only limited range of contractive action. These aspects limit the ability of these models to closely mimic the dynamic gastric contractions and deformations of the biological tract.

The compact size of the nylon coil unit constrictors allows them to be placed side-by-side, providing the ability for multiple constrictors to be placed over a specific region of the gastric tract wall. This mimics the biological gastric wall where muscle layers are made up of

bundles of muscle cells that are interconnected and are aligned along the same orientation. The unit constrictors can be constructed with a width of 1-2 millimetres, meaning that they can be attached to small stomach shells. This facilitates in the construction of artificial stomachs comparable in size to those of children or infants.

The use of Bowden cables within the biomimetic gastric tract simulator, to transmit the pulling and releasing of the unit constrictor tendons, allows the artificial muscles to be decoupled from the actuation system. This physically frees the artificial gastric shell from requiring any surrounding rigid mechanisms or structures, giving the stomach greater ability to deform and move around as it does in the biological system. The surrounding structures of the gastric tract can now involve constraining boundaries that more closely mimic the shape, form, and flexibility of the biological system such as the surrounding organs of the liver, transverse colon, pancreas, spleen, and kidney. Decoupling of the actuation system also reduces the overall weight and size of the stomach reactors' containment vessel, allowing it to be able to be moved or rotated into various orientations more easily. The ability to alter the orientation of an *in vitro* gastric tract reactor facilitates investigation into the effects of body posture or movement on digestion and food structure breakdown.

Actuation of the muscles

Few *in vitro* gastric tract models consider biomimetic transport of food boluses from the oesophagus into the stomach, and the layering of food as it enters the stomach cavity. The pumping action of the linear peristaltic pump, described in Section 5.1, demonstrates mimicry of the swallowing action of the oesophagus and the formation and transportation of food material as a bolus into the stomach. The linear peristaltic pump was integrated into

the biomimetic *in vitro* gastric model to provide a controllable and efficient means for transporting prepared food materials and slurries into the stomach reactor in a bio-relevant manner.

Actuation of the peristaltic swallowing action of the artificial oesophagus was achieved using a novel system of rotating discs used to generate the peristaltic contraction of multiple unit constrictors (Section 5.1). The discs are connected by offset pins that create tension on each of the constrictor tendons in turn as the discs are rotated by a motor. This method simplifies the control system required for actuating the contraction of multiple constrictors over a length of artificial flexible oesophageal tubing. The rotation of the discs and tension pins causes the contractions to occur at the required timing for creating a peristaltic wave formation. The contractive peristaltic wave passes down the length of the artificial oesophagus, propelling a single bolus of food to the stomach during one complete rotation of the discs. Complete closure of the lower oesophageal sphincter occurs at the end of each complete rotation and keeps the food contained within the stomach cavity. The linear peristaltic pump mechanism also displays potential use in the pumping of slurry materials.

The actuation control system used for the unit constrictors placed over the stomach membrane requires independent control over each individual constrictor action. This is because the stomach is more dynamic and varied in its deformation patterns than the oesophagus, and because the volume of the stomach changes over time due to the intake and emptying of digesta. As a substantial number of individual unit constrictors are attached over the stomach membrane surface of the biomimetic gastric tract simulator, each would require a winding motor capable of providing enough torque to actuate the unit constrictors and produce the contractive and expansive deformations that occur during

digestion. The more torque required, the larger the motor tends to be, and this typically translates to more cost for construction of an *in vitro* system.

The individual constrictor control system described in Section 5.2 significantly reduces the number of large electric motors required for the winding of independent unit constrictor tendons by incorporating the use of a capstan mechanism. The motors driving the capstan spindles provide the required torque for contracting all the unit constrictors attached to the spindles, while smaller individual winding motors are used to control the rate and amount of unit constrictor tendon uptake. This method for implementation of the capstan mechanism reduces the models' overall cost while still providing independent control over the actuation of multiple unit constrictors. The capstan mechanism also smooths out variations in the rotational speed of the winding motors because it transfers the torque required for winding and contracting the artificial muscles over to the more powerful capstan motors and spindle. This method of using the capstan mechanism for creating mechanical advantage shows potential to contribute to the design of other tendon or cable driven applications.

Control and feedback

Potential for mapping the active deformation of the *in vitro* model onto a three-dimensional (3D) virtual reconstruction of the stomach shell was investigated (Section 6.3). Physics-based simulation software (SOFA) was used for creating the 3D virtual environment representing the *in vitro* model stomach shell and its containment boundaries. Near real-time deformation of the virtual stomach mesh model, constructed from the dimensions of the physical stomach shell and its surrounding boundary constraints, was simulated using the finite element method. Simulated circumferential contraction patterns of the mesh

model were carried out at the same locations on the virtual stomach as the positions of the unit constrictors on the physical model. Programming of the individual unit constrictor contraction timings, amplitudes, and contraction velocities is carried out using a graphical user interface. The interface also provides real-time plotting of the contraction ratios as they are being applied to each of the unit constrictors throughout the actuation of gastric motility patterns. Virtual simulation of the physical *in vitro* model in this manner presents a user-friendly visual means for programming and testing of the deformation patterns that are intended to be used on the dynamic *in vitro* model.

It was also found that feedback measurements, obtained from the tendon displacement sensors, membrane stretch sensors, and tendon tension sensors, could be used to map the actual deformation taking place on the physical model of the stomach. The intended deformation patterns, pre-programmed into the initial virtual simulation, can then be compared against the actual deformation measurements obtained from the stomach shell during the operation of the physical model. This comparison can provide useful information about how the deformation of the simulated stomach shell reacts to different food materials when using a pre-programmed deformation pattern.

The ability to independently control large numbers of individual unit constrictors over the entire stomach membrane provides significant advantage in recreating a variety of deformation patterns, and in re-forming or morphing the overall shape of the stomach shell. Contractions can be generated over any region of the artificial stomach wall where unit constrictors are located, with varying amplitude, force, and velocity. This means that normal stomach peristaltic contractions could be simulated; slowly travelling from the corpus region down to the pylorus, as well as the simulation of patterns considered to be

dysfunctional or abnormal stomach activity, where peristaltic wave activity is disrupted or erratic. The general overall shape of the stomach can be altered by controlling the constrictions of individual unit constrictors. Thus, the artificial stomach shell could be morphed from the typical J-shaped stomach, the form recognised by most dynamic *in vitro* models, to other radiologically defined stomach shapes such as steer-horn, cascade, or hourglass [1].

With the artificial muscles being decoupled from the muscle actuation system, the entire gastric tract model can be placed inside a compact containment unit and mounted onto a rotational gimbal rig. The artificial gastric tract is surrounded in its containment unit by transparent, soft polymer surfaces. The moulded polymer surfaces serve as the bounding organs that surround the gastric tract in the biological system, and act as both a physical support for the gastric tract and as a constraint to the expansion or movement of the stomach.

Limitations of the study

Many of the novel forms of mechanisms, devices, sensors, and materials presented in this study have not undergone extensive testing or design analysis. The design or fabrication of some of these artefacts may therefore be considered sub-optimal with respect to various factors including durability, component lifetime, repeatability, accuracy, precision, power consumption, susceptibility to interference, and environmental impact of the materials used. These factors can influence the performance of the *in vitro* simulator. Component configurations and software coding of the microcontrollers, user interface, virtual simulations, and calculation algorithms used in the proof-of-concept demonstrations of the simulator may also be considered sub-optimal.

Simulation of biomechanical digestive activity demonstrated by the *in vitro* biomimetic gastric tract simulator has had limited comparison with results from *in vivo* studies. Part of the reason for this is that much of the data from *in vivo* studies relates to the chemical composition, breakdown effects, and gastric emptying rates of ingested food materials, or the electrophysiological aspects of deformation patterns. The simulation of food digestion within the artificial gastric tract model, with the addition of gastric acids to assist in food breakdown, was out of scope for this study. *In vivo* data is limited regarding studies on the biomechanical activity of the gastric tract, particularly 3D imaging and quantification of the temporal deformation patterns involved with the stomach wall.

Despite these limitations, the dynamic *in vitro* gastric tract simulator presented in this thesis provides a novel, low-cost, innovative and advanced approach for studying the effects of gastric tract biomechanics on the digestion of food and the breakdown of food structures.

References

[1] Gregersen, H., & Christensen, J. (2016). *Clinical mechanics in the gut: an introduction*: Bentham Science Publishers.

[2] Lentle, R. G., & Janssen, P. W. (2011). *The physical processes of digestion*: Springer Science & Business Media.

[3] Ehrlein, H., & Schemann, M. Gastrointestinal motility. *Munich, Technische Universität München*. (2005)

[4] Miftahof, R. N. (2017). *Biomechanics of the Human Stomach*: Springer.

[5] Coffey, J. C., & O'Leary, D. P. The mesentery: structure, function, and role in disease. *The lancet Gastroenterology & hepatology, 1*(3), 238-247. (2016)

[6] Mahadevan, V. Anatomy of the stomach. *Surgery (Oxford), 32*(11), 571-574. (2014)

[7] Leung, P. S. (2014). *The Gastrointestinal System: Gastrointestinal, Nutritional and Hepatobiliary Physiology*: Springer.

[8] Dupont, D., Alric, M., Blanquet-Diot, S., et al. Can dynamic in vitro digestion systems mimic the physiological reality? *Critical reviews in food science and nutrition*, 1-17. (2018)

[9] Guerra, A., Etienne-Mesmin, L., Livrelli, V., Denis, S., Blanquet-Diot, S., & Alric, M. Relevance and challenges in modeling human gastric and small intestinal digestion. *Trends Biotechnol, 30*(11), 591-600. (2012)

[10] Kong, F., & Singh, R. P. Disintegration of solid foods in human stomach. *J Food Sci, 73*(5), R67-80. (2008)

[11] Stevenson, A. (2010). *Oxford dictionary of English* (3rd ed.): Oxford University Press, USA.

[12] Cianchetti, M., Laschi, C., Menciassi, A., & Dario, P. Biomedical applications of soft robotics. *Nature Reviews Materials*, 1. (2018)

[13] Laschi, C., & Cianchetti, M. Soft robotics: new perspectives for robot bodyware and control. *Frontiers in bioengineering and biotechnology, 2*, 3. (2014)

[14] Kim, S., Laschi, C., & Trimmer, B. Soft robotics: a bioinspired evolution in robotics. *Trends in biotechnology, 31*(5), 287-294. (2013)

[15] Li, Y., Fortner, L., & Kong, F. Development of a Gastric Simulation Model (GSM) incorporating gastric geometry and peristalsis for food digestion study. *Food Research International, 125*, 108598. (2019)

[16] Donis-Rabanales, L. F., Escalona-Ortiz, M., Ruiz-Huerta, L., de la Fuente, E. B., Caballero-Ruiz, A., & Ascanio-Gasca, G. Distal gastric simulator based on a soft actuator. *Visión electrónica, 14*(1). (2020)

[17] Donis-Rabanales, F., López-Ruiz, T., Ruiz-Huerta, L., Ascanio, G., Brito-de la Fuente, E., & Caballero-Ruiz, A. Development of an In Vitro Distal Gastric Simulator to mimic the mechanical action of the human stomach. *Food Research International*, 111902. (2022)

[18] Dang, Y., Liu, Y., Hashem, R., et al. SoGut: A Soft Robotic Gastric Simulator. *Soft robotics*. (2020)

[19] Dang, Y., Stommel, M., Cheng, L. K., & Xu, W. (2018). *A Soft Ring-shaped Actuator: FE Simulation and Motion Tracking.* Paper presented at the 2018 25th International Conference on Mechatronics and Machine Vision in Practice (M2VIP).

[20] Dang, Y., Cheng, L. K., Stommel, M., & Xu, W. (2016). *Technical requirements and conceptualization of a soft pneumatic actuator inspired by human gastric motility.* Paper presented at the 2016 23rd International Conference on Mechatronics and Machine Vision in Practice (M2VIP).

[21] Hashem, R., Xu, W., Stommel, M., & Cheng, L. K. (2017). *FEA Evaluation of Ring-Shaped Soft-Actuators for a Stomach Robot.* Paper presented at the International Conference on Robot Intelligence Technology and Applications.

[22] Hashem, R., Xu, W., Stommel, M., & Cheng, L. (2016). *Conceptualisation and specification of a biologically-inspired, soft-bodied gastric robot.* Paper presented at the 2016 23rd International Conference on Mechatronics and Machine Vision in Practice (M2VIP).

[23] Li, Z.-t., Zhu, L., Zhang, W.-l., Zhan, X.-b., & Gao, M.-j. New dynamic digestion model reactor that mimics gastrointestinal function. *Biochemical Engineering Journal, 154*, 107431. (2020)

[24] Peng, Z., Wu, P., Wang, J., et al. Achieving realistic gastric emptying curve in an advanced dynamic in vitro human digestion system: experiences with cheese-a difficult to empty material. *Food & function*. (2021)

[25] Wang, J., Wu, P., Liu, M., et al. An advanced near real dynamic in vitro human stomach system to study gastric digestion and emptying of beef stew and cooked rice. *Food & function, 10*(5), 2914-2925. (2019)
[26] Keppler, S., O'Meara, S., Bakalis, S., Fryer, P., & Bornhorst, G. Characterization of individual particle movement during in vitro gastric digestion in the Human Gastric Simulator (HGS). *Journal of Food Engineering, 264*, 109674. (2020)
[27] Hribar, M., Trontelj, J., Berglez, S., et al. Design of an Innovative Advanced Gastric Simulator. *Dissolution Technologies, 26*(2), 20-29. (2019)
[28] Liu, W., Fu, D., Zhang, X., Chai, J., Tian, S., & Han, J. Development and validation of a new artificial gastric digestive system. *Food Research International, 122*, 183-190. (2019)
[29] Mitsuhashi, N., Fujieda, K., Tamura, T., Kawamoto, S., Takagi, T., & Okubo, K. BodyParts3D: 3D structure database for anatomical concepts. *Nucleic acids research, 37*(suppl_1), D782-D785. (2008)
[30] Coffey, J. C., Dockery, P., Moran, B. J., & Heald, B. (2017). *Mesenteric and peritoneal anatomy*: CRC Press, Taylor & Francis Group Boca Raton, FL.
[31] Cheng, L. K., O'Grady, G., Du, P., Egbuji, J. U., Windsor, J. A., & Pullan, A. J. Gastrointestinal system. *Wiley Interdisciplinary Reviews: Systems Biology and Medicine, 2*(1), 65-79. (2010)
[32] Huizinga, J. D., & Lammers, W. J. Gut peristalsis is governed by a multitude of cooperating mechanisms. *American Journal of Physiology-Gastrointestinal and Liver Physiology, 296*(1), G1-G8. (2009)
[33] Bornhorst, G. M. Gastric Mixing During Food Digestion: Mechanisms and Applications. *Annual review of food science and technology, 8*, 523-542. (2017)
[34] Lentle, R. G., & de Loubens, C. A review of mixing and propulsion of chyme in the small intestine: fresh insights from new methods. *Journal of Comparative Physiology B, 185*(4), 369-387. (2015)
[35] Lim, Y. F., & Massey University. (2015). *Factors influencing mixing and mass transfer in the small intestine : a thesis presented in partial fulfilment of the requirements for the degree of Doctor of Philosophy in Digestive Biomechanics (Physical Process of Digestion) at Massey University, Turitea, New Zealand*.
[36] Carniel, E. L., Rubini, A., Frigo, A., & Natali, A. N. Analysis of the biomechanical behaviour of gastrointestinal regions adopting an experimental and computational approach. *Computer methods and programs in biomedicine, 113*(1), 338-345. (2014)
[37] Egorov, V. I., Schastlivtsev, I. V., Prut, E. V., Baranov, A. O., & Turusov, R. A. Mechanical properties of the human gastrointestinal tract. *Journal of biomechanics, 35*(10), 1417-1425. (2002)
[38] Huh, C., Bhutani, M., Farfan, E., & Bolch, W. Individual variations in mucosa and total wall thickness in the stomach and rectum assessed via endoscopic ultrasound. *Physiological measurement, 24*(4), N15. (2003)
[39] Gregersen, H., Kassab, G., & Fung, Y. The zero-stress state of the gastrointestinal tract. *Digestive diseases and sciences, 45*(12), 2271-2281. (2000)
[40] Cleary, P., Sinnott, M., Hari, B., Bakalis, S., & Harrison, S. (2015). Modelling food digestion *Modeling Food Processing Operations* (pp. 255-305): Elsevier.
[41] Singh, H., Ye, A., & Ferrua, M. J. Aspects of food structures in the digestive tract. *Current Opinion in Food Science, 3*, 85-93. (2015)
[42] Drechsler, K. C., & Ferrua, M. J. Modelling the breakdown mechanics of solid foods during gastric digestion. *Food Research International, 88*, 181-190. (2016)
[43] Birmingham, A. The arrangement of the muscular fibres of the stomach. *Transactions of the Royal Academy of Medicine in Ireland, 16*(1), 432. (1898)
[44] Akhmadeev, N., & Miftahof, R. Stress-strain Distribution In The Human Stomach. *Modelling in Medicine and Biology*, 3. (2010)
[45] Gregersen, H., & Kassab, G. Biomechanics of the gastrointestinal tract. *Neurogastroenterology & Motility, 8*(4), 277-297. (1996)
[46] Savin, T., Kurpios, N. A., Shyer, A. E., et al. On the growth and form of the gut. *Nature, 476*(7358), 57. (2011)

[47] Nelson, C. M. On buckling morphogenesis. *Journal of Biomechanical Engineering, 138*(2), 021005. (2016)
[48] Simons, B. D. Getting your gut into shape. *science, 342*(6155), 203-204. (2013)
[49] Shyer, A. E., Tallinen, T., Nerurkar, N. L., et al. Villification: how the gut gets its villi. *science, 342*(6155), 212-218. (2013)
[50] Zhong, C., & Langrish, T. A comparison of different physical stomach models and an analysis of shear stresses and strains in these system. *Food Research International*, 109296. (2020)
[51] Li, C., Yu, W., Wu, P., & Chen, X. D. Current in vitro digestion systems for understanding food digestion in human upper gastrointestinal tract. *Trends in Food Science & Technology*. (2019)
[52] Verhoeckx, K., Cotter, P., López-Expósito, I., et al. (2015). *The Impact of Food Bioactives on Health: in vitro and ex vivo models*: Springer.
[53] Wu, P., & Chen, X. D. On designing biomimic in vitro human and animal digestion track models: ideas, current and future devices. *Current Opinion in Food Science, 35*, 10-19. (2020)
[54] Sensoy, I. A review on the food digestion in the digestive tract and the used in vitro models. *Current Research in Food Science*. (2021)
[55] Mackie, A., Mulet-Cabero, A.-I., & Torcello-Gómez, A. Simulating human digestion: developing our knowledge to create healthier and more sustainable foods. *Food & function*. (2020)
[56] Dixit, Y., Kanojiya, K., Bhingardeve, N., Ahire, J. J., & Saroj, D. In Vitro Human Gastrointestinal Tract Simulation Systems: A Panoramic Review. *Probiotics and Antimicrobial Proteins*, 1-18. (2023)
[57] Lee, S.-J., Lee, S. Y., Chung, M.-S., & Hur, S. J. Development of novel in vitro human digestion systems for screening the bioavailability and digestibility of foods. *Journal of Functional Foods, 22*, 113-121. (2016)
[58] Oomen, A., Rompelberg, C., Bruil, M., Dobbe, C., Pereboom, D., & Sips, A. Development of an in vitro digestion model for estimating the bioaccessibility of soil contaminants. *Archives of environmental contamination and toxicology, 44*(3), 0281-0287. (2003)
[59] Minekus, M., Alminger, M., Alvito, P., et al. A standardised static in vitro digestion method suitable for food–an international consensus. *Food & function, 5*(6), 1113-1124. (2014)
[60] Brodkorb, A., Egger, L., Alminger, M., et al. INFOGEST static in vitro simulation of gastrointestinal food digestion. *Nature protocols*, 1. (2019)
[61] Egger, L., Ménard, O., Delgado-Andrade, C., et al. The harmonized INFOGEST in vitro digestion method: From knowledge to action. *Food Research International, 88*, 217-225. (2016)
[62] Zhao, J., Liao, D., Chen, P., Kunwald, P., & Gregersen, H. Stomach stress and strain depend on location, direction and the layered structure. *Journal of biomechanics, 41*(16), 3441-3447. (2008)
[63] Minekus, M., Marteau, P., Havenaar, R., & Veld, J. H. H. i. t. A multicompartmental dynamic computer-controlled model simulating the stomach and small intestine. *Alternatives to laboratory animals, 23*(2), 197-209. (1995)
[64] Molly, K., Woestyne, M. V., & Verstraete, W. Development of a 5-step multi-chamber reactor as a simulation of the human intestinal microbial ecosystem. *Applied microbiology and biotechnology, 39*(2), 254-258. (1993)
[65] Vardakou, M., Mercuri, A., Barker, S. A., Craig, D. Q., Faulks, R. M., & Wickham, M. S. Achieving antral grinding forces in biorelevant in vitro models: comparing the USP dissolution apparatus II and the dynamic gastric model with human in vivo data. *AAPS PharmSciTech, 12*(2), 620-626. (2011)
[66] Wickham, M. J. S., Faulks, R. M., Mann, J., & Mandalari, G. The Design, Operation, and Application of a Dynamic Gastric Model. *Dissolution Technologies, 19*(3), 15-22. (2012)
[67] Kong, F., & Singh, R. P. A human gastric simulator (HGS) to study food digestion in human stomach. *J Food Sci, 75*(9), E627-635. (2010)
[68] Phinney, D. M., & Singh, R. P. (2013). *Design, construction, and evaluation of a reactor designed to mimic human gastric digestion : thesis submitted in partial satisfaction of the requirements for the degree of Master of Science in Food Science & Technology in the Office of Graduate Studies of the University of California, Davis*: ProQuest LLC.

[69] Condino, S., Harada, K., Pak, N. N., Piccigallo, M., Menciassi, A., & Dario, P. Stomach simulator for analysis and validation of surgical endoluminal robots. *Applied Bionics and Biomechanics, 8*(2), 267-277. (2011)
[70] Kozu, H., Kobayashi, I., Nakajima, M., et al. Mixing characterization of liquid contents in human gastric digestion simulator equipped with gastric secretion and emptying. *Biochemical Engineering Journal, 122*, 85-90. (2017)
[71] Kozu, H., Nakata, Y., Nakajima, M., et al. Development of a Human Gastric Digestion Simulator Equipped with Peristalsis Function for the Direct Observation and Analysis of the Food Digestion Process. *Food Science and Technology Research, 20*(2), 225-233. (2014)
[72] Ménard, O., Picque, D., & Dupont, D. (2015). The DIDGI® System *The Impact of Food Bioactives on Health* (pp. 73-81): Springer, Cham.
[73] Barroso, E., Cueva, C., Peláez, C., Martínez-Cuesta, M. C., & Requena, T. Development of human colonic microbiota in the computer-controlled dynamic SIMulator of the GastroIntestinal tract SIMGI. *LWT - Food Science and Technology, 61*(2), 283-289. (2015)
[74] Cueva, C., Jiménez-Girón, A., Muñoz-González, I., et al. Application of a new Dynamic Gastrointestinal Simulator (SIMGI) to study the impact of red wine in colonic metabolism. *Food Research International, 72*, 149-159. (2015)
[75] Guerra, A., Denis, S., le Goff, O., et al. Development and validation of a new dynamic computer-controlled model of the human stomach and small intestine. *Biotechnology and bioengineering, 113*(6), 1325-1335. (2016)
[76] Chen, L., Xu, Y., Fan, T., et al. Gastric emptying and morphology of a 'near real' in vitro human stomach model (RD-IV-HSM). *Journal of Food Engineering, 183*, 1-8. (2016)
[77] Bellmann, S., Lelieveld, J., Gorissen, T., Minekus, M., & Havenaar, R. Development of an advanced in vitro model of the stomach and its evaluation versus human gastric physiology. *Food Research International, 88*, 191-198. (2016)
[78] Do, D. H. T., Kong, F., Penet, C., Winetzky, D., & Gregory, K. Using a dynamic stomach model to study efficacy of supplemental enzymes during simulated digestion. *LWT-Food Science and Technology, 65*, 580-588. (2016)
[79] Barros, L., Retamal, C., Torres, H., Zúñiga, R. N., & Troncoso, E. Development of an in vitro mechanical gastric system (IMGS) with realistic peristalsis to assess lipid digestibility. *Food Research International, 90*, 216-225. (2016)
[80] Dang, Y. (2020). *Soft Ring Actuation Based Gastric Simulator: Design, Modelling and Experiments.* ResearchSpace@ Auckland.
[81] Wilson, M. J., & Irving, L. Pressures in the Stomach. *Canadian Medical Association journal, 25*(6), 685. (1931)
[82] Thompson, D. A. W., & Bonner, J. T. (1997). *On Growth and Form* (Vol. Abridged edition /. edited by John Tyler Bonner). Cambridge [England]: Cambridge University Press.
[83] Li, B., Cao, Y.-P., Feng, X.-Q., & Gao, H. Mechanics of morphological instabilities and surface wrinkling in soft materials: a review. *Soft Matter, 8*(21), 5728-5745. (2012)
[84] Battista, N. A., Strickland, W. C., & Miller, L. A. IB2d: a Python and MATLAB implementation of the immersed boundary method. *Bioinspiration & biomimetics, 12*(3), 036003. (2017)
[85] Dirven, S., Xu, W., & Cheng, L. K. Sinusoidal peristaltic waves in soft actuator for mimicry of esophageal swallowing. *IEEE/ASME Transactions on Mechatronics, 20*(3), 1331-1337. (2015)
[86] Bhattacharya, D., JV Ali, S., Cheng, L. K., & Xu, W. RoSE: A Robotic Soft Esophagus for Endoprosthetic Stent Testing. *Soft robotics*. (2020)
[87] Miki, H., Okuyama, T., Kodaira, S., et al. Artificial-esophagus with peristaltic motion using shape memory alloy. *International journal of applied electromagnetics and mechanics, 33*(1, 2), 705-711. (2010)
[88] Dirven, S., Allen, J., Xu, W., & Cheng, L. K. Soft-robotic esophageal swallowing as a clinically-inspired bolus rheometry technique. *Measurement Science and Technology, 28*(3), 035701. (2017)

[89] Esser, F., Steger, T., Bach, D., Masselter, T., & Speck, T. (2017). *Development of novel foam-based soft robotic ring actuators for a biomimetic peristaltic pumping system.* Paper presented at the Conference on Biomimetic and Biohybrid Systems.
[90] Esser, F., Krüger, F., Masselter, T., & Speck, T. (2019). *Characterization of Biomimetic Peristaltic Pumping System Based on Flexible Silicone Soft Robotic Actuators as an Alternative for Technical Pumps.* Paper presented at the Conference on Biomimetic and Biohybrid Systems.
[91] Wright, N. D., Kong, F., Williams, B. S., & Fortner, L. A human duodenum model (HDM) to study transport and digestion of intestinal contents. *Journal of Food Engineering, 171*, 129-136. (2016)
[92] Yamada, Y., Ashigaki, K., Yoshihama, S., Negishi, K., Kato, K., & Nakamura, T. Triangular cross-section peristaltic conveyor for transporting powders at high speed in printers. *Advanced Robotics, 32*(12), 646-658. (2018)
[93] Iwasaki, A., Matsumoto, K., Ban, R., Yoshihama, S., Nakamura, T., & Habu, H. The Continuous Mixing Process of Composite Solid Propellant Slurry by an Artificial Muscle Actuator. *TRANSACTIONS OF THE JAPAN SOCIETY FOR AERONAUTICAL AND SPACE SCIENCES, AEROSPACE TECHNOLOGY JAPAN, 14*(ists30), Pa_107-Pa_110. (2016)
[94] Suzuki, K., & Nakamura, T. (2010). *Development of a peristaltic pump based on bowel peristalsis using for artificial rubber muscle.* Paper presented at the 2010 IEEE/RSJ International Conference on Intelligent Robots and Systems.
[95] Slawinski, P. R., Oleynikov, D., & Terry, B. S. Intestinal biomechanics simulator for robotic capsule endoscope validation. *Journal of medical engineering & technology, 39*(1), 54-59. (2015)
[96] Rotman, O. M., Zaretsky, U., Birnboim, Y., Pascal, A., & Einav, S. Mechanical Simulator of the Small Intestine for In-Vitro Practice with Endoscopic Devices. *Journal ISSN: TBA, 3*. (2016)
[97] Stamatopoulos, K. (2017). *Development of a biorelevant dynamic model of human proximal colon: a tool for designing colon–specific drug delivery systems.* University of Birmingham.
[98] Cei, D., Costa, J., Gori, G., et al. A bioreactor with an electro-responsive elastomeric membrane for mimicking intestinal peristalsis. *Bioinspiration & biomimetics, 12*(1), 016001. (2016)
[99] Anderson, I. A., Gisby, T. A., McKay, T. G., O'Brien, B. M., & Calius, E. P. Multi-functional dielectric elastomer artificial muscles for soft and smart machines. *Journal of Applied Physics, 112*(4), 041101. (2012)
[100] Mirfakhrai, T., Madden, J. D., & Baughman, R. H. Polymer artificial muscles. *Materials today, 10*(4), 30-38. (2007)
[101] Acome, E., Mitchell, S. K., Morrissey, T. G., et al. Hydraulically amplified self-healing electrostatic actuators with muscle-like performance. *science, 359*(6371), 61-65. (2018)
[102] Carpi, F., Salaris, C., & Rossi, D. D. Folded dielectric elastomer actuators. *Smart Materials and Structures, 16*(2), S300-S305. (2007)
[103] Zolfagharian, A., Kouzani, A. Z., Khoo, S. Y., Nasri-Nasrabadi, B., & Kaynak, A. Development and analysis of a 3D printed hydrogel soft actuator. *Sensors and Actuators A: Physical, 265*, 94-101. (2017)
[104] Gelebart, A. H., Jan Mulder, D., Varga, M., et al. Making waves in a photoactive polymer film. *Nature, 546*(7660), 632-636. (2017)
[105] Palleau, E., Morales, D., Dickey, M. D., & Velev, O. D. Reversible patterning and actuation of hydrogels by electrically assisted ionoprinting. *Nat Commun, 4*, 2257. (2013)
[106] Wang, E., Desai, M. S., & Lee, S. W. Light-controlled graphene-elastin composite hydrogel actuators. *Nano Lett, 13*(6), 2826-2830. (2013)
[107] Shin, S. R., Migliori, B., Miccoli, B., et al. Electrically Driven Microengineered Bioinspired Soft Robots. *Adv Mater, 30*(10). (2018)
[108] Miriyev, A., Stack, K., & Lipson, H. Soft material for soft actuators. *Nat Commun, 8*(1), 596. (2017)
[109] Martinez, R. V., Fish, C. R., Chen, X., & Whitesides, G. M. Elastomeric Origami: Programmable Paper-Elastomer Composites as Pneumatic Actuators. *Advanced Functional Materials, 22*(7), 1376-1384. (2012)
[110] Mosadegh, B., Polygerinos, P., Keplinger, C., et al. Pneumatic networks for soft robotics that actuate rapidly. *Advanced Functional Materials, 24*(15), 2163-2170. (2014)

[111] Li, S., Vogt, D. M., Rus, D., & Wood, R. J. Fluid-driven origami-inspired artificial muscles. *Proc Natl Acad Sci U S A, 114*(50), 13132-13137. (2017)
[112] Kim, S., Hawkes, E., Choy, K., Joldaz, M., Foleyz, J., & Wood, R. (2009). *Micro artificial muscle fiber using NiTi spring for soft robotics.* Paper presented at the Intelligent Robots and Systems, 2009. IROS 2009. IEEE/RSJ International Conference on.
[113] Yip, M. C., & Niemeyer, G. On the Control and Properties of Supercoiled Polymer Artificial Muscles. *IEEE Transactions on Robotics, 33*(3), 689-699. (2017)
[114] Mirvakili, S. M., & Hunter, I. W. Multidirectional artificial muscles from nylon. *Advanced Materials, 29*(4). (2017)
[115] Kianzad, S. (2015). *A treatise on highly twisted artificial muscle: thermally driven shape memory alloy yarn and coiled nylon actuators.* University of British Columbia.
[116] Mirvakili, S. M., & Hunter, I. W. (2016). *Bending artificial muscle from nylon filaments.* Paper presented at the Electroactive Polymer Actuators and Devices (EAPAD) 2016.
[117] Bar-Cohen, Y., Mirvakili, S. M., Rafie Ravandi, A., et al. Simple and strong: twisted silver painted nylon artificial muscle actuated by Joule heating. *9056*, 90560I. (2014)
[118] Haines, C. S., Li, N., Spinks, G. M., Aliev, A. E., Di, J., & Baughman, R. H. New twist on artificial muscles. *Proc Natl Acad Sci U S A, 113*(42), 11709-11716. (2016)
[119] Fan, J., & Li, G. High performance and tunable artificial muscle based on two-way shape memory polymer. *RSC Advances, 7*(2), 1127-1136. (2017)
[120] Atikah, N. A., Weng, L. Y., Anuar, A., Fat, C. C., Abidin, I. Z., & Sahari, K. S. M. Development of nylon-based artificial muscles for the usage in robotic prosthetic limb. *1883*, 020042. (2017)
[121] Haines, C. S., Lima, M. D., Li, N., et al. Artificial muscles from fishing line and sewing thread. *science, 343*(6173), 868-872. (2014)
[122] Okuzaki, H., Saido, T., Suzuki, H., Hara, Y., & Yan, H. A biomorphic origami actuator fabricated by folding a conducting paper. *Journal of Physics: Conference Series, 127*, 012001. (2008)
[123] Sareh, S., & Rossiter, J. Kirigami artificial muscles with complex biologically inspired morphologies. *Smart Materials and Structures, 22*(1), 014004. (2013)
[124] Onal, C. D., Wood, R. J., & Rus, D. An Origami-Inspired Approach to Worm Robots. *IEEE/ASME Transactions on Mechatronics, 18*(2), 430-438. (2013)
[125] Hou, J., Bonser, R. H., & Jeronimidis, G. Design of a biomimetic skin for an octopus-inspired robot–Part I: Characterising octopus skin. *Journal of Bionic Engineering, 8*(3), 288-296. (2011)
[126] Hou, J., Bonser, R. H., & Jeronimidis, G. Design of a biomimetic skin for an octopus-inspired robot–Part II: Development of the skin artefact. *Journal of Bionic Engineering, 8*(3), 297-304. (2011)
[127] Hou, J., Bonser, R. H., & Jeronimidis, G. Developing skin analogues for a robotic octopus. *Journal of Bionic Engineering, 9*(3), 385-390. (2012)
[128] Wang, Y., Gregory, C., & Minor, M. A. Improving Mechanical Properties of Molded Silicone Rubber for Soft Robotics Through Fabric Compositing. *Soft robotics*. (2018)
[129] Boxerbaum, A. S., Chiel, H. J., & Quinn, R. D. (2010). *A new theory and methods for creating peristaltic motion in a robotic platform.* Paper presented at the Robotics and Automation (ICRA), 2010 IEEE International Conference on.
[130] Winstone, B., Pipe, T., Melhuish, C., Callaway, M., Etoundi, A. C., & Dogramadzi, S. (2016). *Single motor actuated peristaltic wave generator for a soft bodied worm robot.* Paper presented at the Biomedical Robotics and Biomechatronics (BioRob), 2016 6th IEEE International Conference on.
[131] Seok, S., Onal, C. D., Wood, R., Rus, D., & Kim, S. (2010). *Peristaltic locomotion with antagonistic actuators in soft robotics.* Paper presented at the Robotics and Automation (ICRA), 2010 IEEE International Conference on.
[132] Horchler, A. D., Kandhari, A., Daltorio, K. A., et al. Peristaltic locomotion of a modular mesh-based worm robot: precision, compliance, and friction. *Soft robotics, 2*(4), 135-145. (2015)
[133] Park, J.-S., Jeong, S., & Lee, D. H. Recent advances in gastrointestinal stent development. *Clinical endoscopy, 48*(3), 209. (2015)
[134] Someya, T., Bao, Z., & Malliaras, G. G. The rise of plastic bioelectronics. *Nature, 540*(7633), 379-385. (2016)

[135] Kim, H.-J., Sim, K., Thukral, A., & Yu, C. Rubbery electronics and sensors from intrinsically stretchable elastomeric composites of semiconductors and conductors. *Science advances, 3*(9), e1701114. (2017)
[136] Yassi, R., Cheng, L., Rajagopal, V., Nash, M., Windsor, J., & Pullan, A. Modeling of the mechanical function of the human gastroesophageal junction using an anatomically realistic three-dimensional model. *Journal of biomechanics, 42*(11), 1604-1609. (2009)
[137] Brandstaeter, S., Fuchs, S. L., Aydin, R. C., & Cyron, C. J. Mechanics of the stomach: A review of an emerging field of biomechanics. *GAMM-Mitteilungen, 42*(3), e201900001. (2019)
[138] Carniel, E. L., Fontanella, C. G., Polese, L., Merigliano, S., & Natali, A. N. Computational tools for the analysis of mechanical functionality of gastrointestinal structures. *Technology and Health Care, 21*(3), 271-283. (2013)
[139] Liao, D., Lelic, D., Gao, F., Drewes, A. M., & Gregersen, H. Biomechanical functional and sensory modelling of the gastrointestinal tract. *Philosophical Transactions of the Royal Society A: Mathematical, Physical and Engineering Sciences, 366*(1879), 3281-3299. (2008)
[140] Bellini, C., Glass, P., Sitti, M., & Di Martino, E. S. Biaxial mechanical modeling of the small intestine. *journal of the mechanical behavior of biomedical materials, 4*(8), 1727-1740. (2011)
[141] Marra, F., Ferrua, M. J., & Singh, R. P. Experimental characterization of the fluid dynamics in an in-vitro system simulating the peristaltic movement of the stomach wall. *Procedia Food Science, 1*, 1473-1478. (2011)
[142] Ferrua, M. J., & Singh, R. P. Modeling the fluid dynamics in a human stomach to gain insight of food digestion. *J Food Sci, 75*(7), R151-162. (2010)
[143] Ferrua, M. J., Kong, F., & Singh, R. P. Computational modeling of gastric digestion and the role of food material properties. *Trends in Food Science & Technology, 22*(9), 480-491. (2011)
[144] Du, P., O'Grady, G., Gao, J., Sathar, S., & Cheng, L. K. Toward the virtual stomach: progress in multiscale modeling of gastric electrophysiology and motility. *Wiley Interdiscip Rev Syst Biol Med, 5*(4), 481-493. (2013)
[145] Carneiro, A. A., Baffa, O., & Oliveira, R. B. Study of stomach motility using the relaxation of magnetic tracers. *Physics in Medicine and Biology, 44*(7), 1691-1697. (1999)
[146] Angeli, T. R., Du, P., Paskaranandavadivel, N., et al. High-resolution electrical mapping of porcine gastric slow-wave propagation from the mucosal surface. *Neurogastroenterol Motil, 29*(5). (2017)
[147] Berry, R., Paskaranandavadivel, N., Du, P., et al. A novel retractable laparoscopic device for mapping gastrointestinal slow wave propagation patterns. *Surg Endosc, 31*(1), 477-486. (2017)
[148] Cheng, L. K., Pullan, A. J., & Farrugia, G. (Eds.). *New advances in gastrointestinal motility research*.
[149] Lammers, W., Stephen, B., Arafat, K., & Manefield, G. High resolution electrical mapping in the gastrointestinal system: initial results. *Neurogastroenterology & Motility, 8*(3), 207-216. (1996)
[150] O'Grady, G., Paskaranandavadivel, N., Du, P., Angeli, T., Erickson, J. C., & Cheng, L. K. Correct techniques for extracellular recordings of electrical activity in gastrointestinal muscle. *Nat Rev Gastroenterol Hepatol, 14*(6), 372. (2017)
[151] Paskaranandavadivel, N., Cheng, L. K., Du, P., Rogers, J. M., & O'Grady, G. High-resolution mapping of gastric slow-wave recovery profiles: biophysical model, methodology, and demonstration of applications. *Am J Physiol Gastrointest Liver Physiol, 313*(3), G265-G276. (2017)
[152] Paskaranandavadivel, N., G, O. G., & Cheng, L. K. Time-Delay Mapping of High-Resolution Gastric Slow-Wave Activity. *IEEE Trans Biomed Eng, 64*(1), 166-172. (2017)
[153] Wang, T. H., Du, P., Angeli, T. R., et al. Relationships between gastric slow wave frequency, velocity, and extracellular amplitude studied by a joint experimental-theoretical approach. *Neurogastroenterol Motil, 30*(1). (2018)
[154] Aydin, R., Brandstaeter, S., Braeu, F., et al. Experimental characterization of the biaxial mechanical properties of porcine gastric tissue. *journal of the mechanical behavior of biomedical materials, 74*, 499-506. (2017)
[155] Jia, Z., Li, W., & Zhou, Z. Mechanical characterization of stomach tissue under uniaxial tensile action. *Journal of biomechanics, 48*(4), 651-658. (2015)

[156] Fullard, L., Lammers, W., Wake, G. C., & Ferrua, M. J. Propagating longitudinal contractions in the ileum of the rabbit–efficiency of advective mixing. *Food & function, 5*(11), 2731-2742. (2014)
[157] Vassiliadis, S., Kyriakis-Mpitzaros, E., Cay, A., Rangoussi, M., Zachariadou, A., & Papadopoulos, P. Multiaxial Out-of-Plane Tensile Test of Textile Fabrics. (2016)
[158] Vassiliadis, S., Prekas, K., Katsoulis, A., et al. Multiaxial tensile testing of Textile Fabrics. *Journal of Fashion Technology & Textile Engineering, 2015*. (2017)
[159] Zheng, J., Takatera, M., Inui, S., & Shimizu, Y. Measuring technology of the anisotropic tensile properties of woven fabrics. *Textile Research Journal, 78*(12), 1116-1123. (2008)
[160] Gregersen, H., Kassab, G., & Fung, Y. Determination of membrane tension during balloon distension of intestine. *MCB-TECH SCIENCE PRESS-, 1*, 191-200. (2004)
[161] Herbella, F. A. M., Aprile, L. R., & Patti, M. G. High-resolution manometry for the evaluation of gastric motility. *Updates in surgery, 66*(3), 177-181. (2014)
[162] Whitehead, W. E., & Delvaux, M. Standardization of barostat procedures for testing smooth muscle tone and sensory thresholds in the gastrointestinal tract. *Digestive diseases and sciences, 42*(2), 223-241. (1997)
[163] Ang, D. Measurement of gastric accommodation: a reappraisal of conventional and emerging modalities. *Neurogastroenterology & Motility, 23*(4), 287-291. (2011)
[164] De Schepper, H., Cremonini, F., Chitkara, D., & Camilleri, M. Assessment of gastric accommodation: overview and evaluation of current methods. *Neurogastroenterology & Motility, 16*(3), 275-285. (2004)
[165] Schwizer, W., Steingötter, A., Fox, M., et al. Non-invasive measurement of gastric accommodation in humans. *Gut, 51*(suppl 1), i59-i62. (2002)
[166] Schulze, K. S. The imaging and modelling of the physical processes involved in digestion and absorption. *Acta Physiologica, 213*(2), 394-405. (2015)
[167] De Luca, C. J. The use of surface electromyography in biomechanics. *Journal of applied biomechanics, 13*(2), 135-163. (1997)
[168] Marciani, L., Gowland, P. A., Fillery-Travis, A., et al. Assessment of antral grinding of a model solid meal with echo-planar imaging. *American Journal of Physiology-Gastrointestinal and Liver Physiology, 280*(5), G844-G849. (2001)
[169] Laulicht, B., Tripathi, A., Schlageter, V., Kucera, P., & Mathiowitz, E. Understanding gastric forces calculated from high-resolution pill tracking. *Proceedings of the National Academy of Sciences, 107*(18), 8201-8206. (2010)
[170] Zhu, D., Handschuh-Wang, S., & Zhou, X. Recent progress in fabrication and application of polydimethylsiloxane sponges. *Journal of Materials Chemistry A, 5*(32), 16467-16497. (2017)
[171] Choi, S.-J., Kwon, T.-H., Im, H., et al. A polydimethylsiloxane (PDMS) sponge for the selective absorption of oil from water. *ACS applied materials & interfaces, 3*(12), 4552-4556. (2011)
[172] Zhang, S., Guo, J., Ma, X., et al. Smart PDMS sponge with switchable pH-responsive wetting surface for oil/water separation. *New Journal of Chemistry, 41*(17), 8940-8946. (2017)
[173] Zhao, X., Li, L., Li, B., Zhang, J., & Wang, A. Durable superhydrophobic/superoleophilic PDMS sponges and their applications in selective oil absorption and in plugging oil leakages. *Journal of Materials Chemistry A, 2*(43), 18281-18287. (2014)
[174] Park, B.-G., Jung, Y., Shin, M.-G., Ko, J., & Cho, H. (2020). *Self-Recovering 3-Dimensional Micro Pore Structure Pressure Sensor Using Shape Memory Polymer.* Paper presented at the 2020 IEEE 33rd International Conference on Micro Electro Mechanical Systems (MEMS).
[175] Park, S. W., Das, P. S., & Park, J. Y. Development of wearable and flexible insole type capacitive pressure sensor for continuous gait signal analysis. *Organic Electronics, 53*, 213-220. (2018)
[176] Zhou, T., Yang, J., Zhu, D., et al. Hydrophilic Sponges for Leaf-Inspired Continuous Pumping of Liquids. *Advanced Science, 4*(6), 1700028. (2017)
[177] Mazurek, P., Ekbrant, B., Madsen, F., Yu, L., & Skov, A. Glycerol-silicone foams–Tunable 3-phase elastomeric porous materials. *European Polymer Journal, 113*, 107-114. (2019)

[178] Turco, A., Primiceri, E., Frigione, M., Maruccio, G., & Malitesta, C. An innovative, fast and facile soft-template approach for the fabrication of porous PDMS for oil–water separation. *Journal of Materials Chemistry A, 5*(45), 23785-23793. (2017)
[179] Shin, J. H., Heo, J.-H., Jeon, S., Park, J. H., Kim, S., & Kang, H.-W. Bio-inspired hollow PDMS sponge for enhanced oil–water separation. *Journal of hazardous materials, 365*, 494-501. (2019)
[180] Mac Murray, B. C., An, X., Robinson, S. S., et al. Poroelastic Foams for Simple Fabrication of Complex Soft Robots. *Adv Mater, 27*(41), 6334-6340. (2015)
[181] Jia, H., He, Y., Zhang, X., Du, W., & Wang, Y. Integrating Ultra-Thermal-Sensitive Fluids into Elastomers for Multifunctional Flexible Sensors. *Advanced Electronic Materials, 1*(3), 1500029. (2015)
[182] Haffiz, T. M., Izzuddin, M. Y. A., Affidah, D., et al. *Biochar: A "green" carbon source for pressure sensors.* Paper presented at the 2017 IEEE SENSORS.
[183] Kim, J. I., Jeon, S., & Lee, W. C. Fully Stretchable Electromagnet Using Magnetoactive PDMS Sponges and Metallic Coils. *JOM*, 1-6. (2019)
[184] Thomas, S. Foam dressings. *Journal of wound care, 2*(3), 153-156. (1993)
[185] Schneider, C. A., Rasband, W. S., & Eliceiri, K. W. NIH Image to ImageJ: 25 years of image analysis. *Nature methods, 9*(7), 671-675. (2012)
[186] Maziz, A., Concas, A., Khaldi, A., Stålhand, J., Persson, N.-K., & Jager, E. W. Knitting and weaving artificial muscles. *Science advances, 3*(1), e1600327. (2017)
[187] Arena, P., Bonomo, C., Fortuna, L., Frasca, M., & Graziani, S. Design and Control of an IPMC Wormlike Robot. *IEEE Transactions on Systems, Man and Cybernetics, Part B (Cybernetics), 36*(5), 1044-1052. (2006)
[188] Aydin, Y. O., Molnar, J. L., Goldman, D. I., & Hammond, F. L. (2018). *Design of a soft robophysical earthworm model.* Paper presented at the 2018 IEEE International Conference on Soft Robotics (RoboSoft).
[189] Boxerbaum, A., Chiel, H., & Quinn, R. (2009). *Softworm: A soft, biologically inspired worm-like robot.* Paper presented at the Neuroscience Abstracts.
[190] Boxerbaum, A. S., Horchler, A. D., Shaw, K. M., Chiel, H. J., & Quinn, R. D. (2011). *A controller for continuous wave peristaltic locomotion.* Paper presented at the Intelligent Robots and Systems (IROS), 2011 IEEE/RSJ International Conference on.
[191] Boxerbaum, A. S., Shaw, K. M., Chiel, H. J., & Quinn, R. D. Continuous wave peristaltic motion in a robot. *The International Journal of Robotics Research, 31*(3), 302-318. (2012)
[192] Boxerbaum, A. S., Horchler, A. D., Shaw, K. M., Chiel, H. J., & Quinn, R. D. Worms, waves and robots. 3537-3538. (2012)
[193] Cheng, N., Ishigami, G., Hawthorne, S., et al. Design and analysis of a soft mobile robot composed of multiple thermally activated joints driven by a single actuator. 5207-5212. (2010)
[194] Connolly, F., Polygerinos, P., Walsh, C. J., & Bertoldi, K. Mechanical programming of soft actuators by varying fiber angle. *Soft robotics, 2*(1), 26-32. (2015)
[195] Hassan, T., Cianchetti, M., Mazzolai, B., Laschi, C., & Dario, P. Active-braid, a bioinspired continuum manipulator. *IEEE Robotics and Automation Letters, 2*(4), 2104-2110. (2017)
[196] Manwell, T., Vitek, T., Ranzani, T., Menciassi, A., Althoefer, K., & Liu, H. (2014). *Elastic mesh braided worm robot for locomotive endoscopy.* Paper presented at the Engineering in Medicine and Biology Society (EMBC), 2014 36th Annual International Conference of the IEEE.
[197] Menciassi, A., Gorini, S., Pernorio, G., Weiting, L., Valvo, F., & Dario, P. (2004). *Design, fabrication and performances of a biomimetic robotic earthworm.* Paper presented at the Robotics and Biomimetics, 2004. ROBIO 2004. IEEE International Conference on.
[198] Branscomb, D., Beale, D., & Broughton, R. New directions in braiding. *Journal of Engineered Fibers and Fabrics, 8*(2), 155892501300800202. (2013)
[199] Felt, W., Chin, K. Y., & Remy, C. D. Contraction sensing with smart braid McKibben muscles. *IEEE/ASME Transactions on Mechatronics, 21*(3), 1201-1209. (2015)
[200] Koizumi, S., Kurumaya, S., Nabae, H., Endo, G., & Suzumori, K. Braiding thin McKibben muscles to enhance their contracting abilities. *IEEE Robotics and Automation Letters, 3*(4), 3240-3246. (2018)
[201] Chen, D. (2014). *Experimental characterization of Bowden cable friction and compliance.*

[202] Jeong, U., & Cho, K.-J. (2015). *Feedforward friction compensation of Bowden-cable transmission via loop routing.* Paper presented at the 2015 IEEE/RSJ International Conference on Intelligent Robots and Systems (IROS).
[203] Jeong, U., & Cho, K.-J. Control of a Bowden-cable actuation system with embedded boasensor for soft wearable robots. *IEEE Transactions on Industrial Electronics, 67*(9), 7669-7680. (2019)
[204] Arakawa, T., Uno, H., Fukuda, T., Higuchi, K., Kobayashi, K., & Kuroki, T. New aspects of gastric adaptive relaxation, reflex after food intake for more food: involvement of capsaicin-sensitive sensory nerves and nitric oxide. *Journal of smooth muscle research, 33*(3), 81-88. (1997)
[205] Cheng, L. K. Slow wave conduction patterns in the stomach: from W aller's Foundations to Current Challenges. *Acta Physiologica, 213*(2), 384-393. (2015)
[206] Hocke, M., Schone, U., Richert, H., et al. Every slow-wave impulse is associated with motor activity of the human stomach. *Am J Physiol Gastrointest Liver Physiol, 296*(4), G709-716. (2009)
[207] O'Grady, G., Du, P., Cheng, L. K., et al. Origin and propagation of human gastric slow-wave activity defined by high-resolution mapping. *American Journal of Physiology-Gastrointestinal and Liver Physiology, 299*(3), G585-G592. (2010)
[208] Lu, K. H., Liu, Z., Jaffey, D., et al. Automatic assessment of human gastric motility and emptying from dynamic 3D magnetic resonance imaging. *Neurogastroenterology & Motility, 34*(1), e14239. (2022)
[209] Starkey, M. M., & Williams, R. L. (2011). *Capstan as a Mechanical Amplifier.* Paper presented at the ASME 2011 International Design Engineering Technical Conferences and Computers and Information in Engineering Conference.
[210] In, H., Kang, S., & Cho, K.-J. (2012). *Capstan brake: Passive brake for tendon-driven mechanism.* Paper presented at the 2012 IEEE/RSJ International Conference on Intelligent Robots and Systems.
[211] Dhouibi, S., Boujelbene, M., Kharrat, M., Dammak, M., & Maalej, A. Friction behavior of high density polyethylene (HDPE) against 304L steel: An experimental investigation of the effects of sliding direction, sliding history and sliding speed. *Journal of Surfaces and Interfaces of Materials, 1*(1), 71-76. (2013)
[212] Gregory, S. (2018). Physical properties of glycerine *Glycerine* (pp. 113-156): CRC Press.
[213] Nyce, D. S. (2016). *Position sensors*: John Wiley & Sons.
[214] Olson, G., Davies, C., Gupta, G. S., Davies, R., & Fullard, L. (2021). *Positional feedback of a linear track slider using a low-cost stretch sensor.* Paper presented at the 2021 IEEE Sensors Applications Symposium (SAS).
[215] Berg, R. F., Chiodo, N., & Georgin, E. Silicone tube humidity generator. *Atmospheric Measurement Techniques, 15*(3), 819-832. (2022)
[216] Keller, P. E., & Kouzes, R. T. (2017). Water vapor permeation in plastics: Pacific Northwest National Lab.(PNNL), Richland, WA (United States).
[217] Velderrain, M. (2012). *Designing low permeability, optical-grade silicone systems: guidelines for choosing a silicone based on transmission rates for barrier applications.* Paper presented at the Advances in Display Technologies II.
[218] Robb, W. Thin silicone membranes-their permeation properties and some applications. *Annals of the New York Academy of Sciences, 146*(1), 119-137. (1968)
[219] Zhang, H., Lowe, A., Kalra, A., & Yu, Y. A Flexible Strain Sensor Based on Embedded Ionic Liquid. *Sensors, 21*(17), 5760. (2021)
[220] Hoffmann, K. (1974). *Applying the wheatstone bridge circuit*: HBM Darmstadt, Germany.
[221] Wilson, J. S. (2004). *Sensor technology handbook*: Elsevier.
[222] Suprapto, S., Setiawan, A., Zakaria, H., Adiprawita, W., & Supartono, B. (2017). *Low-cost pressure sensor matrix using velostat.* Paper presented at the 2017 5th International Conference on Instrumentation, Communications, Information Technology, and Biomedical Engineering (ICICI-BME).
[223] Valle-Lopera, D. A., Castaño-Franco, A. F., Gallego-Londoño, J., & Hernández-Valdivieso, A. M. Test and fabrication of piezoresistive sensors for contact pressure measurement. *Revista Facultad de Ingeniería Universidad de Antioquia*(82), 47-52. (2017)

[224] Hopkins, M., Vaidyanathan, R., & Mcgregor, A. H. Examination of the performance characteristics of velostat as an in-socket pressure sensor. *IEEE Sensors Journal, 20*(13), 6992-7000. (2020)
[225] Vehec, I., & Livovsky, L. (2020). *Flexible resistive sensor based on velostat.* Paper presented at the 2020 43rd International Spring Seminar on Electronics Technology (ISSE).
[226] Fatema, A., Kuriakose, I., Devendra, D., & Hussain, A. M. (2022). *Investigation of the Mechanical Reliability of a Velostat-based Flexible Pressure Sensor.* Paper presented at the 2022 IEEE International Conference on Flexible and Printable Sensors and Systems (FLEPS).
[227] Giovanelli, D., & Farella, E. Force sensing resistor and evaluation of technology for wearable body pressure sensing. *Journal of Sensors, 2016*. (2016)
[228] Dzedzickis, A., Sutinys, E., Bucinskas, V., et al. Polyethylene-carbon composite (Velostat®) based tactile sensor. *Polymers, 12*(12), 2905. (2020)
[229] Barba, R., de Madrid, Á. P., & Boticario, J. G. Development of an inexpensive sensor network for recognition of sitting posture. *International Journal of Distributed Sensor Networks, 11*(8), 969237. (2015)
[230] Martinez-Cesteros, J., Medrano-Sanchez, C., Plaza-Garcia, I., Igual-Catalan, R., & Albiol-Pérez, S. A Velostat-Based Pressure-Sensitive Mat for Center-of-Pressure Measurements: A Preliminary Study. *International Journal of Environmental Research and Public Health, 18*(11), 5958. (2021)
[231] Lee, B. W., & Shin, H. Feasibility study of sitting posture monitoring based on piezoresistive conductive film-based flexible force sensor. *IEEE Sensors Journal, 16*(1), 15-16. (2015)
[232] Jeong, E., Lee, J., & Kim, D. (2011). *Finger-gesture recognition glove using velostat (ICCAS 2011).* Paper presented at the 2011 11th International Conference on Control, Automation and Systems.
[233] Carrozzino, M., Avveduto, G., Tecchia, F., Gurevich, P., & Cohen, B. (2014). *Navigating immersive virtual environments through a foot controller.* Paper presented at the Proceedings of the 20th ACM symposium on virtual reality software and technology.
[234] Fairman, E., & Santimore, D. (2011). *The Smart Vest.* Worcester Polytechnic Institute.
[235] Faure, F., Allard, J., Cotin, S., et al. (2007). *SOFA: A modular yet efficient simulation framework*.
[236] Allard, J., Cotin, S., Faure, F., et al. (2007). *Sofa-an open source framework for medical simulation*.
[237] Faure, F., Duriez, C., Delingette, H., et al. (2012). Sofa: A multi-model framework for interactive physical simulation *Soft tissue biomechanical modeling for computer assisted surgery* (pp. 283-321): Springer.
[238] Comas, O., Taylor, Z. A., Allard, J., Ourselin, S., Cotin, S., & Passenger, J. (2008). *Efficient nonlinear FEM for soft tissue modelling and its GPU implementation within the open source framework SOFA.* Paper presented at the International Symposium on Biomedical Simulation.
[239] Comas, O. (2010). *Real-time soft tissue modelling on GPU for medical simulation.*
[240] Pedersen, A., Bardow, A., Jensen, S. B., & Nauntofte, B. Saliva and gastrointestinal functions of taste, mastication, swallowing and digestion. *Oral diseases, 8*(3), 117-129. (2002)
[241] Kessing, B., Bredenoord, A., & Smout, A. Mechanisms of gastric and supragastric belching: a study using concurrent high-resolution manometry and impedance monitoring. *Neurogastroenterology & Motility, 24*(12), e573-e579. (2012)
[242] Nguyen, H., Silny, J., Albers, D., et al. Dynamics of esophageal bolus transport in healthy subjects studied using multiple intraluminal impedancometry. *American Journal of Physiology-Gastrointestinal and Liver Physiology, 273*(4), G958-G964. (1997)

Appendix A: Moving and mixing materials with a mechanical intestine

Reprinted, with permission, from Olson, G. K., Davies, C. E., Fullard, L., Davies, R. Y., & Gupta, G. S. (2019, January). Moving and mixing materials with a mechanical intestine. In *13th International Conference on Bulk Materials Storage, Handling and Transportation (ICBMH 2019)* (pp. 521-526). Barton, ACT: Engineers Australia.

Moving and mixing materials with a mechanical intestine

Gerald K. Olson[1,2], Clive E. Davies[1,2], Luke Fullard[1,3,4], Rose Y. G. Davies[5], Gourab Sen Gupta[2]

[1]*Riddet Institute, Massey University, Palmerston North, 4410 New Zealand*
[2] *School of Food and Advanced Technology, Massey University, Palmerston North, 4410 New Zealand*
[3]*School of Fundamental Sciences, Massey University, Palmerston North, 4410 New Zealand*
[4]*School of Agriculture and Environment, Massey University, Palmerston North, 4410 New Zealand*
[5]*School of Aviation, Massey University, Palmerston North, 4410 New Zealand*
Contact email: g.olson@massey.ac.nz

Abstract

Mimicry of the bio-mechanical action of the gastrointestinal tract could provide a novel method for simulating the transportation and mixing of various materials. The actions of the muscles of the gastrointestinal tract produce peristaltic waves and segmented contraction activity for the efficient mixing and evacuation of digesta. A biomimetic physical model of the gastrointestinal tract has been developed using controlled actuators (unit constrictors) to simulate the contraction / expansion action of these muscles. The unit constrictors incorporate a compressive / expansive action in combination with material flexibility, allowing the artificial muscle segments to flex and form in response to applied forces. Flexible tendons provide cable-driven actuation for compression and expansion of the unit constrictors against a tubular membrane. The membrane displays high flexibility, good resistance to tear and fracture, and can be fabricated to provide a water-tight seal at low strains. Controlled contraction of the unit constrictors is carried out with motors and a programmable microcontroller, allowing for wide variation in the speed and pattern of wave motions being applied to the membrane. Initial results show that the physical model achieves good basic peristaltic deformation and segmented contraction of the tubular membrane, as well as good potential for providing effective propulsion and gentle mixing for a variety of solid, semi-solid or liquid materials.

1. Introduction

The gastrointestinal tract can be regarded as nature's biological slurry pump. Through wave-like muscle wall contractions, or 'peristalsis', the gastrointestinal tract is capable of moving and mixing a wide variety of edible materials and liquids. In the stomach, these wave-like contractions also act in the grinding of food matter into smaller particles, thereby assisting in the uptake of nutrients as the slurry of food and gastric secretions (or 'chyme') are transported through the intestine [1].

The employment of peristalsis as a mechanism for pumping materials is not new. Rotary peristaltic hose pumps use rollers or cams to compress a flexible hose and propel liquids and gases [2]. The pressure exerted by the rollers forces the fluid through the remaining length of hose but little or no control is possible over the possible mixing of contents, and the hoses frequently experience excessive wear. The progressing cavity pump (also referred as an orbital lobe or 'mono' pump) is comprised of a metallic rotor and an elastomeric stator, each being helical in form, creating a series of cavities as the rotor is rotated and propelling the material in a peristaltic-like manner [3]. Typically, the progressing cavity pump consists of large, heavy, solid parts that lack any flexibility and pump only to a limited distance. The solid rotor of this type of pump also requires being in contact with the material being propelled. Recent studies have shown the potential for use of segments of artificial muscle actuators as the driving mechanism for the peristaltic propulsion and continuous mixing of materials, including the use of pneumatic constrictors for the mixing and moving of highly sensitive solid rocket propellant slurry [4] and transportation of other highly

viscous liquids or solid-liquid mixtures [5]. Being pneumatically driven these constrictor segments are relatively solid and heavy, with little flexibility available for bending or redirection of flow.
Soft-robotics research on biomimetic, worm-like, peristaltic locomotion of platforms over various surfaces offer a variety of methods for applying peristaltic waveform patterns to a tubular shell [6-9]. In peristaltic locomotion, the wave-like deformations of a shell applies directional forces to an external surface, propelling the platform forward via frictional contact [7]. Alternatively, forces can also be directed inwards through a patterned constriction of the shell surface, thereby manipulating and moving the internal cavity contents instead.
Of particular interest are the robotic models that incorporate a braided shell structure [7-9], as control of the peristaltic deformation pattern over the length of the platform is maintained by passive, mechanical means rather than through precise control and actuation of a large number of localised constrictions.
Artificial intestine: To study the effects of peristalsis on the transport, breakdown and mixing of food materials within the human gastrointestinal tract a nature-inspired, flexible, soft-walled mechanical model was created to mimic the peristaltic action of a biological intestine. The characteristics of the mechanical intestine could offer insights towards the potential continuous bulk moving and mixing of a wide range of other materials.

2. Method

The mechanical artificial intestine model was comprised of two layers – an outer sleeve connecting a series of unit constrictors to be used in the actuation of the waveform, and an inner composite sleeve providing a flexible and elastic surface that would come in contact with the material to be moved.
The outer sleeve of the physical model used a commercially available expandable braided sleeve made from polyethylene terephthalate (PET). A section of the unexpanded flat braided sleeve was cut to length with a hot knife to prevent further fraying of the ends. It was then spread over rigid polyvinyl chloride (uPVC) tubing and heat-set in its expanded form using a heat-gun.
A flexible monofilament nylon line was used to act as a unit constrictor. Several nylon lines were evenly spaced over the length of the outer sleeve and directly attached to it via threading of the lines over and under the braid yarns at similar intervals (Figure 1). Remaining lengths of nylon line exiting the braid were then used to act as tendons for the constrictors. A range of actuation of the constrictions could therefore be achieved by applying a varying amount of tension to each tendon.

Figure 1: Nylon line constrictors threaded through expandable braided tubing. At the top of the image can be seen Bowden cables through which the constrictor tendons run before connecting to winding spindles.

The flexible inner membrane sleeve was made from an elastic textile encased in elastomer rubber. A section of the textile was cut and positioned over a length of polycarbonate tubing, ensuring there was an even coverage over the tubing with no folds or overlapping. An additional length of braided sleeve was then placed over the textile to provide reinforcement for the artificial membrane tube.
The prepared textile and braid tubing was then dipped into liquid elastomer and left to drain off, leaving an even layer over the entire surface. Once cured, additional coats could subsequently be applied to ensure the sleeve was sufficiently encased. However, repeated coats increased the thickness of the composite tube and in turn the overall stiffness of the material, affecting the deformation response of the tubing.
The outer braided sleeve with connected constrictors is positioned over the inner composite sleeve and the tendons attached to winders on a motor driver unit by feeding them through a set of flexible Bowden cables. A programmable microcontroller was used to control the rotor positions of a series of servo motors, each having spindles attached to their rotors. The turning spindles would wind the constrictor tendons, causing the constrictors to reduce in diameter and deform a particular section of the tubing.
Patterning of servo rotor positions, programmed into the microcontroller, could then constrict different sections of the tubing as desired. Different patterns of deformation are subsequently achieved through alteration of the programmed timing of the constrictions.

3. Discussion

A periodic sine-wave contraction pattern of the unit constrictors provided a smooth, wave-like deformation of the braided tubing (Figure 2). This deformation pattern was maintained even when the tubing was bent or flexed up to 45 degrees away from its central longitudinal axis.

Figure 2: (Left) An example of linear peristaltic waveform deformation of the braided tubing. (Right) A similar deformation pattern is maintained while bending the length of tubing.

As a section of the braid is compressed through constriction, the length of the braided tube is extended. Likewise, the tube's length contracts as constrictors relax and expand (Figure 3). A similar mechanism can be found in biological smooth muscle layers that form the peristaltic waves in gastrointestinal tract organs. As the longitudinal muscle contracts the relaxed circumferential muscle bundles expand and bunch closer together. As the circumferential muscle contracts, the longitudinal muscle relaxes, and the bundles of circumferential muscle begin to spread apart from each other, propelling the internal contents of the tract forward as they do so [10].

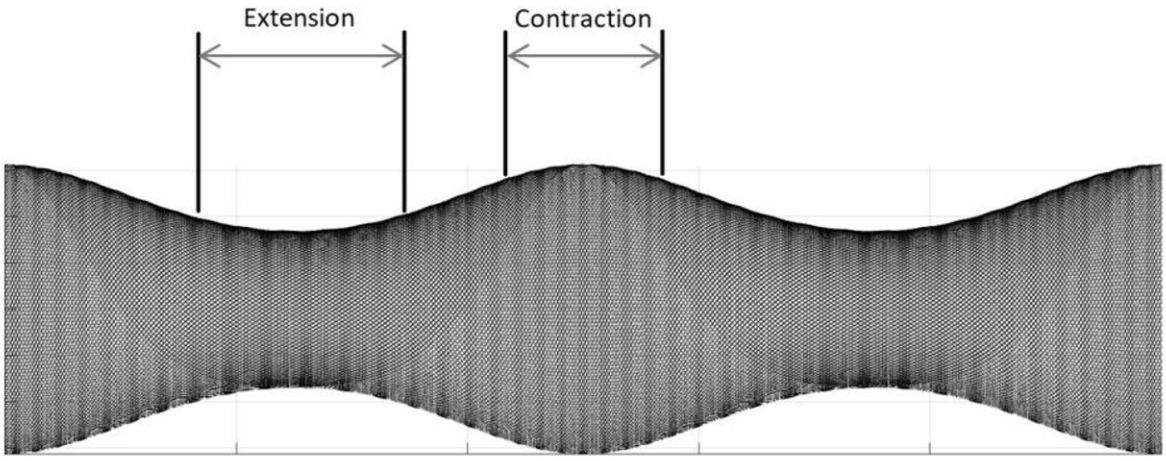

Figure 3: A side-on graphical representation of the deformation of a braided tube under a sine-wave constriction pattern. Localised extension of the braid occurs at sections where the tubing is constricted radially, whilst the braid contracts where constrictors relax and expand in diameter.

The contraction of the unit constrictors mimics circumferential muscle contraction. The elastic returning force resulting from stretching of the inner composite sleeve has been used to mimic the longitudinal muscle contraction, eliminating the need for additional constrictors to be placed for control of contraction in the axial direction.

The angle of the braid yarns to the longitudinal axis is a factor affecting the limits for longitudinal extension and circumferential constriction of the tubing [11]. This angle constantly changes with the extension and contraction of the braid, reducing in size as the tubing is constricted radially / extended longitudinally and increasing in size as the tubing expands radially and contracts longitudinally.

As the braided tube is contracted radially a minimum diameter occurs where the braid yarns will begin to collide against each other. For the original braided tube, this limit was reached at a minimum diameter of 45mm, and the force required on pulling the constrictor tendons further begins to increase steeply. From observation, the small servo motors used would begin to reach their torque output limit on approaching this minimum diameter. When further application of force was applied to the constrictor tendons the braided tube would show signs of buckling and folding rather than form a clearly circular contraction profile, affecting the symmetry and appearance of the patterned peristaltic wave. If the tube is attached directly to the entire circumference of the constrictors it more closely follows the pattern of expansion/contraction, and reduces instances of buckling. However, a reduction in the number of yarns comprising the braided pattern can help extend the minimum limit of contraction and reduce the occurrence of buckling. This was observed in the model by stripping out every second yarn from the original braiding, reducing the number of yarns in the clockwise and counter-clockwise directions by half. In doing so, the minimum constricted diameter of the braided tubing was reduced by up to half as the distance between points of contact between yarns travelling in the same direction was effectively doubled.

Friction is another factor for consideration as it affects the amount of force required for effective constriction of the tubing. Friction points of particular interest lie between the constrictor lines and the braided yarns, between the constrictor lines and the surface of the inner sleeve, within the Bowden cable and associated bends as the tendons enter and exit the cable, and between the surfaces of the inner and outer sleeves as they impress upon each other.

Constrictor spacing on the braided tubing affects the resulting constriction characteristics of the applied patterned waveform. Too far apart and the contraction of adjacent constrictors would cause a ‘bubble’ of tubing to appear between constrictors, reducing the effectiveness of the constrictors to propel contents forward. Placing unit constrictors closer together would provide greater strength to the tubing as it deforms, but also require the use of additional controls and material. The optimal

spacing to be determined between constrictors is likely to be dependent on the type of material that is to be moved within the tubing.
The peristaltic waveform pattern used for actuating the constrictors requires timing with regard to the distance between constrictors and the response of the longitudinal elastic contraction provided by the composite inner sleeve. Incorrect timing of constrictor actuation can lead to ineffective deformation of the braided tubing, poorly tensioned constrictor tendons and additional stress on motors. The creation of standing wave patterns for the mixing of contents is likely to be more reliant on the distance between actuated constrictions rather than by inaccurate timing.
Alternative methods could potentially be employed to achieve similar peristaltic deformation of the tubing while reducing the number of motors used or the total number of constrictors required. However, the ability to gently mix contents through the creation of standing waves may be sacrificed as a result. More efficient distribution of the Bowden cables over larger distances may also be achieved by attaching them to the braided tube in a helix, following the angle of the braid yarns, and therefore allowing them to bend in response to the deformation of the tubing.

4. Conclusions

The nature-inspired artificial intestine model presented here successfully applies an approximated peristaltic deformation pattern to the surface of a flexible braided tube. A series of unit constrictors connected around the circumference of the tubing, and evenly spaced along its length, constrict and expand via the drawing and releasing of tendons attached to motorised spindles. A timed pattern of actuation is achievable through programmable control of the motorised spindles, which can be employed to produce peristaltic-like motion in either direction (for potential moving of internal contents) or a segmental contraction and expansion of localised sections (to potentially induce content mixing). The tubing also displays good ability to flex and bend from its central axis whilst maintaining a continuous peristaltic deformation pattern.
Further research of the geometry and mechanics underlying the braid structure, and the effects of constrictions upon it, could improve the ability to completely close or seal the internal surface of the tubing during peristaltic deformation.

5. References

[1] Kong, F., & Singh, R. P. (2008). Disintegration of solid foods in human stomach. *J Food Sci, 73*(5), R67-80. doi:10.1111/j.1750-3841.2008.00766.x
[2] Nesbitt, B. (2006). *Handbook of pumps and pumping: Pumping manual international*: Elsevier.
[3] Cholet, H. (1997). *Progressing Cavity Pumps*: Editions Technip.
[4] Iwasaki, A., Matsumoto, K., Ban, R., Yoshihama, S., Nakamura, T., & Habu, H. (2016). The Continuous Mixing Process of Composite Solid Propellant Slurry by an Artificial Muscle Actuator. *Transactions of the Japan Society for Aeronautical and Space Sciences, Aerospace Technology Japan, 14*(ists30), Pa_107-Pa_110.
[5] Suzuki, K., & Nakamura, T. (2010). *Development of a peristaltic pump based on bowel peristalsis using for artificial rubber muscle.* Paper presented at the Intelligent Robots and Systems (IROS), 2010 IEEE/RSJ International Conference on.
[6] Menciassi, A., Gorini, S., Pernorio, G., Weiting, L., Valvo, F., & Dario, P. (2004). *Design, fabrication and performances of a biomimetic robotic earthworm.* Paper presented at the Robotics and Biomimetics, 2004. ROBIO 2004. IEEE International Conference on.
[7] Horchler, A. D., Kandhari, A., Daltorio, K. A., Moses, K. C., Ryan, J. C., Stultz, K. A., . . . Bachmann, R. J. (2015). Peristaltic locomotion of a modular mesh-based worm robot: precision, compliance, and friction. *Soft Robotics, 2*(4), 135-145.
[8] Hassan, T., Cianchetti, M., Mazzolai, B., Laschi, C., & Dario, P. (2017). Active-braid, a bioinspired continuum manipulator. *IEEE Robotics and Automation Letters, 2*(4), 2104-2110.

[9] Manwell, T., Vitek, T., Ranzani, T., Menciassi, A., Althoefer, K., & Liu, H. (2014). *Elastic mesh braided worm robot for locomotive endoscopy.* Paper presented at the Engineering in Medicine and Biology Society (EMBC), 2014 36th Annual International Conference of the IEEE.
[10] Gregersen, H., & Christensen, J. (2016). *Clinical mechanics in the gut: an introduction*: Bentham Science Publishers.
[11] Connolly, F., Polygerinos, P., Walsh, C. J., & Bertoldi, K. (2015). Mechanical programming of soft actuators by varying fiber angle. *Soft Robotics, 2*(1), 26-32.

MASSEY UNIVERSITY
TE KUNENGA KI PŪREHUROA
UNIVERSITY OF NEW ZEALAND

GRADUATE RESEARCH SCHOOL

STATEMENT OF CONTRIBUTION
DOCTORATE WITH PUBLICATIONS/MANUSCRIPTS

We, the candidate and the candidate's Primary Supervisor, certify that all co-authors have consented to their work being included in the thesis and they have accepted the candidate's contribution as indicated below in the *Statement of Originality*.

Name of candidate:	Gerald Keith Olson
Name/title of Primary Supervisor:	Prof. Clive E. Davies
In which chapter is the manuscript /published work:	Appendix A

Please select one of the following three options:

(●) The manuscript/published work is published or in press

- Please provide the full reference of the Research Output:

Olson, G. K., Davies, C. E., Fullard, L., Davies, R. Y., & Gupta, G. S. (2019, January). Moving and mixing materials with a mechanical intestine. In 13th International Conference on Bulk Materials Storage, Handling and Transportation (ICBMH 2019) (pp. 521-526). Barton, ACT: Engineers Australia.

( ) The manuscript is currently under review for publication – please indicate:

- The name of the journal:
- The percentage of the manuscript/published work that was contributed by the candidate:
- Describe the contribution that the candidate has made to the manuscript/published work:

( ) It is intended that the manuscript will be published, but it has not yet been submitted to a journal

Candidate's Signature:	Gerald Keith Olson — Digitally signed by Gerald Keith Olson, Date: 2023.04.28 12:59:33 +12'00'
Date:	28-Apr-2023
Primary Supervisor's Signature:	Digitally signed by Clive E Davies, DN: cn=Clive E Davies, c=NZ, email=C.Davies@massey.ac.nz, Date: 2023.04.28 13:21:24 +12'00'
Date:	28-Apr-2023

This form should appear at the end of each thesis chapter/section/appendix submitted as a manuscript/ publication or collected as an appendix at the end of the thesis.

Appendix B: Positional feedback of a linear track slider using a low-cost stretch sensor

Positional feedback of a linear track slider using a low-cost stretch sensor

Gerald Olson
School of Food & Advanced Technology
Massey University, New Zealand
g.olson@massey.ac.nz

Clive Davies
School of Food & Advanced Technology
Massey University, New Zealand
c.davies@massey.ac.nz

Gourab Sen Gupta
School of Food & Advanced Technology
Massey University, New Zealand
g.sengupta@massey.ac.nz

Rose Davies
School of Aviation
Massey University, New Zealand
r.g.davies@massey.ac.nz

Luke Fullard
School of Agriculture and Environment
Massey University, New Zealand
lukeafullard@gmail.com

Abstract - **The artificial muscles of a biomimetic model of the human stomach require positional control of the (linear track) sliders that the actuated muscles are attached to. A novel servomechanism for positional control of a slider on a linear track has been explored using a basic, low-cost stretch sensor as a means in determining the sliders' absolute position over time. The stretch sensor was constructed from a silicone (PDMS) tube filled with an ionic liquid (saline) and exhibited good characteristics of linearity and low hysteresis. A microcontroller was used for conditioning the sensor feedback and software control over the slider positioning. Initial results indicate a coarse approximation is attainable of the slider position relative to its targeted position. However, further testing is required to determine operational life-time and other factors such as repeatability, drift and potential for improved accuracy.**

Keywords - stretch sensor, low-cost, position, servo

I. Introduction

Simulating how the stomach wall dynamically deforms during digestive activity can greatly improve our understanding of the effects of these deformations on the digestion of foods. A biomimetic artificial stomach model has been developed with multiple (> 30) synthetic muscles that require individual actuation via the pulling and releasing of cables. Measurement of the amount of cable displacement during actuation of the muscles can provide for determination of, and allow for control over, the amount of contraction that takes place on the stomach model. The muscle cables have been connected to sliders that travel along a 250 mm long linear track, with slider movement provided via the motorised winding and unwinding of a pulley system that each slider is attached to. Due to the number of muscles (sliders) involved, a low-cost system determining individual slider position is desired in order to provide effective feedback control for the muscle actuation system.

Many types of position sensor are available including resistive / potentiometer, cable extension transducers ("string pots"), capacitive sensing, inductive sensing, linear variable differential / inductive transformer (LVDT & LVIT), hall effect, magneto-resistive, magneto-strictive, encoders (brush type, optical, magnetic, and capacitive), optical triangulation (laser, infra-red) and time-of-flight (ultrasonic, laser) [1-4]. Among these sensors the resistive, cable extension transducer, LVIT, hall effect and encoder types can be considered relatively low-cost but can vary widely on performance factors such as range, linearity, repeatability and hysteresis, resolution, accuracy, complexity and the need for support electronics. They can also differ from being absolute or incremental (relative) in position indication and the lifetime of the device can be influenced from whether they use contact or non-contact forms of sensing. Rotary encoder position sensors [5, 6] have also been considered here as rotational displacement of the winding motors can be converted into a linear displacement of the cable; however these sensors (among others) typically require dedicated hardware interrupts that are generally limited in number on microcontroller devices.

A novel, low-cost approach to position sensing of a slider on a linear track is to use a basic resistive stretch-sensor made from silicone (polydimethylsiloxane) tubing filled with an ionic liquid (saline). This type of sensor can be stretched up to 300% of its original length with a change in resistance being measurable between its electrode terminals as it is being stretched. This change in resistance can be applied from the resistance equation for a piece (cable/wire) of homogenous material (Eqn. (1)).

$$R = \frac{l}{A}\rho \tag{1}$$

Where: R = resistance; l = length; A = cross-sectional area; ρ = resistivity.

An experimental setup was trialled where a silicone tubing-type stretch-sensor was attached to a pulley driven slider on a linear track. The stretch-sensor provided feedback of the absolute position of the slider and a microcontroller was used to control the position of the slider from this feedback. Measurements of the actual slider position were then compared to the desired (target) position output from the microcontroller.

II. Method and Materials

An ionic liquid was prepared by dissolving 10 grams of sodium chloride in 500 grams of water. The conductivity of the liquid was 33.65 mS/cm (18.5 °C) when measured with a conductivity meter (Thermo Scientific Orion Star A Series). The liquid was then degassed in a vacuum chamber for five minutes at 90 kPa to remove dissolved gases.

Silicone tubing was made via extrusion of a room-temperature vulcanising silicone (Sika Sikasil RTV Fast Cure Glazing Sealant Acetic Cure Silicone) through a plastic extrusion die screwed to the nozzle of the silicone tube. The die had a circular extrusion exit with a 4 mm outer diameter and 2 mm internal diameter to create the tubing and was printed in ultra-violet setting resin using a 3D resin printer

(AnyCubic Photon Mono). The silicone was extruded into a plastic tray containing water and a laundry detergent (Vanish NapiSan OxiAction). The addition of the detergent was to prevent the tubing from adhering to itself and the tray. The silicone was then left overnight to fully cure for 24 hours.

After injecting the saline solution into a 170 mm length of silicone tubing, one end was sealed with a 4 mm diameter barbed plastic connector that had a 40 mm length of 2.4 mm diameter stainless steel rod inserted into it to act as an electrode (Fig. 1). This sealing was carried out while the tubing was immersed in water to prevent any air from entering into the tube. Before sealing the other end of the tubing, in a similar manner as above, it is beneficial to degas the tubing in a vacuum chamber several times at 90 kPa for 3 minutes to remove any compressed air bubbles in the liquid. The tubing was placed vertically within the vacuum chamber with the open end pointing upwards so that air bubbles could drift to the tube opening and be released from the liquid. Some tapping of the tubing after degassing helped to release the trapped bubbles towards the tube opening. Rubber bands were then wrapped around the silicone tubing and plastic barb connector to prevent the tubing from pulling off the connector during stretching. A small amount of cyanoacrylate adhesive was also applied at the contact point of the connector and the steel rod to complete the sealing of the sensor.

The experimental motor-driven pulley system (Fig. 2 & 3) used a small brushed DC motor (N20-6V-600) to wind a braided nylon cable that was coiled around a pair of constantly rotating spindles. This approach applies the capstan principle to provide a mechanical advantage for the pulling of cables [7]. A small amount of tension applied on one side of the capstan spindle results in a much larger pulling force on the other side. The rotating capstan spindles were driven by two 70 RPM 12 VDC reversible gearhead motors providing up to 2.1 kg.cm of torque. The braided nylon cable was attached to a plastic slider that would move along a pair of stainless-steel rods. The fabricated stretch-sensor was attached to the plastic slider with a cable-tie and the other end of the sensor was fixed onto the motor housing. A 100 kΩ resistor placed in series with the sensor formed a voltage divider circuit, allowing for voltage measurements indicating the change in resistance to take place.

A microcontroller (STMicroelectronics STM32F103C) was used for determining the desired (target) position of the slider, directional and speed control of the pulley-winding motor and for measurement of the voltage across the sensor using a 12-bit ADC. A sine-wave displacement of the slider position was calculated by the microcontroller to represent the type of contraction typically involved in the desired application i.e., contraction of an artificial muscle. In order to move the slider to the targeted position the current position needed to be determined. This was achieved by determining the voltage of the sensor at several fixed positions over its range of stretch and calculating a line of best fit.

The sensor / shunt resistor contact point of the voltage divider circuit was connected to the ADC input pin of the microcontroller via an op-amp voltage buffer. Two 3.3V digital pins were connected to the terminals to alternatingly act as both current source and sink. The direction of current flow through the sensor and shunt resistor was reversed by the microcontroller between voltage readings in order to create an alternating current through the ionic liquid. This reversing of the current flow was necessary for the elimination of electrolysis at the sensor electrodes and to minimise the impedance of the ionic liquid from affecting the stability of the voltage readings.

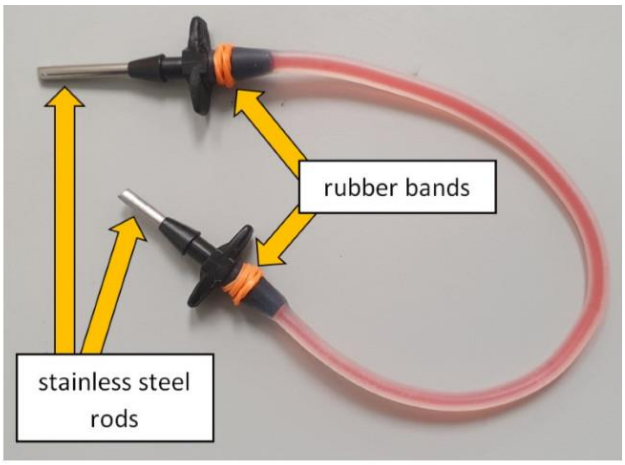

Fig. 1: Image of fabricated stretch sensor with plastic barbed connectors housing the stainless steel electrodes. The conductive liquid has been dyed red for observation of potential bubbles.

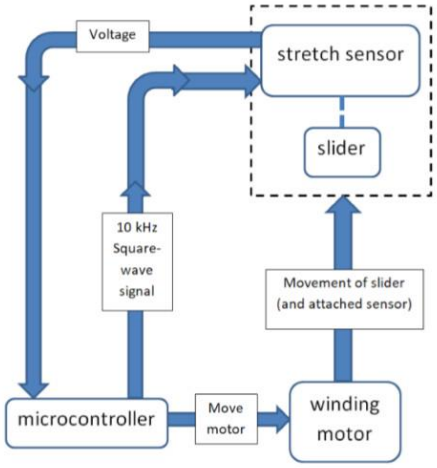

Fig. 2: Block diagram of experimental motor-driven pulley system.

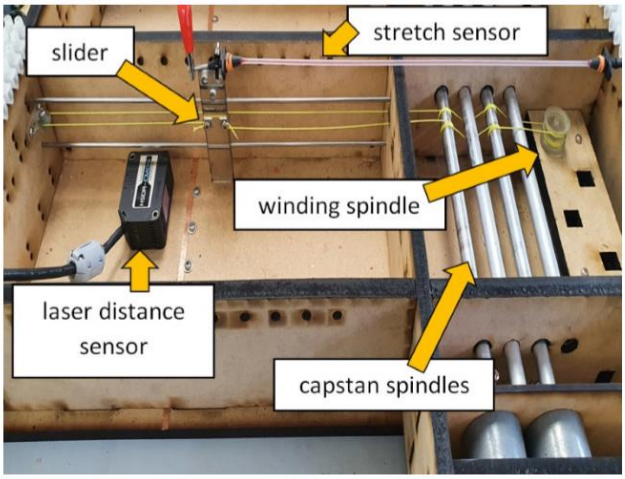

Fig. 3: Image of experimental motor drive system with attached stretch-sensor and slider.

The position of the plastic slider as it moved was measured using a laser distance sensor and amplifier (Omron ZX2-LD50L and ZX2-LDA) and logged to computer via data acquisition device (Measurement Computing USB-1208FS). The laser sensor provided measurement of the position of the slider within a 20 mm (±1 µm) range of distance. Positional measurements were sampled every 100 microseconds (10 kHz), timestamped, and logged to a data file.

III. Results

Although the voltage versus position plot (Fig. 4) exhibits some amount of non-linearity, a 2nd order polynomial was able to be fitted closely to the results using a spreadsheet graphing application (Microsoft Excel). The resulting polynomial (Eqn. (2)) was used to provide the microcontroller software with a means for translating the analogue-to-digital conversion of the sensor voltage into a meaningful absolute position of the slider.

$$y = -0.00001x^2 + 0.0069x + 1.3943 \qquad (2)$$

Where: y = position from origin (mm)

x = voltage from sensor output (V)

The voltage response of the sensor at various slider positions along the track provides a smooth yet non-linear curve (Fig. 4). On stretching, some of the tubing would be dragged over the barbs, returning again upon relaxation, and this could be contributing to the overall shape of curvature of the voltage response. This may be from a slight increase in the overall length (amount) of viscoelastic silicone tubing material as it stretches when compared to the constant volume of conductive liquid that is contained.

IV. Discussion

The measured displacement of the slider over the 6 second time period (Fig. 5) shows a close fit to the targeted sine-wave displacement set by the microcontroller. Deviation from the targeted position was minimal and some delay occurs, up to 100 milliseconds, as the slider position was updated by the microcontroller. However, the actual displacement is not a smooth curve and this can be visually observed as a slight jittering in the slider during its motion, particularly as it begins its motion and the required torque for the motor is significantly increased causing a sudden jerk in response. Various factors may be attributing to the motion jittering including the update rate of motor movement calculated by the microcontroller being too slow, slider friction on the track rails, inadequate starting-torque requirements of the winding motor, tension of the capstan pulley cables and backlash from the motor / winding pulley.

The hysteretic response of the sensor was tested to discern how much of an effect it may have on the performance of the sensor (Fig. 6 & 7). A series of three cycles of stretching and relaxing of the sensor from 0 to 200% strain was performed in a tensile testing machine (Instron 5960 Dual Column Table Frame), and using a signal generator to produce a 2 Vpp 10 kHz square-wave and a digital multi-meter to obtain the voltage. The results show a significant lack of hysteresis being present during the loading and unloading of the sensor. This may be attributable to the geometric cross-sectional area of the sensor, both the ionic channel and surrounding silicone encapsulate, being circular rather than the typical rectangular specimens as presented in

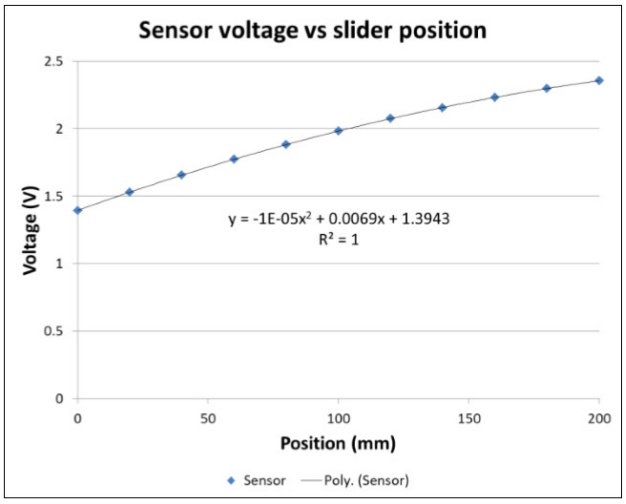

Fig. 4: Plot of sensor voltages over a series of slider positions with a polynomial line-of-best-fit.

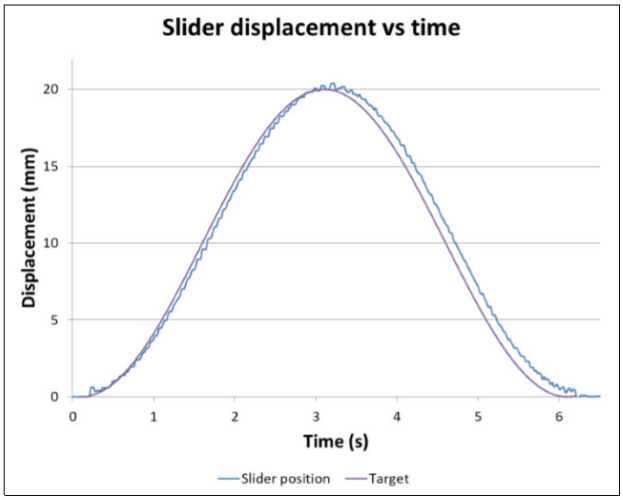

Fig. 5: Plot of sine-wave slider displacement from a point-of-origin over a period of 6 seconds. The point-of-origin of the displacement was in a mid-range position along the linear track (100 mm from one end of the track).

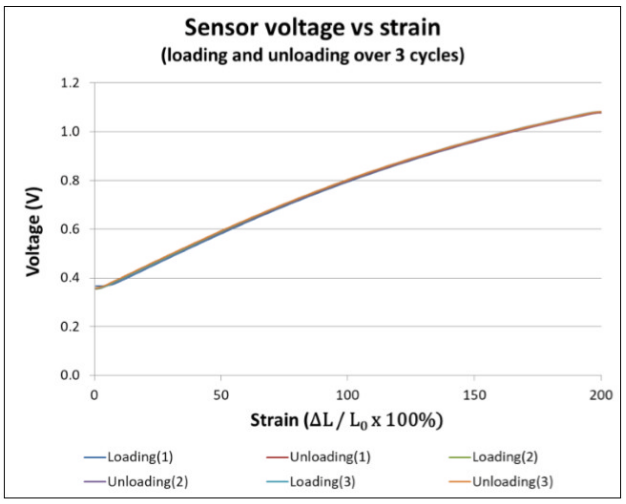

Fig. 6: Voltage versus strain of the sensor during several cycles of stretching up to 200%.

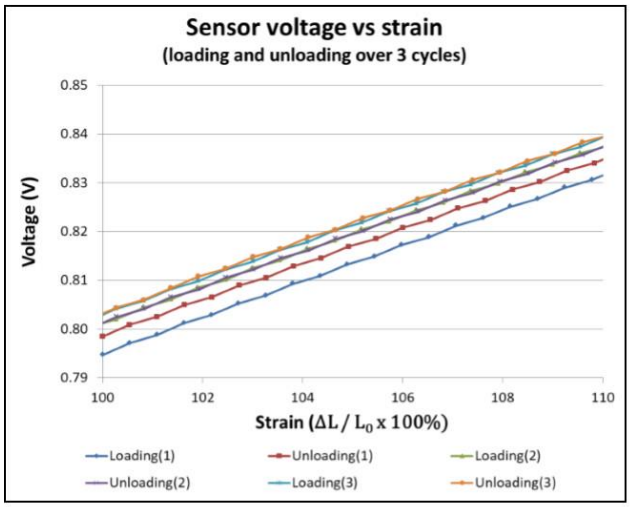

Fig. 7: Magnified view of the sensor voltage versus strain curve (Fig. 6) between the range of 100 - 110% strain showing the slight differentiation (hysteresis) that occurs between loading and unloading cycles.

Fig. 8: Altered stretch-sensor terminal with an attached reservoir of conductive liquid.

other works regarding the hysteresis of ionic liquid / silicone sensors [8]. These results are promising as they suggest that there is little need for countering the effects of hysteresis, such as through a deep-learning approach as suggested by [9].

With regard to the sensor's relevance to its intended application it shows promise as a suitable low-cost candidate for determining the absolute position of a slider on a linear track. However, use of the presented solution to the synchronous positioning of multiple sliders will be highly reliant on the processing speed and capabilities of the specific microcontroller being used. As the slider position is being updated at a rate of 10 kHz by the microcontroller, other program aspects such as the inclusion of serial communications may impinge on its ability to maintain an accurate position at all times, and cause considerable jittering to occur as the slider consistently overshoots its target position due to lapses in position update. This could be alleviated by transferring motor control to dedicated hardware, such as is provided by the position error-comparator control boards found in servo motors, rather than presently driving the motor speed and direction by software-based means. The controller would then be updating position signals to the dedicated motor control hardware rather than constantly having to drive and hold the motor(s) in position itself.

Fabrication of the tubing stretch-sensor may also require further modification if air bubbles are continuously observed to diffuse into the tubing over time. The possibility of this diffusion occurring may be mitigated by adding a small reservoir and air trap to one of the terminals of the stretch sensor in the form of a barbed tee (Fig. 8). The reservoir allows for some amount of conductive fluid to be drawn into the tubing as the sensor is stretched while the air trap acts as a compressive / expansive material, reducing the likelihood of air bubbles from diffusing through the silicone via the surrounding environment. This does however slightly alter the slope of the sensor voltage versus displacement curve and appropriate adjustments to the calibration of the sensor will be required.

V. Conclusions

The results show promise for the use of a basic, low-cost stretch-sensor as a means of determining the coarse absolute position of a linear track slider. However, additional testing is required to determine characteristics such as repeatability, non-linearity, hysteresis, accuracy, drift and sensitivity over its full range of stretch. Other factors also require further investigation such as long-term consistency and potential life-time.

Another challenge is the determination of a suitable means of motor control using the feedback from the sensor. The method of slider positioning trialled here relies heavily on using microprocessor control for providing conditioning of the feedback signal from the sensor and movement of the motors. This creates a significant drain on microprocessor resources as constant updating of the position of the slider is required. As a result, serial communications with the microprocessor can affect the smooth movement of the slider and contribute to some amount of motion jittering. To mitigate these effects, dedicated hardware for maintaining the slider position and monitoring of sensor feedback is to be considered as an alternative control mechanism.

References

[1] Nyce, D. S. (2016). *Position sensors*: John Wiley & Sons.
[2] Golby, J. (2010). Advances in inductive position sensor technology. *Sensor Review*.
[3] Wilson, J. S. (2004). *Sensor technology handbook*: Elsevier.
[4] Ripka, P., & Tipek, A. (2007). *Modern sensors handbook*: Wiley Online Library.
[5] Ellin, A., & Dolsak, G. (2008). The design and application of rotary encoders. *Sensor Review*.
[6] Miyashita, K., Takahashi, T., & Yamanaka, M. (1987). Features of a magnetic rotary encoder. *IEEE Transactions on Magnetics, 23*(5), 2182-2184.
[7] Starkey, M. M., & Williams, R. L. (2011). *Capstan as a Mechanical Amplifier*. Paper presented at the ASME 2011 International Design Engineering Technical Conferences and Computers and Information in Engineering Conference.
[8] Hara, Y., Yoshida, K., Khosla, A., Kawakami, M., Hosoda, K., & Furukawa, H. (2020). Very Wide Sensing Range and Hysteresis Behaviors of Tactile Sensor Developed by Embedding Soft Ionic Gels in Soft Silicone Elastomers. *ECS Journal of Solid State Science and Technology, 9(6),* 061024.
[9] Oldfrey, B., Jackson, R., Smitham, P., & Miodownik, M. (2019). A deep learning approach to non-linearity in wearable stretch sensors. *Frontiers in Robotics and AI, 6*, 27.

MASSEY UNIVERSITY
TE KUNENGA KI PŪREHUROA
UNIVERSITY OF NEW ZEALAND

GRADUATE RESEARCH SCHOOL

STATEMENT OF CONTRIBUTION
DOCTORATE WITH PUBLICATIONS/MANUSCRIPTS

We, the candidate and the candidate's Primary Supervisor, certify that all co-authors have consented to their work being included in the thesis and they have accepted the candidate's contribution as indicated below in the *Statement of Originality*.

Name of candidate:	Gerald Keith Olson
Name/title of Primary Supervisor:	Prof. Clive E. Davies
In which chapter is the manuscript /published work:	Appendix B

Please select one of the following three options:

(●) The manuscript/published work is published or in press

- Please provide the full reference of the Research Output:

Olson, G., Davies, C., Gupta, G. S., Davies, R., & Fullard, L. (2021). Positional feedback of a linear track slider using a low-cost stretch sensor. Paper presented at the 2021 IEEE Sensors Applications Symposium (SAS).

( ) The manuscript is currently under review for publication – please indicate:

- The name of the journal:
- The percentage of the manuscript/published work that was contributed by the candidate:
- Describe the contribution that the candidate has made to the manuscript/published work:

( ) It is intended that the manuscript will be published, but it has not yet been submitted to a journal

Candidate's Signature:	Gerald Keith Olson — Digitally signed by Gerald Keith Olson Date: 2023.04.27 18:34:57 +12'00'
Date:	27-Apr-2023
Primary Supervisor's Signature:	
Date:	27-Apr-2023

This form should appear at the end of each thesis chapter/section/appendix submitted as a manuscript/ publication or collected as an appendix at the end of the thesis.

GRS Version 5 – 13 December 2019
DRC 19/09/10

Appendix C: Preliminary investigation into low-cost stretch sensors for stomach deformation measurement

Preliminary investigation into low-cost stretch sensors for stomach deformation measurement

Gerald Olson
School of Food & Advanced Technology
Massey University, New Zealand
geraldolson@whatever-works.co.uk

Clive Davies
School of Food & Advanced Technology
Massey University, New Zealand
c.davies@massey.ac.nz

Gourab Sen Gupta
School of Food & Advanced Technology
Massey University, New Zealand
g.sengupta@massey.ac.nz

Rose Davies
School of Aviation
Massey University, New Zealand
r.g.davies@massey.ac.nz

Luke Fullard
School of Agriculture and Environment
Massey University, New Zealand
l.fullard@massey.ac.nz

***Abstract*— Physical simulation of gastric tract motility, through the use of controlled flexi-walled reactors, can benefit from measured feedback of the amount of stretch that regions of the deformable membrane wall undergo. Appropriate sensors need to be at least as flexible as the surface they are mounted on, and have the ability to stretch to the same extent. One method for measuring the stretch of highly flexible membrane walls is through the use of conductive ionic fluids encased in a flexible elastomer. A change in resistance can be measured between two terminals of the ionic liquid pathway as the sensor strip undergoes stretch deformation. A simple, low-cost approach to fabricating this form of sensor is to encase a conductive saline solution in a highly flexible silicone tube, with electrodes placed in contact with the fluid at the two ends of the sealed tube. Initial results indicate that this basic approach provides good stability and repeatability of resistance measurement readings during stretching. Further testing of the characteristics of this type of sensor is required to properly assess its capabilities against commercial stretch sensors and state-of-the-art devices.**

Keywords*— *Stretch sensor, deformation measurement

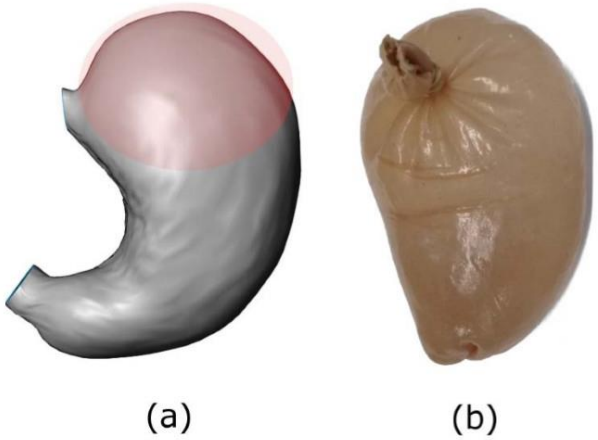

Fig. 1. (a) CAD virtual image of a stomach showing the anticipated region of greatest expansion highlighted in red. (b) A physical example of the simulated stomach membrane requiring stretch sensor measurement.

I. Introduction

Physical simulation of gastric tract motility, through the use of controlled flexi-walled reactors, can benefit from receiving measured feedback of the amount of stretch that specific regions of the deformable membrane wall perform. Natural stretch receptors within the human stomach trigger the relaxation of the oesophageal sphincter and assist in the intake of more food [1]. The most significant region of expansion of the stomach occurs in its upper half and over its greater curvature (fig. 1). The muscular membrane in this section of the stomach can stretch up to 200% of its original length in order to allow for the accommodation of ingested food. At the same time, the lower half of the stomach undergoes extensive wave-like contractive deformations, mixing and breaking down food matter as it does so.

One difficulty in measuring stomach deformation is the potential for sensor interference on the characteristic deformation pattern of the membrane it is attached to. In order to accurately measure the amount of stretch of a flexible membrane wall, sensors need to be at least as flexible as the surface they are mounted on, and have the ability to stretch to the same extent.

Typical stretch sensors can be classified into several types including capacitive and resistive. Capacitive sensors employ layers of conductive material acting as capacitive plates. Stretching of the sensor causes a measurable change in capacitance to be observed. Resistive sensors rely on the changing resistance of a conductive material to determine the amount of stretch that occurs.

A variety of materials have been used in the fabrication of stretch sensors including conductive fabric or textiles [2][3] and conductive fillers such as carbon black [4], graphene nano-platelets, or carbon-nanotubes embedded in an elastomer [5] to act as a deformable conductive material. However, increasing the concentration of a conductive filler within elastomeric rubbers improves overall conductivity, but also decreases the elastic properties of the rubber [6].

Another method of fabrication is through the use of conductive ionic fluids or gels encased in a flexible protective strip of elastic polymer [7][8][9][10][11]. A change in resistance can be measured between two terminals of the ionic conductor pathway as the sensor strip undergoes stretch deformation. The ability of these fluids to infinitely deform provides an advantage over other sensors that use solid conductive fillers encased within a flexible material.

The resistance (R) of an enclosed channel of conductive fluid depends upon the (temperature dependent) resistivity of the fluid (ρ), the cross-sectional area of the channel (A) and the distance between its electrodes (Equation l):

$$R = \frac{l}{A}\rho \quad (1)$$

A conductive ionic fluid channel (or series of channels), suitably terminated with electrode connections and enclosed within a stretchable elastic structure, can produce a measurable change in conductivity as the geometric dimensions of the channel becomes altered. Basic stretch sensors can therefore be constructed from a variety of common materials. A preliminary investigation into several simple, low-cost approaches to fabricating this form of sensor was therefore undertaken. The typical approach involved encasing a conductive saline solution within a highly flexible silicone tube or channel, with electrodes placed in contact with the conductive tract at each end of the sealed channel.

II. Method and Materials

A variety of low-cost, fabricated stretch sensors were investigated for their efficacy in determining the stretch of an elastic membrane. The types of sensors involved can be categorised into: 1) linear channel-type stretch sensors; and 2) conductive fluids, gels or pastes embedded within a flexible membrane.

A. Channel-type sensors

Sample stretch sensors were fabricated from several different elastic tubular source materials to determine their appropriateness for further testing (fig. 2). Rubber balloons, silicone tubing and silicone encased channels were all found to be suitable as enclosures for fabricating basic linear stretch sensors.

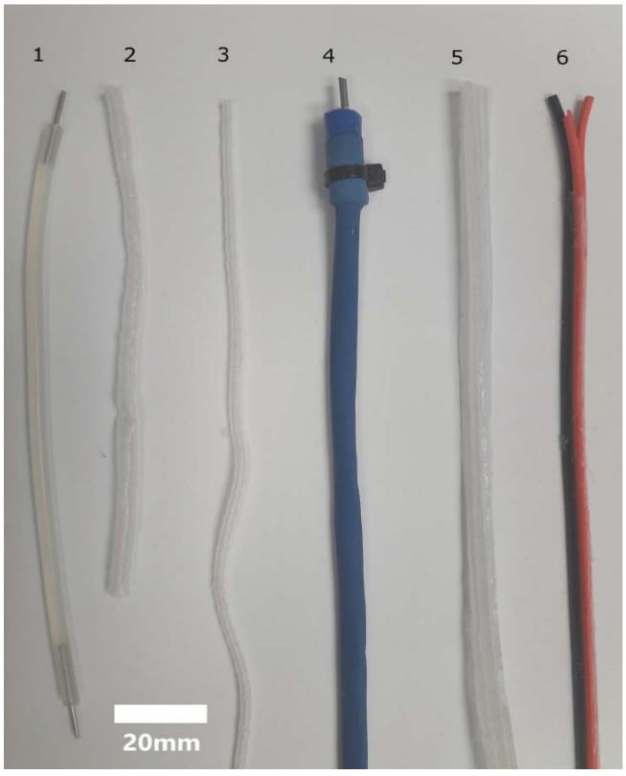

Fig. 2. A selection of trialled sensor materials: (1) commercially available silicone tubing; (2) a thin-walled tube made of silicone; (3) coiled nylon line coated with silicone; (4) a rubber balloon; (5) three tubes sealed together in a triangular shape; (6) a triangular shape made from three silicone-insulated electrical wire sheaths.

A conductive electrolyte solution was obtained by dissolving sodium chloride (NaCl) in tap water to provide an electrolytic fluid. The conductivity of the fluid was measured using a Thermo Scientific Orion Star A325 pH/Conductivity Portable Meter. The electrolyte was further diluted or concentrated in order to bring the conductivity to approximately 0.05 S/cm (@ 18.0° C).

The electrolytic fluid was introduced into the channels of each of the channel-type sensors using a syringe. The ends of the channels were then sealed with a tight-fitting electrode and a small amount of silicone sealant. The terminal electrodes typically consisted of a zinc rod to reduce the effects of corrosion from contact with the salt solution. Care was taken not to allow any air bubbles into the fluid channel during the filling and sealing stages.

A 10 kHz square-wave signal, in series with a shunt resistor, was applied to the terminals of each sensor. Voltage readings were taken across both the shunt resistor and the sensor terminals at various stages of stretching. Calculation of the sensor current was made by dividing the known resistance of the shunt resistor from the measured voltage dropped across it. The sensor current was then divided from the measured voltage drop across the sensor terminals to determine the resistance. A BitScope Micro BS05U USB oscilloscope was used to generate the square-wave signal and measure voltages.

Each sensor was also attached to a semi-inflated silicone balloon using a film of silicone sealant (Selley's Silicone 401 RTV). The balloon was then gradually inflated. This test was used to observe any effects of the attached sensor on altering the natural deformation pattern of the balloon membrane during inflation.

B. Conductive membrane sensors

Two further types of embedded conductive membrane sensors were fabricated for comparison against the channel-type sensors: i) a spreadable composite conductive rubber made from thickened conductive gel and silicone sealant elastomer; and ii) a conductive gel separating an inner and outer membrane layer that employed capacitive coupling for measurement readings.

The conductive paste for the composite conductive elastomer was made by dissolving 5 grams of sodium chloride (NaCl) in 20 ml of water and 5 grams of tapioca (cassava root) starch. The paste was then heated in a microwave oven for 40 seconds, with stirring taking place every 10 seconds to ensure that the gel had an evenly distributed texture. The resulting texture of the gel was then matched to that of the acetic-cure silicone sealant it was to be mixed with (Selley's Silicone 401 RTV).

The thickened gel was then stirred into the silicone sealant at a ratio of 1:1. During mixing the combined materials became opaque as the silicone encased the water-based gel. The resulting paste was then evenly spread out on a smooth surface to cure for 24 hours. Once set, the silicone/gel composite membrane layer was peeled from the surface and cut into strips for testing. Two strips of the conductive gel / silicone composite material were tested for their resistive stretch response in a similar manner to the channel-type stretch sensors.

Two silicone balloons were used for testing of the second conductive membrane sensor, representing the elastic

membranes separated by a conductive gel. A second batch of conductive gel was made with a reduced amount of corn starch (2 grams), producing a gel of thinner consistency. One balloon was then pushed inside the other with the openings aligned together, and the gel inserted between the balloon layers using a syringe. The inner balloon was then able to be inflated, causing the conductive gel to spread out internally between the elastic layers. An electrode was placed between the layers at the balloon opening and a hole was cut at the opposite end of the outer balloon to allow for placement of a secondary electrode.

A 10 kHz square-wave signal, in series with a shunt resistor of suitable value, was passed between the electrodes. Capacitive coupling was used to obtain a reading of the change in voltage between two selected points on the balloon surface, which was then converted to a measure of resistance. The inflation level of the inner balloon was then altered and additional voltage readings repeated over the same two points to obtain the change in resistance as the surface stretched.

III. Results

In general, the tested channel-type sensors displayed linear increase in resistance at low strains (i.e. strains of less than 50%). However, some sensors exhibited non-linear (exponential) changes in resistance at larger strains and when external pressure was applied to the sensor surface (fig. 3). This was due to the differing geometrical cross-sectional areas of the conductive channels as they buckled under compression, as well as the stiffness and thickness of the materials the sensors had been constructed from.

For the purposes of matching the strain required of the expanding artificial stomach only the balloon channel-type sensor (fig. 2(#4)) showed ability to stretch up to 200% from its original length. The sensor made from coiled nylon line coated with silicone (fig. 2(#3)) could not be stretched as a fully sealed unit due to the structural stability of the coil restricting the cross-sectional area from changing. However, the nylon coil sensor was able to be stretched when a reservoir of conductive fluid was attached to one end of the channel, allowing for additional fluid to be drawn into the channel during stretching.

Repeatability of measurements over several stretches, and over different fabricated versions of the same sensor, was not always obtainable due to the inadvertent introduction of gas bubbles within the conductive fluid channels. On observation, bubbles at times formed as the solid metal electrodes moved during stretching, allowing a small amount air to enter into the conductive tract. Imperfections along the inner surfaces of the sensors also prevented the complete expulsion of air bubbles as the conductive fluid was being introduced into the channel. However, the appearance of air bubbles along the (more uniform) internal channels of commercially available silicone tubing was not as prevalent.

Attachment of the channel-type sensors to an inflating balloon membrane resulted in significant alteration to the expected deformation pattern of the membrane material. The stiffness of the encasing materials of each sensor determined to a large extent the amount of alteration to the membrane deformation pattern.

In the balloon tests, the two types of conductive membrane sensors both had less effect on the balloon's natural deformation patterns than the channel-type sensors. The conductive gel sandwiched between two balloons showed the best response as the viscous fluid would evenly spread between the two layers of expanding membrane. The other membrane stretch sensor (i.e. the conductive gel / silicone composite material) adhered well to the balloon surface and would expand with it until rupture of the sensor material or separation occurred from the substrate surface. Both sensor types were able to produce repeatable voltage feedback readings so long as their conductive pathways remained intact.

Uni-directional (i.e. lengthwise) stretch tests of the conductive gel/silicone composite material stretch sensor indicate an approximate linear response in resistance when stretched (fig. 4). Inconsistencies in the dispersion of conductive gel throughout the silicone were found to create locations of increased stress upon stretching. The areas where the cross-sectional dispersion of connected silicone was minimal tended to to be locations where breakages and ruptures in the material would first occur.

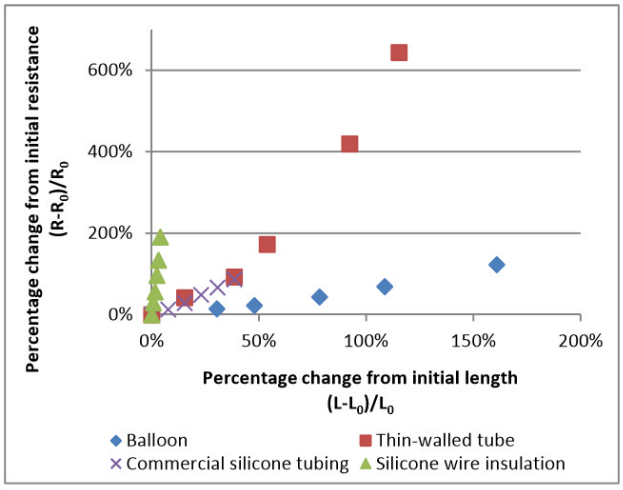

Fig. 3. Resistance response from four of the channel-type sensors being stretched in a lengthwise direction.

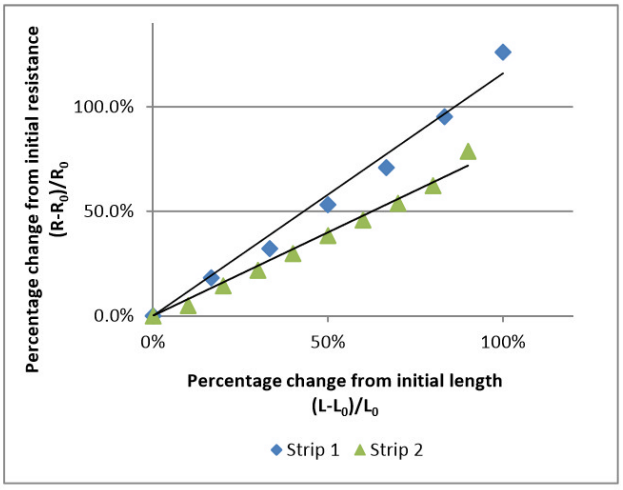

Fig. 4. Resistance response from two strips of the conductive gel & silicone composite stretch sensor being stretched in a lengthwise direction.

IV. Discussion

Assessing the location and extent of stretch that occurs on a simulated stomach membrane during digestion would assist in our understanding of the mechanical processes of digestion. The construction of low-cost, basic stretch sensors that can deform closely alongside the natural deformation of the artificial membrane can provide a means for rapid prototyping and determination of suitable sensor arrangements and material properties.

Initial results indicate that the channel-type sensors could provide good stability and repeatability of resistance measurement readings as the sensors were stretched. The amount of stretch that could be applied to each sensor, as well the amount of force required to stretch them, was dependent upon the materials they were constructed from.

Care must be taken in the design and fabrication of the fluidic channel sensors so that no air bubbles can be introduced into the fluid. Air bubbles (as well as other internal obstructions) significantly impact the cross-sectional area of the conductive channel, returning larger than anticipated resistance readings. This was a consistent problem with the majority of sensors tested as solid metal electrodes tended to spread away from the surrounding elastic material and create air pockets within the conductive fluid channel.

One means of minimising the separation of the electrodes from the connecting elastic material was to sheath the solid electrode with a flexible yet less-extensible material. In this case a silicone-insulated solid-core electrical wire was found to improve the connection to the sensor body whilst the core acted as the electrode in contact with the conductive fluid. However, the tin-coated copper electrical wire was not an ideal electrode material as the saline concentration of the conductive fluid would corrode the wire over time. Another solution may be to use a silicone embedded with solid conductive filler (such as carbon black) as an intermediary connection between the silicone tubing / conductive fluid and solid electrode, although the resistance of the intermediary connection will also need to be taken into account during measurements.

The channel-type sensors may not be suitable for membrane deformation measurements as their own mechanical properties affected the membrane deformation pattern. One possibility for addressing this problem may be to directly construct the conductive channels within the fabricated membrane itself. This approach would help to maintain the original elastic properties of the stomach membrane material, but would also require the embedded channels (subsequently filled with conductive fluid) to have negligible impact on the original membrane deformation pattern.

An added complexity in using channel-type sensors for measuring membrane stretch is that the sensors are primarily designed for stretching in one direction only. When a membrane is stretched it can deform along multiple directions, meaning that several stretch sensors may be required to adequately assess any amount of stretching that takes place. The possible effects on a membrane's natural deformation pattern from the placement of multiple stretch sensors may be considerable.

Capacitive coupling of a signal passed through a conductive channel offers an alternative means for obtaining voltage readings during stretching. The use of capacitive coupling eliminates the need for making a direct electrode contact with the conductive medium. This was demonstrated through experimentation with a double-layered balloon sensor. Voltage readings over the surface of the outer balloon membrane were achieved by passing a square-wave voltage through a conductive gel that was sandwiched between membrane layers. However, due to the nature of the conductive material being spread over an area rather than a pre-defined geometric channel, the resulting conductive tracks involved with this type of sensor are more complex and non-linear than those found in the single-channel type of sensor. The readings obtained are also highly dependent on the location and placement of the signal electrodes that provide the voltage gradient over the membrane.

Although still at a very early stage of development, the conductive gel / silicone composite material shows good potential as a base material for the fabrication of a conductive membrane stretch sensor. The embedded gel exhibited repeatable measures of resistance during initial trials of stretching, and resilience to penetration and leakage of the conductive material. As the gel remains sealed within the silicone it displays good ability to withstand dehydration and therefore maintain a consistent measure of conductivity (fig. 5(a)). At the same time, the mechanical properties of the silicone elastomer do not seem to be significantly affected by the addition of the gel, although the maximum elongation of the silicone is somewhat reduced.

The silicone / gel composite stretch sensor effectively eliminates the potential for air bubbles to enter into the conductive pathway. Inserting a solid electrode or wire into the silicone / gel composite material provides a direct contact with the conductive material, whilst at the same time sealing the electrode with the flexible silicone elastomer. Furthermore, this novel composite material allows for metal

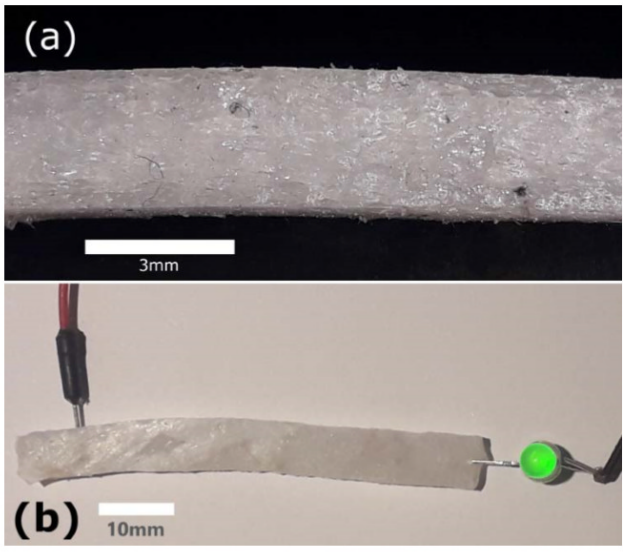

Fig. 5. (a) Close-up image showing a cross-section of the conductive gel / silicone composite material after it has been cut into a strip. (b) A strip of the conductive gel / silicone composite material used in lighting an LED. The contact electrodes can be seen pushed directly into the material without any need for further sealing of the sensor.

electrodes (such as contact wires) to be directly inserted and removed from the sensor at will, without significantly affecting the operation of the sensor (fig. 5(b)).

The ability to manually spread thin films out of the conductive gel / silicone composite material is limited by the viscosity of the mixed components. The minimum thickness of the spread film that could readily be obtained was approximately 3mm. Thinner films affected the ability of the composite material to hold together as a cohesive elastomer, causing the film to become more susceptible to tearing and rupture. This may be in part to a non-optimal mix ratio of the gel and silicone, inconsistencies in distribution of the materials throughout the mixture, and the physical properties of the silicone sealant and conductive gel being used. However, the composite material shows potential to be applied as a conductive thin-film onto other silicone membrane substrates, so long as careful matching of the mechanical properties of the gel / silicone composite material and the substrate are taken into consideration.

Dissolution of the starch gel from the sensor strip reveals a silicone skeletal structure resembling that of a flexible / stretchable open-cell sponge (fig. 6). This interesting characteristic of the (mixed) composite material suggests another potential direction for fabrication of a membrane stretch sensor - by creating a flat, sponge-like structural layer for the encasement of the conductive gel. Such elastomeric sponges can be fabricated by a variety of techniques including direct templating (dissolution of a soluble template material such as sugar or salt), emulsion templating, phase separation and 3D printing [12]. An ionic fluid or gel, encased within the absorbent network of cells, could therefore provide a means from which multi-directional measurements of stretch over a single membrane structure may be made.

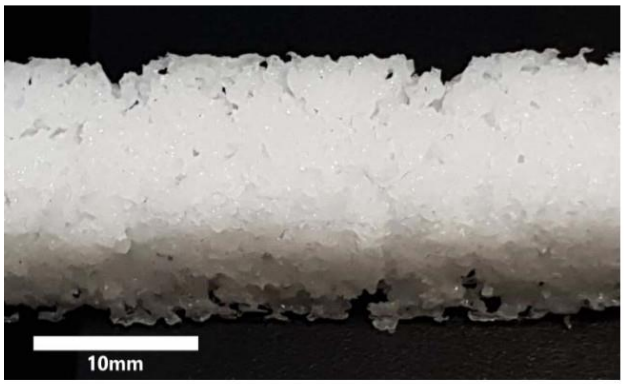

Fig. 6. Close-up image showing a strip of the conductive gel / silicone composite sensor after the gel was dissolved away from the silicone body.

V. Conclusions

Basic resistive stretch sensors constructed from elastic tubing and similar materials can be a viable option for measuring membrane stretch. However, some degree of experimentation is further required in determining appropriate sensor material properties, conductive channel geometry, and electrode contact methods in order to: a) minimize interference with the membrane deformation; and b) eliminate the potential for the formation of air bubbles within the conductive channel.

Further testing of the characteristics of the conductive gel / silicone composite type of sensor will be undertaken to optimise its material properties and assess its capabilities against commercial stretch/pressure sensors and state-of-the-art devices.

References

[1] Penagini, R., Carmagnola, S., Cantù, P., Allocca, M., & Bianchi, P. A. (2004). Mechanoreceptors of the proximal stomach: Role in triggering transient lower esophageal sphincter relaxation. Gastroenterology, 126(1), 49-56.

[2] Tairych, A., & Anderson, I. A. (2017). Distributed sensing: multiple capacitive stretch sensors on a single channel. Paper presented at the Electroactive Polymer Actuators and Devices (EAPAD) 2017.

[3] Stoppa, M., & Chiolerio, A. (2014). Wearable electronics and smart textiles: a critical review. Sensors, 14(7), 11957-11992.

[4] Tairych, A., & Anderson, I. A. (2018). A variable RC transmission line model for resistive stretch sensors. Paper presented at the Electroactive Polymer Actuators and Devices (EAPAD) XX.

[5] Devaraj, H., Giffney, T., Petit, A., Assadian, M., & Aw, K. (2018). The development of highly flexible stretch sensors for a robotic hand. Robotics, 7(3), 54.

[6] Saleem, A., Frormann, L., & Soever, A. (2010). Fabrication of extrinsically conductive silicone rubbers with high elasticity and analysis of their mechanical and electrical characteristics. Polymers, 2(3), 200-210.

[7] Choi, D. Y., Kim, M. H., Oh, Y. S., Jung, S.-H., Jung, J. H., Sung, H. J., Lee, H. M., et el. (2017). Highly stretchable, hysteresis-free ionic liquid-based strain sensor for precise human motion monitoring. ACS applied materials & interfaces, 9(2), 1770-1780.

[8] Wang, Y., Gong, S., Wang, S. J., Simon, G. P., & Cheng, W. (2016). Volume-invariant ionic liquid microbands as highly durable wearable biomedical sensors. Materials Horizons, 3(3), 208-213.

[9] Yoon, S. G., Park, B. J., & Chang, S. T. (2017). Highly sensitive microfluidic strain sensors with low hysteresis using a binary mixture of ionic liquid and ethylene glycol. Sensors and Actuators A: Physical, 254, 1-8.

[10] Zhang, S.-H., Wang, F.-X., Li, J.-J., Peng, H.-D., Yan, J.-H., & Pan, G.-B. (2017). Wearable Wide-Range Strain Sensors Based on Ionic Liquids and Monitoring of Human Activities. Sensors, 17(11), 2621.

[11] Manandhar, P., Calvert, P. D., & Buck, J. R. (2012). Elastomeric ionic hydrogel sensor for large strains. IEEE Sensors Journal, 12(6), 2052-2061.

[12] Zhu, D., Handschuh-Wang, S., & Zhou, X. (2017). Recent progress in fabrication and application of polydimethylsiloxane sponges. Journal of Materials Chemistry A, 5(32), 16467-16497.

MASSEY UNIVERSITY
TE KUNENGA KI PŪREHUROA
UNIVERSITY OF NEW ZEALAND

GRADUATE RESEARCH SCHOOL

STATEMENT OF CONTRIBUTION
DOCTORATE WITH PUBLICATIONS/MANUSCRIPTS

We, the candidate and the candidate's Primary Supervisor, certify that all co-authors have consented to their work being included in the thesis and they have accepted the candidate's contribution as indicated below in the *Statement of Originality*.

Name of candidate:	Gerald Keith Olson
Name/title of Primary Supervisor:	Prof. Clive E. Davies
In which chapter is the manuscript /published work:	Appendix C

Please select one of the following three options:

(●) The manuscript/published work is published or in press

- Please provide the full reference of the Research Output:

Olson, G., Davies, C., Gupta, G. S., Davies, R., & Fullard, L. (2020). Preliminary investigation into low-cost stretch sensors for stomach deformation measurement. Paper presented at the 2020 IEEE Sensors Applications Symposium (SAS).

( ) The manuscript is currently under review for publication – please indicate:

- The name of the journal:
- The percentage of the manuscript/published work that was contributed by the candidate:
- Describe the contribution that the candidate has made to the manuscript/published work:

( ) It is intended that the manuscript will be published, but it has not yet been submitted to a journal

Candidate's Signature:	Gerald Keith Olson — Digitally signed by Gerald Keith Olson, Date: 2023.04.27 18:34:57 +12'00'
Date:	27-Apr-2023
Primary Supervisor's Signature:	
Date:	27-Apr-2023

This form should appear at the end of each thesis chapter/section/appendix submitted as a manuscript/ publication or collected as an appendix at the end of the thesis.

Appendix D: Resistance measurements of polydimethylsiloxane (PDMS) stretch-sensors embedded with a conductive starch gel

Resistance measurements of polydimethylsiloxane (PDMS) stretch-sensors embedded with a conductive gel

Gerald Olson
School of Food & Advanced Technology
Massey University, New Zealand
g.olson@massey.ac.nz

Clive Davies
School of Food & Advanced Technology
Massey University, New Zealand
c.davies@massey.ac.nz

Gourab Sen Gupta
School of Food & Advanced Technology
Massey University, New Zealand
g.sengupta@massey.ac.nz

Rose Davies
School of Aviation
Massey University, New Zealand
r.g.davies@massey.ac.nz

Luke Fullard
School of Agriculture and Environment
Massey University, New Zealand
lukeafullard@gmail.com

***Abstract*— A novel conductive gel and soft silicone (PDMS) composite material was investigated as a potential stretch-sensor material for measuring deformation of elastic surfaces. Initial trials involved resistance measurements on un-stretched sample strips and when strips were stretched to 200% of initial length, resulting in good consistency in resistive feedback between all samples tested. Temperature effect on resistance was also explored. However, due to the small sample size used more extensive testing is suggested in order to confirm these results.**

***Keywords*— PDMS, conductive gel, resistance, measurement**

I. Introduction

Development of an artificial biomimetic stomach, and its complex three-dimensional expanding surface, can benefit from obtaining measurements on the amount of stretch that various sections of the elastic stomach wall undergo during the simulated digestion of food. One option for approaching this challenge is to attach stretch-sensors to the elastic wall that provided measurable feedback on the amount of stretch taking place.

Initial explorations into the development of a stretch sensor for deformation measurement of an artificial stomach membrane revealed potential in the use of sheets or strips of polydimethylsiloxane (PDMS) when combined with a conductive gel [1]. The objective of this work is to develop an elastic sensing material that could stretch up to 200%, deform with the same characteristics and directions as an artificial stomach membrane, and provide measurable feedback as to how much stretch is occurring. Solid contact electrodes and probes could be physically placed on or inserted into the developed sensor material without causing the conductive material to escape or leak out, while changes in resistance between points on the material could be measured as it is stretched. However, the method of fabrication of the original PDMS composite sensor resulted in inconsistent distributions of the conductive material throughout the elastomer and widely varying resistance feedback between samples.

Conductive elastomer stretch sensors have been fabricated using a variety of conductive materials, including solid conductive fillers [2-6], ionic fluids [7-15], liquid metals [16], and conductive gels [17-20]. These stretch sensors typically involve geometrically designed channels or layers encased within an elastomer. The channel-type designs offer measurable dimensions to the cross-sectional area of a homogenous conductive material, from which the resistance equation for a piece (cable/wire) of homogenous material can apply (Eqn. (1)).

$$R = \frac{l}{A}\rho \tag{1}$$

Where: R = resistance; l = length; A = cross-sectional area; ρ = resistivity.

However, many of these stretch sensors may be considered unsuitable for our purpose as they are unable to stretch sufficiently, difficult or too costly to fabricate, or made from materials that affect the required deformation of the stomach membrane. Stretch sensors incorporating ionic conductors may be more suitable as they are able to deform (infinitely) along with their encasing, yet the conductive fluids are limited to working within channels and prove difficult to employ over a complicated expanding three-dimensional elastic surface (such as an artificial stomach wall) as readings can also be affected by compression on the ionic liquid sensor.

The conductive elastomer stretch sensor proposed here is an emulsion-type composite material made from a platinum-cure PDMS and gelatinous vegetable gum (guar). A liquid surfactant (detergent) is used to produce a conductive gel with the gum and bind it with the liquid PDMS as it cures.

II. Method and Materials

A. Sensor fabrication

A gel paste was first produced by mixing 12 grams of guar gum with 44 grams of liquid detergent (Palmolive Original) for 3 minutes at 300 RPM in a stirrer (Velp Scientifica Stirrer DLH). Conductivity of the liquid detergent was 21.87 mS/cm (21.1° C) when measured with a conductivity meter (Thermo Scientific Orion Star A Series). Sixty grams of liquid silicone (Smooth-On Ecoflex 00-30 Platinum Cure Silicone Rubber Compound) resin (part A) was mixed with the gel at 800 RPM for fifteen minutes, followed by the addition of 60 grams of the liquid silicone hardener (part B) and mixing for a further 3 minutes at 300 RPM. The mixture was degassed for five minutes in a vacuum chamber at 90 kPa and poured into a 50 ml plastic syringe. The filled syringe was then spun at approximately 1200 RPM for 1 minute by connecting it to a cordless hand drill via a short length of 3 mm diameter flexible vinyl tubing plugged over the syringe nose.

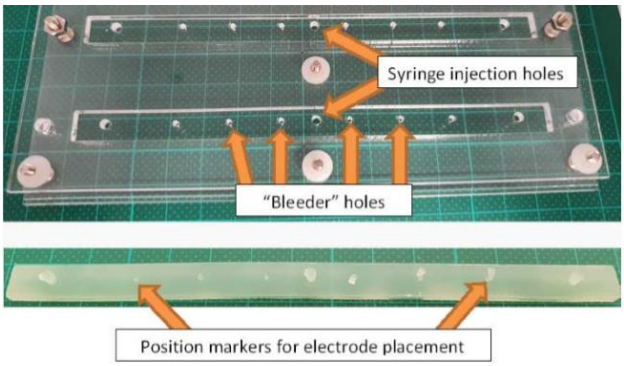

Fig. 1: (Top) An acrylic mould used in creating the sample strips. (Bottom) An example stretch sensor strip removed from the mould.

A mould was made using 3 mm thick acrylic (PMMA) sheet and cut with a laser machine (Epilog Fusion Laser 120W) to form the sample sensor strips. A plate containing a series of slots, each 8 mm wide by 140 mm long, was sandwiched between a base and top plate and held together with screw fixtures (Fig. 1). The top plate had 2 mm diameter holes positioned over the centre of each of the slots so that the gel / PDMS mixture could be injected into the mould using the syringe. 'Bleeder' holes were also cut into the top plate to assist in removing any bubbles that may have found their way into the injected mixture. When the PDMS mixture had cured within the mould (4-6 hours at 20° C) they were removed and sealed with a thin layer of PDMS.

Electrical contact with the conductive material was attained by first threading each end of the strips through a series of rectangular slots cut into short lengths of acrylic 12 mm wide by 52 mm long (Fig. 2). The pieces of slotted acrylic act in a manner to that of standard strap adjusters, allowing the silicone strip to be held in place (via frictional contact force) without applying direct compression to it. A 3 mm diameter hole was made in the acrylic to allow a short section of 3 mm diameter aluminium rod to be pushed through both the hole and the conductive material of the sensor strip. The contact points were positioned 30 mm from each end of the conductive sample strips, so that the resulting initial distance between contact electrodes, when the sensor is un-stretched, was 80 mm.

B. Resistance measurements

Initial resistances of the un-stretched sample strips were made using a 4-wire resistance measurement in order to eliminate contact resistances from the resistance calculations. The four-wire resistance measurements were made by passing an alternating current of 10 microamperes between the ends of the sensor strips and measuring a resulting voltage between the two electrode contact points with a digital multi-meter. The fixed current was provided from a waveform generator feeding a 10 volt (peak-to-peak) 100 Hz square-wave voltage to an adjustable current source (Fig. 3). Resistance of the sample strips was calculated by dividing the known current from the voltage measured across the two electrode contact points. Ten samples of the voltage measurement between the contact probes were taken, with the probes being removed and replaced each time prior to sampling, and a mean value of the resistance of the un-stretched sensor was calculated from the obtained voltages.

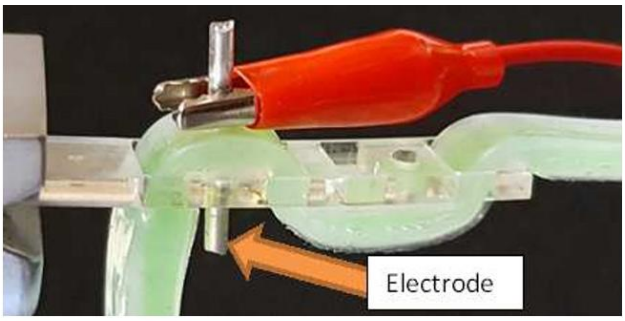

Fig. 2: A sample stretch-sensor strip threaded through a slotted piece of PMMA that is gripped in the jaws of a tensile testing machine. The contact electrode (aluminium rod) is pushed through both the PMMA and sensor material.

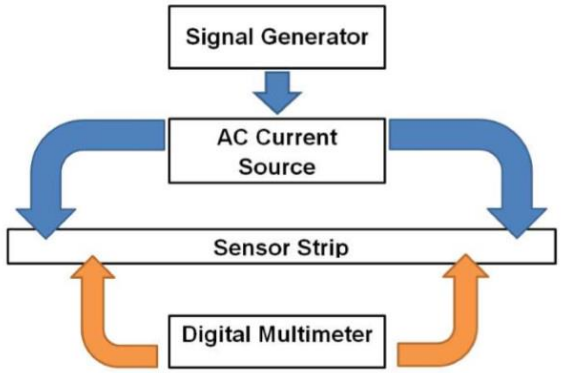

Fig. 3: Schematic of the resistance measurement setup. The blue arrows indicate the connections of the alternating current probes while the orange arrows represent voltage probe positions along the length of the sensor strip.

Six sample strips were placed in the jaws of a universal testing machine (Instron 5960 Dual Column Table Frame) with the starting distance between the two voltage electrodes set to 100mm to remove any slack on the strip. Alligator clips and leads connected the sensors to the measurement equipment. The strips were then subjected to a displacement of 200 mm (200% elongation from the starting length) at a rate of 500 mm per minute.

The resistance of an un-stretched sensor at different temperatures was measured by placing a sensor strip, with electrodes connected to measuring equipment via alligator clips and leads, within a flat-bottomed container of oil and then heating the container in a water bath to 55° Celsius. The glass container was then removed from the bath and resistance readings taken at several intervals as it cooled to room temperature. Temperature readings were recorded at the same time as resistance with a digital thermometer and K-type thermocouple. The thermometer probe was placed in direct contact with the sensor, and located mid-way between the two electrode contact points.

III. Results

Sensor resistance was negatively correlated with change in temperature and resulted in approximately -1.3% change in resistance per degree Celsius increase in temperature (Fig. 4).

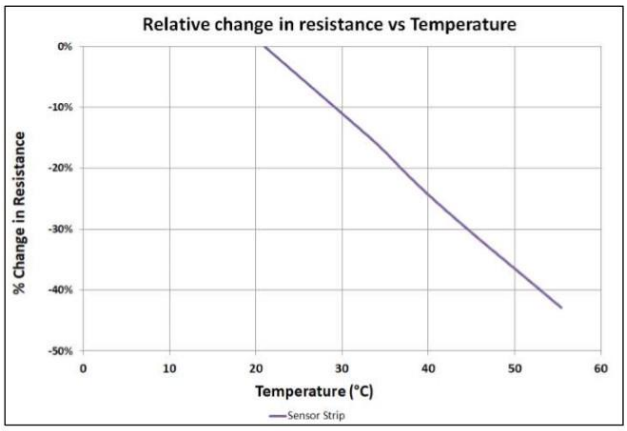

Fig. 4: Relative resistance (from initial sensor resistance at 21.0° C) of a stretch sensor over temperatures ranging between 21° C to 55° C.

Table 1: Mean resistance measurements taken between two contact electrodes on un-stretched stretch-sensor strips.

Sensor sample	Mean resistance (n=10) (kΩ)	Standard deviation (kΩ)	% error (from average of all samples)
1	169.0	3.7	1.4%
2	170.8	10.0	2.5%
3	168.2	7.7	0.9%
4	161.8	4.8	-2.8%
5	169.0	5.3	1.4%
6	160.7	5.8	-3.5%
Mean resistance – all samples	166.6	4.2	

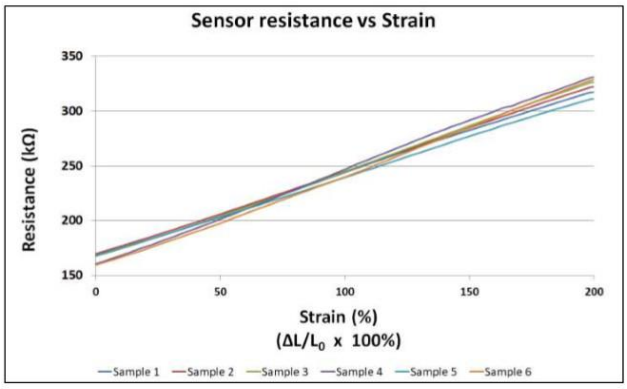

Fig. 5: Resistance response of the stretch-sensor samples as they were stretched to 200% of their initial length.

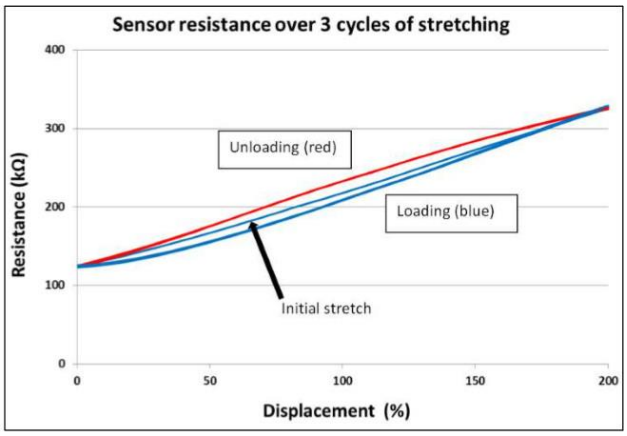

Fig. 6: Resistive response of a stretch sensor over 3 cycles of stretching from 0% to 200% of its initial length.

Initial (un-stretched) resistances of the samples showed good consistency, with resistance values falling within a ±5% margin of the mean (all samples) resistance of 167 kΩ (Table 1). Response in the change in resistance, as samples were stretched to 200% of their initial length, also showed good consistency (Fig. 5). However, some hysteresis appears when a sensor is loaded and unloaded repeatedly (Fig. 6). For all samples the resistance approached a linear response to strain (Fig. 5) but there is still indication that the conductive material is not completely homogenous over the length of the sensor. This may explain why the slopes of the curves differ somewhat between samples. The samples all share a similar bulk resistance over the distance between the electrodes, but the resistivity of the material between the probes may still be unevenly distributed from sample to sample.

IV. Discussion

Several factors are important in maintaining material homogeneity when fabricating these sensors. These include adequate mixing of the combined gel paste and liquid PDMS, rigorous removal of air or gas bubbles and attention to the rate of injection or dispersion of the mixed materials when forming the sensors in moulds or on surfaces.

Mechanical mixing of the gel and liquid PDMS over a sufficient duration and speed was required to produce an adequate distribution of the conductive gel throughout the mixture. Initial trials were carried out via hand-mixing but resulted in significant variations of conductivity occurring between the samples produced. Extended duration of mixing and increased speeds resulted in improved consistency of the composite material. However, this required the liquid PDMS to be mixed in separate parts to prevent the silicone from curing during the mixing process. Increased mixing speeds also introduced more air bubbles, particularly as a liquid detergent was involved in the mixture.

The paste formed during mixing of the gel and PDMS is thicker in viscosity to that of the liquid PDMS in its native form. This property introduces challenges in the adequate removal of bubbles from the mixture prior to curing; hence it is important to undertake appropriate levels of degassing, centrifugal spinning, and provision of 'bleeder' holes within the mould. The presence of gas bubbles can significantly affect the measured resistance of the sensors by reducing the conductive cross-sectional area available for current flow. However, not all bubbles could be removed via degassing or

centrifuge so additional 1 mm diameter bleeder holes were placed in the top plate of the moulds to eject remaining bubbles passing through the mould channels during injection. The bleeder holes also produced small nodes on the surface of the cured sensor when extracted from the mould that provided convenient markers for placement of the contact electrodes.

Although the resulting composite paste was thicker in viscosity than the native liquid PDMS, application of the paste during fabrication of sensor forms can be treated in much the same way. Conductive films of the composite material can be made having a thickness as low as one millimetre by compressing the paste between two plates before curing. Elastomeric conductive cords can also be made by injecting the paste into suitably dimensioned tubing, allowing it to cure, and then extracting the elastomer 'wire' from the tubing (Fig. 7). Alternatively, the PDMS / gel paste can be directly applied to other non-conductive (elastic or inelastic) material surfaces in order to form a conductive layer; however, the materials applied to would need to be known not to inhibit the curing of the PDMS.

The different viscosities of the liquid PDMS and gel paste have significant effect on the resulting homogeneity of the composite material (and therefore its resistivity) as it is injected into a mould. A faster rate of injection appears to cause the lower viscosity PDMS to flow faster than the gel, resulting in some degree of separation between the two materials during the flow process. Slow injection rates resulted in the two materials appearing to move more uniformly and at the same speed through the mould cavity. A constant rate of compression on the syringe plunger was therefore employed during injection of the material into the mould. This was achieved by housing the syringe within a universal testing machine frame and applying a 10 mm/min compression rate to the top of the syringe plunger. A 500 mm length of 3 mm diameter flexible tubing was attached to the syringe tip to feed the PDMS /gel into the moulds.

Initial stretch sensor trials focused on development of suitable PDMS sponge structures into which a conductive gel could be embedded. The sponge structures were filled with a starch slurry (tapioca / cassava root) that was then heated in order to gelatinise it within the sponge. Although many of these early trials succeeded in creating working conductive elastomer stretch sensors, the resistances between samples remained highly variable.

The resistances of the emulsion-type stretch sensors tested here display an improved consistency between samples over the previously trialled embedded sponge-type sensors, and the fabrication process for the emulsion-type is also much faster and less complicated. Another significant improvement is that once the silicone mixture has set, the sensor does not require further absorption of water in order for adequate conductive gelatinisation to occur as the vegetable gun has already gelatinised during the mixing phase.

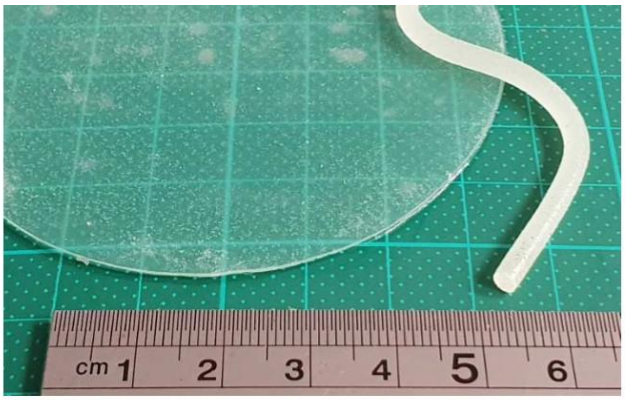

Fig. 7: Examples of fabricated conductive thin-film sheet and elastomeric 'wire'.

The requirement of the sponge-type trial sensors to take on additional water after the silicone has set means that the conductivity of each sensor may vary depending on the amount of water that has been absorbed. The overall volume of the sponge-type sensors typically also increase, sometimes significantly, from their initial (moulded) size. The resistivity of the embedded conductive material of the emulsion-type sensors can potentially be altered during fabrication by soaking the sensor strips in a saline solution. However, it is undetermined as to what effect this would have on increasing the overall volume of the strips and whether this causes measures of resistivity to differ between samples.

During sensor voltage measurements, a 100Hz alternating voltage frequency was required for generating the 10 microampere current as higher frequencies affected the performance of the current source, resulting in lower than anticipated current outputs and fluctuations between sensors being tested. The use of the 4-wire sensing setup was considered for testing purposes only as it prevents contact resistances appearing at the voltage measurement electrodes. However, for operational means, these resistance measurements can be undertaken using a standard 2- wire sensing setup, but the obtained readings would include the associated contact resistances.

The 'strap adjuster', used in maintaining constant electrode contact with the elastomeric sensor material during tensile tests, plays a significant role in obtaining reliable sensor readings. When electrodes are attached to a stretching sensor (either on the surface or inserted into it) they can move around and separate from the conductive material, resulting in erratic sensor readings. The strap adjuster holds both the elastic sensor and solid electrode in place, allowing only a certain section of the sensor to stretch rather than the entire strip. However, this approach is difficult to apply on sensors that are not in 'strap' form, such as flat elastic sheets, as it is difficult in these cases to restrict only certain parts of the material from moving. A potential solution may be to add peripheral nodes to the sensor that extend beyond the stretching surface but are not subjected to the same amount of physical movement (Fig. 8). The electrodes are still required to make contact with the conductive material within the node but the contact is less affected by any stretching of the sensor.

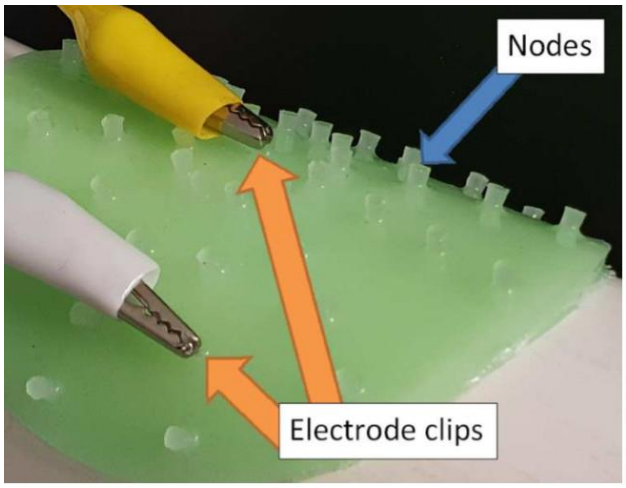

Fig. 8: A flat-sheet sensor showing numerous 'peripheral nodes' extending from the surface and acting as flexible contact points for electrodes. The electrodes require breaking the silicone surface of the sensor (if it has been sealed prior to use) to make contact with the embedded conductive gel.

PDMS / gel sensors are sensitive to temperature changes and require either operation within a temperature-controlled environment or use of temperature compensation methods, such as using a Wheatstone bridge or compensation factor, when computing resistance change. For instance, the sensor material was able to register the heat fluctuations from a person breathing at a distance of 100 mm (when the sensor was placed on a table), and could also detect inhaling (cool air - increasing resistance) and exhaling (hot air - decreasing resistance) when attached to a medical face mask.

Measuring change in resistance of the sensor over its length could help indicate the level of material homogeneity and explain some of the variances that occur. This measurement may be possible by using a set of rolling voltage probes to measure the voltage between the rollers as they move over the surface of the conductive material. The resulting measures of resistance over the entire length of the strips could provide useful information as to how evenly the conductive material is distributed throughout the strips.

As yet there is no understanding of long-term effects on sensor operation such as durability, repeatability, bacterial blooming and changing resistances due to dehydration or chemical change of the conductive gel. These aspects need to be considered before any practical application of this type of stretch sensor can be made.

V. Conclusions

The embedding of a vegetable gum-based gel within PDMS is a novel method for fabricating a conductive elastomer. Near linear responses in resistance can be measured during stretching and the conductive composite material shows good potential for repeatability, as well as resistive consistency between samples trialled. However, the sample size in this trial was very small and extensive testing of this type of sensor is required before any conclusions can be reached. These sensors are at an early stage of development and little is understood about the resistivity of the composite material used, or long-term effects on the sensor. However, they offer interesting potential for the fabrication of conductive sheet-type sensors that could be useful in measuring the deformation of complex three-dimensional surfaces.

References

[1] Olson, G., Davies, C., Gupta, G. S., Davies, R., & Fullard, L. (2020). Preliminary investigation into low-cost stretch sensors for stomach deformation measurement. Paper presented at the 2020 IEEE Sensors Applications Symposium (SAS).

[2] Bojtos, A., & Huba, A. (2011). *Electrical and mechanical testing of conductive silicone rubber filled by carbon black nanoparticles.* Paper presented at the Mechanismentechnik in Ilmenau, Budapest und Niš: Technische Universität Ilmenau, 29.-31. August 2012.

[3] Devaraj, H., Giffney, T., Petit, A., Assadian, M., & Aw, K. (2018). The development of highly flexible stretch sensors for a robotic hand. *Robotics, 7*(3), 54.

[4] Fadzil, F., Sidek, R., Jaafar, H., & Hamidon, M. (2017). *Fabrication and characterization of carbon-based flexible strain sensor.* Paper presented at the 2017 IEEE Regional Symposium on Micro and Nanoelectronics (RSM).

[5] Giffney, T., Bejanin, E., Kurian, A. S., Travas-Sejdic, J., & Aw, K. (2017). Highly stretchable printed strain sensors using multi-walled carbon nanotube/silicone rubber composites. *Sensors and Actuators A: Physical, 259*, 44-49.

[6] Lacasse, M.-A., Duchaine, V., & Gosselin, C. (2010). *Characterization of the electrical resistance of carbon-black-filled silicone: Application to a flexible and stretchable robot skin.* Paper presented at the 2010 IEEE International Conference on Robotics and Automation.

[7] Yoon, S. H., Paredes, L., Huo, K., & Ramani, K. (2018). MultiSoft: Soft sensor enabling real-time multimodal sensing with contact localization and deformation classification. *Proceedings of the ACM on Interactive, Mobile, Wearable and Ubiquitous Technologies, 2*(3), 145.

[8] Choi, D. Y., Kim, M. H., Oh, Y. S., Jung, S.-H., Jung, J. H., Sung, H. J., . . . Lee, H. M. (2017). Highly stretchable, hysteresis-free ionic liquid-based strain sensor for precise human motion monitoring. *ACS applied materials & interfaces, 9*(2), 1770-1780.

[9] Keplinger, C., Sun, J.-Y., Foo, C. C., Rothemund, P., Whitesides, G. M., & Suo, Z. (2013). Stretchable, transparent, ionic conductors. *science, 341*(6149), 984-987.

[10] Wang, Y., Gong, S., Wang, S. J., Simon, G. P., & Cheng, W. (2016). Volume-invariant ionic liquid microbands as highly durable wearable biomedical sensors. *Materials Horizons, 3*(3), 208-213.

[11] Yin, X.-Y., Zhang, Y., Cai, X., Guo, Q., Yang, J., & Wang, Z. L. (2019). 3D printing of ionic conductors for high-sensitivity wearable sensors. *Materials Horizons, 6*(4), 767-780.

[12] Yoon, S. G., Park, B. J., & Chang, S. T. (2017). Highly sensitive microfluidic strain sensors with low hysteresis using a binary mixture of ionic liquid and ethylene glycol. *Sensors and Actuators A: Physical, 254*, 1-8.

[13] Zhang, S.-H., Wang, F.-X., Li, J.-J., Peng, H.-D., Yan, J.-H., & Pan, G.-B. (2017). Wearable Wide-Range Strain Sensors Based on Ionic Liquids and Monitoring of Human Activities. *Sensors, 17*(11), 2621.

[14] Zhu, Y., Chao, C., Cheng, C.-H., & Leung, W. W.-F. (2009). A novel ionic-liquid strain sensor for large-strain applications. *Ieee electron device letters, 30*(4), 337-339.

[15] Jia, H., He, Y., Zhang, X., Du, W., & Wang, Y. (2015). Integrating Ultra-Thermal-Sensitive Fluids into Elastomers for Multifunctional Flexible Sensors. *Advanced Electronic Materials, 1*(3), 1500029.

[16] Chossat, J.-B., Park, Y.-L., Wood, R. J., & Duchaine, V. (2013). A soft strain sensor based on ionic and metal liquids. *IEEE Sensors Journal, 13*(9), 3405-3414.

[17] Yuk, H., Zhang, T., Parada, G. A., Liu, X., & Zhao, X. (2016). Skin-inspired hydrogel–elastomer hybrids with robust interfaces and functional microstructures. *Nature Communications, 7*, 12028.

[18] Sun, J. Y., Keplinger, C., Whitesides, G. M., & Suo, Z. (2014). Ionic skin. *Advanced Materials, 26*(45), 7608-7614.

[19] Tan, Z., Dini, D., y Baena, F. R., & Forte, A. E. (2018). Composite hydrogel: A high fidelity soft tissue mimic for surgery. *Materials & Design, 160*, 886-894.

[20] Manandhar, P., Calvert, P. D., & Buck, J. R. (2012). Elastomeric ionic hydrogel sensor for large strains. *IEEE Sensors Journal, 12*(6), 2052-2061.

MASSEY UNIVERSITY
TE KUNENGA KI PŪREHUROA
UNIVERSITY OF NEW ZEALAND

GRADUATE RESEARCH SCHOOL

STATEMENT OF CONTRIBUTION
DOCTORATE WITH PUBLICATIONS/MANUSCRIPTS

We, the candidate and the candidate's Primary Supervisor, certify that all co-authors have consented to their work being included in the thesis and they have accepted the candidate's contribution as indicated below in the *Statement of Originality*.

Name of candidate:	Gerald Keith Olson
Name/title of Primary Supervisor:	Prof. Clive E. Davies
In which chapter is the manuscript /published work:	Appendix D

Please select one of the following three options:

(●) The manuscript/published work is published or in press

- Please provide the full reference of the Research Output:

Olson, G., Davies, C., Gupta, G. S., Davies, R., & Fullard, L. (2021). Resistance measurements of polydimethylsiloxane (PDMS) stretch-sensors embedded with a conductive gel. Paper presented at the 2021 IEEE International Instrumentation and Measurement Technology Conference (I2MTC).

( ) The manuscript is currently under review for publication – please indicate:

- The name of the journal:

- The percentage of the manuscript/published work that was contributed by the candidate:

- Describe the contribution that the candidate has made to the manuscript/published work:

( ) It is intended that the manuscript will be published, but it has not yet been submitted to a journal

Candidate's Signature:	Gerald Keith Olson — Digitally signed by Gerald Keith Olson Date: 2023.04.27 18:34:57 +12'00'
Date:	27-Apr-2023
Primary Supervisor's Signature:	
Date:	27-Apr-2023

This form should appear at the end of each thesis chapter/section/appendix submitted as a manuscript/ publication or collected as an appendix at the end of the thesis.